

University of Louisville

ThinkIR: The University of Louisville's Institutional Repository

Electronic Theses and Dissertations

5-2012

Carbon-sulfur bond formation/cleavage reactions of metal-stabilized thiyl radicals by electrochemical and chemical methods.

Kagna Ouch Sampson 1983-
University of Louisville

Follow this and additional works at: <https://ir.library.louisville.edu/etd>

Recommended Citation

Sampson, Kagna Ouch 1983-, "Carbon-sulfur bond formation/cleavage reactions of metal-stabilized thiyl radicals by electrochemical and chemical methods." (2012). *Electronic Theses and Dissertations*. Paper 1257.

<https://doi.org/10.18297/etd/1257>

This Doctoral Dissertation is brought to you for free and open access by ThinkIR: The University of Louisville's Institutional Repository. It has been accepted for inclusion in Electronic Theses and Dissertations by an authorized administrator of ThinkIR: The University of Louisville's Institutional Repository. This title appears here courtesy of the author, who has retained all other copyrights. For more information, please contact thinkir@louisville.edu.

**CARBON-SULFUR BOND FORMATION/CLEAVAGE REACTIONS OF
METAL-STABILIZED THIYL RADICALS BY ELECTROCHEMICAL AND
CHEMICAL METHODS**

By

Kagna Ouch Sampson
B.A., RUPP, Cambodia, 2004
M.S., University of Louisville, 2008

A Dissertation
Submitted to the Faculty of the
College of Arts and Sciences of the University of Louisville
in Partial Fulfillment of the Requirements
for the Degree of

Doctor of Philosophy

Department of Chemistry
University of Louisville
Louisville, Kentucky

May 2012

Copyright 2012 by Kagna Ouch Sampson

All rights reserved

**CARBON-SULFUR BOND FORMATION/CLEAVAGE REACTIONS OF
METAL-STABILIZED THIYL RADICALS BY ELECTROCHEMICAL AND
CHEMICAL METHODS**

By

Kagna Ouch Sampson
B.A., RUPP, Cambodia, 2004
M.S., University of Louisville, 2008

A Dissertation Approved on

March 23, 2012

by the following Dissertation Committee:

Advisor: Dr. Craig A. Grapperhaus

Dr. Mark E. Noble

Dr. Francis P. Zamborini

Dr. Christopher T. Burns

Dr. Cindy K. Harnett

DEDICATION

This dissertation is dedicated to my both parents

Mr./Mrs. Ouch

And

Mr./Mrs. Sampson

who have given me invaluable educational opportunities.

ACKNOWLEDGMENTS

I would like to thank my mentor Dr. Grapperhaus, for this patience, insight and the opportunity to join his group for this research over the past six years. Being a part of his group has helped me develop as a chemist and analytical thinker. Dr. Grapperhaus also pushed me to reach my potential, even when I doubted myself.

I would like to thank all my committee members Dr. Noble, Dr. Zamborini, Dr. Burns and Dr. Cindy for their advices and for their time in evaluating my dissertation. Special thanks to Dr. Mark Mashuta for his X-ray expertise and Dr. Neal Stolowich for his help with NMR collection. Thanks to my friend, Davinder Kumar for his help with density functional theory (DFT) calculations.

I would like to thank the members of the Grapperhaus research group, both past and present: Martin O'Toole, Cesar Masitas, Kiran Venna, Rajat Chauhan, and Jinlan Cui. I am grateful for their support and their friendship.

Finally, I would like to give a big thank to my both parents and sibling who made all of my dreams possible and stood behind my every decision and problems.

ABSTRACT

**CARBON-SULFUR BOND FORMATION/CLEAVAGE REACTIONS OF
METAL-STABILIZED THIYL RADICALS BY ELECTROCHEMICAL AND
CHEMICAL METHODS**

Kagna Ouch Sampson

March 23, 2012

The oxidation of metalthiolates is complicated by “non-innocence” or potential redox activity of sulfur to yield thiyl ($RS\cdot$) radicals. In some instances, the one-electron oxidation of metal thiolates yields a product with the unpaired electron nearly equally delocalized between metal and sulfur such that, a specific site of oxidation cannot be defined. We refer to these complexes as metal-stabilized thiyl radicals. This dissertation explores reversible carbon-sulfur bond formation between metal-stabilized thiyl radicals and unsaturated hydrocarbons. Oxidation of the metal thiolate precursors $[Ru(DPPBT)_3]$, **Ru-1**, and $Re(DPPBT)_3$, **Re-1**, (DPPBT = diphenylphosphino-benzenethiolato), generates reactive species that add with alkenes, alkynes, and dienes to yield metal-dithioether products. The electrochemical experiment reveals the addition of alkenes to $[Ru-1]^+$ as an irreversible process. The oxidized intermediate $[Re-1]^+$ binds alkenes reversibly with equilibrium binding constants that vary with complex charge. This dissertation employs the complex, $[Ru-1]$, to investigate metal-stabilized thiyl radical reactivity with alkenes, alkynes, and dienes. The successful works allow us to establish the scope and limits of these reactions. The rate constants of substrates are obtained through digital simulation of

cyclic voltammograms at multiple scan rates. The electronic effects provide a measure of the relative reactivity of the substituted styrenes toward the metal-coordinated thiyl radicals, which yields a Hammett correlation ($\rho = -0.7(1)$) consistent with an electrophilic character for our thiyl radical complexes. Experimentally determined rate constants range from $4.6(5) \times 10^7 \text{ M}^{-1} \text{ s}^{-1}$ for electron-rich alkenes to $2.7(2) \times 10^4 \text{ M}^{-1} \text{ s}^{-1}$ for electron-poor alkenes. For cyclic alkenes, the rate of addition correlates with ring strain; $k_{\text{norbornene}} > k_{\text{cyclopentene}} > k_{\text{cyclohexene}}$. The rate constant of alkyne addition are found to be approximately 100 times lower than alkenes as well-known. The dienes are obtained the addition rate in range between alkenes and alkynes. Crystalline samples of the ethylene addition products $[\text{Ru-1}\cdot\text{C}_2\text{H}_4]^+$ and $[\text{Re-1}\cdot\text{C}_2\text{H}_4]^+$ are obtained from preparative scale reactions using chemical oxidants. Chemical oxidation of $[\text{Ru-1}]^-$ in the presence of *m*-methylstyrene, *p*-methylstyrene, cyclohexene, and 1-octyne yields the dithioether complexes $[\text{Ru-1}\cdot\textit{m}\text{-methylstyrene}]^+$, $[\text{Ru-1}\cdot\textit{p}\text{-methylstyrene}]^+$, $[\text{Ru-1}\cdot\text{cyclohexene}]^+$, and $[\text{Ru-1}\cdot\text{octyne}]^+$. All chemically synthesized complexes were fully characterized including ^{31}P NMR and mass spectrometry.

TABLE OF CONTENTS

	PAGE
ACKNOWLEDGMENTS	iv
ABSTRACT.....	v
LIST OF TABLES.....	ix
LIST OF FIGURES	xi
CHAPTER	
I. INTRODUCTION	1
II. EXPERIMENTAL.....	19
Material and physical methods	19
Electrochemical methods	20
Cyclic voltammetry.....	20
CV simulation parameters.....	24
Square wave voltammetry.....	27
Routine electrochemical measurements.....	29
Kinetic study to determine rate constants	29
Reactivity study to determined rate constants	30
Experimental for chapter III.....	31
Experimental for chapter IV	36
Chemical synthesis.....	38
III. KINETIC STUDY OF $[\text{Ru}(\text{DPPBT})_3]^+$ WITH ALKENES	47

Styrene addition to [Re-1]⁺	51
Rate constant of addition of styrene to [Ru-1]⁺	54
Rate constant of addition of acyclic and cyclic alkenes to [Ru-1]⁺	58
Chemical syntheses	67
IV. REACTIVITY OF [Ru(DPPBT)₃]⁺ WITH OTHER UNSATURATED SUBSTRATES	78
Electrochemical measurements	83
Reactivity of [Ru-1]⁺ with multi-substituted alkenes	84
Reactivity of [Ru-1]⁺ with alkynes	89
Reactivity of [Ru-1]⁺ with dienes	93
Chemical syntheses	97
V. CONCLUSIONS	105
REFERENCES	113
APPENDICES	118
CURRICULUM VITAE	211

LIST OF TABLES

CHAPTER	PAGE
II-1	Rate constant (k_f) data for [Ru-1]⁺ in presence of styrene in 4 mL of dry degassed chlorobenzene.....32
III-1	Cyclic voltammetry simulation parameters57
III-2	Experimentally determined second-order rate constants for the addition of alkenes to [Ru-1]⁺59
III-3	Second-order rate constants for the addition of substituted styrene derivatives to [Ru-1]⁺ in acetonitrile at 298 K.....62
III-4	Relatives rates of substituted styrenes toward [Ru-1]⁺ intermediate.....63
III-5	Selected bond distances (Å) and bond angles (deg) for [Ru-1·C₂H₄]⁺ , [Ru-1·<i>m</i>-methylstyrene]⁺ , [Ru-1·<i>p</i>-methylstyrene]⁺74
III-6	Selected bond distances (Å) and bond angles (deg) for [Ru-1·C₂H₄]⁺ , [Ru-1·cyclohexene]⁺ , [Ru-1·<i>p</i>-methylstyrene]⁺77
IV-1	CV data for [Ru-1·alkene]^{2+/+} with rate constants89
IV-2	CV data for [Ru-1·alkyne]^{2+/+} with rate constants93
IV-3	CV data for [Ru-1·diene]^{2+/+} with rate constants96
IV-4	CV data for [Ru-1·substrate]^{2+/+} with rate constants97
IV-5	Selected bond distances (Å) and bond angles (deg) for [Ru-1·octyne]⁺ , [Ru-1·C₂H₄]⁺ , and [Ru-1]⁺100
IV-6	Properties of Ru(II)-substrate complexes102

IV-7	^{31}P NMR of (4)-(11).....	103
------	--------------------------------------	-----

LIST OF FIGURES

CHAPTER	PAGE
I-1	A qualitative overview of the frontier molecular orbitals shows π interactions between Ru d-orbitals and S p-orbitals13
I-2	Views of the xz-planes highlighting interactions between S p-orbitals and C-C bond orbitals.....16
II-1	Cyclic voltammetry.....22
II-2	Simulation screens in DigiSim program27
II-3	Square wave voltammetry.....28
III-1	A truncated MO diagram depicting only the p-interactions, M(d)-S(p) (filled-filled), which “activate” the thiolate lone pair48
III-2	Cyclic voltammograms of complex Re-1 obtained under a nitrogen atmosphere in dichloromethane49
III-3	Absorbance spectra showing the reversible binding of ethylene to [Re-1] ⁺50
III-4	Cyclic voltammogram of Re-1 in presence of 2.0 M styrene obtained in acetonitrile.....52
III-5	Kinetic study of [Re-1] ⁺ in presence of 2.0 M styrene obtained in chlorobenzene53

III-6	Cyclic voltammograms of 2.0 mM complex [Ru-1]⁻ recorded in the absence (top) and presence (bottom) of 0.2 M styrene	55
III-7	Experimental (–) and simulated (---) cyclic voltammograms of [Ru-1]⁻ in presence of styrene were obtained at a scan rate 400 mV/s	56
III-8	Correlation of log (k/k _H) for styrenes with Hammett σ parameter	64
III-9	Correlation of E _{1/2} for styrenes with Hammett σ parameter	66
III-10	Four possible isomers of [Ru-1·alkene]⁺	69
III-11	ORTEP representations of the complex cations [Ru-1·p-methylstyrene]⁺	69
III-12	³¹ P NMR of [Ru-1·p-methylstyrene]⁺	70
III-13	³¹ P NMR second order spectra.....	71
III-14	³¹ P NMR of [Ru-1·p-methylstyrene]⁺ as isolated crystal	72
III-15	ORTEP representations of the complex cation [Ru-1·m-methylstyrene]⁺	73
III-16	³¹ P NMR of [Ru-1·cyclohexene]⁺	75
III-17	ORTEP representations of the complex cation [Ru-1·cyclohexene]⁺	76
IV-1	Cyclic voltammogram of 2.0 mM complex [Ru-1]⁻ in acetonitrile with 0.1 M TBAHFP was obtained in the presence of <i>cis</i> -stilbene (0.20 M)...	84
IV-2	Cyclic voltammogram of 2.0 mM complex [Ru-1]⁻ in acetonitrile with 0.1 M TBAHFP was obtained in the presence of <i>trans</i> -stilbene (0.20 M)	86
IV-3	Cyclic voltammogram of 2.0 mM complex [Ru-1]⁻ in acetonitrile with 0.1 M TBAHFP was obtained in the presence of 2-methyl-2-butene (0.20 M).....	87
IV-4	Cyclic voltammogram of 2.0 mM complex [Ru-1]⁻ in acetonitrile	

	with 0.1 M TBAHFP was obtained in the presence of 2,3-dimethyl-2-butene (0.20 M)	88
IV-5	Cyclic voltammogram of 2.0 mM complex [Ru-1]⁻ in acetonitrile with 0.1 M TBAHFP was obtained in the presence of 1-octyne (0.20 M)	90
IV-6	Cyclic voltammogram of 2.0 mM complex [Ru-1]⁻ in acetonitrile with 0.1 M TBAHFP was obtained in the presence of phenyl acetylene (0.20 M)	91
IV-7	Cyclic voltammogram of 2.0 mM complex [Ru-1]⁻ in acetonitrile with 0.1 M TBAHFP was obtained in the presence of 1-phenyl-1-propyne (0.20 M)	92
IV-8	Cyclic voltammogram of 2.0 mM complex [Ru-1]⁻ in acetonitrile with 0.1 M TBAHFP was obtained in the presence of 1,3-butadiene (0.20 M)	94
IV-9	Cyclic voltammogram of 2.0 mM complex [Ru-1]⁻ in acetonitrile with 0.1 M TBAHFP was obtained in the presence of 2,3-dimethyl-1,3-butadiene (0.20 M).....	95
IV-10	Cyclic voltammogram of 2.0 mM complex [Ru-1]⁻ in acetonitrile with 0.1 M TBAHFP was obtained in the presence of dipentene (0.20 M)	96
IV-11	ORTEP representations of the complex cations [Ru-1·octyne]⁺	100
IV-12	³¹ P NMR of [Ru-1·octyne]⁺	101
V-1	(a) Qualitative overview of the frontier molecular orbitals of [Ru-1]⁺ and (b) site of alkene addition	109

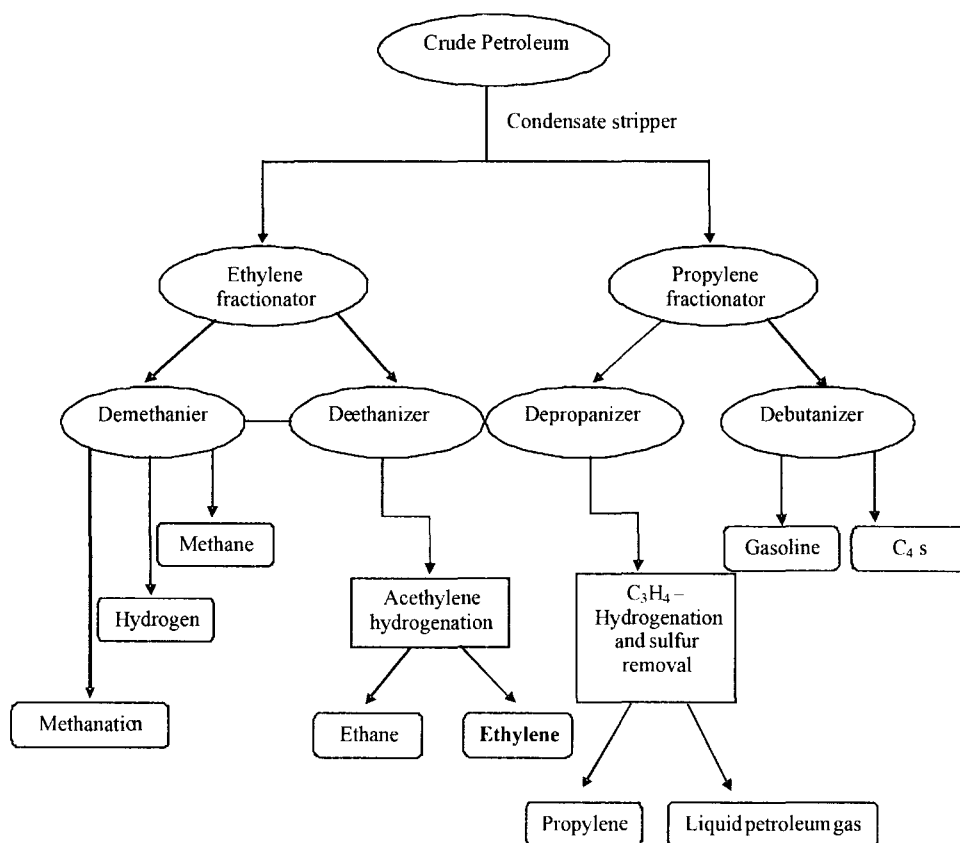
CHAPTER I

INTRODUCTION

Ethylene is the simplest unsaturated hydrocarbon and is classified as an alkene, or olefin. Although ethylene is small in molecular weight it is the largest organic molecule in terms of industrial production. Annual U.S. production of ethylene has averaged 2.4×10^7 metric tons since 1999 and worldwide production in 2011 was estimated as 14.0×10^7 metric tons.^{1,2} The large scale production of ethylene is required since it is a feedstock for polyethylene, ethylene oxide, ethylene chloride and other products. Also ethylene is used for welding, anesthetic agent, and fruit ripening. Ethylene is manufactured by various methods such as thermal cracking of hydrocarbons, catalytic pyrolysis, membrane dehydrogenation of ethane, and other methods.³

Mainly, ethylene is produced from thermal cracking of naphtha in the petrochemical industry. Scheme I-1 outlines the basic steps in the process.⁴ Naphtha feedstock is heated up to 750-950 °C. This process converts large hydrocarbons to small and unsaturated molecules. Then, this step passes by compression and distillation resulting in cracked gas stream. The cryogenic treatment is operated to cool down the cracked gas stream. The gas stream is then separated by two fractionators. The first is the ethylene fractionators and the second is the propylene fractionators. In the dissertation, only the ethylene fractionator is of interest. All of the cold cracked gas stream transfers

through the demethanizer tower, which produces an overhead consisting of all hydrogen and methane. Methanation is used to purify hydrogen. The pure hydrogen is withdrawn from the lowest temperature stage separator. The bottom stream from demethanizer tower goes to the deethanizer tower. This tower contains C_2 's that are sent to a C_2 splitter. The ethylene product obtained from the overhead of the tower is subjected to acetylene removal and hydrogenation to purify the ethylene. Ethane is also obtained as base product from the C_2 increase and ethylene production remains high there is increased need to improve efficiency.



Scheme I-1. Flow diagram of an ethylene plant.

An alternate separation technique involves chemically specific reagents that react with ethylene reversibly. An important area of petroleum industry is based on the

influence of inorganic chemistry and diverse field investigations. Carbon-sulfur bond formation and cleavage reactions between alkenes and transition metal complexes are focused on the synthetic research. The new design and control of metal complexes with “non-innocent” sulfur donors that yield metal-stabilized thiyl radicals upon oxidation.

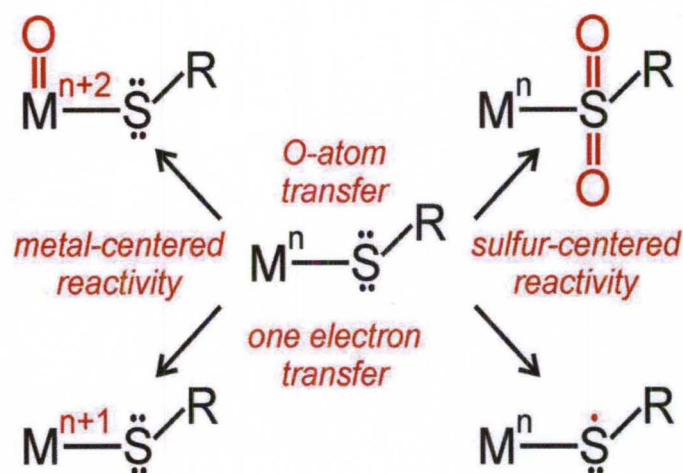
Metal-coordinated radical ligands have received significant attention as alternates to traditional transition metal catalysts. Metal-coordinated radical-ligand complexes are of current interest as demonstrated by Chirik, Heyduck, and Soper.⁵⁻¹⁰ Chirik and coworkers has reported that the bis(imino)pyridine iron bis(dinitrogen) complex [ⁱPr₂PDI₂Fe(N₂)₂] (iPr = isopropyl, PDI = pyridinediimine) is functional-group tolerant precatalyst in a number of reactions such as hydrogenation and hydrosilylation of olefins, as well as the cyclization of enynes and diynes. Also, in galactose oxidase, a copper center with tyrosine ligand is using to oxidize alcohols to aldehydes in a two-electron oxidation process.^{8,10} Using two-electron redox reactivity of [N₂O₂^{red}]ZrL₃ (N₂O₂^{red} = *N,N'*-bis(3,5-di-*tert*-butyl-2-phenoxy)-1,2-phenylene-diamide, L = THF), this complex was found to be catalyst for the disproportionation of diphenylhydrazine to azobenzene and aniline.⁶ The addition of alkyl halides to square planar cobalt(III) complexes with redox-active amidophenolate ligand generates stable square pyramidal alkylcobalt(III) complexes. The formation is required two-electron oxidation of the metal fragment, but the metal oxidation state is the same so the reaction occurs with 2 electrons oxidation from the active ligands.⁵

The redox active ligands help the base metals (Fe, Cu, Zr, Co), which normally have one-electron redox chemistry constraining their application in organic reactions, participate in two-electron transfers. For our system, we develop a series of metal-thiolate

complexes that yield metal-stabilized thiyl radical complexes upon oxidation. Metal-stabilized thiyl radicals can offer an advantage over strictly organic thiyl radicals, if the metal can tune the radical reactivity or selectivity.

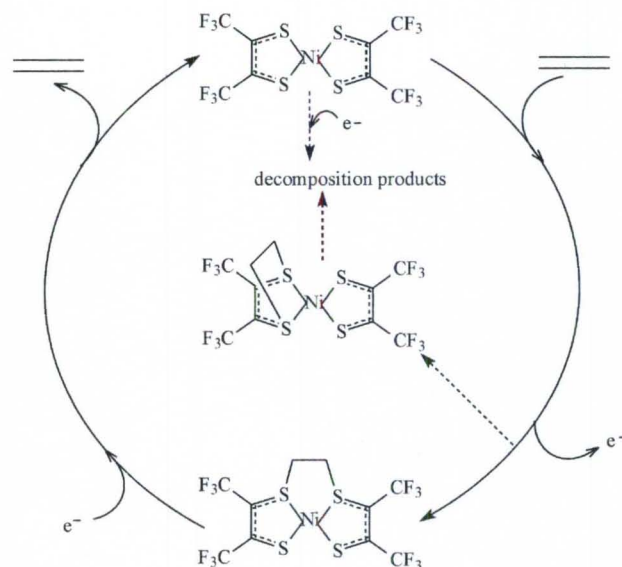
The well-studied reactivity of nucleophilic metal-thiolate presents a new method for the synthesis of metal-sulfur complexes. Transition metal-coordinated thiolate complexes are of interest due to their biological significance as well as their potential applications in catalysis and industry.¹¹⁻¹³ Cytochrome P450s, blue copper proteins, zinc finger proteins, nitrile hydratase, and hydrogenase contain metal-coordinated thiolates at their active site, which provides an impetus to understand the mechanism and electron transfer. However, the elucidation of the chemistry of these systems is complicated due to the crucial reactivity at both the sulfur and the metal center.¹⁴

A significant challenge in the study and synthesis of metal thiolate complexes comes up from their complicated oxidation chemistry, especially for electron-rich metals, Scheme I-2. When dioxygen is the oxidant, which can result in the oxidation and/or oxygenation (oxidation where oxygen atoms are transferred) at the metal and also at the ligand is possible. Metal oxygenation normally yields in the formation of an M=O bond. In addition, ligand-centered oxygenation can produce sulfenato (MSOR), sulfinato (MSO₂R), or sulfonato (MSO₃R) complexes. Thiolate ligand oxidation often results in the formation of a thiyl radical, which often rearranges to form a disulfide bond. However, as described in this dissertation, the thiyl radical may also be intercepted in reactions with unsaturated hydrocarbons.



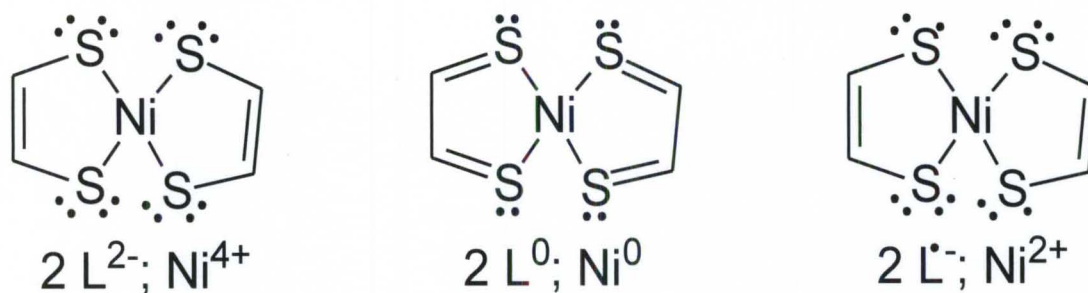
Scheme I-2. Oxygen reactivity of metal-thiolates.

Alkene addition to oxidized metal-sulfur complexes has been previously reported, although a metal-coordinated thiyl radical was not invoked in the mechanism. Most notably, Stiefel and coworkers revealed binding of alkenes to an oxidized nickel dithiolene with subsequent release upon reduction, Scheme I-3 (dark line).¹⁵ Inter-ligand addition resulted in formation of an S_4^{2-} chelate for nickel which was reportedly stable unless reduced. In fact, this process was proposed to potentially be of great industrial importance in olefin purification. The electronic structure of the oxidized dithiolene complex was studied by Wieghardt and determined to be a diradical $[Ni(II)(L)_2]$, (L = dithiolene).¹⁶ Upon introduction of an alkene, the diradical reacts resulting in C-S bond formation. In the reversed direction, controlled by switching the potential for a one electron reduction, C-S bond cleavage regenerates the original nickel complex and releases the alkene.



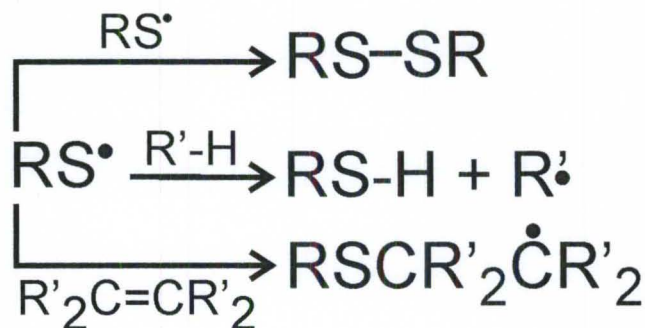
Scheme I-3. Redox initiated alkene binding/release. The solid lines represent the desired pathway. The dashed lines show competing paths leading to decomposition.

However, later studies elucidated the reaction is more complex, Scheme I-3 (dash lines). Deleterious intraligand alkenes addition, leading to dihydrodithiin and complex degradation, dominates while the desired interligand addition is a minor product.¹⁷ From studies by Geiger, complications regarding the alkenes release were distinguished. The potential required for alkene release is also to reduce the initial nickel dithiolene leading to decomposition products.¹⁸ For nickel dithiolene, intraligand is preferred by symmetry. As noted above and in Scheme I-4, the electronic structure of nickel dithiolene has radical character. Further, alkene binding is dependent on the diradical ligand character of the Ni(II) complex.¹⁶



Scheme I-4. Electronic structure of nickel dithiolene has radical character.

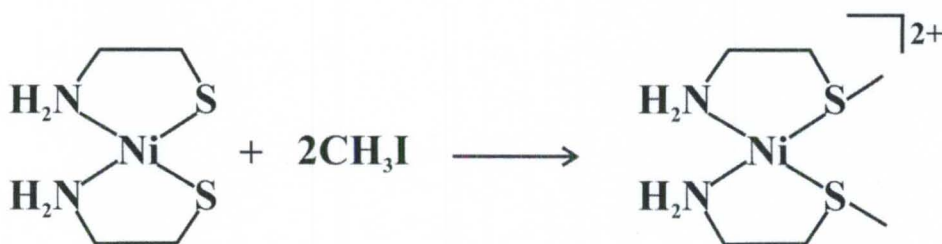
Reactions of organic thiyl radicals typically correspond to one of three major classes, Scheme I-5. First, thiyl radicals may react with each other forming disulfide. Second, thiyl radicals can abstract hydrogen from activated C-H bonds. Finally, thiyl radicals can react with unsaturated hydrocarbons in a C-S bond forming reaction.¹⁹ Carbon-sulfur bond formation between organic thiyl radicals and unsaturated hydrocarbons has exploited for *cis/trans* isomerization, sulfide synthesis, and polymerization. In 1958, Helmreich and coworkers reported thiyl radical initiated isomerization of *cis*-alkenes to *trans*-alkenes in a reversible reaction.²⁰ The addition of thiyl radicals to alkene to form C-S bond was utilized by the Ichinose group for the synthesis of sulfides.²¹ Apart from the C-S bond formation reaction, thiyl radicals have also been used in the initiation of block polymerization.



Scheme I-5. Reaction categories for thiyl radicals.

The study of our group is to use metal-thiolate to promote C-S bond formation by hindering disulfide and H-atom abstraction. Geometrical or steric constraints are sufficient to hinder disulfide formation. Hydrogen abstraction from C-H bonds by thiyl radical is only favored for activated hydrogen atoms since the S-H bond enthalpy typically is weaker than the C-H bond enthalpy.²² Coordination of the thiolate to a metal should further decrease S-H bond enthalpy.

The first metal-coordinated thiolate complex that demonstrated reactivity analogous to an organothiolate compound was the nickel dithiolate complex, bis(mercaptoethylamine)nickel(II), studied by Busch *et al.* in 1964.²³ When the complex is reacted with methyl iodide, C-S bond formation on the sulfur ligand occurs, Scheme I-6.

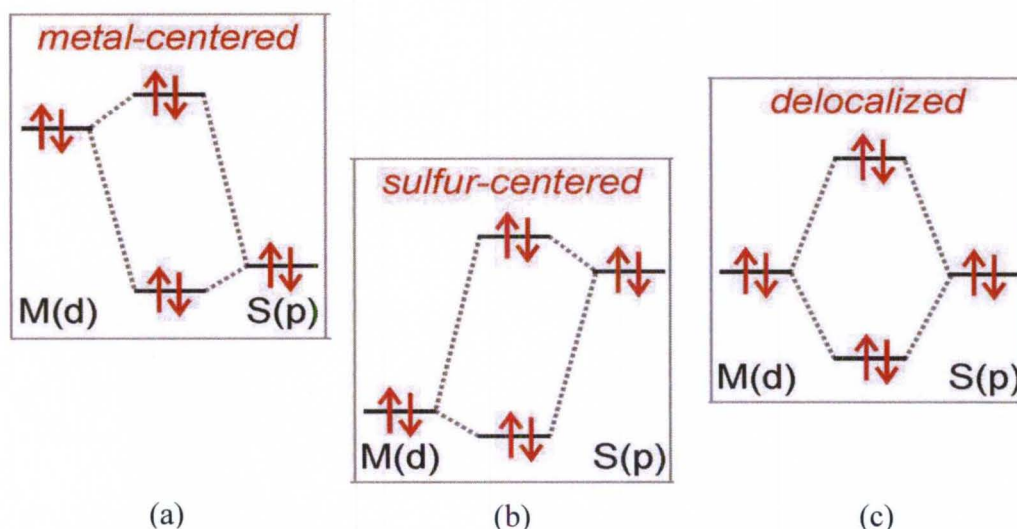


Scheme I-6. Sulfur alkylation of a nickel dithiolate.

Alkylation of metal-coordinated thiolates indicates that the sulfurs are nucleophilic, analogous to non-coordinated organothiolate compounds. In either case, thiolate undergoes a two-electron oxidation producing a new C-S bond formation. These two families are further investigated through the electron density distribution by density functional theory (DFT) calculations. Theoretical examinations for numerous synthetic thiolate complexes have supported that the electron density is highly delocalized on the sulfur.²⁴⁻²⁹ Therefore, the nucleophilicity of the thiolates observed in both metal-

coordinated and alkyl thiolates is assigned to the sulfur p-orbital of the HOMO. However, coordination to a metal is also promoted delocalization of electrons into the metal d-orbitals, thus decreasing the nucleophilicity of the thiolate.

The reactivity of the thiolate has been attributed to the interaction of the sulfur p lone-pair with a “ t_{2g} ” metal d-orbital.³⁰ As illustrated in Scheme I-7, there are three general cases for these interactions depending on the relative energies of the orbitals.

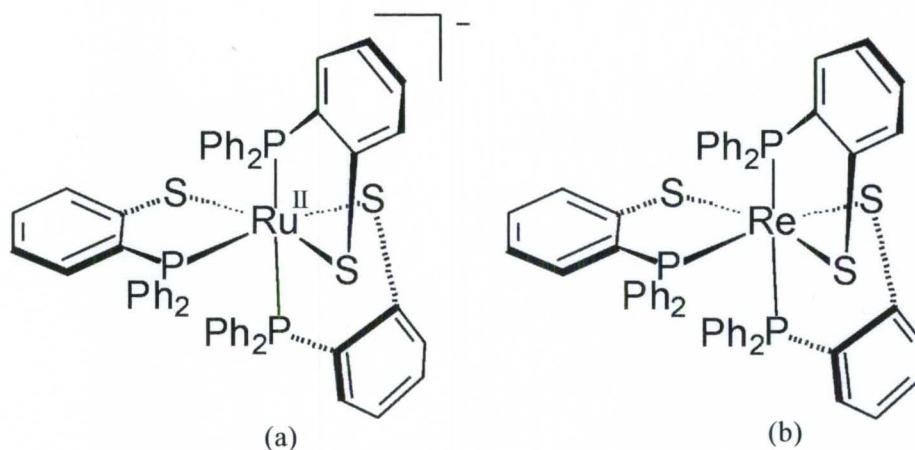


Scheme I-7. Partial molecular diagrams are showing interactions of metal d-orbital and sulfur p-orbital to generate a π -bonding and π -antibonding orbital.

When the t_{2g} metal d-orbital is higher in energy than the sulfur p-orbital, there is also no significant interaction. The thiolate is not expected to be as nucleophilic and oxidation is regarded as metal-based (Scheme I-7a). When the sulfur p lone-pair orbital has higher energy than t_{2g} metal d-orbital, there is no significant interaction between each other. The higher energy orbital is sulfur-centered and may be a nucleophilic, but it is not “activated” (Scheme I-7b). Oxidation would be expected to be sulfur based. When the metal d-orbital and sulfur p lone-pair have similar energies, (Scheme I-7c), there is a strong interaction that yields a remarkable stabilized π -bonding orbital and π -antibonding

orbital. Each of these orbitals is delocalized between sulfur and metal character. Although there is no net π -bond, the increased energy of the antibonding orbital “activates” the thiolate nucleophilicity. Moreover, since the orbital is not localized on the metal or sulfur, it is difficult to assign oxidation as metal or ligand centered upon the oxidation. Rather, “metal-stabilized thiyl radical”, or complexes that enjoy stability but maintain some reactive properties of thiyl radicals are generated.

The focus of this dissertation will be the exploration of carbon-sulfur bond formation/cleavage reactions of metal-stabilized thiyl radical by the electrochemical and chemical methods. The one-electron oxidation of metal thiolates results in an increased oxidation state of the metal ion or the formation of a sulfur-based, thiyl radical in limiting extremes. For complexes with highly covalent M-S bonds, the unpaired electron may be delocalized over the metal and the sulfur, yielding a metal-stabilized thiyl radical. Our investigations with metal-stabilized thiyl radical will largely focused on the Ru and Re complexes $[\text{Ru}(\text{DPPBT})_3]^-$, **[Ru-1]**⁻, and $\text{Re}(\text{DPPBT})_3$, **Re-1** (DPPBT = diphenylphosphinobenzenethiolato), initially reported by Dilworth *et al.*, Scheme I-8. The tri-chelate ligand environment and an electron rich metal center makes it a suitable candidate to investigate metal versus ligand centered reactivity. Since each chelate contains a single sulfur donor, the addition must be interligand. The bulky ligand environment increases the possibility for radical stabilization.



Scheme I-8. Representation of $[\text{Ru}(\text{DPPBT})_3]^-$, $[\text{Ru-1}]^-$ (a) and $\text{Re}(\text{DPPBT})_3$, **Re-1** (b) (DPPBT = 2-diphenylphosphinobenzenethiolato).

The complex $[\text{Ru-1}]^-$ was earlier studied by Dilworth *et al.* as the HNEt_3^+ salt.³¹ In those reports, the oxidation behavior was reported as solvent dependent. Oxidation of $[\text{Ru-1}]^-$ by one electron occurred upon the exposure to O_2 in dichloromethane solvent layered with methanol. Ligand centered oxygenation was obtained in a mixture of solvents including toluene, dichloromethane, and methanol. Unfortunately, the poor solubility of this complex as the triethylammonium salt prevented the further study of these reactions by the various spectroscopic methods. This limitation hinders our understanding of the reactivity. In the Grapperhaus group, the HNEt_3^+ counter-ion of this complex was substituted with PPN^+ ($\text{PPN} = \text{bis}(\text{triphenylphosphoranylidene})\text{ammonium}$) to improve the solubility.³²

Previously in the Grapperhaus group, the complex $[\text{Ru-1}]^-$ has been shown to be a good nucleophile, reacting even with poor electrophile like dichloromethane. This clearly indicates the thiolates of this complex are good nucleophiles.³² This strongly suggests oxidation will remove an electron from an orbital with significant metal and sulfur character.

To further understand the reactivity of **[Ru-1]**⁻, the electrochemical investigations are undertaken with *in situ* monitoring by UV-visible spectroscopy. This intermediate species increases intensity in short lived time then before completed electron process, the band is disappeared. However, further oxidation by one electron results in proposed intramolecular S-S formation via an observed intermediate. Spectroscopic characterization of the intermediate is consistent with a metal-coordinated thiyl radical.³³ The rate of radical decay determines as $5.8(0.7) \times 10^{-3} \text{ s}^{-1}$ at 253 K. The short lived intermediate decays to a proposed Ru (II)-disulfide product.^{32,34} The disulfide is not thermally stable and therefore not structurally characterized or fully explored.

Density functional theory (DFT) investigations by Frye in the Grapperhaus group have determined the ground state of the reactive intermediate **[Ru-1]**⁺. The ground state of **[Ru-1]**⁺ is best considered as a singlet diradical which is consistent with experimental data. A qualitative overview of the frontier molecular orbitals shows π interactions between Ru d-orbitals and S p-orbitals in the xz, yz, and xy planes, Figure I-1. The configuration of ground state **[Ru-1]**⁺ is shown as $(S2(p_x) - S6(p_z))^2$, $(dxz - S2(p_x) - S6(p_z))^1$, and $(dxz - S3(p_y))^1$.³⁵ This diradical ground state has unpaired electrons delocalized over the metal and sulfur donors in nearly orthogonal orbitals. The relative orientation of the half-occupied orbitals inhibits disulfide formation and favors addition of unsaturated hydrocarbons across adjacent atoms.

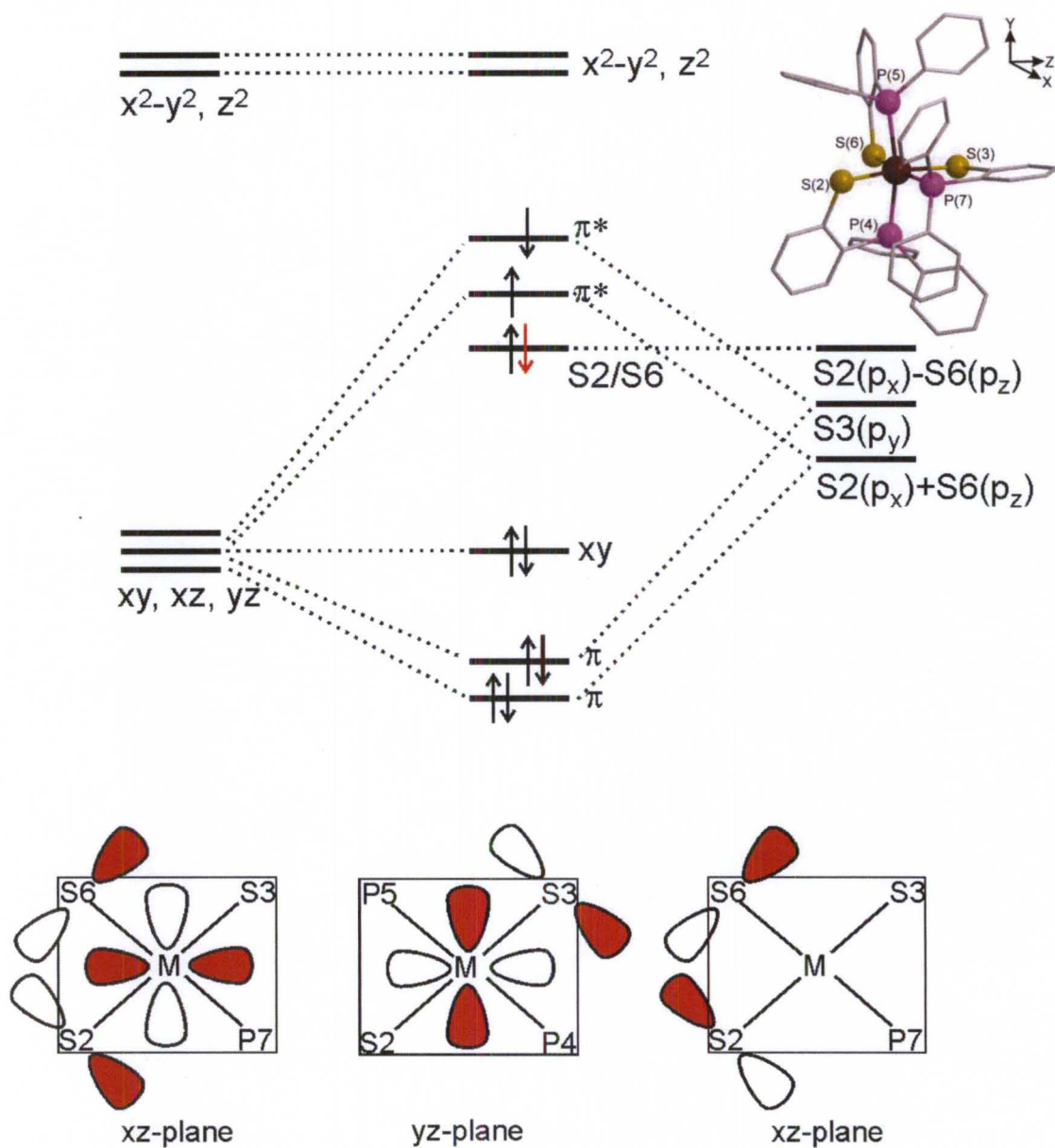
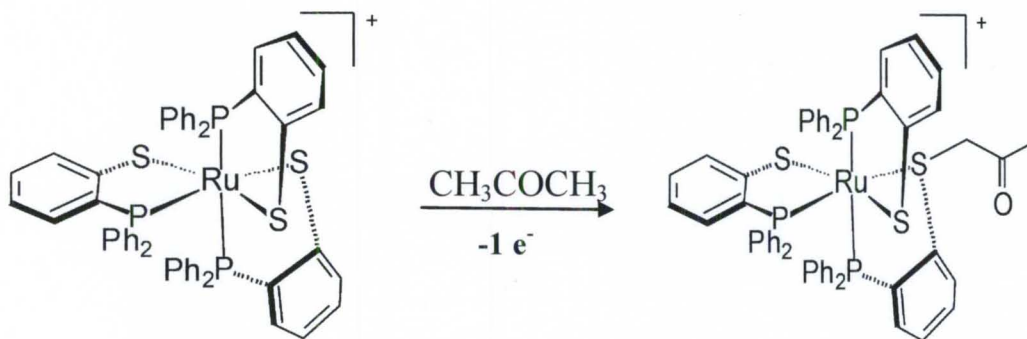


Figure I-1. A qualitative overview of the frontier molecular orbitals shows π interactions between Ru d-orbitals and S p-orbitals in the xz , yz , and xz planes.

From the results of combined spectroscopic and electrochemical investigation along with computational studies, a nearly degenerate electronic ground state was revealed that is best described as a singlet diradical.³⁶⁻³⁹ In acetonitrile and most organic solvents, the radical intermediate slowly decays to form disulfide complex. The diradical

ground state is contributed to delocalize the unpaired electrons over the metal and sulfur donors in nearly orthogonal orbitals. The slow rate of decay was observed at $0.0101(6) \text{ s}^{-1}$ at 273 K.⁴⁰

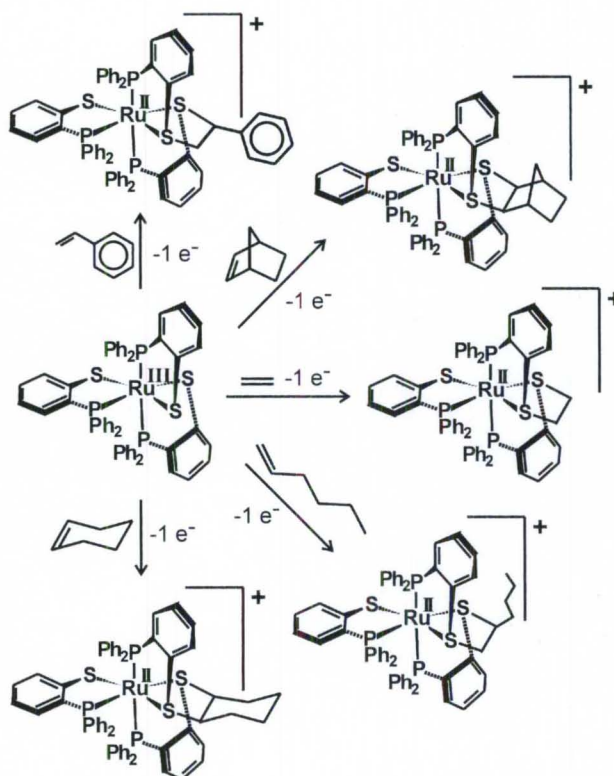
In previous work by Poturovic, the intermediate reacts with methyl ketones to generate new C-S bonds, Scheme I-9.⁴¹ The identity of the product is further characterized by the chemical method in which $[\text{Ru-1}]^+$ is reacted with chloroacetone. Using this approach, single crystals of this monoalkylated product were obtained for X-ray crystallographic studies, which confirmed the proposed structure. In addition other ketones were also investigated using a similar protocol, which identified the similar product for methyl ketones. The reaction is proposed to proceed via the enol tautomer of the ketone as the reactive species.³³



Scheme I-9. The reaction of $[\text{Ru-1}]^+$ with acetone resulted thioether.

These reactions suggested alkenes should also add to the reactive intermediate species. This work was done by Venna who showed a variety of alkenes add across the cis sulfur sites to generate dithioether complexes. The C-S bond formation is also wholly explored in the presence of the various alkenes such as 1-hexene, cyclohexene, styrene, and norbornene, Scheme I-10. However, the kinetic study and chemical synthesis are not

confirmed in detailed previously. Thereafter, the further understanding of these approaches needs to investigate and fully characterize with the various alkenes.



Scheme I-10. $[\text{Ru-1}]^+$ reacts with various alkenes to yield respective Ru (II)-dithioether compounds.

While oxidation of $[\text{Ru-1}]^+$ lead to facile alkene addition, the complexes could not be reduced and C-S bonds could not break.⁴² Report of C-S bond cleavage with ethylene release upon reduction has been reported for the Re (II) complex $[\text{Re}(\text{TTCN})]^{2+}$ (TTCN = 1,4,7-trithiacyclononane) by Went *et al.*⁴³ Density functional theory (DFT) and first-principles molecular dynamics studies have been applied by Rothlisberger to investigate the basis of C-S bond cleavage upon reduction of metal-thioethers. The high energy of the t_{2g} orbitals of Re (I) as compared to Ru (II) is largely responsible for bond

breaking.^{44,45} This investigation of reversible alkene binding is turned our group's attention to the rhenium derivative, **Re-1**.

In my prior thesis work, the focus was directed towards understanding oxidation and reduction induced C-S formation and cleavage, respectively, employing the related rhenium complex $\text{Re}(\text{DPPBT})_3$ **Re-1**. Although **Re-1** and $[\text{Ru-1}]^-$ are isoelectronic addition of ethylene proceeds through the ruthenium, but not the rhenium complex. This may be due to a lower lying excited state of ruthenium that is reactive or a change in orbital ordering between the two metals. In addition to, one oxidation of **Re-1** results in C-S bond formation and gives an expected configuration as $(\text{S}2(\text{p}_x) - \text{S}6(\text{p}_z))^1$, $(\text{dxz} - \text{S}2(\text{p}_x) - \text{S}6(\text{p}_z))^1$, and $(\text{dxz} - \text{S}3(\text{p}_y))^1$. It is proposed that $[\text{Re-1}]^+$ reacts with ethylene as shown in Figure I-2. The filled π^* -orbital of sulfur interacts with LUMO empty p-orbital of C-C double bond (Figure I-2, left) and also vacant orbital of sulfur correlated with higher orbital HOMO of σ -bond alkene (Figure I-2, right).

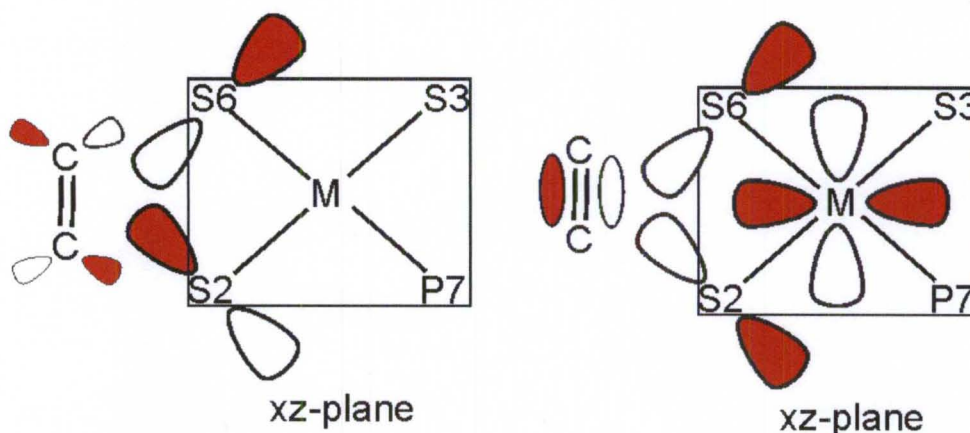
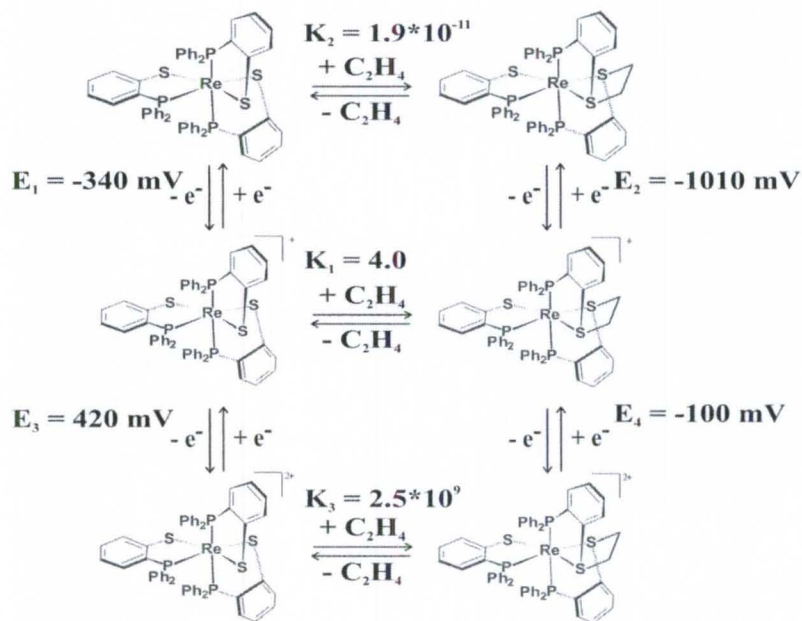


Figure I-2. Views of the xz-planes highlighting interactions between S p-orbitals and C-C bond orbitals.

My work on the reversible C-S bond formation/cleavage between a rhenium-thiolate complex and ethylene was published in 2009. The C-S bond formation/cleavage process can be repeated in multiple times with no remarkable changes in efficiency. The kinetic and equilibrium parameters associated with C-S bond formation/cleavage were extracted from cyclic voltammograms at multiple scan rates using DigiSim software package. From the redox potentials of $[\text{Re-1}]^n$ and $[\text{Re-1}\cdot\text{C}_2\text{H}_4]^n$ and the equilibrium constant of $[\text{Re-1}]^+$ binding ethylene, the thermodynamic boxes were constructed as shown in Scheme I-11. From these studies, we established reversible C-S bond formation/release that is regulated by the oxidation state of the complex with access to “lock on”, “lock off”, or concentration dependent ethylene addition. The rate of ethylene C-S formation/cleavage allows facile trap and release of ethylene over in multiple cycles. We next sought to further study rate constants for the addition of various alkenes to $[\text{Re-1}]^+$ by CV measurements to establish the selectivity of ethylene addition.



Scheme I-11. Thermodynamic squares for $[\text{Re-1}]^n$ and $[\text{Re-1}\cdot\text{C}_2\text{H}_4]^n$ ($n = 0, +1, +2$).

The generated metal-stabilized thiyl radicals react with unsaturated substrates (alkenes, alkynes and dienes) to yield dithioether-metal products or S-alkylated dithiolene-metal products. There are two main chapters which will be focused on the kinetic and reactivity studies. The kinetic study will be employed mono-substituted alkenes to investigate the steric and electronic effect. The results will be reported in Chapter III. Furthermore, the addition of alkynes and dienes to metal-stabilized thiyl radicals will be explored to establish the scope and limits of this reactivity. The results will be presented in Chapter IV.

CHAPTER II

EXPERIMENTAL METHODS

Material and Physical Methods

All chemicals were purchased from commercial sources (Aldrich, VWR Chemicals, TCI, Acros Organic, Alfa Aesar, and Strem Chemicals) and used without further purification unless otherwise stated. All solvents were purified utilizing standard methods and were freshly distilled and degassed using the freeze-pump-thaw method immediately before use.⁴⁶ Ferrocenium hexafluorophosphate (FcPF₆) was obtained from Aldrich and was recrystallized according to published protocols prior to use and stored in an argon filled dry box.⁴⁷ The ligand H(DPPBT) (2-diphenylphosphinobenzenethiolate) was synthesized as previously described in the literature.⁴⁸ The [Ru(DPPBT)₃]⁻ thiolate complex **PPN[Ru-1]**⁴⁰ (PPN = bis(triphenylphosphoranylidene)ammonium) and **HNEt₃[Ru-1]**³¹ and the Re(DPPBT)₃ thiolate complex **Re-1**⁴⁹ were synthesized according to established literature methods. Deuterated acetonitrile was obtained from Cambridge Isotope Laboratories, Inc. and used as received. All reactions were performed under anaerobic condition via standard Schlenk-line techniques unless otherwise noted. IR spectra were measured with a Thermo Nicolet Avatar 360 spectrometer with a resolution of 4 cm⁻¹. An Agilent 8453 diode array spectrometer was used for all

electronic absorption measurements utilizing a custom designed quartz cell. NMR spectra were recorded on a Varian 400 MHz spectrometer and referenced to TMS (^1H NMR) or 85% phosphoric acid (^{31}P NMR). Element analyses were performed by the Midwest Microlab (Indianapolis, IN). Electrospray ionization mass spectra (ESI-MS) were obtained from the Mass Spectrometry Application and Collaboration Facility in the Chemistry Department at Texas A&M University. X-ray crystallographic analyses were conducted by Dr. Mark Mashuta at the University of Louisville's X-ray diffraction laboratory. X-ray crystallographic data were collected on a Bruker SMART APEX CCD. All published X-ray structural data has been deposited in the Cambridge Crystallographic Deposit Centre (CCDC). A summary of data collection and refinement methods are provided in the Appendix G along with the CCDC deposit number and atomic coordinates. Unpublished X-ray structural data is fully described in the Appendix G.

Electrochemical Methods

All electrochemical measurements were performed by using a PAR 273 potentiostat/galvanostat with a three-electrode cell (glassy carbon working electrode, platinum wire counter electrode, and Ag/Ag^+ pseudo reference electrode (used in rate constant study) or Ag/AgCl reference electrode (used in reactivity study). Potentials are reported versus ferrocenium/ferrocene (Fc^+/Fc), which was measured as an internal reference for each sample.

Cyclic Voltammetry (CV)

Cyclic voltammetry is a simple technique and the choice to determine precise kinetic data for our system. Cyclic voltammetry is a type of linear sweep voltammetry

which involves sweeping the electrode potential between potential limits E_{initial} and E_{final} at sweep rate of v . The scan direction can then be switched E_{final} and the potential returned to E_{initial} . The technique uses a triangular potential waveform that can be repeated over multiple cycles as shown in Figure II-1a. A typical current response for a reduction event over one cycle is shown in Figure II-1b. When the electrode potential reaches the vicinity of the analyte standard reduction potential, $E^{0'}$, a cathodic current is recorded with increasing intensity. During this initial period the current follows Nernstian behavior as sufficient analyte is near the electrode. However, as the potential continues to grow more negative, the concentration of the analyte drops and the current becomes dependent on the mass transfer of analyte to the electrode surface. The cathodic current is at a maximum when this transition occurs. The direction of the potential sweep is switched at time t_2 . As the potential approaches $E^{0'}$ in the anodic direction, the reduced species becomes oxidized according to the Nernst equation. The anodic current increases while the potential becomes more positive. Once the reduced complex near the electrode is consumed, the anodic current reaches a minimum and the system is mass transfer limited. The cycle can be repeated as noted by the potentials at t_3 and t_4 . The advantage of cyclic voltammetry is a reversal technique and is the potential-scan equivalent of double potential step chronoamperometry.

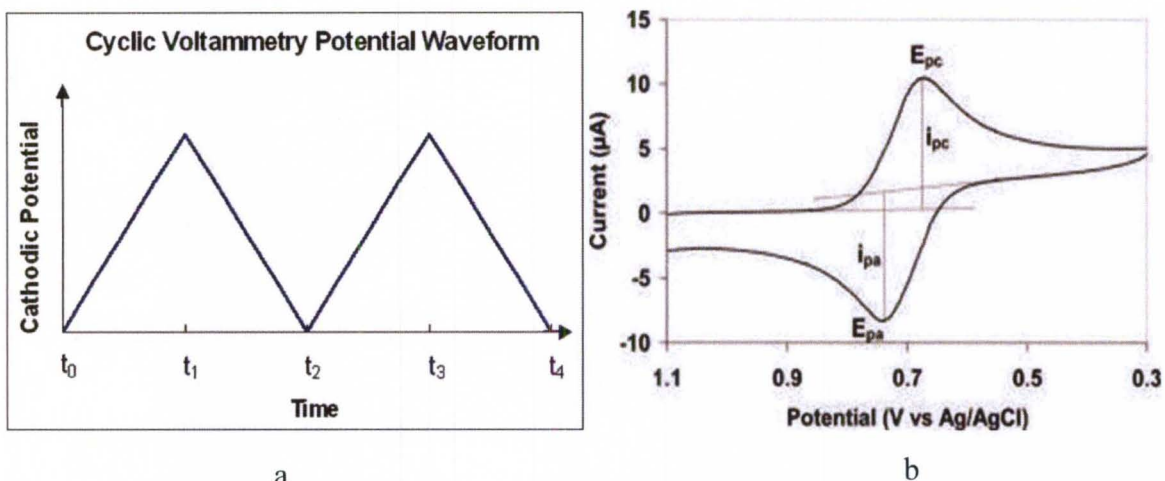


Figure II-1. Cyclic voltammetry. (a) A cyclic voltammetry potential waveform with switching potentials. (b) The expected response of a reversible redox couple during a single potential cycle.

In a cyclic voltammetry experiment, the potential is scanned from an initial value to a switching point, after which the potential is scanned back to the original value.^{50,51} In this way, cyclic voltammetry probes both the oxidation (anodic) and reduction (cathodic) events associated with a redox couple, so that the reversibility of the redox events can be determined. A reversible cyclic voltammogram is observed if the oxidation and reduction species are stable and the kinetics of electron transfer processes are fast and independent of the potential scan rate. Also, the electron transfer on the electrode surface is in Nernstian equilibrium; that is, diffusion limit with electrochemical events to species at the electrodes' surface. The current peak (i_p) is proportional to the concentration of reactant species (C_0), the square root of scan rate ($v^{1/2}$), and the diffusion coefficient (D_0). Therefore, the peak potentials (E_p) for both oxidation and reduction are independent of scan rates. In addition, the value of the peak separation, $\Delta E_p = E_{pa} - E_{pc} = 59/n$ when $n =$ number of electrons, a = anode, and c = cathode, indicates the electrochemically

reversible event. That is, for a single-electron transfer, $\Delta E_p = 59 \text{ mV}$; for two-electron transfer, $\Delta E_p = 29.5 \text{ mV}$. The peak shapes are generally superimposable for all scan rates. For reversible events, voltammograms for experiments with different scan rates are generally identical (that is, superimposable). The half potential ($E_{1/2}$) is calculated from the average of cathodic and anodic potentials.

In some cases, the electron transfer is quasireversible or irreversible. In the first instance, the rate of electron transfer (k_s) is inadequate to maintain equilibrium; this changes the shape of the cyclic voltammogram. Consequently, $E_{1/2}$ varies with scan rate. In contrast with the reversible system, the peak current is proportional to the electron transfer coefficient (α). The i_p is reached at lower values than those in a reversible system. The ΔE_p increases with an increased in scan rate and the peak observed eventually disappears.

A totally electrochemically irreversible process (E) is also a common observation. The irreversibility of the reduction shows up in the difference between the forward and reverse scans. In this case, the cathodic potential or anodic potential is reported, not the average $E_{1/2}$. Sometimes, the difference between the forward and reversed scan is not due to an irreversible electron transfer event but the fast process of the chemical step (C) known as the chemically irreversible event.^{50,51}

The electrochemically quasireversible event is identified for the value of k_s and the observed current due to slow Nernstian equilibrium at the surface of the electrode. In general, the experimental value of k_s can be as high as 1 cm/s . In general, ΔE_p increases in a quasireversible system. ΔE_p is greater than $59/n \text{ mV}$ as described in the reversible system above. However, neither reversible nor irreversible events account for

uncompensated resistance (R_u) which depends upon measuring R_u . The effect of iR_u drop is consistent and undistinguishable from slow kinetic study due to ΔE_p increasing with scan rate (v). For the increase in ΔE_p is slow electron transfer, that is, high R_u has the effect similar to a quasireversible electrochemical event.

For cyclic voltammetry experiments, a Dr. Bob's cell was used as a three-electrode cell with a 6.5 mm diameter glassy carbon working electrode (area = 0.071 cm²), a platinum wire counter electrode, and an Ag/Ag⁺ pseudo or an Ag/AgCl reference electrode, the first was utilized for the determination of rate constants and the second for the measurement of reactivity and routine analysis. The Dr. Bob's cell kit was purchased from Gamry Instruments, Warminster, PA, USA. The Dr. Bob's cell can be used with solvent volumes from 2.0 mL to 50 mL and actual volume was determined for each experiment as described.

Prior to the addition of analyte, a background voltammogram was collected using 5.0 mL (rate constants study, routine analysis) or 3.0 mL (reactivity study) of dry, degassed acetonitrile with 0.1 M tetrabutylammonium hexafluorophosphate (TBAHFP) as the supporting electrolyte. Nitrogen gas was bubbled through to the solution for 5 minutes to remove dissolved oxygen, and then the solution was allowed to settle for 2 minutes without disturbance under a nitrogen gas atmosphere. The initial, switching and final potentials were set between the solvent limits of -1.5 V to 1.5 V versus the reference at scan rate of 200 mV/s.

CV Simulation Parameters

A cyclic voltammogram of the analyte was obtained in a smaller potential window at scan rate of 200 mV/s. Prior to scanning; the solution was purged with

nitrogen for several minutes and then held under a nitrogen atmosphere during analysis. The voltammograms for analyte solutions, including the complex of interest and the unsaturated hydrocarbon (0.2 M), were collected at multiple scan rates of 100, 200, 400, 600, 800, and 1000 mV/s with a larger potential window. Three independent samples were analyzed.

For each set of data, the CV results over all scan rates were fit simultaneously using the DigiSim software package (Bioanalytical Systems).⁵² Prior to data analysis, the potential was adjusted to the Fc^+/Fc standard (0.00 V). Preliminary investigations with the glassy carbon working electrode and the Ag/Ag^+ reference electrode proved the background signal to be small and negligible. Its subtraction from the measured sample data did not significantly alter the simulation results and the practice was discontinued. All data were input into a text data file format. These data files were converted to the **.use** format as described in DigiSim the instruction manual.⁵³ Critical parameters in the CV simulation which determine the peak current response are described in more detailed below:

$$i_p = FAD_0^{1/2}C_0^*f^{1/2}\nu^{1/2}\Psi(E)$$

i_p = peak current

F = Faraday's constant

A = area of electrode

D_0 = diffusion coefficient

C_0^* = initial concentration

$f = F/RT$

ν = scan rate

$\Psi(E) = k_s/(\pi D_0 f \nu)^{1/2}$

Uncompensated resistance was estimated using the iR measurements technique within potentiostat software (IR measurement technique). The resistance of the solution

between the reference and the working electrode combines with the cell current to produce an iR_u drop that prevents the working electrode from being at the programmed potential. To estimate the uncompensated resistance, a measurement was taken at a potential where no redox processes occur and a current applied at a value that attended the maximum amount of current that would be measured in the experiment. Moreover, IR mode was switched to “measured” command

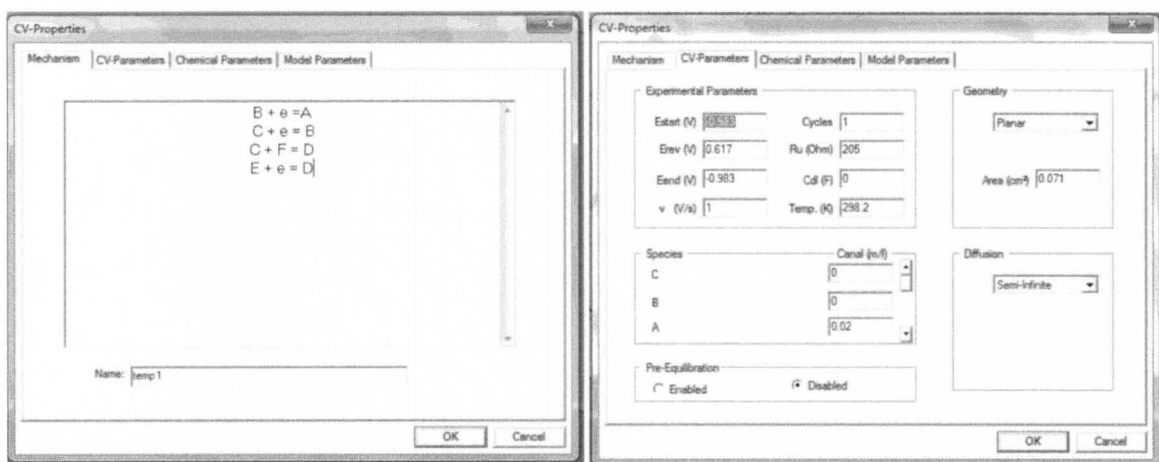
The diffusion coefficient (D_0) was treated as a variable parameter with an initial setting of 10^{-6} cm²/s. The electron transfer rate constant (k_s) was treated as a variable parameter with initial values estimated from equations (1) and (2). Note that the simulation improves the value of k_s through comparison of ΔE_p at different scan rates.

$$k_s = \Psi * a \quad (1)$$

$$a = (\pi D_0 f v)^{1/2} \quad (2)$$

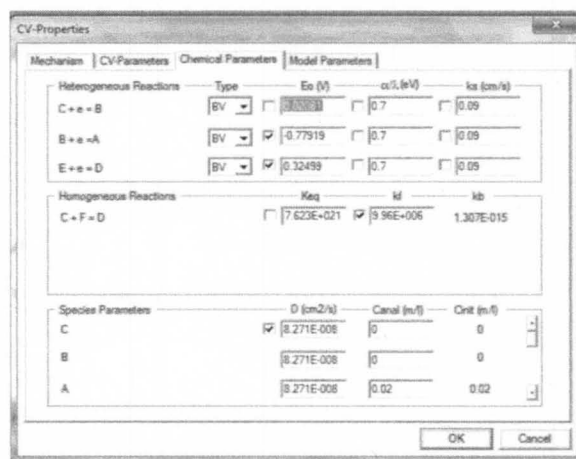
The transfer coefficient, α , a simulation parameter which defines peak shape and current was set to 0.7.^{50,54} The initial value of simulation's standard-half potential parameter was estimated from the potentials of minimum and maximum. The data was fit according to a mechanism with redox events and a chemical step associated with the equilibrium constant, K , rate constant, k_f , and k_r .

All fitting parameters were refined simultaneously over all scan rates and reported values are the average of three independently prepared samples. All simulation screens are shown in Figure II-2.



a

b



c

Figure II-2. Simulation screens in DigiSim program, (a) mechanism dialog box, (b) CV-parameters dialog box, and (c) chemical parameters dialog box for fitting routine.

Square Wave Voltammetry

Square wave voltammetry is a derivative of step-sweep voltammetry in which the potential scan begins at the initial potential and ends at the final potential. In square wave voltammetry, series of forward and reverse pulses of current are superimposed on a linear scan of potential. The potential wave form consists of a square wave of constant amplitude superimposed on a staircase wave form, Figure II-3a. The current is measured

at the end of each half cycle. The current measured on the reversed half-cycle (i_r) is subtracted from the current measured on the forward half-cycle (i_f), Figure II-3b (dotted line). This difference current ($i_f - i_r$) is displayed as a function of the applied potential, Figure II-3b (dark lines). For a cathodic scan, $E_{\text{initial}} > E_{\text{final}}$, the difference current is positive. For an anodic scan, $E_{\text{initial}} < E_{\text{final}}$, the difference current is negative. The subtraction of the reverse current from the forward current results in a flat baseline with clearly identifiable peaks corresponding to the electroactive species. The difference current maximum (or minimum) occurs exactly at the standard reduction potential of the analyte, $E_{1/2}$. The peak height directly provides the concentration for these species. The advantage of this technique is providing high resolution with the elimination of background noise present in a fast scan. Square wave voltammetry is an excellent preliminary experiment to evaluate a system because it requires low concentration and can be performed quickly.

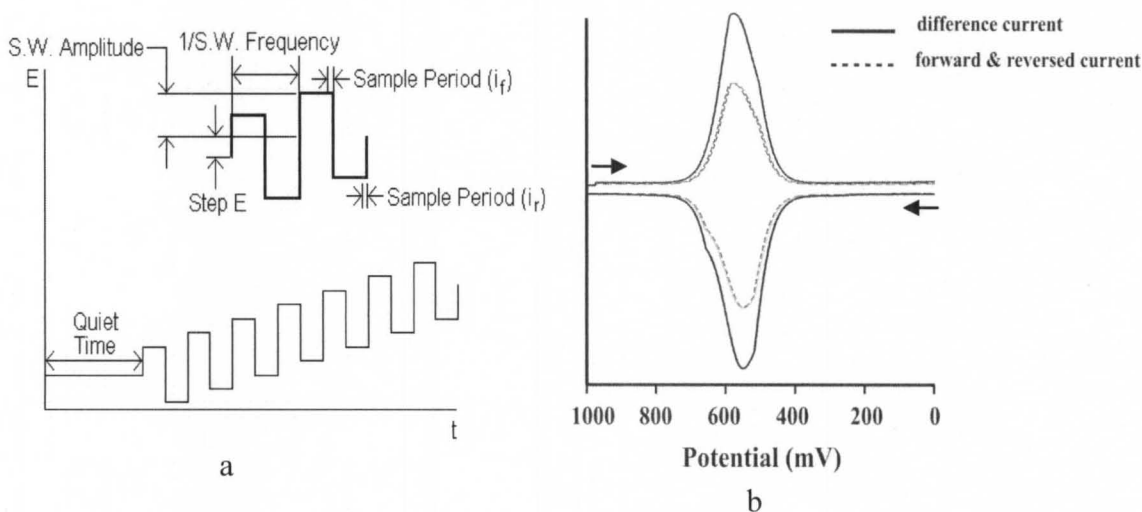


Figure II-3. Square wave voltammetry. (a) Potential wave form for square wave voltammetry. (b) Square wave voltammograms.

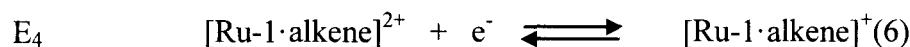
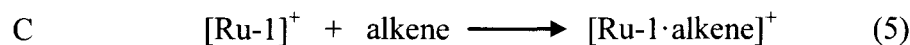
Square wave measurements were obtained using a glassy carbon working electrode, a platinum wire counter electrode, and an Ag/AgCl reference electrode. The initiation of the scan starts without a holding time. Data was collected in the cathodic and anodic direction for all samples. The cathodic scan (reduction) was obtained from a range of -0.6 V to 1.1 V and anodic scan (oxidation) was scanned in reverse. The resulting peaks were plotted as current versus potential.

Routine Electrochemical Measurements

For routine characterization, cyclic voltammograms and square wave voltammograms were conducted at room temperature using the Dr. Bob cell described previously. The cell was filled with 3.0 mL freshly distilled acetonitrile containing TBAHFP (0.1 M) as supporting electrolyte. The analyte concentration was 1.0 mM. Cyclic voltammetry data were recorded at various scan rates from 100 to 1000 mV/s. For square wave measurements, data was collected in both the anodic and cathodic directions. The potentials were recorded versus a ferrocenium/ ferrocene reference.

Kinetic Study to Determine Rate Constants

For experiments to determine chemical rate constants for alkene addition, the same cell noted above was used with an Ag/Ag⁺ pseudo-reference employed as reference electrode. The analyte concentration was increased to 2.0 mM in 5.0 mL acetonitrile. The concentration of alkene was 0.2 M. voltammograms were obtained at Multiple scan rates and the data were fit based on an EECE mechanism (E = electrochemical step, C = chemical step) as shown in equations 3 to 6. As convention, all electrochemical processes are written as reduction.



After each experiment, uncompensated resistance was estimated using the iR compensation method from the potentiostat instrument as mentioned earlier. The average value of R_u was used for the simulation parameters input. The diffusion coefficient was defined as a variable parameter with an initial setting value of $10^{-6} \text{ cm}^2/\text{s}$. The standard rate constant for electron transfer between the electrode and solutes (k_s) and the electron transfer coefficient (α/λ) were set to 0.08 cm/s and 0.7, respectively, as determined in earlier work.⁵⁵ The standard-half potential E_1 was set to -770 mV and allowed to refine freely. The half-potential (E_2) was not allowed to vary., the E_2 half potential was fixed at a position equal to $E_1 + 800 \text{ mV}$ based on reported separation of these two redox events.⁴⁰ A single irreversible chemical step is assumed with the equilibrium constant, K , set to an initial large value ($>10^{10} \text{ M}^{-1}$) to affect the irreversible step. The forward rate constant (k_f) for this step was allowed to vary. The standard half potential, E_4 , was based on the observed value and allow varying slightly. The chemical step (C) was fit as an irreversible process. All fitting parameters were defined simultaneously over all scan rates for a given alkene and observed values are of the average of three independently prepared samples.

Reactivity Study to Determined Rate Constants

All measurements were similar to those in the previous setup except an Ag/AgCl was used as the reference electrode. The voltammogram of analyte (2.0 mM) in 3.0 mL

acetonitrile was scanned, and then data were collected in the presence of alkynes, dienes, and substituent alkenes at 0.2 M concentration. The data over all scan rates were fit based on an ECEE mechanism. Parameters used in the simulation were freely defined and constrained based on the results of the simulation. The average value of uncompensated resistance was obtained as $R_u = 187 \Omega$. The standard electron transfer rate constant and the electron transfer coefficient were set at 0.09 cm/s and 0.7, respectively. E_1 , E_2 , and K were set as mentioned previously. The diffusion coefficient (D_0), k_f , and E_4 were allowed to define freely for fitting process.

Chapter III

Kinetic Study

Electrochemical measurement was performed for substituted styrenes and all data are summarized in Table H-2, Table H-3 and Table H-4, Appendix H. The data for alkenes are reported in Table H-5, Appendix H.

Electrochemical investigation of Re-1 in the presence of styrene: The electrochemical cell was filled with 10 mL of dichloromethane and 0.387 g (0.1 M) TBAHFP was added to record the backgrounds for cyclic voltammetry. Then 10.7 mg (0.01 mmol) of **Re-1** was added resulting in a burgundy colored solution. Nitrogen was bubbled through the solution to ensure proper mixing followed by adding 2.29 mL (19.9 mmole) of styrene. The cyclic voltammograms were collected in multiple scan rates from 100 mV/s to 1000 mV/s. The observed voltammograms in small window were not changed as compared to the original events. The event was shown at -329 mV.

Kinetic study of [Re-1]⁺ in the presence of styrene through room temperature UV-visible spectroscopy: In drybox, 0.9 mg (0.8 μ mol) of **Re-1** in 5 mL chlorobenzene was

prepared in UV-visible cell resulting a burgundy solution. Then 2 equivalents of AgPF_6 (1 mg, 1.6 μmol) was added to the burgundy solution while shaking, a blue color appeared corresponding to $[\text{Re-1}]^+$. Before the kinetic measurement performed, 4 mL of chlorobenzene as a blank solution was run. Then the blue solution cell was replaced in the UV-visible chamber. Settings up kinetic parameters were described as shown below.

Wavelength	WL1 = 390 nm
	WL2 = 581 nm
Y scaling from	0 to 2.5
Run time	300000 seconds
Cycle time	120 seconds
Increment cycle time	10%
Start after	120 seconds

Then styrene (0.5 μL) was added via microsyringe through the reaction solution. After 3 days, the solution was changed color to an orange. Based on the pseudo first order rate law, the rate constant was obtained $(4.9 \pm 2) \times 10^{-5} \text{ M}^{-1} \text{ s}^{-1}$. Three trials were analyzed and data was demonstrated on Table II-1.

Table II-1. Rate constant (k_f) data for $[\text{Re-1}]^+$ in presence of styrene in 4 mL of dry degassed chlorobenzene.

Styrene	Wavelength (nm)		
	390	581	693
Trial 1	$(2.0 \pm 2) \times 10^{-4}$	$(4.9 \pm 4) \times 10^{-4}$	$(5.2 \pm 3) \times 10^{-4}$
Trial 2	$(6.7 \pm 2) \times 10^{-5}$	$(2.0 \pm 2) \times 10^{-4}$	$(1.6 \pm 2) \times 10^{-4}$
Trial 3	$(6.1 \pm 1) \times 10^{-5}$	$(2.0 \pm 1) \times 10^{-4}$	$(2.0 \pm 1) \times 10^{-4}$
Average	10.9×10^{-5}	3.0×10^{-4}	2.9×10^{-4}

Electrochemical investigation of PPN[Ru-1] in the presence of styrene: The electrochemical cell was purged with nitrogen gas for 30 minutes to avoid dissolved oxygen. 5.0 mL of acetonitrile and 0.194 g (0.5 mmol) of TBAHFP was added via syringe to record the background for cyclic voltammetry. Then 0.015 g (0.01 mmol) of PPN[Ru-1] was dissolved in the schlenk flask with supporting electrolyte resulting in an orange-colored solution under nitrogen atmosphere. The solution was transferred to the cell and nitrogen gas allowed to bubble through the solution to deoxygenate. Two oxidation redox events were obtained at scan rate of 200 mV/s. Using a syringe, 0.115 mL (43.6 mmol) of styrene was added and the solution was purged with nitrogen to ensure proper mixing for 2 minutes. The resulting events appeared at -830 mV, -117 mV, and +276 mV. After all scans were recorded, IR compensation data were collected three times. The average value of uncompensated resistance (R_u) was 200 Ω .

Electrochemical investigation of PPN[Ru-1] in the presence of *p*-chlorostyrene: All measurements were performed as for styrene. With the addition of 0.120 mL (41.7 mmol) *p*-chlorostyrene, the voltammograms were obtained at -830 mV, -112 mV, and +286 mV and $R_u = 188 \Omega$.

Electrochemical investigation of PPN[Ru-1] in the presence of *p*-fluorostyrene: The three redox events in the presence of 0.119 mL (41.9 mmol) *p*-fluorostyrene were recorded at -830 mV, -101 mV, and +281 mV and $R_u = 210 \Omega$.

Electrochemical investigation of PPN[Ru-1] in the presence of *p*-methylstyrene: The three redox events in the 0.132 mL (37.9 mmol) *p*-methylstyrene solution were observed at -830 mV, -109 mV, and +275 mV. $R_u = 267 \Omega$.

Electrochemical investigation of PPN[Ru-1] in the presence of *p*-methoxystyrene:

The three redox events with the addition of 0.133 mL (37.6 mmol) *p*-methoxystyrene were determined at -830 mV, -174 mV, and +213 mV and $R_u = 255 \Omega$.

Electrochemical investigation of PPN[Ru-1] in the presence of *m*-chlorostyrene:

The voltammograms in the presence of 0.127 mL (39.3 mmol) *m*-chlorostyrene were recorded at -830 mV, -82 mV, and +286 mV and $R_u = 225 \Omega$.

Electrochemical investigation of PPN[Ru-1] in the presence of *m*-fluorostyrene:

The voltammograms with the addition of 0.119 mL (41.9 mmol) *m*-fluorostyrene were obtained at -830 mV, -103 mV, and +283 mV and $R_u = 222 \Omega$.

Electrochemical investigation of PPN[Ru-1] in the presence of *m*-methylstyrene:

The voltammograms with the addition of 0.133 mL (37.7 mmol) *m*-methylstyrene were measured at -830 mV, -115 mV, and +274 mV and $R_u = 222 \Omega$.

Electrochemical investigation of PPN[Ru-1] in the presence of *m*-methoxystyrene:

The voltammograms with the addition of 0.139 mL (36.0 mmol) *m*-methoxystyrene were defined at -830 mV, -111 mV, and +271 mV and $R_u = 210 \Omega$.

Electrochemical investigation of PPN[Ru-1] in the presence of *o*-fluorostyrene:

The voltammograms with the addition of 0.119 mL (23.8 mmol) *o*-fluorostyrene were obtained at -830 mV, -126 mV, and +278 mV and $R_u = 200 \Omega$.

Electrochemical investigation of PPN[Ru-1] in the presence of *o*-methylstyrene:

The voltammograms with the addition of 0.129 mL (25.9 mmol) *o*-methylstyrene were measured at -830 mV, -128 mV, and +255 mV and $R_u = 202 \Omega$.

Electrochemical investigation of PPN[Ru-1] in the presence of *o*-methoxystyrene:

The voltammograms with the addition of 0.134 mL (26.9 mmol) *o*-methoxystyrene were defined at -830 mV, -124 mV, and +269 mV and $R_u = 234 \Omega$.

Electrochemical investigation of PPN[Ru-1] in the presence of *n*-propyl vinyl ether:

All measurements were performed as described in presence of styrene. The orange solution of PPN[Ru-1] (0.0152g, 0.01 mmol) in 5 mL of acetonitrile containing 0.194 g (0.5 mmol) TBAHFP was measured. Then 0.112 mL (1 mmol) of *n*-propyl vinyl ether was added and the solution was mixed by purging nitrogen for 2 minutes. The cyclic voltammograms were observed at -830 mV, -113 mV, and +270 mV. $R_u = 182 \Omega$.

Electrochemical investigation of PPN[Ru-1] in the presence of *tert*-butyl vinyl ether:

The cyclic voltammograms of PPN [Ru-1] solution in the presence of *tert*-butyl vinyl ether (0.131 mL, 1 mmol) was collected under nitrogen atmosphere. The events were revealed at -830 mV, -87 mV, and +273 mV and $R_u = 196 \Omega$.

Electrochemical investigation of PPN[Ru-1] in the presence of 1-hexene: Follow the same process as stated previously except 1-hexene (0.125 mL, 1 mmol) was used for measurement. The voltammograms were obtained at -830 mV, -65 mV, and +263 mV and $R_u = 179 \Omega$.

Electrochemical investigation of PPN[Ru-1] in the presence of acrylonitrile: The cyclic voltammograms were collected in an orange solution of PPN[Ru-1] in the presence of 0.066 mL (1 mmol) acrylonitrile resulting the standard half potentials at -830mV, -71 mV, and +347 mV and $R_u = 210 \Omega$.

Electrochemical investigation of PPN[Ru-1] in the presence of cyclohexene: To a solution of PPN[Ru-1], 0.101 mL of cyclohexene (1 mmol) was added and nitrogen

purging was completed for 2 minutes. The events were determined at -830 mV, -12 mV, and +238 mV and $R_u = 185 \Omega$.

Electrochemical investigation of PPN[Ru-1] in the presence of cyclopentene: 0.088 mL of cyclopentene (1 mmol) was mixed in an orange solution of **PPN[Ru-1]** under nitrogen atmosphere. The redox events were recorded at -830 mV, -73 mV, and +260 mV and $R_u = 171 \Omega$.

Electrochemical investigation of PPN[Ru-1] in the presence of norbornene: The mixing solution of **PPN[Ru-1]** containing 0.094 g of norbornene (1 mmol) was collected the cyclic voltammograms which observed three redox peaks at -830 mV, -113 mV, and +285 mV and $R_u = 179 \Omega$.

Chapter IV

Reactivity Study

Electrochemical measurement of PPN[Ru-1] in presence of *cis*-stilbene: Initially, acetonitrile (5 mL) was mixed with 0.194 g (0.5 mmol) of TBAHFP as electrolyte and degassed via nitrogen bubbling. A blank solution was measured via cyclic voltammetry at a scan rate, 200 mV/s. Then 0.0152 g of **PPN[Ru-1]** (0.01 mmol) was added, resulting an orange-colored solution in the Schlenk flask and transferred to an electrochemical cell via syringe. The cell was purged with nitrogen gas was purged for 2 minutes to deoxygenate the solution before run the CV. The scan rate of 200 mV/s was used to collect the CV of analyte and also square wave voltammogram was obtained for both oxidation and reduction. An aliquot of 0.0178 mL of *cis*-stilbene was added. The resulting redox events were shown at -830 mV, -32 mV, and 314 mV and the cyclic voltammograms collected at multiple scan rates 100, 200, 400, 600, 800, and 1000 mV/s for rate constant

investigations. The square wave voltammograms revealed events at -830 mV, -79 mV, and 310 mV.

Electrochemical measurement of PPN[Ru-1] in presence of *trans*-stilbene: All measurements were performed as mentioned in presence of *cis*-stilbene. Next, an amount of *trans*-stilbene (0.0901 g) was added and mixed via nitrogen bubbling through the solution. The three events were obtained at -830 mV, 19 mV, and 307 mV. The square wave peaks were resulted at -830 mV, -23 mV, and 307 mV.

Electrochemical measurement of PPN[Ru-1] in presence of 2-methyl-2-butene: In the presence of 2-methyl-2-butene (0.106 mL), the cyclic voltammograms displayed redox couples at -830 mV, -31 mV, and 238 mV. The square wave displayed three redox peaks at -830 mV, -65 mV, and 232 mV.

Electrochemical measurement of PPN[Ru-1] in presence of 2,3-dimethyl-2-butene: The 2,3-dimethyl-2-butene (0.119 mL) was dissolved in the orange solution of PPN[Ru-1] yielding the half potentials at -830 mV, -44 mV and 226 mV. The square wave events were determined at -830 mV, -43 mV, and 226 mV.

Electrochemical measurement of PPN[Ru-1] in presence of 1-octyne: The redox events were collected in the presence of (0.148 mL) 1-octyne yielding at -830 mV, -60 mV, and 302 mV. The square wave events were obtained at -830 mV, -98 mV, and 249 mV.

Electrochemical measurement of PPN[Ru-1] in presence of phenyl acetylene: 0.110 mL of phenyl acetylene was added to the orange solution of PPN[Ru-1] then the voltammograms were performed. The cyclic voltammograms were revealed at -830 mV, -61 mV, and 311 mV. The wave events were shown at -830 mV, -94 mV, and 310 mV.

Electrochemical measurement of PPN[Ru-1] in presence of 1-phenyl-1-propyne: The PPN[Ru-1] solution was mixed with 1-phenyl-1-propyne (0.125 mL). Then the cyclic voltammograms recorded events at -830 mV, -25 mV, and 304 mV. The square wave events were appeared at -830 mV, -57 mV, and 309 mV.

Electrochemical measurement of PPN[Ru-1] in presence of 1,3-butadiene: The mixing solution of PPN[Ru-1] and 1,3-butadiene (0.0671 mL) was performed the voltammograms. The redox events were revealed at -830 mV, -101 mV, 271 mV and the wave events showed at -830 mV, -173 mV, and 267 mV.

Electrochemical measurement of PPN[Ru-1] in presence of 2,3-dimethyl-1,3-butadiene: The cyclic voltammograms of PPN[Ru-1] in the presence of 2,3-dimethyl-1,3-butadiene (0.113 mL) were observed at -830 mV, -25mV, and 267 mV. Moreover, the square wave events were determined at -830 mV, -80 mV, and 265 mV.

Electrochemical measurement of PPN[Ru-1] in presence of dipentene: The voltammograms were measured in PPN [Ru-1] solution and dipentene (0.160 mL) yielding the redox potentials at -830 mV, -65 mV, and 269 mV. The square wave obtained events at -830 mV, -119 mV, and 268 mV.

Chemical Synthesis

Chemical synthesis of $\{[(1\text{-ethylbenzene-1,2-diylbis(thio-2,1-phenylene)diphenylphosphine)](2\text{-diphenylphosphinobenzene-thiolato})\text{rhenium(III) hexafluorophosphate [Re-1-styrene]}][\text{PF}_6]_2$: To a burgundy solution of Re-1 (20 mg, 0.019 mmol) in chlorobenzene (5 mL) was added AgPF_6 (9.5 mg, 0.038 mmol). The resulting solution was added with styrene (2.17 mL, 19 mmol) during which a purple color developed. Then allow stirring over 2 days for completing reaction yielding an

orange color. The mixture filtered through wool cotton to remove Ag (s). The solvent was removed via vacuum. The cyclic voltammetry showed event at -101 mV consistent with **[Re-1·styrene]^{2+/+}**.

Chemical synthesis of {{{(1-ethyl-3-methylbenzene-1,2-diylbis(thio-2,1-phenylene)diphenylphosphine)}(2-diphenylphosphinobenzene-thiolato)ruthenium(II)} hexafluorophosphate [Ru-1·*m*-methylstyrene][PF₆]: To a yellow solution of HNEt₃[Ru-1] (100 mg, 0.0935 mmol) in dry, degassed acetonitrile (40 mL) was added *m*-methylstyrene (0.0621 mL, 0.468 mmol) via syringe. The solution was cooled in an ice bath and a blue solution of FcPF₆ (0.0619 g, 0.187 mmol) in acetonitrile (30 mL) was added by cannula transfer. The resulting solution was stirred for 3 hours during which time a yellow green color developed. The solvent was removed by rotary evaporation to yield a yellow residue. The crude product was washed with an excess of hot water (~300 mL) and diethyl ether (25 mL) and dried in vacuo. Yield: 0.090 g (82 %). The crude product (30 mg) was dissolved with a mixture of dichloromethane (1 mL) and hexane (1 mL). Slow evaporation of the solvent results yellow X-ray quality crystals. $E_{1/2}(\text{Ru}^{\text{III}}/\text{Ru}^{\text{II}}) = +224 \text{ mV}$. +ESI-MS for C₆₃H₅₂P₃S₃Ru: theoretical *m/z* (*Z* = 1), 1099.15; observed, 1099.20. Element analysis for C₆₃H₅₂P₄S₃F₆Ru: calculated C, 61.34; H, 4.44, found: C, 61.50; H, 4.73. ³¹P NMR of **[Ru-1·*m*-methylstyrene]⁺** as isolated in CD₃CN shows a pair of second-order spectra assigned to a pair of structural isomers. The major component (65%) displays chemical shift (ppm) of $\delta_1 = 59.3$, $\delta_2 = 39.1$, $\delta_3 = 35.2$ and coupling constants (Hz) of $J_{12} = J_{13} = 30$ and $J_{23} = 300$. The minor component (35%) displays $\delta_1 = 54.8$, $\delta_2 = 44.3$, $\delta_3 = 35.9$ and $J_{12} = J_{13} = 32$ and $J_{23} = 318$ Hz.

Chemical synthesis of $\{[(1\text{-ethyl-4-methylbenzene-1,2-diylbis(thio-2,1-phenylene)diphenylphosphine)](2\text{-diphenylphosphinobenzene-thiolato)ruthenium(II)}\}$ hexafluorophosphate $[\text{Ru-1}\cdot p\text{-methylstyrene}][\text{PF}_6]$: To a 40 mL solution of $\text{HNEt}_3[\text{Ru-1}]$ (100 mg, 0.0935 mmol) in acetonitrile which cooled in an ice bath was added *p*-methylstyrene (0.0618 mL, 0.468 mmol). Upon complete mixture solution, a blue solution of FcPF_6 (0.0619 g, 0.187 mmol) in 30 mL acetonitrile was added. After vigorous stirring for 3 hours, a yellow green color solution appeared. The solvent was evaporated. The residue was washed with 3×100 mL hot water and 3×25 mL diethyl ether. Yield: 0.088 g (80 %). Recrystallization from slow evaporation of the mixture of dichloromethane and hexane afforded yellow X-ray quality crystals. $E_{1/2}(\text{Ru}^{\text{III}}/\text{Ru}^{\text{II}}) = +284$ mV. +ESI-MS for $\text{C}_{63}\text{H}_{52}\text{P}_3\text{S}_3\text{Ru}$: theoretical m/z ($Z = 1$), 1099.15; observed, 1099.20. Element analysis for $\text{C}_{63}\text{H}_{52}\text{P}_4\text{S}_3\text{F}_6\text{Ru}$: calculated C, 61.35; H, 4.44, found: C, 60.99; H, 4.73. ^{31}P NMR of $[\text{Ru-1}\cdot p\text{-methylstyrene}]^+$ as isolated in CD_3CN shows a pair of second-order spectra assigned to a pair of structural isomers. The major component (65%) displays chemical shift (ppm) of $\delta_1 = 59.2$, $\delta_2 = 39.2$, $\delta_3 = 35.1$ and coupling constants (Hz) of $J_{12} = J_{13} = 30$ and $J_{23} = 300$. The minor component (35%) displays $\delta_1 = 54.7$, $\delta_2 = 44.4$, $\delta_3 = 35.9$ and $J_{12} = J_{13} = 28$ and $J_{23} = 316$ Hz.

Chemical synthesis of $\{[(\text{cyclohexane-1,2-diylbis(thio-2,1-phenylene)diphenylphosphine)](2\text{-diphenylphosphinobenzenethiolato)ruthenium(II)}\}$ hexafluorophosphate $[\text{Ru-1}\cdot \text{cyclohexene}][\text{PF}_6]$: To a 40 mL solution of $\text{HNEt}_3[\text{Ru-1}]$ (100 mg, 0.0935 mmol) in acetonitrile with cyclohexene (0.947 mL, 9.35 mmol) was slowly added a 30 mL of FcPF_6 (0.0619 mg, 0.187 mmol) in acetonitrile via cannula transfer. The mixture was cooled in ice bath and allowed to stir for 3 hours. The color of the solution

transformed from yellow to yellow green. The solvent was removed through use of a roto-evaporator, followed by washing with an excess of hot water (~300 mL) and diethyl ether (25 mL). Yield: 85 mg (76%). Single crystals suitable for X-ray diffraction studies were grown through slow evaporation into 1:1 CH₂Cl₂:hexane mixture. $E_{1/2}(\text{Ru}^{\text{III}}/\text{Ru}^{\text{II}}) = +269$ mV. +ESI-MS for C₆₀H₅₂P₃S₃Ru: theoretical m/z (Z = 1), 1063.31; observed, 1063.17. Element analysis for C₆₀H₅₂P₄S₃F₆Ru: calculated C, 59.64; H, 4.35, found: C, 59.9; H, 4.75. Electronic absorption: λ_{max} (ϵ , M⁻¹ cm⁻¹): 367 nm (6993), 440 nm (shoulder). FT-IR (KBr pellet, cm⁻¹) 3052, 2925, 2852, 1434, 1086, 845, 559, 518. ³¹P NMR of **[Ru-1·cyclohexene]⁺** as isolated in CD₃CN shows a second-order spectra displays chemical shift (ppm) of $\delta_1 = 54.8$, $\delta_2 = 39.5$, $\delta_3 = 36.5$ and coupling constants (Hz) of $J_{12} = J_{13} = 29$ and $J_{23} = 313$.

Chemical synthesis of {[(diphenylethane-1,2-diylbis(thio-2,1-phenylene)diphenylphosphine)](2-diphenylphosphinobenzenethiolato)ruthenium(II)} hexafluorophosphate [Ru-1·cis stilbene][PF₆]: 100 mg of HNEt₃[Ru-1] (0.0935 mmol) in 40 mL acetonitrile resulting an yellow solution in schlenk flask was transferred the *cis*-stilbene (1.67 mL, 9.35 mmol) via syringe then the flask was cooled in an ice bath. Following the addition of a blue solution of FcPF₆ (0.0619 mg, 0.187 mmol) in 30 mL acetonitrile, the reaction solution was stirred overnight after which the solvent was removed by rotary evaporation to produce yellow green residue. The residue was washed 3 times with hot water (~100 mL) and diethyl ether (25 mL). The crude product was the yellow solid (69 mg, 57%). $E_{1/2}(\text{Ru}^{\text{III}}/\text{Ru}^{\text{II}}) = +361$ mV. +ESI-MS for C₆₈H₅₄P₃S₃Ru: theoretical m/z (Z = 1), 1161.34; observed, 1161.20. Element analysis for C₆₈H₅₄P₄S₃F₆Ru: calculated C, 62.52; H, 4.17, found: C, 63.17; H, 5.63. Electronic absorption: λ_{max} (ϵ , M⁻¹ cm⁻¹): 366

nm (10093). FT-IR (KBr pellet, cm^{-1}) 3052, 2917, 2848, 1434, 1091, 837, 694, 522. ^{31}P NMR of **[Ru-1·cis stilbene]⁺** as isolated in CD_3CN shows a pair of second-order spectra assigned to a pair of structural isomers. The major component (70%) displays chemical shift (ppm) of $\delta_1 = 52.5$, $\delta_2 = 42.9$, $\delta_3 = 35.6$ and coupling constants (Hz) of $J_{12} = J_{13} = 29$ and $J_{23} = 315$. The minor component (30%) displays $\delta_1 = 54.0$, $\delta_2 = 43.7$, $\delta_3 = 35.2$ and $J_{12} = J_{13} = 30$ and $J_{23} = 317$ Hz.

Chemical synthesis of {[(diphenylethane-1,2-diylbis(thio-2,1-phenylene)diphenylphosphine)](2-diphenylphosphinobenzenethiolato)ruthenium(II)} hexafluorophosphate [Ru-1·trans stilbene][PF₆]. The complex is prepared by the method mentioned above except that *trans*-stilbene (1.69 g, 0.187 mmol) was added instead of *cis* stilbene. Yield: 85mg (70%). $E_{1/2}(\text{Ru}^{\text{III}}/\text{Ru}^{\text{II}}) = 337$ mV. + ESI-MS for $\text{C}_{68}\text{H}_{54}\text{P}_3\text{S}_3\text{Ru}$, theoretical: m/z ($Z = 1$) 1161.34. Observed: 1161.17. Element analysis for $\text{C}_{68}\text{H}_{54}\text{P}_4\text{S}_3\text{F}_6\text{Ru}$, calculated: C, 62.52; H, 4.17. Found: C, 58.63; H, 4.30. Electronic absorption: λ_{max} (ϵ , $\text{M}^{-1} \text{cm}^{-1}$): 370 nm (6811), 441 nm (shoulder). FT-IR (KBr pellet, cm^{-1}) 3040, 2921, 2851, 1484, 1091, 833, 698, 523. ^{31}P NMR of **[Ru-1·trans stilbene]⁺** as isolated in CD_3CN shows a pair of second-order spectra assigned to a pair of structural isomers. The major component (69%) displays chemical shift (ppm) of $\delta_1 = 57.9$, $\delta_2 = 38.5$, $\delta_3 = 35.6$ and coupling constants (Hz) of $J_{12} = J_{13} = 30$ and $J_{23} = 303$. The minor component (31%) displays $\delta_1 = 54.1$, $\delta_2 = 43.7$, $\delta_3 = 35.2$ and $J_{12} = J_{13} = 30$ and $J_{23} = 318$ Hz.

Chemical synthesis of {[(1-octene-1,2-diylbis(thio-2,1-phenylene)diphenylphosphine)](2-diphenylphosphinobenzenethiolato)ruthenium(II)} hexafluorophosphate [Ru-1·octyne][PF₆]: To a acetonitrile (40 mL) solution of $\text{HNEt}_3[\text{Ru-1}]$ (100

mg, 0.0935 mmol) was added 1-octyne (1.38 mL, 9.35 mmol) via syringe. The solution was cooled at 0°C in ice bath. The resulting yellow solution was slowly added a blue solution of FcPF₆ (0.0619 mg, 0.187 mmol) via cannula. After the addition, the mixture was allowed to stir overnight. The observed color was a dark orange. The removal of solvent resulted in oily orange residue. The crude product was washed with an excess of hot water (~300 mL) and diethyl ether (100 mL) and recrystallized from THF/hexane yielding the yellow solid (49 mg, 43 %). X-ray quality crystals were obtained by slow evaporation of 1:2 chlorobenzene:hexane mixture. $E_{1/2}(\text{Ru}^{\text{III}}/\text{Ru}^{\text{II}}) = +356 \text{ mV}$. +ESI-MS for C₆₂H₅₆P₃S₃Ru: theoretical m/z (Z = 1), 1091.37; observed, 1091.18. Element analysis for C₆₂H₅₆P₄S₃F₆Ru: calculated C, 60.23; H, 4.57, found: C, 58.03; H, 3.72. Electronic absorption: $\lambda_{\text{max}} (\epsilon, \text{M}^{-1} \text{cm}^{-1})$: 305 nm (9527), 361 nm (shoulder). FT-IR (KBr pellet, cm⁻¹) 3052, 2929, 2852, 1434, 1086, 837, 559, 531. ³¹P NMR of **[Ru-1·octyne]⁺** as isolated in CD₃CN shows a pair of second-order spectra assigned to a pair of structural isomers. The major component (60%) displays chemical shift (ppm) of $\delta_1 = 57.2$, $\delta_2 = 42.8$, $\delta_3 = 35.8$ and coupling constants (Hz) of $J_{12} = J_{13} = 31$ and $J_{23} = 313$. The minor component (40%) displays $\delta_1 = 57.2$, $\delta_2 = 43.0$, $\delta_3 = 36.2$ and $J_{12} = J_{13} = 31$ and $J_{23} = 313$ Hz.

Chemical synthesis of {[(phenylethylene-1,2-diylbis(thio-2,1-phenylene)diphenylphosphine)](2-diphenylphosphinobenzenethiolato)ruthenium(II)} hexafluorophosphate [Ru-1·phenylacetylene][PF₆]: 100 mg of HNEt₃[Ru-1] (0.0935 mmol) in 40 mL acetonitrile resulting an yellow solution in schlenk flask was transferred the phenylacetylene (1.38 mL, 9.35 mmol) via syringe then the flask was cooled in an ice bath. Following the addition of a blue solution of FcPF₆ (0.0619 mg, 0.0817 mmol) in 30 mL acetonitrile, the reaction solution was stirred overnight after which the solvent was

removed by rotary evaporation to produce yellow green residue. The residue was washed 3 times with hot water (~100 mL) and diethyl ether (25 mL). The crude product was recrystallized via the mixture of THF/hexane yielding the yellow solid (49 g, 42%). $E_{1/2}(\text{Ru}^{\text{III}}/\text{Ru}^{\text{II}}) = +361$ mV. +ESI-MS for $\text{C}_{62}\text{H}_{48}\text{P}_3\text{S}_3\text{Ru}$: theoretical m/z ($Z = 1$), 1083.29; observed, 1083.12. Element analysis for $\text{C}_{62}\text{H}_{48}\text{P}_4\text{S}_3\text{F}_6\text{Ru}$: calculated C, 60.62; H, 3.95, found: C, 57.32; H, 4.28. Electronic absorption: λ_{max} (ϵ , $\text{M}^{-1} \text{cm}^{-1}$): 305 nm (6919), 437 nm (shoulder). FT-IR (KBr pellet, cm^{-1}) 3052, 2917, 2848, 1434, 1091, 837, 559, 523. ^{31}P NMR of **[Ru-1-phenylacetylene] $^+$** as isolated in CD_3CN shows a pair of second-order spectra assigned to a pair of structural isomers. The major component (57%) displays chemical shift (ppm) of $\delta_1 = 56.7$, $\delta_2 = 42.7$, $\delta_3 = 36.5$ and coupling constants (Hz) of $J_{12} = J_{13} = 30$ and $J_{23} = 312$. The minor component (43%) displays $\delta_1 = 57.2$, $\delta_2 = 43.0$, $\delta_3 = 36.0$ and $J_{12} = J_{13} = 30$ and $J_{23} = 312$ Hz.

Chemical synthesis of $\{[(1\text{-methyl-2-phenylethylene-1,2-diylbis(thio-2,1-phenylene)diphenyl-phosphine)](2\text{-diphenylphosphinobenzene-thiolato})\text{ruthenium(II)}\}$ hexafluoro-phosphate $[\text{Ru-1-phenylpropyne}][\text{PF}_6]$. The complex is synthesized the same method as described above except 1-phenyl-1-propyne (0.112 mL, 9.35 mmol) was added instead of phenylacetylene. Yield: 88 mg (76%). $E_{1/2}(\text{Ru}^{\text{III}}/\text{Ru}^{\text{II}}) = 368$ mV. + ESI-MS for $\text{C}_{63}\text{H}_{50}\text{P}_3\text{S}_3\text{Ru}$, theoretical: m/z ($Z = 1$) 1097.26. Observed: 1097.13. Element analysis for $\text{C}_{63}\text{H}_{50}\text{P}_4\text{S}_3\text{F}_6\text{Ru}$, calculated: C, 60.86; H, 4.06. Found: C, 58.5; H, 4.33. Electronic absorption: λ_{max} (ϵ , $\text{M}^{-1} \text{cm}^{-1}$): 374 nm (5302), 446 nm (shoulder). FT-IR (KBr pellet, cm^{-1}) 3052, 2917, 2848, 1434, 1086, 841, 694, 523. ^{31}P NMR of **[Ru-1-phenylpropyne] $^+$** as isolated in CD_3CN shows a pair of second-order spectra assigned to a pair of structural isomers. The major component (55%) displays

chemical shift (ppm) of $\delta_1 = 55.8$, $\delta_2 = 43.3$, $\delta_3 = 37.1$ and coupling constants (Hz) of $J_{12} = J_{13} = 25$ and $J_{23} = 315$. The minor component (45%) displays $\delta_1 = 55.5$, $\delta_2 = 45.0$, $\delta_3 = 35.7$ and $J_{12} = J_{13} = 25$ and $J_{23} = 316$ Hz.

Chemical synthesis of $\{[(1\text{-butene-1,2-diylbis(thio-2,1-phenylene)diphenylphosphine)](2\text{-diphenylphosphinobenzenethiolato)ruthenium(II)}\}$ hexafluorophosphate $[\text{Ru-1-butadiene}][\text{PF}_6]$: To a solution of $\text{HNEt}_3[\text{Ru-1}]$ (100 mg, 0.0935 mmol) in 40 mL of acetonitrile was added via syringe 3 mL of 1,3-butadiene (9.35 mmol) which cooled in a ice bath. To the resulting yellow mixture was added a blue solution of FcPF_6 (0.0619 mg, 0.187 mmol) in degassed acetonitrile (30 mL) via cannula during which time the solution developed instantaneous color from yellow to yellow green. The solution was stirred for 3 hours followed by solvent removal under the roto-evaporator. The residue was washed with an excess of hot water (~300 mL) and diethyl ether (25 mL). The resulting yellow solid was dried under vacuum yielding as a crude product (86 mg, 78 %). $E_{1/2}(\text{Ru}^{\text{III}}/\text{Ru}^{\text{II}}) = +321$ mV. +ESI-MS for $\text{C}_{58}\text{H}_{48}\text{P}_3\text{S}_3\text{Ru}$: theoretical m/z ($Z = 1$), 1035.19; observed, 1035.12. Element analysis for $\text{C}_{58}\text{H}_{48}\text{P}_4\text{S}_3\text{F}_6\text{Ru}$: calculated C, 59.02; H, 4.11, found: C, 58.82; H, 4.25. Electronic absorption: λ_{max} (ϵ , $\text{M}^{-1} \text{cm}^{-1}$): 294 nm (8640), 361nm, 433 nm (shoulder). FT-IR (KBr pellet, cm^{-1}) 3048, 1475, 1091, 837, 698, 523.

Chemical synthesis of $\{[(2,3\text{-dimethyl-1-butene-1,2-diylbis(thio-2,1-phenylene)diphenyl-phosphine)](2\text{-diphenylphosphinobenzene-thiolato)ruthenium(II)}\}$ hexafluoro-phosphate $[\text{Ru-1-dimethylbutadiene}][\text{PF}_6]$. The compound is prepared by the same method as notified above except using 2,3-dimethyl-1,3-butadiene (1.06 mL, 9.35 mmol) instead of 1,3-butadiene. The resulting yellow solid

was dried under vacuum yielding as a crude product (70 mg, 62 %). $E_{1/2}$ (Ru^{III}/Ru^{II}) = 332 mV. + ESI-MS for C₆₄H₅₈P₃S₃Ru, theoretical: m/z ($Z = 1$) 1064.25. Observed: 1063.15. Element analysis for C₆₄H₅₈P₄S₃F₆Ru, calculated: C, 59.65; H, 4.34. Found: C, 56.62; H, 4.50. Electronic absorption: λ_{\max} (ϵ , M⁻¹ cm⁻¹): 374 nm (12472), 439 nm (shoulder). FT-IR (KBr pellet, cm⁻¹) 3052, 1434, 1091, 841, 694, 519.

Chemical synthesis of {[(dipentene -1,2-diylbis(thio-2,1-phenylene)diphenylphosphine)](2-diphenylphosphinobenzene-thiolato)ruthenium(II)} hexafluorophosphate [Ru-1-dipentene][PF₆]. The compound is prepared by the same method as performed above except utilizing dipentene (1.50 mL, 9.35 mmol) instead of 1,3-butadiene. The resulting yellow solid was dried under vacuum yielding as a crude product (66 mg, 56 %). $E_{1/2}$ (Ru^{III}/Ru^{II}) = 320 mV. + ESI-MS for C₆₄H₅₈P₃S₃Ru, theoretical: m/z ($Z = 1$) 1117.33. Observed: 1117.20. Element analysis for C₆₄H₅₈P₄S₃F₆Ru, calculated: C, 60.9; H, 4.63. Found: C, 58.8; H, 4.85. Electronic absorption: λ_{\max} (ϵ , cm⁻¹ M⁻¹): 369 nm (6150), 439 nm (shoulder). FT-IR (KBr pellet, cm⁻¹) 3048, 1434, 1091, 833, 698, 519. ³¹P NMR of [Ru-1-dipentene]⁺ as isolated in CD₃CN shows a pair of second-order spectra assigned to a pair of structural isomers. The major component (62%) displays chemical shift (ppm) of $\delta_1 = 55.0$, $\delta_2 = 39.7$, $\delta_3 = 34.8$ and coupling constants (Hz) of $J_{12} = J_{13} = 30$ and $J_{23} = 299$. The minor component (38%) displays $\delta_1 = 58.9$, $\delta_2 = 43.7$, $\delta_3 = 35.8$ and $J_{12} = J_{13} = 30$ and $J_{23} = 316$ Hz.

CHAPTER III
KINETIC STUDY OF [Ru(DPPBT)₃]⁺ WITH ALKENES

As noted in Chapter I, ethylene is a major product of the petroleum industry with annual US production topping 28.7×10^3 kilotons in 2009.⁵⁶ The alternate separation technique proposed by Wang and Stiefel in 2001 offers promise for the development of similar systems that overcome the limitations noted in the Introduction. Our Re complexes [**Re-1**]ⁿ provide the best alternate system to date with efficient ethylene binding and release as a function of applied potential. In this Chapter, I describe a series of kinetic experiment to determine the electronic and steric effects of alkene addition to [**M-1**]ⁿ (M = Re, Ru).

As described in the introduction, the metal-sulfur orbital interactions enhance the nucleophilicity of metal-thiolates for “t_{2g}-rich” metals. An idealized interaction in which the energies of the metal-d and sulfur-p orbitals are perfectly matched is reviewed in Figure III-1. This type of interaction in our [**M-1**]ⁿ complexes is responsible for the thiol radical character in our oxidized complexes.

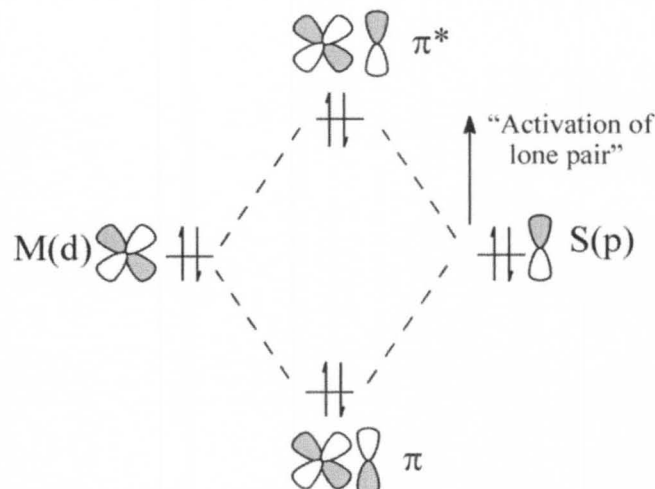


Figure III-1. A truncated MO diagram depicting only the p-interactions, M(d)-S(p) (filled-filled), which “activate” the thiolate lone pair.

In my prior thesis work, the focus was directed towards understanding oxidation and reduction induced C-S formation and cleavage, respectively, employing the related rhenium complex $\text{Re}(\text{DPPBT})_3$ **Re-1**. My work on the reversible C-S bond formation/cleavage between a rhenium-thiolate complex and ethylene was published in 2009.⁵⁵ **Re-1** displays two reversible one electron oxidations and a single reduction based on cyclic voltammetric data, Figure III-2. The two oxidation events obtain at -340 mV and +420 mV assigned as the $[\text{Re-1}]^{+/0}$ and $[\text{Re-1}]^{2+/+}$, respectively. The $[\text{Re-1}]^{0/-}$ reduction event shows at -1620 mV. The events span formal oxidation states from Re(II) to Re (V) although significant ligand participation in the redox events makes these formal assignments misleading with respect to the electronic structure of the complexes.⁴⁹

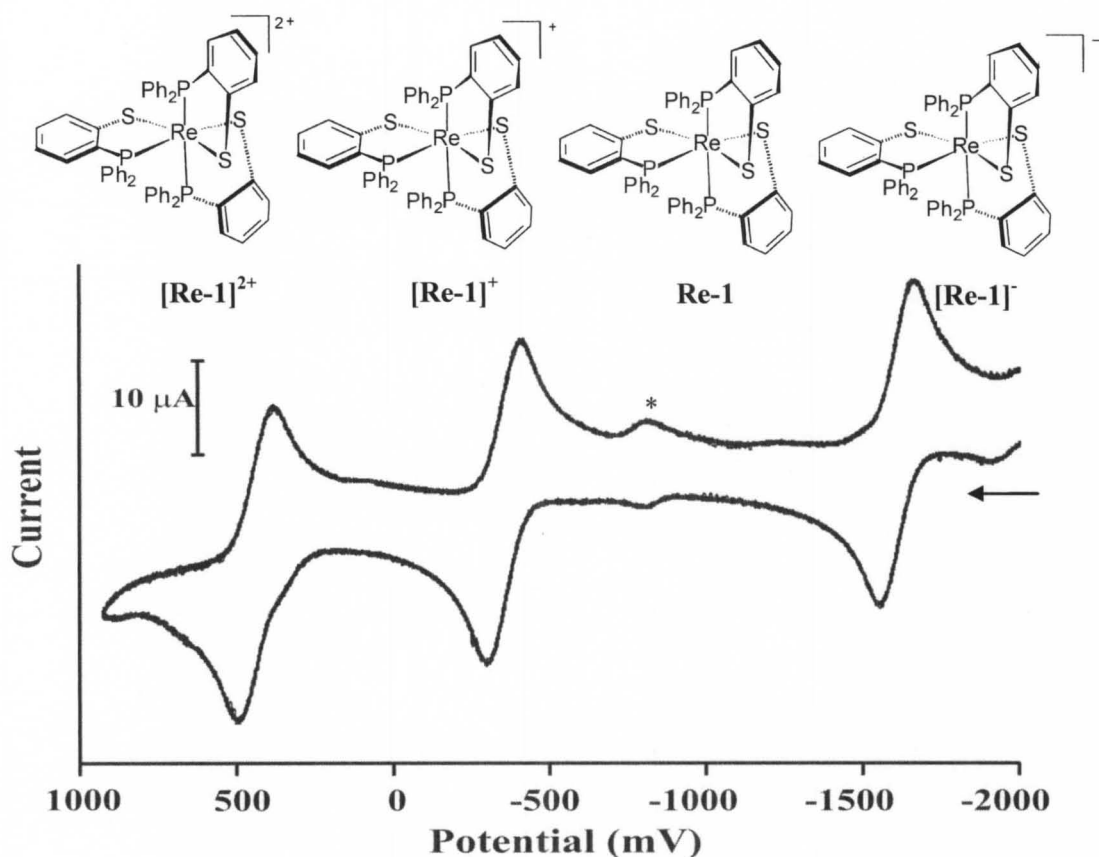


Figure III-2. Cyclic voltammograms of complex **Re-1** obtained under a nitrogen atmosphere in dichloromethane at room temperature with 0.1 M TBAHFP as supporting electrolyte. * is indicated as the impurity.

The oxidized complex $[\text{Re-1}]^+$ is a blue solution prepared by chemical method and electrochemical method. Solutions of $[\text{Re-1}]^+$ are stable under nitrogen gas for several hours at room temperature and a trace of the electronic spectra recorded at 581 nm. In the presence of ethylene, the blue solutions rapidly generate a purple solution consistent with $[\text{Re-1}\cdot\text{C}_2\text{H}_4]^+$ and spectra were collected every 30 seconds. After 150 seconds, the absorbance at 581 nm was 46 % of initial absorbance. Longer purge times resulted in no further significant changes thereafter, Figure III-3. Assuming ethylene saturation of the solution (0.4642 M in dichloromethane), an equilibrium binding

constant, K_2 , is estimated at 2.5.⁶⁰ A nitrogen purge restored the initial spectrum of $[\text{Re-1}]^+$. Spectra were collected every 30 seconds. After 480 seconds, the absorbance at 581 nm reached a maximum value. The C-S bond formation/cleavage process can be repeated in multiple times with no remarkable changes in efficiency.

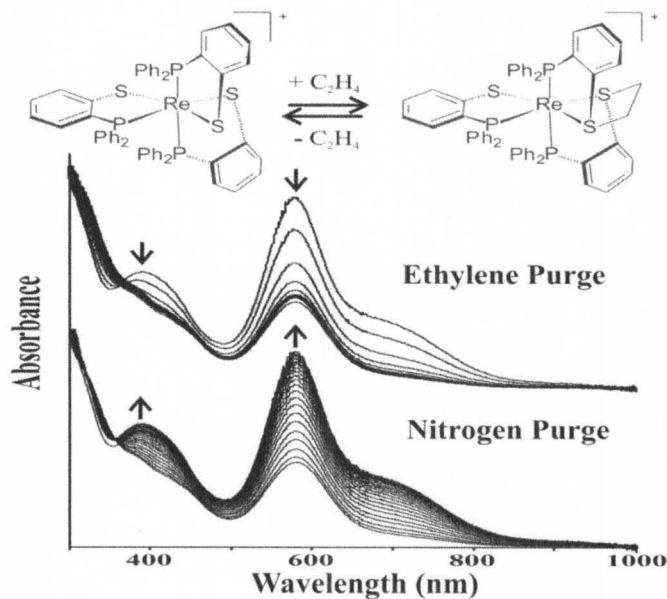


Figure III-3. Absorbance spectra showing the reversible binding of ethylene to $[\text{Re-1}]^+$.

The kinetic and equilibrium parameters associated with C-S bond formation/cleavage were extracted from cyclic voltammograms at multiple scan rates using DigiSim software package. Rate constants for C-S bond formation between $[\text{Re-1}]^+$ and ethylene, k_f , and for C-S bond cleavage, k_r , for $[\text{Re-1}\cdot\text{C}_2\text{H}_4]^+$ were extracted from simulation of the CV data at 7 scan rates ranging from 100 to 1000 mV/s for 3 independent trials. Average values for k_f and k_r are $0.12(2) \text{ M}^{-1} \text{ s}^{-1}$ and $0.03(4) \text{ s}^{-1}$, respectively. From these, the equilibrium binding constant was calculated as $4.0(0.8) \text{ M}^{-1}$ in agreement with the prediction from the UV-visible study.

From the redox potentials of $[\mathbf{Re-1}]^n$ and $[\mathbf{Re-1}\cdot\mathbf{C}_2\mathbf{H}_4]^n$ and the equilibrium constant of $[\mathbf{Re-1}]^+$ binding ethylene, the thermodynamic boxes were constructed as shown in Scheme I-11. K_2 has calculated value of $1.9(4) \times 10^{-11} \text{ M}^{-1}$ consistent with observation of an unstable C-S bond of $[\mathbf{Re-1}\cdot\mathbf{C}_2\mathbf{H}_4]$. In contrast, the calculated value of K_3 , $2.5(9) \times 10^9 \text{ M}^{-1}$, is large and corresponds to the observed stability of $[\mathbf{Re-1}\cdot\mathbf{C}_2\mathbf{H}_4]^{2+}$. The large differences in equilibrium constants as a function of oxidation state provide a mean to easily gate ethylene addition and release. In addition to electrochemical methods, $[\mathbf{Re-1}\cdot\mathbf{C}_2\mathbf{H}_4]^{2+}$ can be isolated by preparing with chemical oxidant via the ECE pathway. Full characterization was completely performed by the spectroscopic methods and X-ray crystal structure was modified.

From these studies, we established reversible C-S bond formation/release that is regulated by the oxidation state of the complex with access to “lock on”, “lock off”, or concentration dependent ethylene addition. The rate of ethylene C-S formation/cleavage allows facile trap and release of ethylene over in multiple cycles. We next sought to further study rate constants for the addition of various alkenes to $[\mathbf{Re-1}]^+$ by CV measurements to establish the selectivity of ethylene addition.

Styrene addition to $[\mathbf{Re-1}]^+$

To investigate the addition of other alkenes to $[\mathbf{Re-1}]^+$, we attempted to employ a strategy similar to that used for ethylene addition. The CV of $\mathbf{Re-1}$ was measured in the presence of 2.0 M styrene at multiple scan rates. As shown in Figure III-4, the voltammogram is identical to that recorded in the absence of styrene. This indicates that either styrene is unreactive with $[\mathbf{Re-1}]^+$ or that the reaction is too slow to measure on the

CV timescale. To resolve the issue, the chemical (as opposed to electrochemical) reaction of $[\text{Re-1}]^+$ with styrene was investigated.

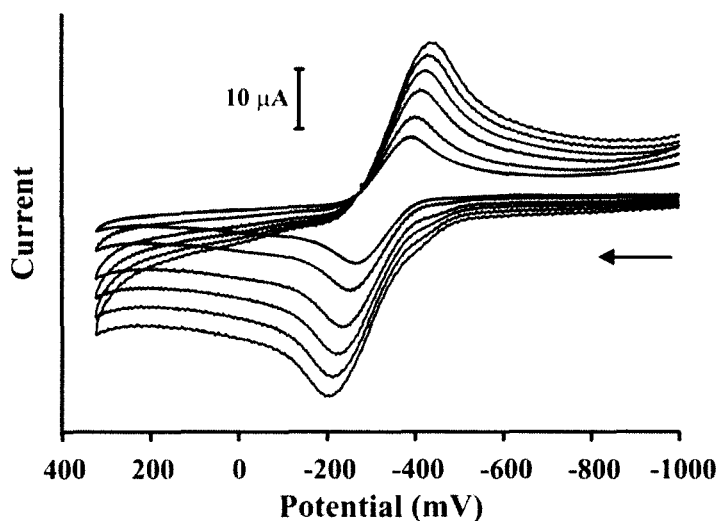


Figure III-4. Cyclic voltammogram of **Re-1** in presence of 2.0 M styrene obtained in acetonitrile. The voltammograms at multiple scan rates from 100 to 1000 mV/s.

A blue solution of $[\text{Re-1}]^+$ was prepared by chemical oxidation of **Re-1** with AgPF_6 . Then styrene was added to the blue solution yielding the purple solution of $[\text{Re-1}\cdot\text{styrene}]^+$. Due to the limited stability of $[\text{Re-1}\cdot\text{styrene}]^+$ an additional equivalent of AgPF_6 was added to oxidize one electron on $[\text{Re-1}\cdot\text{styrene}]^+$ resulting $[\text{Re-1}\cdot\text{styrene}]^{2+}$. This $[\text{Re-1}\cdot\text{styrene}]^{2+}$ was isolated as orange complex. The CV was performed which provides the redox event potential at -101 mV consistent with that expected for the $[\text{Re-1}\cdot\text{styrene}]^{2+/+}$ redox couple, Appendix E-1. The results clearly indicate that styrene will add to $[\text{Re-1}]^+$, but not at rates detectable by CV. Using simulation parameters similar to those employed for ethylene and along with a styrene concentration of 2.0 M, we can predict that the addition rate must be slower than 10^{-2} s^{-1} .

UV-visible studies were conducted to establish an approximate rate for the addition of styrene to $[\text{Re-1}]^+$. As shown in Figure III-5, the reaction can be monitored by absorbance versus time in the kinetic study. The observed absorbance of $[\text{Re-1}]^+$ shows at 390 nm and 581 nm. In the presence of styrene (2.0 M), the pre-equilibrium baseline occurred then the 581 nm absorbance started to decay within the times until the completion of the reaction. The assumption of baseline is related to the complication of oxidizing agent. The formal potential of AgPF_6 is 650 mV versus Fc^+/Fc reference which allows to perform the equilibrium between $[\text{Re-1}]^+$ to $[\text{Re-1}]^{2+}$. The rate constant of the styrene addition is on the order of $10^{-5} \text{ M}^{-1} \text{ s}^{-1}$. This rate constant is 4 orders of magnitude slower than the ethylene addition rate constant confirming ethylene selectively in the presence of styrene. As described below, most other alkenes are expected to add more slowly than styrene confirming a general selectivity for ethylene over all other alkenes.

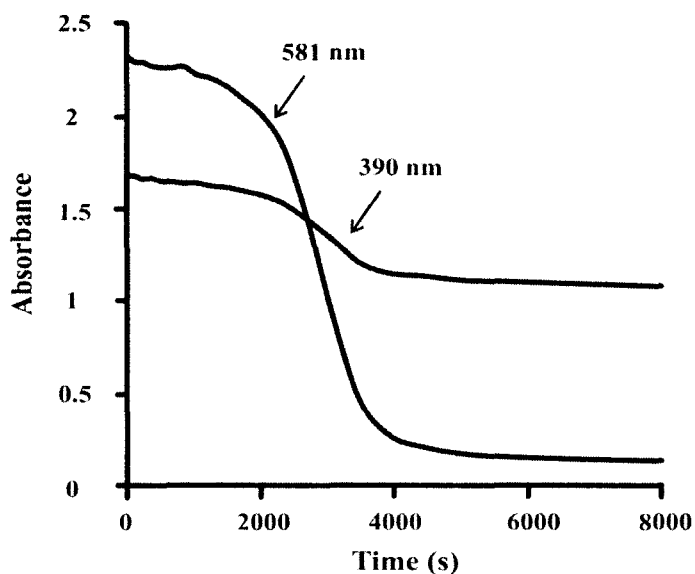


Figure III-5. Kinetic study of $[\text{Re-1}]^+$ in presence of 2.0 M styrene obtained in chlorobenzene. The trace was recorded absorbance versus time.

Rate constant of addition of styrene to $[\mathbf{Ru-1}]^+$

While the results with $[\mathbf{Re-1}]^+$ and styrene confirm the desired selectivity of our reversible binding system for ethylene, the relatively low reaction rates impede further studies to determine general reactivity trends. For these studies, reactions with the $[\mathbf{Ru-1}]$ analogue are more appropriate. As described below, styrene addition to $[\mathbf{Ru-1}]^+$ is 12 order magnitude faster higher than its addition to $[\mathbf{Re-1}]^+$. The fast irreversible addition of alkenes to $[\mathbf{Ru-1}]^+$ make it ideal for the rate constants investigations by cyclic voltammetry.

As previously reported by Venna, oxidation of $[\mathbf{Ru-1}]$ in the presence of various alkene yields the corresponding $[\mathbf{Ru-1}\cdot\text{alkenes}]^+$.³³ The reaction is rapid with no detectable $[\mathbf{Ru-1}]^+$ intermediate in the UV-visible trace recorded during the reaction.⁴² This suggests the rate constant must be faster than 10^{-2} s^{-1} , which is suitable for measuring the rate of C-S bond formation on the CV timescale. To obtain further insight into the alkene addition mechanism, the CV was used to determine rate constants for the addition of various alkenes to oxidized intermediate $[\mathbf{Ru-1}]^+$.

For a 2.0 mM solution of $[\mathbf{Ru-1}]$, the cyclic voltammogram was recorded in the absence of styrene under a nitrogen atmosphere. The voltammogram was collected over a wide potential that was scanned from negative to positive potentials. As shown Figure III-6 (top), the CV shows the two expected reversible redox events at -22 mV and -830 mV assigned as $[\mathbf{Ru-1}]^{+0}$ and $[\mathbf{Ru-1}]^{0/-}$, respectively.

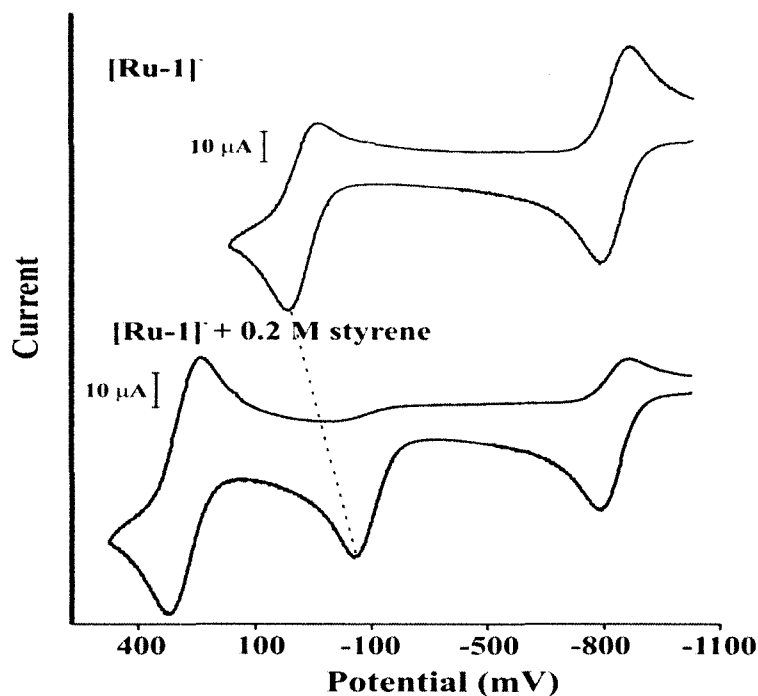


Figure III-6. Cyclic voltammograms of 2.0 mM complex $[\text{Ru-1}]^-$ recorded in the absence (top) and presence (bottom) of 0.2 M styrene. Data were collected at 200 mV/s in acetonitrile at 0°C temperature with 0.1 M TBAHFP as supporting electrolyte. Potential referred to a Fc^+/Fc .

In the presence of 0.2 M styrene, a new redox couple assigned to $[\text{Ru-1}\cdot\text{sty}]^{2+/+}$ is observed at +277 mV, while the cathodic return peak currents for $[\text{Ru-1}]^{+/0}$ and $[\text{Ru-1}]^{0/-}$ events greatly diminished due to the irreversible chemical formation of $[\text{Ru-1}\cdot\text{sty}]^{2+/+}$, Figure III-6 (bottom). The difference in potential between the formal $\text{Ru}^{\text{III/II}}$ potentials of thiolate precursor $[\text{Ru-1}]^{0/-}$ and dithioether product, $[\text{Ru-1}\cdot\text{sty}]^{2+/+}$ of +1107 mV is consistent with the modification of two thiolate donors to thioether donors.^{32,34,42,61} Additionally, the potential shift of anodic peak minimum for $[\text{Ru-1}]^{+/0}$ from 0 to -96 mV, results from the rapid chemical reaction of $[\text{Ru-1}]^+$ with styrene. According to Le Chatelier's principle, a change in one of the variables such as concentration, pressure, and

temperature will allow the system shift the equilibrium position. In our case, the shift potential can describe as the change of the equilibrium concentration of $[\text{Ru-1}]^+$ in the chemical step. As soon as the $[\text{Ru-1}]^+$ intermediate is generated, styrene reacts with it, which shifts the apparent anodic potential to lower potential.

In order to estimate the rate constant of C-S bond formation, cyclic voltammograms were measured at scan rates of 100 to 1000 mV/s, Figure E-2 in Appendix E. A representative voltammogram at a scan rate of 400 mV/s is shown in Figure III-7 (dark line). The current peak is proportional to the scan rate. As mentioned above, the $[\text{Ru-1}]^{+/0}$ potential shifts due to the chemical reaction. This redox event is observed at more negative potentials at higher scan rates. Moreover, a current peak is varied depending on the scan rates. By performing various scan rates a set of consistent and reliable CV parameters were obtained.

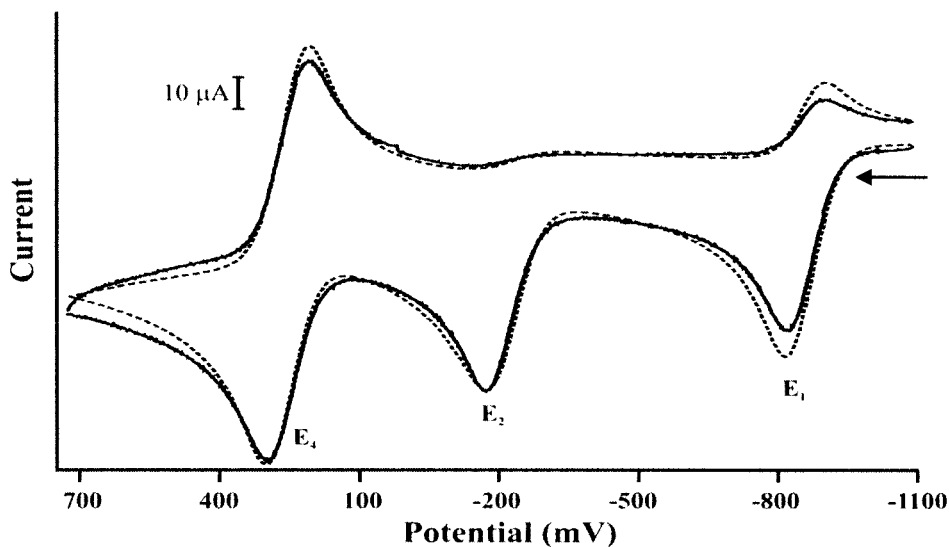
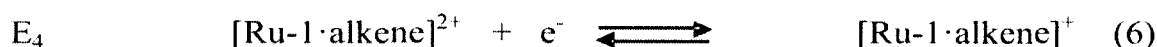
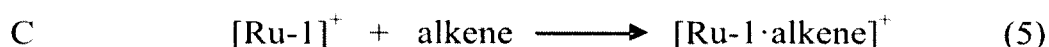


Figure III-7. Experimental (—) and simulated (---) cyclic voltammograms of $[\text{Ru-1}]^+$ in presence of styrene were obtained at a scan rate 400 mV/s.

Recorded CVs were simulated over all the scan rates simultaneously using the DigiSim software package to extract the kinetic and equilibrium parameters of styrene addition.⁵² These voltammograms were simulated with an EECE mechanism as shown in Scheme III-1. The experimental and simulated CV at a scan rate of 400 mV/s is shown in Figure III-7 (dash line).



Scheme III-1. EECE mechanism.

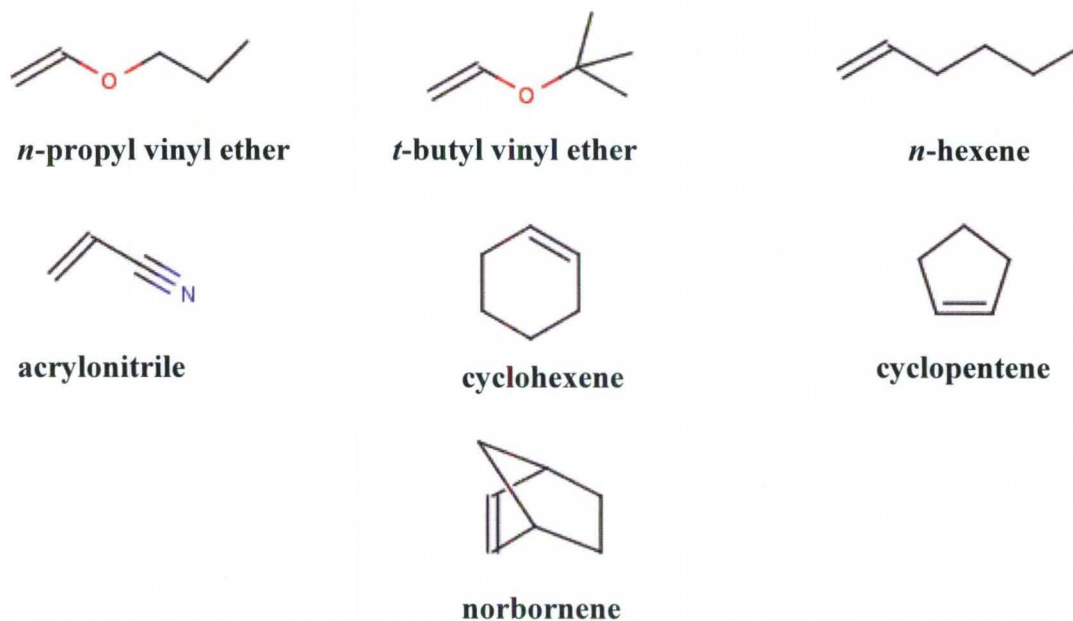
Simulation details and average fitting parameters are summarized in Table III-1. All parameters input for the program are defined or set as noted on Chapter II. The rate constant for C-S bond formation between $[\text{Ru-1}]^+$ and styrene, k_f , was refined from simulation of the CV data at 7 scan rates ranging from 100 to 1000 mV/s for 3 independent trials. The addition reaction between $[\text{Ru-1}]^+$ and styrene follow a second-order rate law with an average value for k_f of $4.6(5) \times 10^7 \text{ M}^{-1} \text{ s}^{-1}$.

Table III-1: Cyclic voltammetry simulation parameters						
$[\text{Ru-1}]^-$ 2.0 mM with Styrene 0.2 M, EECE Mechanism						
	Potential (vs Fc^+/Fc) (mV)			Rate constant (* $10^7 \text{ M}^{-1} \text{ s}^{-1}$)	Diffusion coefficient (cm^2/s)	Uncompensated resistance (Ω)
	E_2	E_1^1	E_4	k_f	D_0	R_u
Trial 1	-30.0	-830	269	4.798	7.426	205
Trial 2	-29.9	-830	269	4.021	8.759	177
Trial 3	-30.0	-830	272	4.860	8.401	210

¹ This was set as internal reference

Rate constant of addition of acyclic and cyclic alkenes to $[\text{Ru-1}]^+$

The previous studies by Venna revealed carbon-sulfur bond formation readily occurs between $[\text{Ru-1}]^+$ and a variety of alkenes including 1-hexene, styrene, cyclohexene, and norbornene.⁴² To evaluate the influence of alkene substituent on the rate of reaction, addition reactions of $[\text{Ru-1}]^+$ with various alkenes were investigated by cyclic voltammetry as described above. The alkenes included in this study are shown in Scheme III-2. The alkenes of interest are an electron-rich like vinyl ether, an electron-neutral hexene, and an electron poor acrylonitrile. The cyclic alkenes are varied based on ring strain which increase from cyclohexene to, cyclopentene to, norbornene. The selection of these alkenes defines on the steric and electronic effects, solid or liquid at room temperature with the boiling point $\geq 60^\circ\text{C}$.



Scheme III-2. Selected alkenes.

Based on the calculated electronic structure of $[\text{Ru-1}]^+$, C-S bond formation behavior occurs in matter of electronic imbalance between the metal-stabilized thiyl radicals and alkenes. Since the transition metal serves as an electron withdrawing group of the thiyl radical, the fastest rates are expected for alkenes with electron-donating groups. Moreover, alkenes with electron-releasing groups presumably results the slow reaction rate. Steric effect are expected to be lowered the reaction rates, although the cyclic alkenes with ring strain are expected to promote the rate of addition.

Representative cyclic voltammograms for $[\text{Ru-1}]^-$ in the presence of each alkene are provided in Figure B-2 to B-7 in Appendix B. In total, each alkene was investigated at least three times at scan rates of 100 to 1000 mV/s, Appendix E. Simulations of the data according to an EECE mechanism was shown in Figure III-7 and used to extract rate constants data as described below. Results from individual trials are summarized in Table A-1 to A-8, Appendix A. Average experimentally determined second-order rate constants and measured redox potentials are provided in Table III-2

Table III-2: Experimentally determined second-order rate constants for the addition of alkenes to $[\text{Ru-1}]^+$.

Alkene	k	E ₄	E ₄	E _{exp.}	E _{sim.}
	(M ⁻¹ s ⁻¹)	exp.	sim.	shift	shift
mono-substituted linear alkenes		(mV)	(mV)	(mV)	(mV)
styrene	4.6(5) × 10 ⁷	278	270	1108	1100
<i>n</i> -propyl vinyl ether	2.0(1) × 10 ⁷	271	263	1101	1093
<i>t</i> -butyl vinyl ether	2.6(8) × 10 ⁶	270	261	1100	1091
<i>n</i> -hexene	7.0(2) × 10 ⁵	264	251	1094	1081
acrylonitrile	2.7(4) × 10 ⁴	332	343	1162	1173
cyclic alkenes					
norbornene	4(2) × 10 ⁷	286	274	1116	1104
cyclopentene	6(1) × 10 ⁶	258	254	1088	1074
cyclohexene	2.9(3) × 10 ³	241	236	1071	1066

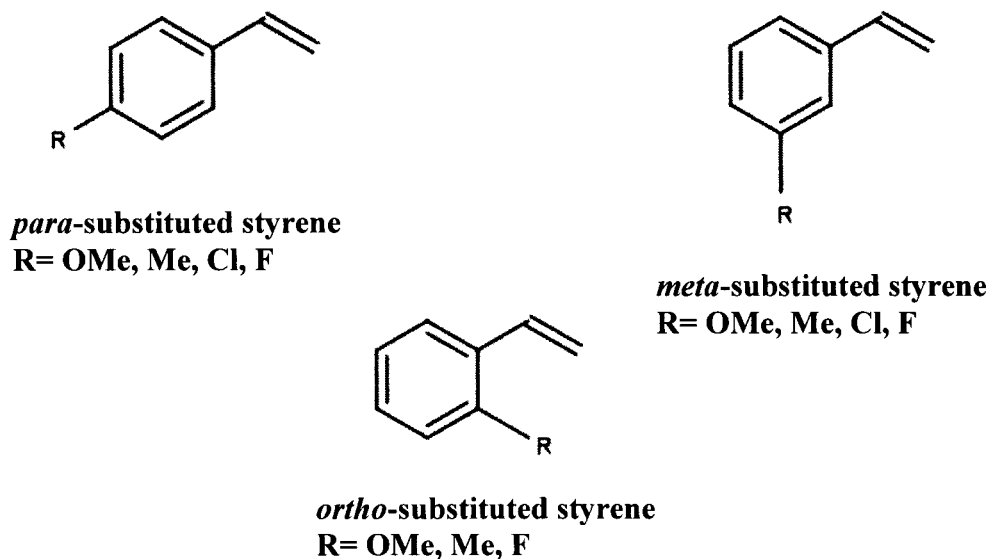
The non-functionalized alkene *n*-hexene displays a second-order rate constant of $7.0(2) \times 10^5 \text{ M}^{-1} \text{ s}^{-1}$. The electron-rich alkenes including *n*-propyl vinyl ether, *t*-butyl ether increase the addition reaction rate with the metal-stabilized thiyl radicals by 10-100 folds. Similar observations for the addition of haloalkyl and butoxyl radicals to alkenes were investigated by Hosomi et al.^{62,63} In contrast, the electron-deficient alkene, acrylonitrile, reduces the addition rate constant by 100-1000 folds. The results are consistent with the electrophilic radicals.

For cyclic alkenes, the higher ring-strain alkene, norbornene, adds most rapidly to form the metal dithioether complex. The rate is $4(2) \times 10^7 \text{ M}^{-1} \text{ s}^{-1}$ which is 4 orders of magnitude as compared to cyclohexene. The rate constants for the significant ring chains of cyclic alkenes are similar as compared to electron rich linear alkenes. The decreasing ring chain alkenes are accompanying along with the electron deficient alkenes.

The E_4 potentials for the $[\text{Ru-1}\cdot\text{alkene}]^{2+/+}$ of various alkenes both experimental and simulated data indicate that they are close to each other and these value ranges correspond to a shift of approximately +1100 mV which is translated as two sulfur donors alkylation to form dithioether complexes. The different potentials of $[\text{Ru-1}\cdot\text{alkene}]^{2+/+}$ and $[\text{Ru-1}]^+$ are increased consistent with the fast rate constants from the opening alkenes, styrene to *n*-hexene and from the cyclic alkene, norbornene to cyclohexene.

The alkenes group will include a series of styrene derivatives with various para, meta, and ortho substituent positions as shown in Scheme III-3 are used to evaluate electronic effect. The R-substituent can be methoxyl (OMe), methyl (Me), chloro (Cl), and fluoro (F) groups. This selection of functional groups for our study is based on the

physical state of the alkene and its commercial availability. Liquid alkenes are preferred for the electrochemical investigations and they must also be miscible in the acetonitrile solvent.



Scheme III-3. Selected *para*, *meta*, and *ortho*-substituted styrene derivatives.

The cyclic voltammograms of each substituted styrene were collected over multiple scan rates to determine the rate constants for addition using the same protocol as mentioned above. The representative cyclic voltammograms from simulation versus experiment are provided in Figure B-8 to B-18, Appendix B. In this study, the rate constant for each individual styrene derivative was measured 10 times to obtain reliable data, Table A-8 to A-19 in Appendix A. The average rate constant was obtained as demonstrated in Table III-3.

Table III-3: Second-order rate constants for the addition of substituted styrene derivatives to [Ru-1]⁺.in acetonitrile at 298 K

Substituent Styrene Derivatives	k × 10⁷
<i>para</i>-substituted styrene	
OCH ₃	4.2(2)
CH ₃	3.6(1)
Cl	2.0(1)
F	1.8(1)
<i>meta</i>-substituted styrene	
OCH ₃	5.3(2)
CH ₃	7.2(3)
Cl	2.3(1)
F	1.5(1)
<i>ortho</i>-substituted styrene	
OCH ₃	12.3(9)
CH ₃	2.3(1)
F	1.3(1)

The fastest rate constants occurred for substituted styrenes with electron-donating groups (methoxyl and methyl) while electron-withdrawing groups (chloro, fluoro) lowered the addition rate constants. Even though the error bars are large but the results are showing a general Trans. The methoxyl group is known as more powerful electron donor group than the alkyl group which increases the electron density in the ring and enhances reactive with an electrophile corresponding to an increased rate. Besides, the chloro group is more electrons attracting than fluoro group providing the faster addition rate constants.

However, the haloalkyl and oxygen radicals have been widely investigated.^{62,63} The observations on the rates of addition to styrene were analyzed the data by way of a Hammett correlation indicated that radicals are electrophilic based on the negative value ρ . When the Hammett equation is written in the form of $\log (k/k_H) = \sigma\rho$. k and k_H are the rate constants for the reaction of the substituted and unsubstituted compounds,

respectively. ρ is the reaction constant (a measure of the sensitivity of the reaction series to changes in electron density at the reaction sites). The σ parameter is the substituent constant (a measure of the ability of the substituent to change the electron density at the reaction sites).⁶⁴ From this overview, the rate constants will be evaluated according to a Hammett σ ρ correlation that is expected to yield a negative value ρ , as observed for alkyl and oxygen radicals consistent with electrophilic character of metal-coordinated thiyl radicals.

The *ortho*-substituted styrenes do not have corresponding σ constants in the literature protocol. The relative rates (k/k_H , where k_H is the rate constant for reaction with styrene) toward the addition of $[\text{Ru-1}]^+$ radical intermediate are demonstrated in Table III-4. The electronic effect of the *para*-substituent on the formation of the dithioether complex is expressed in the terms of the reaction constant ρ , which is determined as -0.7 ± 0.2 from the Hammett plot of logarithm of the relative rates of additions against σ constants in Figure III-8. The negative ρ -value is consistent with the view of the thiyl radical as an electrophilic nature. Thus a nucleophilic character on the substituted styrene is promoted by further resonance stabilization from the second-order substituent effect especially on the *para*-position. All *para*-positions result increase reactivity.

Table III-4: Relative rates of substituted styrenes toward $[\text{Ru-1}]^+$ intermediate at 298 K

Substituents	k/k_H	$\log(k/k_H)$
<i>para</i>-substituted styrene		
OCH ₃	0.97	-0.02 ± 0.22
CH ₃	0.83	-0.08 ± 0.14
Cl	0.47	-0.33 ± 0.27
F	0.41	-0.39 ± 0.26
<i>meta</i>-substituted styrene		
OCH ₃	1.24	0.09 ± 0.25
CH ₃	1.68	0.22 ± 0.46

Cl	0.53	-0.28 ± 0.18
F	0.35	-0.45 ± 0.22

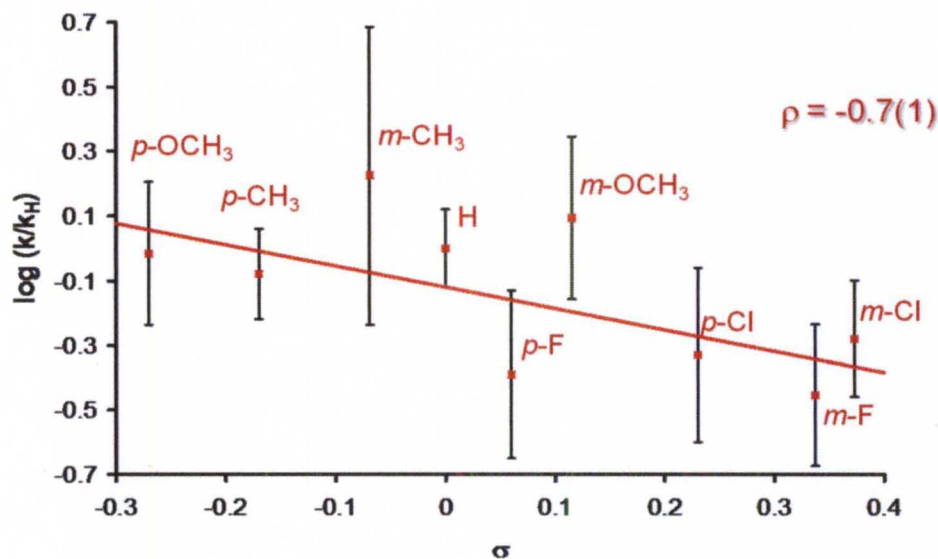


Figure III-8. Correlation of $\log(k/k_H)$ for styrenes with Hammett σ parameter. The solid line is the result of a least best fit to all points for the *para*-substituted styrenes and for the *meta*-substituted styrenes.

The ρ value obtained in the *meta*-position is higher than *para*-position ($\rho = -1.3 \pm 0.1$ with best fit linear), Figure III-8. The negative value can be explained as the same *para*-position interaction. However, the higher value of the *meta*-position disobeys the Hammett correlation along the resonance effect. This fact indicates that *meta*-position adds faster than the *para*-position; although, the addition reaction is enhanced for *para* series. Therefore, the limits of experimental error for these can be assumed. There are no Hammett parameters available for *ortho*-substituents. One might expect the effect on the reaction constant ρ value of *ortho*-substituted styrenes to be similar in magnitude to *para*-substituted styrenes, because of resonance effects through the aromatic ring.

Interestingly, the effect of substitution can also be described by the electrochemical properties. This study has been reported by Graham in 2001 focused on the electrochemical and xerographic properties of triarylamine and correlation to the Hammett parameters of the substituent and calculated HOMO energy level.⁶⁵ Our study will demonstrate the same method. The Hammett linear relationship can be applied to measure changes in half-wave potentials of electrochemical redox reactions following the term of $\Delta E_{1/2} = \sigma \rho$.⁶⁶ In this case, σ , a substituent constant, measures the electron-donating or electron-withdrawing characteristic of styrene derivatives, and ρ , the reaction constant, determines the sensitivity of the reaction of the electron-donating or attracting characteristic of substituent.

The cyclic voltammograms of **[Ru-1]** are obtained in the presence of *para*- and *meta*-substituted styrenes resulting **[Ru-1·alkene]^{2+/+}**. The half-wave potential ($E_{1/2}$) are calculated from the average between the oxidation and reduction peak for a given couple. Plots of $E_{1/2}$ versus Hammett σ yield a linear relationship from which the reaction constants are defined, Figure III-9. The ρ values for *para* and *meta*-substituent are 34.5 and 23.6, respectively. The higher reaction constant of *para*-position increases the reactivity as expected. As a result of changing the second order substituent, the electrochemical properties are found to obey the Hammett relationship. A positive Hammett parameter is referred that the functional group is electrophilic. The binding ability of these styrene derivatives is elucidated that the electron-donating groups are easily reduced than the electron-withdrawing groups and the oxidations are occurred in the opposite.

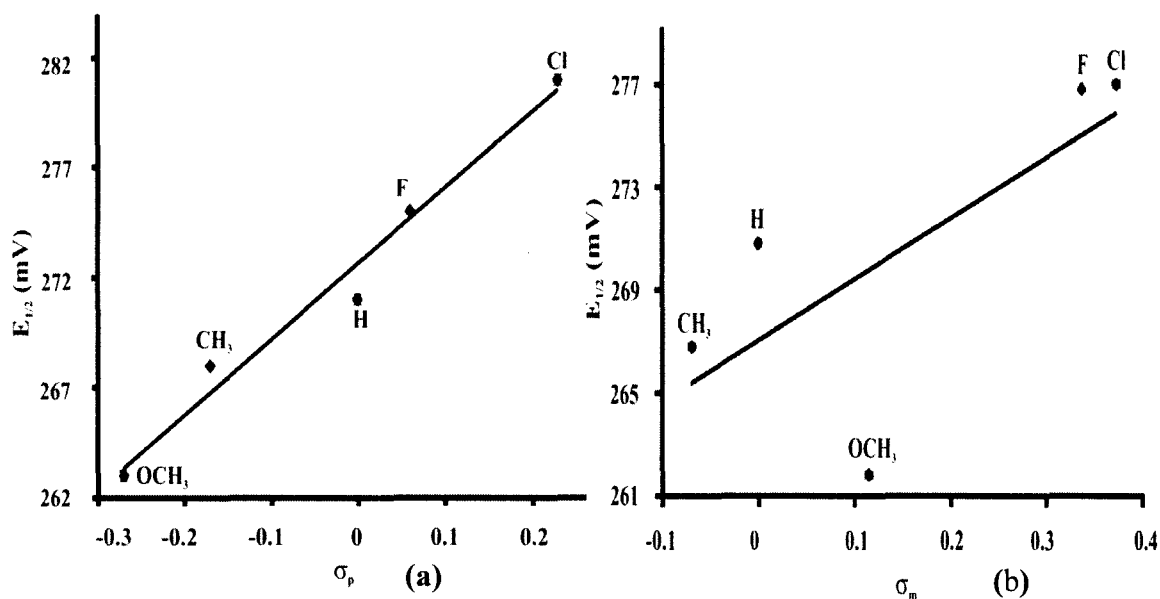


Figure III-9. Correlation of $E_{1/2}$ for styrenes with Hammett σ parameter. The solid line is the result of a least best fit to all points. (a) is the result of best fit for the *para*-substituted styrenes and (b) for the *meta*-substituted styrenes.

In summary, the occurrence new peaks in the CV and the shifted potentials clearly note that the intermediate $[\text{Ru-1}]^+$ reacts with various alkenes to yield respective Ru(II) dithioether compounds. Moreover, the rate constants of substituted alkenes are obtained from the powerful simulation program based on the recorded CV in the multiple scan rates. From the addition of alkenes, the metal-thiolate complex suggests as the electrophilic behavior. The faster rate constants are observed with for electron-rich alkenes and cyclic alkenes with ring strain. The shift potentials evaluation allows predicting the rate constant of reaction. Furthermore, the electronic effects also provide a measure of the relative reactivity of the substituted styrene toward the metal-coordinated thiyl radicals. The results for both *para* and *meta*-substituent confirm the electrophilic character of thiyl radicals from the reaction constant in the Hammett correlation. Few

compounds with *ortho*-substituent also measured the rate constants; although, no Hammett parameters are available to investigate the effect of *ortho*-substitution on styrenes with the intermediate radicals behavior. However, the experimental methods could not be applied accurately to an investigation of the corresponding reaction with substituted styrenes. The electrochemical investigations on the second order substituent are supported the Hammett correlation.

Chemical Syntheses

In addition to electrochemical methods, $[\text{Ru-1}\cdot\text{alkene}]^{2+/+}$ derivatives can be prepared by chemical oxidants via the EECE pathway. Selected alkene derivatives were prepared including those based on styrenes and cyclohexene.

$[\text{Ru-1}]^-$ with *m*-methylstyrene and *p*-methylstyrene

To solution of $[\text{Ru-1}]^-$ and *m*-methylstyrene or *p*-methylstyrene in acetonitrile was added to the blue solution of FcPF_6 (2.0 equiv.) in acetonitrile resulting in a green-yellow solution after 3 hours stirring. The solvent was removed and washed with hot water and diethyl ether yielding a desired yellow product, as the hexafluorophosphate salt. X-ray quality crystals were obtained by slow evaporation of a CH_2Cl_2 /hexane solution of $[\text{Ru-1}\cdot\textit{m}\text{-methylstyrene}]^+$ or $[\text{Ru-1}\cdot\textit{p}\text{-methylstyrene}]^+$. The spectroscopic and electrochemical figures are shown in Appendix C, D, and E. The (+)ESI-MS $[\text{Ru-1}\cdot\textit{m}\text{-methylstyrene}]^+$ derivatives display a dominate peak at $m/z = 1099.20$, consistent with the expected value of 1099.15. The $[\text{Ru-1}\cdot\textit{p}\text{-methylstyrene}]^+$ and $[\text{Ru-1}\cdot\textit{m}\text{-methylstyrene}]^+$ complexes have a single absorbance band in the visible region with λ_{max} (ϵ , $\text{M}^{-1} \text{cm}^{-1}$) values of 370 nm (6227) and 370 nm (9280), respectively. These bands are assigned as charge transfer bands from the thiolate ligand to the metal. The cyclic

voltammograms of $[\text{Ru-1}\cdot p\text{-methylstyrene}]^+$ and $[\text{Ru-1}\cdot m\text{-methylstyrene}]^+$ show $E_{1/2}$ values of +284 mV and +224 mV, correspondingly. The $\text{Ru}^{\text{III/II}}$ couples are shifted by approximately +1100 mV with respect to $[\text{Ru-1}]^{0/+}$.

When $[\text{Ru-1}\cdot\text{alkene}]^+$ complexes are synthesized from mono-substituted alkenes such as *p*-methylstyrene, one of several isomers may be obtained. The alkene addition can position the substituent group nearest the sulfur trans to phosphorous or nearest the sulfur trans to sulfur as shown in Figure III-10. Moreover, the five member chelate ring may be in the δ or λ configuration. The geometrical preference of DPPBT ligand in octahedral metal complexes has been exclusively meridional and exists as an enantiomeric mixture of the Λ and Δ isomers.⁶⁷ For the alkene addition products, the “trans to S” product has been observed, Figure III-11. This observation is consistent with Tedder’s Rules for radical species with alkene addition, which demonstrates that the substitution initially occurs at the non-substituted carbon atom in alkene.^{68,69} The sulfur trans to π accepting phosphine is firstly reacted with the non-substituted carbon and the R-group of alkene is added to nearest sulfur trans to sulfur. This mechanistic insight is consistent with electron density calculation.³⁵ The chelate ring conformation correlates with the overall chirality of the complex with Δ isomers yielding δ rings and Λ isomers favoring λ rings.

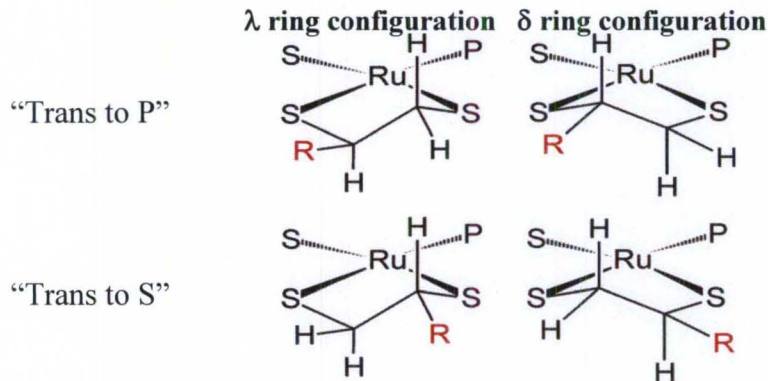


Figure III-10. Four possible isomers of $[\text{Ru-1-alkene}]^+$, only isomers with the R group in the “equatorial” position were considered. The R substituent can be located nearest S “trans to P” or “trans to S”. The ligand chelate ring can be a λ or δ configuration.

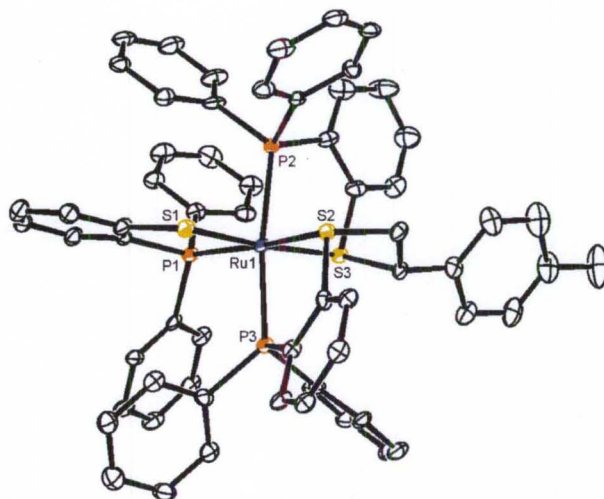


Figure III-11. ORTEP representations of the complex cation $[\text{Ru-1-}p\text{-methylstyrene}]^+$. This structure shows only the “trans to S” isomer. Crystals contain both the Λ and Δ isomers of the complex with λ or δ chelate rings, respectively.

Even though the mass spectrum and the cyclic voltammograms of $[\text{Ru-1-}p\text{-methylstyrene}]^+$ are presented as a single product, the ^{31}P NMR spectra of $[\text{Ru-1-}p\text{-}$

methylstyrene]⁺ is unique as it shows two sets of peaks consistent with two similar isomer products, but non-magnetically equivalent meridional P₃ donor sets. This is associated with the presence of isomers of **[Ru-1-*p*-methylstyrene]⁺, Figure III-12. The results are reliable with the explanation above. The chemical shifts are temperature-independent, ruling out interconverting configurational isomers.**

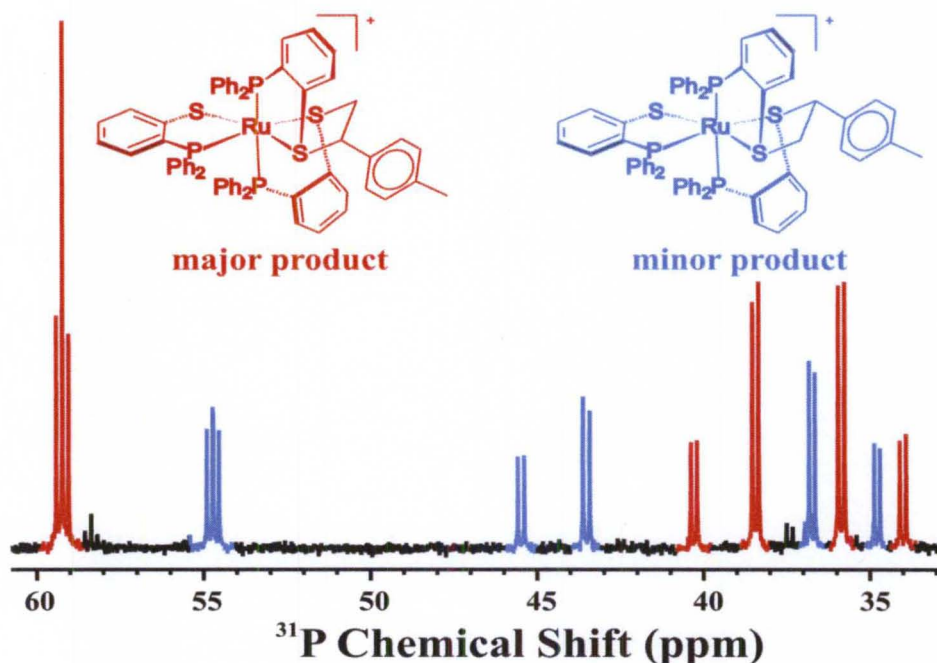


Figure III-12. ³¹P NMR of **[Ru-1-*p*-methylstyrene]⁺ as isolated in CD₃CN shows a pair of second order spectra assigned to a pair of structural isomers that differ by the relative position of the alkene substituent. Chemical shifts and coupling constants are provided**

The meridional arrangement of the three P donors positions one phosphorus, P₁, trans to S1 and two phosphorus donors, P₂ and P₃, trans to each other. Due to the chirality of the complex, the P₂ and P₃ donors are in the similar, but inequivalent magnetic environments resulting in slightly different chemical shifts for both. Additionally, these trans P nuclei are strongly coupled (~300 Hz). Since the difference in the resonance

frequency for these nuclei is similar to the coupling between them, a second order spectrum is observed. The actual position of the chemical shifts δ_2 and δ_3 are calculated using second order equation, Figure III-13.⁷⁰

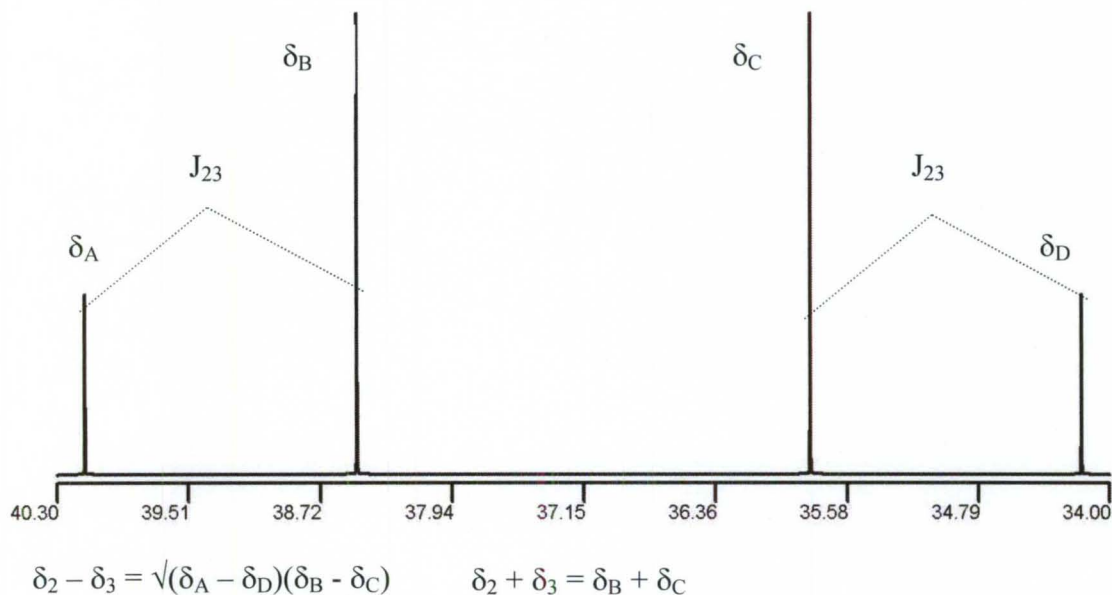


Figure III-13. ³¹P NMR second order spectra.

The major product (65%) displays a second-order spectrum with chemical shifts (ppm) of $\delta_1 = 59.2$, $\delta_2 = 39.2$, and $\delta_3 = 35.1$ and coupling constants (Hz) of $J_{12} = J_{13} = 30$ and $J_{23} = 300$. These coupling constants and chemical shift values are very close to that of anticipated values and are very much similar to the data recorded from the previous literatures indicating that the phosphorus environment has not changed.^{31,32,42,71} A similar second-order spectrum of the minor product accounts for 35% of the NMR intensity with chemical shifts (ppm) of $\delta_1 = 54.7$, $\delta_2 = 44.4$, and $\delta_3 = 35.9$ and coupling constants (Hz) of $J_{12} = J_{13} = 28$ and $J_{23} = 316$. The major isomer of **[[Ru-1-*p*-methylstyrene]⁺** is separable by recrystallization. A yellow crystals sample is prepared and then the ³¹P

NMR is collected. Finally, the spectrum shows the major component, Figure III-14. The mother liquor contains a mixture of major and minor isomer. The ^{31}P NMR spectrum of $[\text{Ru-1-}m\text{-methylstyrene}]^+$ shows similarly three chemical shifts and coupling constants at 59.3 ppm, 39.1 ppm, 35.2 ppm, and 30 Hz, 300 Hz for the major component, and 54.8 ppm, 44.3 ppm, 35.9 ppm, and 32 Hz, 318 Hz for the minor component, Figure F-1 in Appendix F.

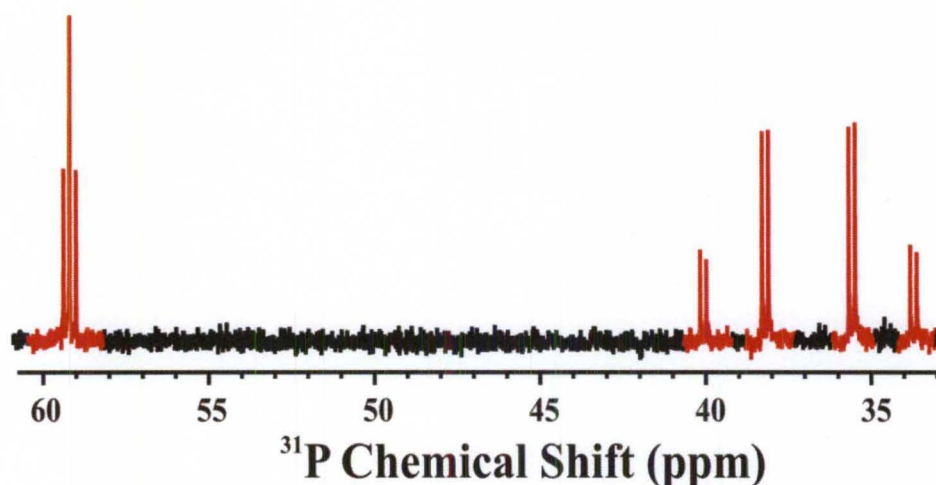


Figure III-14. ^{31}P NMR of $[\text{Ru-1-}p\text{-methylstyrene}]^+$ as isolated crystal in CD_3CN shows a pair of second order spectra assigned to a pair of structural isomers that differ by the relative position of the alkene substituent.

Yellow X-ray quality crystals of $[\text{Ru-1-methylstyrene}]^+$ were obtained by the slow evaporation of $\text{CH}_2\text{Cl}_2/\text{hexane}$. The complexes of $[\text{Ru-1-}m\text{-methylstyrene}]^+$ and $[\text{Ru-1-}p\text{-methylstyrene}]^+$ crystallize as yellow plates in the monoclinic and triclinic space group, correspondingly, with unit cell dimensions, Table G-1 to G-4 Appendix G.⁷²⁻⁷⁴ An ORTEP representation of the $[\text{Ru-1-}m\text{-methylstyrene}]^+$ is shown in Figure III-15 and $[\text{Ru-1-}p\text{-methylstyrene}]^+$ has been displayed on Figure III-11.

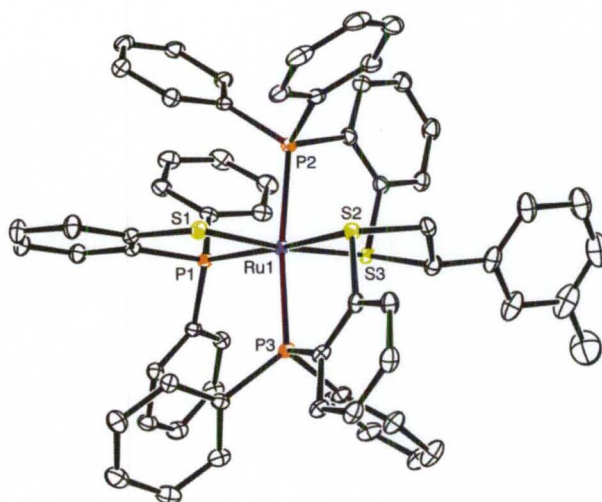


Figure III-15. ORTEP representations of the complex cation **[Ru-1·*m*-methylstyrene]⁺**. This structure shows only the “trans to S” isomer. Crystals contain both the Λ and Δ isomers of the complex with λ or δ chelate rings, respectively.

The selected bond distances and angles provided in the Table III-5. The cation of **[Ru-1·methylstyrene]⁺** contains a single ruthenium ion situated in a pseudo-octahedral P_3S_3 donor environment with phosphorus and sulfur donors arranged in a meridional fashion. The thioether sulfur donors S2 and S3 are bridged by C-C bond linker, while S1 is a thiolate donor. As comparison within these two methylstyrene derivative complexes, C55-C56 bond lengths are approximately between 1.483(13) Å to 1.501(6) Å consistent with a single bond character which well supports with the ethylene addition. The carbon sulfur bond lengths for S2-C55 and S3-C56 are from 1.818(4)Å to 1.838(9) Å and from 1.883(4)Å to 1.867(10) Å, respectively. These values are very close to expected values for a C-S single bond. All bond distances and angles are similarly close each other, which agree the formation of the thioether bridge.^{32,42,55,75}

Table III-5. Selected bond distances (Å) and bond angles (deg) for **[Ru-1·C₂H₄]⁺**, **[Ru-1·*m*-methylstyrene]⁺**, and **[Ru-1·*p*-methylstyrene]⁺**

	[Ru-1·C₂H₄]⁺	[Ru-1·<i>m</i>-methylstyrene]⁺	[Ru-1·<i>p</i>-methylstyrene]⁺
Ru-S1	2.3856(9)	2.3735(9)	2.389(3)
Ru-S2	2.3749(9)	2.3707(9)	2.373(3)
Ru-S3	2.3365(9)	2.3404(9)	2.320(2)
Ru-P1	2.3290(9)	2.3423(9)	2.333(3)
Ru-P2	2.3965(10)	2.3623(9)	2.350(3)
Ru-P3	2.3648(9)	2.3717(9)	2.391(3)
S2-C55	1.836(4)	1.818(4)	1.838(9)
S3-C56	1.843(4)	1.883(4)	1.867(10)
C55-C56	1.510(5)	1.501(6)	1.483(13)
S2-Ru-S3	87.71(3)	87.86(3)	87.67(9)
P2-Ru-P3	168.81(3)	170.64(3)	169.64(10)
S1-Ru-S2	87.06(3)	85.81(3)	87.14(9)
S1-Ru-S3	173.73(3)	172.50(3)	174.37(11)
S2-C55-C56	114.0(3)	114.1(3)	113.8(7)
S3-C56-C55	112.8(3)	112.0(3)	110.1(7)

[Ru-1]⁺ with Cyclohexene

Following with the same experimental methodology as mentioned in methylstyrene complexes, cyclohexene addition to the **[Ru-1]⁺** is chemically synthesized. This was confirmed by all applicable techniques including electrochemical, basic spectroscopic methods. Figure C-3 in Appendix C, Figure D-3 in Appendix D, and Figure E-12 in Appendix E are reported. Tables for crystallographic data are provided in Table G-5 to G-7, Appendix G. The cyclic voltammograms of isolated **[Ru-1·cyclohexene]⁺** show $E_{1/2}$ value of +269 mV at scan rate, 200 mV/s. A larger Ru^{III/II} shift potential ($\Delta = 1099$ mV) is consistent with the modification of two thiolates. The shift potential from the chemical method and from the electrochemical method is slightly different, which is explained due to experimental error. The mass spectra show parent peaks at 1063.17 amu and theoretical mass at 1063.31 amu.

Furthermore, the ^{31}P NMR of the product yields in high percentages, which allow estimating the chemical shifts and coupling constants. A second-order spectrum is defined with chemical shifts (ppm) of $\delta_1 = 54.8$, $\delta_2 = 39.5$, and $\delta_3 = 36.5$ and coupling constants (Hz) of $J_{12} = J_{13} = 29$ and $J_{23} = 313$. These anticipated values of **[Ru-1·cyclohexene]⁺** are very much similar to the data acquired from **[Ru-1·methylstyrene]⁺** indicating that the phosphorus environment has not changed.^{42,75} The ^{31}P NMR results the desired product in the spectrum, Figure III-16.

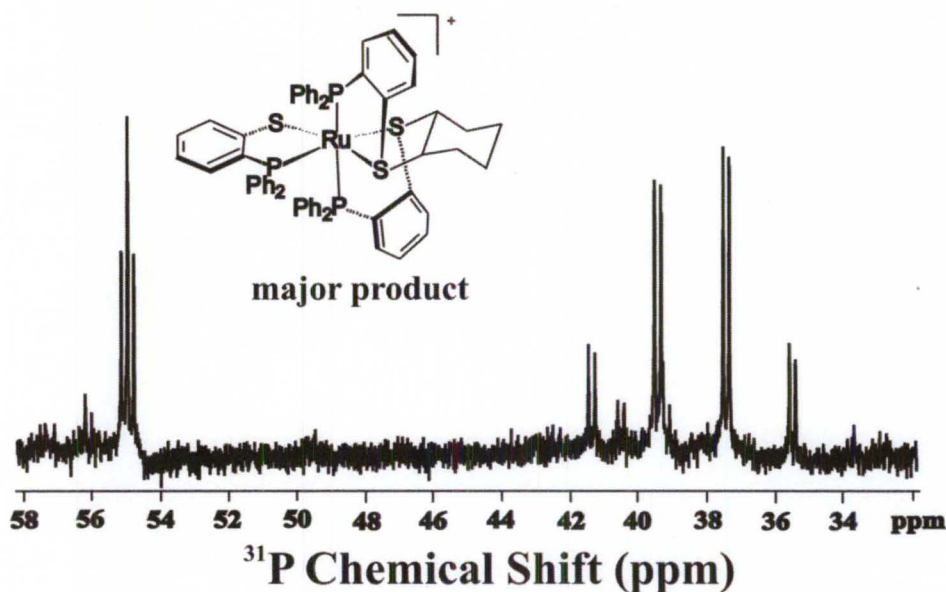


Figure III-16. ^{31}P NMR of **[Ru-1·cyclohexene]⁺** as isolated in CD_3CN shows second order spectrum.

The structure of **[Ru-1·cyclohexene]⁺** has been determined by single-crystal X-ray techniques. The space group and unit cell dimensions table are demonstrated in Appendix G. An ORTEP representation of the ruthenium containing cation of asymmetric unit is displayed in Figure III-17. The structural model has one full occupancy and occupancy dichloromethane solvate molecules. The Ru ion sits in pseudo-

octahedral P_3S_3 donor arranged in an environment with phosphorus and sulfur donors arranged in a meridional fashion. The thioether sulfur donors S2 and S3 are bound with carbon-carbon linker, while S1 is a thiolate donor. Even though, the cyclohexene is disubstituted alkene as cis configuration, the selective bond distances and angles are not quite variable values as compared with the other two structures of $[Ru-1 \cdot C_2H_4]^+$ and $[Ru-1 \cdot p\text{-methylstyrene}]^+$, Table III-6. The C-C and C-S bonds correlated with the cyclohexene bridge are corresponds with single bond character with values of 1.515(5) Å, 1.865(4) Å, and 1.886(4) Å for C55-C60, S2-C55, and S3-C60, respectively.

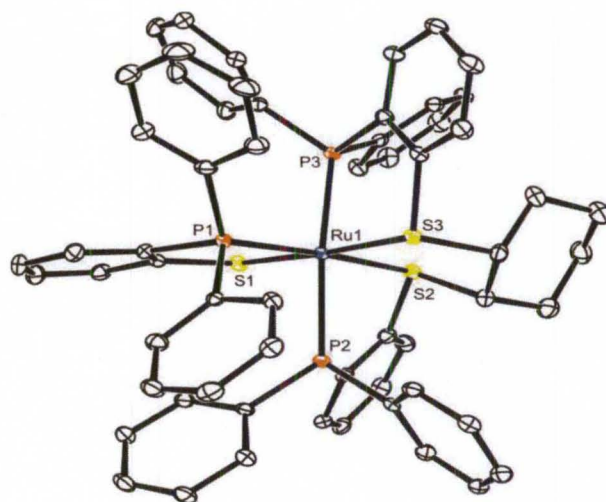


Figure III-17. ORTEP representations of the complex cation $[Ru-1 \cdot \text{cyclohexene}]^+$.

Table III-6. Selected bond distances (Å) and bond angles (deg) for **[Ru-1·C₂H₄]⁺**, **[Ru-1·cyclohexene]⁺**, and **[Ru-1·*p*-methylstyrene]⁺**

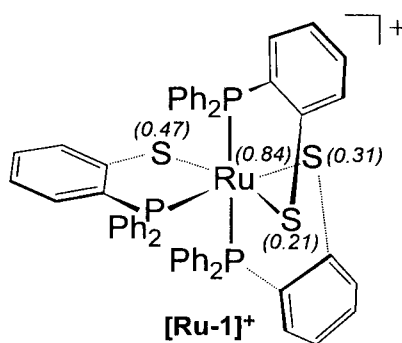
	[Ru-1·C₂H₄]⁺	[Ru-1·cyclohexene]⁺	[Ru-1·<i>p</i>-methylstyrene]⁺
Ru-S1	2.3856(9)	2.3899(9)	2.389(3)
Ru-S2	2.3749(9)	2.3722(9)	2.373(3)
Ru-S3	2.3365(9)	2.3363(9)	2.320(2)
Ru-P1	2.3290(9)	2.3351(9)	2.333(3)
Ru-P2	2.3965(10)	2.4172(9)	2.350(3)
Ru-P3	2.3648(9)	2.3273(9)	2.391(3)
S2-C55	1.836(4)	1.865(4)	1.838(9)
S3-C56	1.843(4)	1.886(4) S3-C60	1.867(10)
C55-C56	1.510(5)	1.515(5) C55-C60	1.483(13)
S2-Ru-S3	87.71(3)	85.07(3)	87.67(9)
P2-Ru-P3	168.81(3)	168.71(3)	169.64(10)
S1-Ru-S2	87.06(3)	92.77(3)	87.14(9)
S1-Ru-S3	173.73(3)	175.70(3)	174.37(11)
S2-C55-C56	114.0(3)	114.1(3)	113.8(7)
S3-C56-C55	112.8(3)	110.4(2)	110.1(7)

This chapter provided an in depth study of the reactivity of the ruthenium coordinated DPPBT ligand. The intermediate **[Ru-1]⁺** has the electrophilic behavior leading to the C-S bond formation This study focuses on the steric and electronic effects with mono-substituted alkenes. The observed rate constants obtain using the digital simulation from the cyclic voltammograms. The isolated products are performed by the electrochemical and chemical methods. The similar reactivity will be explored in the next chapter with the selected group of other substrates.

CHAPTER IV

REACTIVITY OF $[\text{Ru}(\text{DPPBT})_3]^+$ WITH OTHER UNSATURATED SUBSTRATES

As reported on Chapter III, the oxidized metal thiolate complex of $[\text{Ru-1}]^+$ reacts with alkenes to form thioether complexes. The addition rates were investigated for a variety of mono-substituted alkenes. The reactivity of the intermediate $[\text{Ru-1}]^+$ is consistent with its assignment as a metal-stabilized thiyl radical complex.^{35,75} Based on DFT calculations, the electronic ground state of $[\text{Ru-1}]^+$ can be best described as a singlet diradical. Significant spin density is observed as Ru (0.84), S1 (0.47), S2 (0.31), and S3 (0.21) as shown in Scheme IV-1.



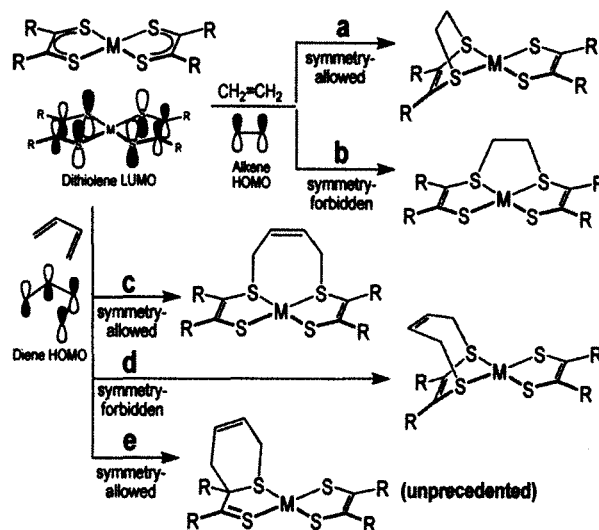
Scheme IV-1. Metal-coordinated thiyl radical complex with calculated spin density values (*italics*).

The addition of alkenes occurs selectively across the S2/S3 sulfur pair which is clearly explained by the different directionality of these lone pairs as compared with S1 as mentioned earlier. The in-phase combination of the S2/S3 p-type orbitals interacts in an antibonding capacity with the metal d_{yz} orbital generating a half-occupied, frontier molecular orbital. This orbital has the proper symmetry to interact with the HOMO of approaching alkene.

The addition of alkenes to the metal-stabilized thiyl radical $[\mathbf{Ru-1}]^+$ requires a net two electrons process including a two electron reduction in the formal oxidation state of the metal ion. Oxidation of the Ru(II) precursor $[\mathbf{Ru-1}]^-$ by two electrons yields the formally Ru(IV) the intermediate $[\mathbf{Ru-1}]^+$, which can react with alkenes resulting in reduction of the metal back to a formal Ru(II) product. Combined bulk electrolysis and cyclic voltammetry experiments demonstrate the alkenes addition to the reactive $[\mathbf{Ru-1}]^+$ with an irreversible process that allows the experimental determination of the rate constants. The rate constants range from $4.6(5) \times 10^7 \text{ M}^{-1} \text{ s}^{-1}$ for the electron-rich alkenes to $2.7(2) \times 10^4 \text{ M}^{-1} \text{ s}^{-1}$ for electron-poor alkenes. The rate constants for cyclic alkenes range from $4(2) \times 10^7 \text{ M}^{-1} \text{ s}^{-1}$ to $2.9(3) \times 10^3 \text{ M}^{-1} \text{ s}^{-1}$.

The dithiolene metal complexes were described to be ligand-centered reactivity toward olefins. Stiefel and coworkers reported binding of alkenes to an oxidized nickel dithiolene with subsequent release upon reduction, Scheme I-3.¹⁵ Later investigation showed that alkene addition is more complicated.¹⁸ The desired interligand addition is a minor product and a major product as intra-ligand ethylene addition leading to decomposition products.^{15,17,76} Even though the reactivity study had been discovered for decades ago, the mechanism is not well-understood and further. The fundamental

reactivity is needed to fully exploit these systems. Geiger explored further reactivity of the trifluoromethyldithiolato-nickel complex $\text{Ni}(\text{S}_2\text{C}_2(\text{CF}_3)_2)$ with diolefins including norbornadiene, norbornene, and 2,3-dimethyl-1,2-butadiene. The electrochemical data revealed adduct formation between the olefinic donors and oxidized Ni-dithiolene. The reactions achieved a reversible process.¹⁸ In later studies by Fekl, diene addition to metal-dithiolenes was predicted based on molecular orbitals diagrams. The addition of 2,3-dimethyl-1,2-butadiene yields interligand C-S bond formation on $[\text{Pt}(\text{tfd})_2]$ ($\text{tfd} = \text{S}_2\text{C}_2(\text{CF}_3)_2$). The product was characterized using the NMR spectroscopy. However, not only the desired product was obtained but also symmetry allowed complex was discovered during the characterization. The formation of C-S intraligand complex is unprecedented for the dithiolene ligand. The new ligand reactivity is underway to discover, Scheme IV-2.⁷⁷



Scheme IV-2

Initially works by Stiefel on the alkene addition products of metal-dithiolenes were proposed as the inter-ligand addition, which is not symmetry allowed product. The

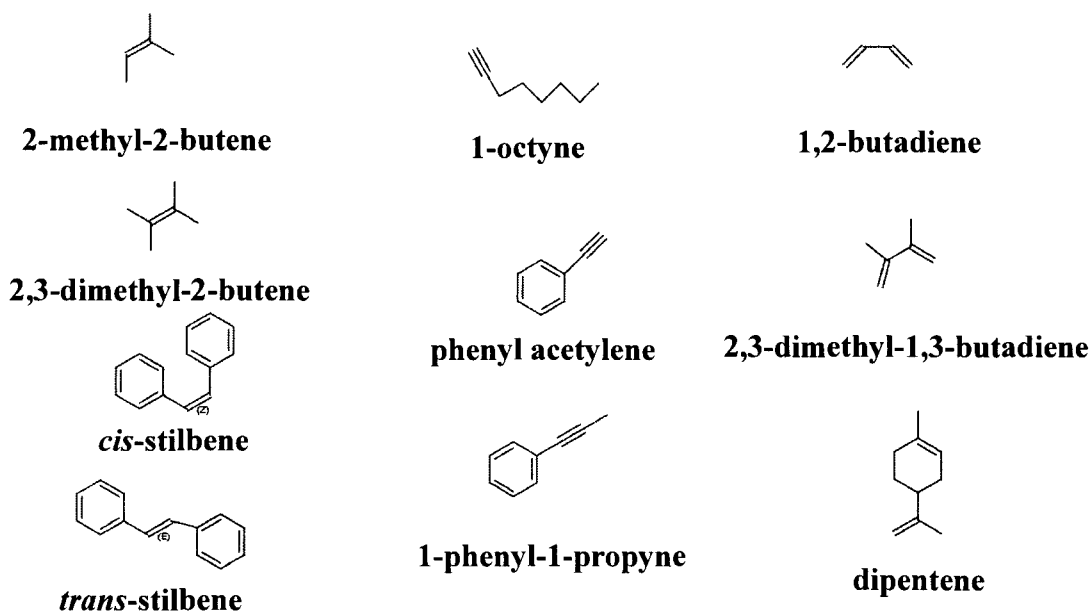
reaction is slow resulting in the intraligand byproduct and complex decomposition attributed to the electronical and steric effects of the ligand. To improve the addition reaction, a push-pull molybdenum complex was prepared through a new design of ligand which contains the electron donating and electron withdrawing groups. The present work from Fekl group introduces a new reactivity of molybdenum trisdithiolenes complex toward alkenes. The first investigation focused on reactivity of $[\text{Mo}(\text{tfd})_3]$ and $[\text{Mo}(\text{bdt})_3]$ ($\text{bdt} = \text{S}_2(\text{C}_6\text{H}_4)$) with ethylene. The ethylene addition is shown to yield the intra-ligand complex on the S-alkylated dithiolene donor as the product with no evidence of side reactions.⁷⁸⁻⁸¹ This Mo-trisdithiolene complex was also employed for alkyne addition which displayed selective side-on coordination to a single dithiolene donor. However, this intraligand product was not further isolated during the reaction.⁸²

Yan and coworkers described disulfuration and hydrosulfuration of an alkyne at 1,2-dicarba-*clos*o-dodecaborane-1,2-dithiolate ligand from the alkyne addition to the chelating cobalt complex.⁸³ The dinuclear ruthenium(I)/ruthenium(III) half sandwich = complexes were synthesized using the same ligand. The purpose of study focused on the addition of alkyne to the diruthenium complex to activate B-H bond formation from metal-chacologens.^{84,85}

For our $[\text{Ru-1}]^+$ intermediate, the ground state is a diradical that can react with various alkenes at rate sufficient to prevent the formation of disulfide. Further reactions will focus on whether the diradical will react more preferentially towards double bond with multi-substituted alkenes instead of mono-substituted alkenes, alkynes, and dienes. This reactivity can lead to many interesting facts for olefin purification.

The work reported in this chapter is focused on the reactivity of **[Ru-1]⁺** with a variety of poly-substituted alkenes, alkynes, and dienes. To investigate this reactivity, a 5 mL acetonitrile solution of **PPN[Ru-1]** with TBAHFP as supporting electrolyte was prepared and the square wave voltammetry was used to screen the reactions. Moreover, the rate constants are also obtained by the collection cyclic voltammograms (CV) data after screening process with all the scan rates applying to the simulation program. All CV data are provided in the detailed in above. Then square wave voltammograms (SW) are recorded in the Appendix E-13 to Appendix E-22. Therefore, our new approach is focused on substrates as shown in Scheme IV-3.

The alkenes employed include 2-methyl-2-butene, 2,3-dimethyl-2-butene, *cis*-stilbene, and *trans*-stilbene. The alkynes are 1-octyne, phenyl acetylene, and 1-phenyl-1-propyne. The dienes group ranges from 1,3-butadiene, 2,3-dimethyl-1,3-butadiene to the monocyclic ring, dipentene. Then the selective substrates will be further investigated by preparation via the chemical method. The products are fully characterized.



Scheme IV-3. Selected alkenes, alkynes, and dienes.

Electrochemical Measurements

The scope of reactivity is screened using the cyclic voltammetry (CV) technique for the fast scanning. A 2.0 mM solution of **PPN[Ru-1]** is prepared in the electrochemical cell with three electrodes. With a pre-equilibrium time set to 15 seconds, the potential is scanned from an initial value (-600 mV) to a switching point (1200 mV) versus Ag/AgCl reference, after which the potential is scanned back to the original value. All potentials are reported versus ferrocenium/ferrocene (Fc^+/Fc). The CV shows two events at -830 mV and -20 mV assigned as $[\text{Ru-1}]^{-/0}$ and $[\text{Ru-1}]^{+/0}$, respectively.⁴⁰ A 0.2 M of substrate is added to the analyte. The solution is mixed by purging the nitrogen gas for 3 minutes. The CV reveals three events. The two events attributed to the thiolate complex are still observed at the negative potentials but they are slightly shifted toward the negative potential. The $[\text{Ru-1}]^{+/0}$ redox couple decreases the intensity as compared in

the absence of substrate. This results from a shift in equilibrium according to LeChatlier's principle. The reason is pointed out that the chemical step occurs to generate the Ru-dithioether product with this thiolate complex, $[\text{Ru-1}]^+$. A new event is consistent with the formation of $\text{Ru}^{\text{III}}/\text{Ru}^{\text{II}}$ dithioether complex shown potential between +260 mV to +320 mV which is shifted from +1090 mV to +1150 mV as compared to the trithiolate, $[\text{Ru-1}]^{-/0}$. The large shift is explained as the conversion of two thiolate donors to thioethers.

Reactivity of $[\text{Ru-1}]^+$ with multi-substituted Alkenes

The protocol is performed as mentioned above. The CV was performed in the presence of *cis*-stilbene. The three events obtain potential at -830 mV, -32 mV, and +314 mV. This voltammogram is recorded after the addition of substrate, Figure IV-1.

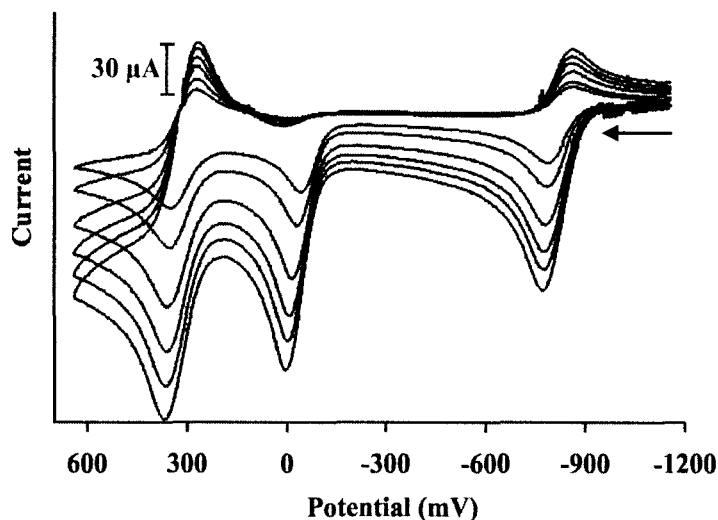


Figure IV-1. Cyclic voltammogram of 2.0 mM complex $[\text{Ru-1}]^+$ in acetonitrile with 0.1 M TBAHFP was obtained in the presence of *cis*-stilbene (0.20 M) at multiple scan rates, 100 mV/s to 1000 mV/s. Potentials referenced to Fc^+/Fc .

The addition reaction is proposed to proceed via an EC mechanism in which **[Ru-1]**⁺ occurs in the electrochemical step and then reacts with *cis*-stilbene to form **[Ru-1·cis stilbene]**⁺ in the chemical step. This **[Ru-1·cis stilbene]**⁺ is further oxidized by one more electron to form the new event which is shifted around +1140 mV corresponding to the dithioether complex. The rate constant is observed as $8.8 \times 10^2 \text{ M}^{-1}\text{s}^{-1}$ using the DigiSim software package.⁵² This rate is approximately 5 orders of magnitudes slower than styrene addition rate due to the second substituent group on the alkene.

The next observation is applied with *trans*-stilbene. The voltammogram shows no reactivity with this *trans* substituted alkene as demonstrated in Figure IV-2. Two possibilities can be used to explain this observation. Either the addition rate is too slow to measure on the scale time for the electrochemical method or no reaction occurs under any condition. Presuming the former, the CV data collected over multiple scan rates predicts a maximum second order rate constant of $1.1 \times 10^1 \text{ M}^{-1} \text{ s}^{-1}$. The rate constant of *trans*-stilbene addition would be approximately 80 times lower than *cis*-stilbene. Instead of the electrochemical method, the chemical method will be utilized to investigate the reactivity with the fully characterizations as mentioned below section.

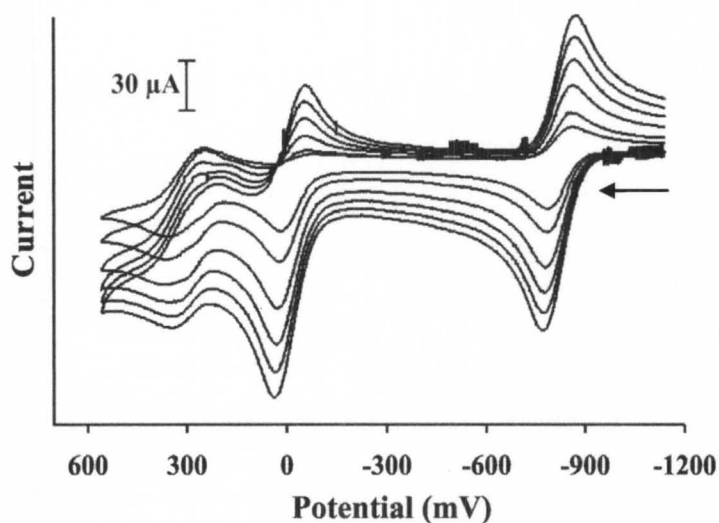
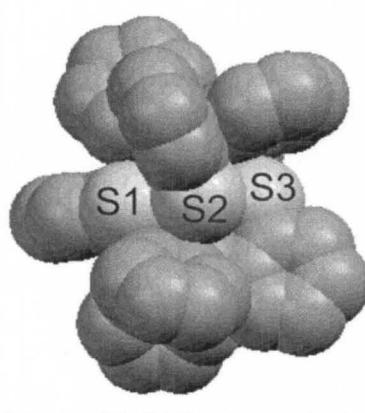


Figure IV-2. Cyclic voltammogram of 2.0 mM complex $[\text{Ru-1}]^+$ in acetonitrile with 0.1 M TBAHFP was obtained in the presence of *trans*-stilbene (0.20 M) at multiple scan rates, 100 mV/s to 1000 mV/s. Potentials referenced to Fc^+/Fc .

The slow reactivity of the *trans*-stilbene may be ascribed to the steric bulk effect from the bidentate PS chelate 2-diphenylphosphine benzenethiolate (DPPBT), Scheme IV-4. The slow reaction rate may be due to a high entropic barrier, which is consistent with a large structural reorganization required for C-S bond formation with a large R-group alkene. DFT calculation by Davinder will investigate cis and trans effect.



Scheme IV-4. Space filling model of $[\text{Ru-1}]^+$.

Addition of tri-substituted alkene 2-methyl-2-butene to $[\text{Ru-1}]^+$ results a dithioether complex with a distinct $[\text{Ru-1}\cdot\text{alkene}]^{2+/+}$ redox couple. The cyclic voltammogram of $[\text{Ru-1}]$ in presence of 2-methyl-2-butene is shown in Figure IV-3. In presence of 2-methyl-2-butene, a new event assigned to $[\text{Ru-1}\cdot\text{Mebutene}]^{2+/+}$ is observed at +238 mV, while the anodic peak current associated with $[\text{Ru-1}]^{+/0}$ is greatly diminished at -31 mV. This result is proved the reaction with rapid addition upon oxidation of $[\text{Ru-1}]^0$ to $[\text{Ru-1}]^+$. Data fitting for the addition of 2-methyl-2-butene to $[\text{Ru-1}]^+$ reveals the rate constant of $1.4 \times 10^2 \text{ M}^{-1} \text{ s}^{-1}$.

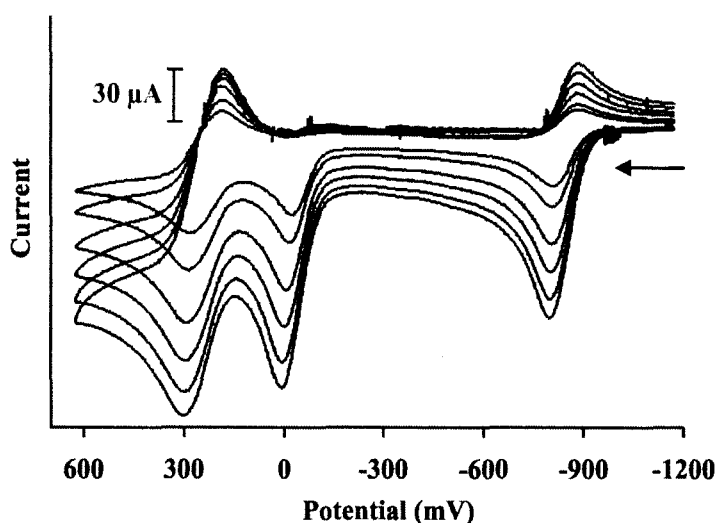


Figure IV-3. Cyclic voltammogram of 2.0 mM complex $[\text{Ru-1}]$ in acetonitrile with 0.1 M TBAHFP was obtained in the presence of 2-methyl-2-butene (0.20 M) at multiple scan rates, 100 mV/s to 1000 mV/s. Potentials referenced to Fc^+/Fc .

The CV investigation of $[\text{Ru-1}]$ in the presence of the tetra-substituted alkene 2,3-dimethyl-2-butene (Figure IV-4) reveals only small, but slightly detectable changes. Based on the DigiSim simulations, the observed rate constant requires for C-S bond formation in this reaction is $3.2 \times 10^1 \text{ M}^{-1} \text{ s}^{-1}$. From tri-substituted to tetra-substituted

alkenes, the addition rate is 5 times faster, which is associated with the least substituted carbon binding with sulfur to form C-S bond first and then the di-substituted carbon reacts to form the second C-S bond. When each carbon contains two R groups the increased steric environment, slows the alkene addition.

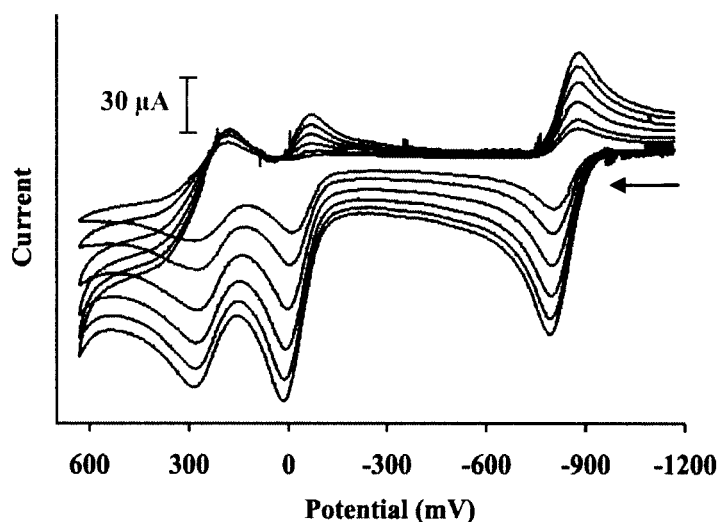


Figure IV-4. Cyclic voltammogram of 2.0 mM complex [Ru-1]⁻ in acetonitrile with 0.1 M TBAHFP was obtained in the presence of 2,3-dimethyl-2-butene (0.20 M) at multiple scan rates, 100 mV/s to 1000 mV/s. Potentials referenced to Fc⁺/Fc.

In reality, the most stable double bonds are those with the most R groups attached. In other words, the R groups attached to the double-bonded carbon stabilize the alkene. The relative energies of typical π bonds compared with ethylene using molar heats of hydrogenation method shows the sequences of increase from tetra-substituted alkene to unsubstituted. Overall, the mono-substituted alkene employs higher addition rate than the di-substituted alkene approximately 5000 times. Between cis and trans position, the reaction occurs with cis conformation due to the allowed symmetry and detectable time scale on the techniques. However, alkenes substituted in the trans positions are slow to

add due to the steric effect of chelating ligand around metal coordination. Tri-substituted alkene reacts with the metal-stabilized thiyl radical faster than tetra-substituted alkene due to vacant R group allowance. The steric and substituent effects of alkenes lower the reaction rate. The summary of square wave data with the rate constants are provided on Table IV-1.

Table IV-1: CV data for [Ru-1·alkene]^{2+/+} with rate constants.

	Potential (vs Fc ⁺ /Fc) (mV)	Rate Constant (M ⁻¹ s ⁻¹)	Shift Potential (mV)
	E ₄	k _f	ΔE
<i>cis</i> -stilbene	314	8.8 × 10 ²	1144
<i>trans</i> -stilbene	307	1.1 × 10 ¹	1137
2-methyl-2-butene	238	1.4 × 10 ²	1068
2,3-dimethyl-2-butene	226	3.2 × 10 ¹	1056

Reactivity of [Ru-1]⁺ with Alkynes

Regarding alkene addition investigations, oxidation and charge state of the metal-stabilized thiyl radical requires a net two electron reduction to yield an accessible oxidation state in the alkene addition product. As reported earlier, alkene addition to the electrophilic character of the metal-stabilized thiyl radicals enhances with less substituted alkenes and vice-verse with the more substituted alkenes. The addition product can further oxidize to generate accessible redox couples. However the reduction product is not observed due to the unavailable solvent window. The result is likely to be irreversible process for the addition alkene product. The product is more stable, which allow evaluating the rate constants of reaction. Further efforts to develop new complexes to demonstrate the scope and limits of this reactivity, addition reaction of alkenes to the metal-stabilized thiyl radical [Ru-1]⁺ will be extended to alkynes. Alkynes investigated include 1-octyne, phenyl acetylene, and 1-phenyl-1-propyne. The expected addition

products include S-alkylated dithiolene ligands using similar electrochemical oxidation strategies as mentioned on alkenes.

The addition of 1-octyne to electrochemically generated $[\text{Ru-1}]^+$ is monitored in fast scan by cyclic voltammetry. As illustrated in Figure IV-5, the voltammogram of $[\text{Ru-1}]^-$ records in the presence of 1-octyne displays two anodic peaks associated with the oxidation of $[\text{Ru-1}]^-$ to $[\text{Ru-1}]^0$ and $[\text{Ru-1}]$ to $[\text{Ru-1}]^+$ at -830 mV and -60 mV, respectively. Following the third oxidation, 1-octyne rapidly adds to $[\text{Ru-1}]^+$ producing $[\text{Ru-1}\cdot\text{octyne}]^+$ as identified by $\text{Ru}^{\text{III/II}}$ redox couple at +302 mV.

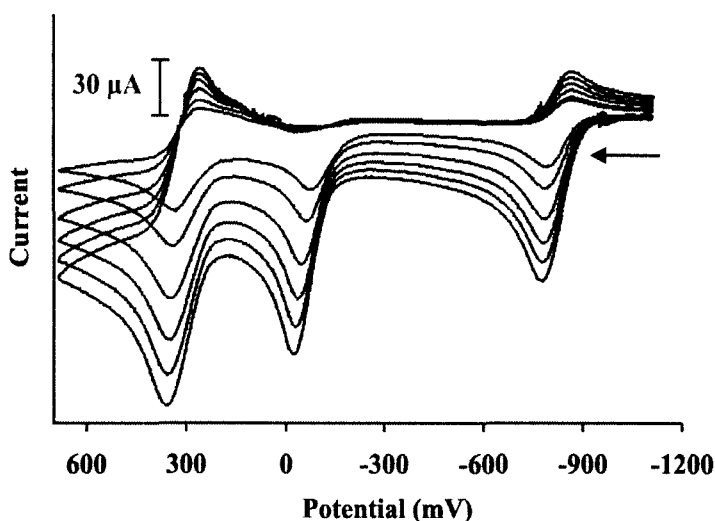


Figure IV-5. Cyclic voltammogram of 2.0 mM complex $[\text{Ru-1}]^-$ in acetonitrile with 0.1 M TBAHFP was obtained in the presence of 1-octyne (0.20 M) at multiple scan rates, 100 mV/s to 1000 mV/s. Potentials referenced to Fc^+/Fc .

The binding product is also evident by the decrease in anodic current for the $[\text{Ru-1}]^{+/0}$ couples. The rate constant for 1-octyne addition to $[\text{Ru-1}]^+$ is evaluated using the methods previously described for alkene addition. A series of cyclic voltammograms are collected over a range of scan rates, 100 to 1000 mV/s, for solutions containing $[\text{Ru-1}]^-$

and 1-octyne . A second-order rate constant of $8.7 \times 10^3 \text{ M}^{-1} \text{ s}^{-1}$ is obtained for this addition reaction. This value is two orders of magnitude lower than the corresponding alkene addition rate constant for 1-hexene to $[\text{Ru-1}]^+$, $7.0 \times 10^5 \text{ M}^{-1} \text{ s}^{-1}$. A rate decrease between 100 to 1000 times is typical for the electron donating group of alkynes and alkenes.

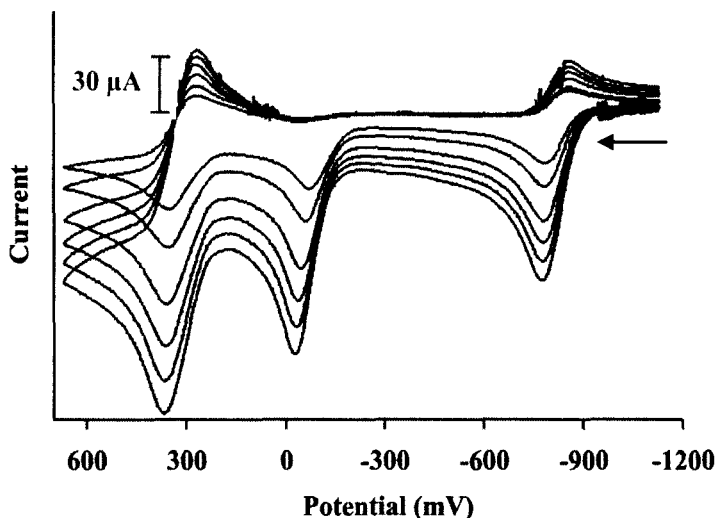


Figure IV-6. Cyclic voltammogram of 2.0 mM complex $[\text{Ru-1}]$ in acetonitrile with 0.1 M TBAHFP was obtained in the presence of phenyl acetylene(0.20 M) at multiple scan rates, 100 mV/s to 1000 mV/s. Potentials referenced to Fc^+/Fc .

The alkyne addition rates also correspond to our earlier observation based on the substituent effects of alkenes to the $[\text{Ru-1}]^+$ which interacts as the electrophilic character as demonstrated with phenyl acetylene as adduct. The phenyl acetylene is electron rich, which enhances the nucleophilicity on the triple bond. The rate constant increases as compared to 1-octyne. Next, the CV obtains with $[\text{Ru-1}]$ in presence of phenyl acetylene. The similar result reveals as three events potentials at -830 mV, -61 mV, and +311 mV, Figure IV-6. The rate constant for phenyl acetylene is determined as 1.2×10^4

$M^{-1} s^{-1}$. This value affects the rate in two orders of magnitudes corresponding to the addition rate of styrene, $4.6 \times 10^7 M^{-1} s^{-1}$. The evidence shows the rate is significantly faster as compared with 1-octyne.

In addition of mono-substituted alkynes, di-substituted alkynes are utilized to evaluate the reactivity. The CV of $[Ru-1]^-$ solutions in presence of 1-phenyl-1-propyne reveal a new peak. The new peak is identified at potential of +304 mV, while the reactive species of $[Ru-1]^{+/0}$ redox couple diminishes its intensity peak at -25 mV providing the evidence of the addition reaction take place, as noted in Figure IV-7. This alkyne, 1-phenyl-1-propyne, displays a second order rate constant of $2.3 \times 10^2 M^{-1} s^{-1}$.

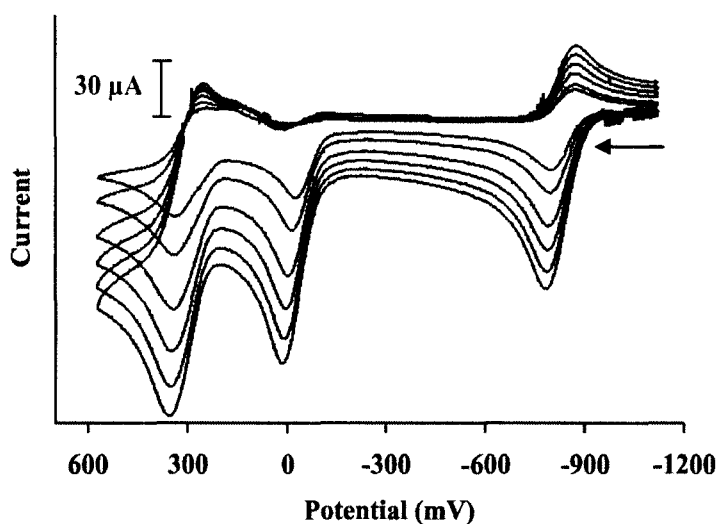


Figure IV-7. Cyclic voltammogram of 2.0 mM complex $[Ru-1]^-$ in acetonitrile with 0.1 M TBAHFP was obtained in the presence of 1-phenyl-1-propyne(0.20 M) at multiple scan rates, 100 mV/s to 1000 mV/s. Potentials referenced to Fc^+/Fc .

For alkynes, the rate constant is related to the substituent effect; $k_{\text{phenylacetylene}} > k_{\text{octyne}} > k_{\text{phenylpropyne}}$, Table IV-2. A variety of alkynes can be added to $[Ru-1]^+$ upon the oxidation to yield the corresponding S-alkylated dithiolenes-Ru(II) derivatives. The

addition proceeds via an electrophilic behavior of $[\text{Ru-1}]^+$ with faster rate constants observed with mono-alkynes. Moreover, the addition rate is found to be approximately 100 times lower than corresponding alkenes in line with the electrophilic character of the ruthenium-stabilized thiyl radical.

Table IV-2: CV data for $[\text{Ru-1}\cdot\text{alkyne}]^{2+/+}$ with rate constants.

	Potential (vs Fc^+/Fc) (mV)	Rate Constant ($\text{M}^{-1} \text{s}^{-1}$)	Shift Potential (mV)
	E_4	k_f	ΔE
1-octyne	302	8.7×10^3	1132
phenyl acetylene	311	1.2×10^4	1141
1-phenyl-1-propyne	304	2.3×10^2	1134

Reactivity of $[\text{Ru-1}]^+$ with Dienes

The study of reactions between alkenes and alkynes and metal complexes has been mentioned above. In these addition reactions, unsaturated hydrocarbons coordinate directly across two sulfur atoms, forming the dithioether or dithiolene complexes. The scope of reactivity is investigated by using cyclic voltammetry technique. The new peak shows the formation of C-S bonds; however, the further structure characterization will be fully described in the next chemical method. The addition rate constants are determined from the simulation program DigiSim. As a result, the rates accelerate or decelerate depending on not only electronic effect but also steric effect from the substituent side of alkenes and alkynes. So the next reactivity scenario is different, which will focus on dienes group. The reason is the competitive addition as 1,2-addition or 1,4-addition. The dienes group is including 1,3-butadiene, 2,3-dimethyl-1,3-butadiene, and dipentene. In this stage, we concentrate on the reactivity. The characterization will explain in the next section.

The cyclic voltammogram of $[\text{Ru-1}]^-$ recorded in the presence of 1,3-butadiene reveals these three events at -830 mV, -101 mV, and +271 mV, Figure IV-8. The new intense peak at +271 mV occurs; meanwhile the decreased peak at -101 mV is consistent with the intermediate, $[\text{Ru-1}]^+$. This observation confirms the C-S bond formation in the reaction scheme. From scan rates dependence of CV data, the rate constant value for this C-S bond formation is determined as $2.4 \times 10^5 \text{ M}^{-1} \text{ s}^{-1}$. The fast rate of 1,3-butadiene is consistent with an electron rich behavior.

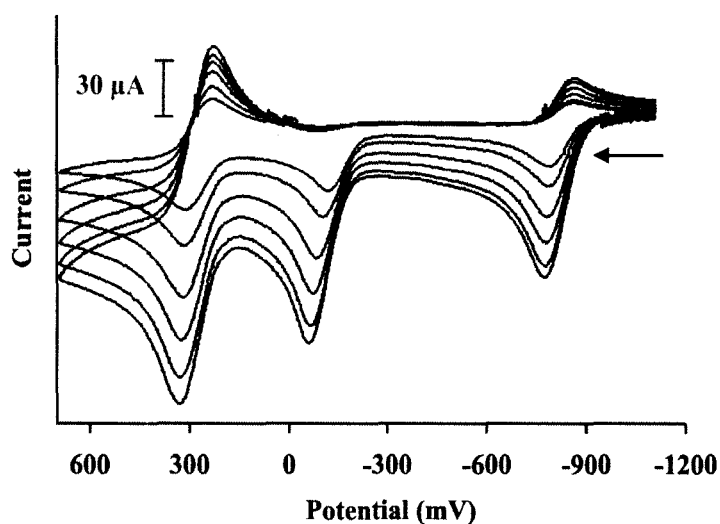


Figure IV-8. Cyclic voltammogram of 2.0 mM complex $[\text{Ru-1}]^-$ in acetonitrile with 0.1 M TBAHFP was obtained in the presence of 1,3-butadiene (0.20 M) at multiple scan rates, 100 mV/s to 1000 mV/s. Potentials referenced to Fc^+/Fc .

2,3-dimethyl-1,3-butadiene is employed to view the reactivity with $[\text{Ru-1}]^+$. The solution of $[\text{Ru-1}]^-$ measures the voltammogram in the presence of 2,3-dimethyl-1,3-butadiene. In Figure IV-9 a new peak with high intensity at +267 mV is shown. This is evidence of the formation of C-S bonds corresponding to the addition of dienes to two across sulfur atoms. The observed rate value is $1.1 \times 10^3 \text{ M}^{-1} \text{ s}^{-1}$.

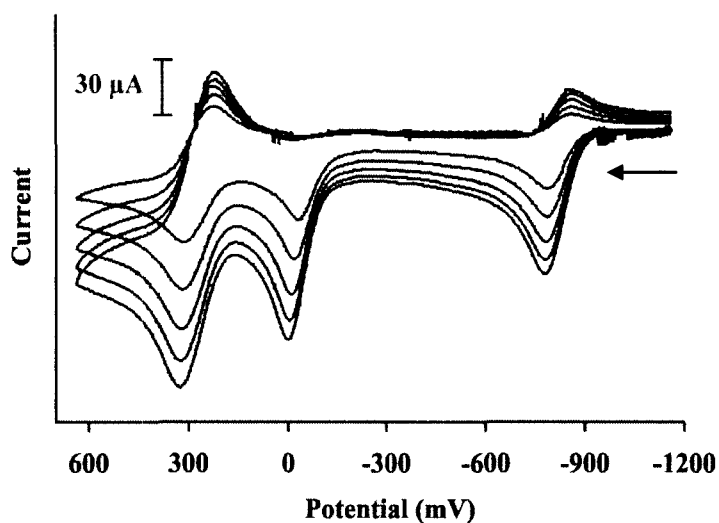


Figure IV-9. Cyclic voltammogram of 2.0 mM complex **[Ru-1]** in acetonitrile with 0.1 M TBAHFP was obtained in the presence of 2,3-dimethyl-1,3-butadiene (0.20 M) at multiple scan rates, 100 mV/s to 1000 mV/s. Potentials referenced to Fc^+/Fc .

The discovery of reactivity is expected to show in the presence of dipentene which contains the side selection and the possibility is on alkene or cyclic alkene. The further description is explored in the synthesis section. In here, the CV is collected in the presence of dipentene for the **[Ru-1]** solution, as illustrated in Figure IV-10. The potential of +269 mV is corresponding to the C-S generation. For CV scan rates dependence, the rate value is evaluated as $2.5 \times 10^4 \text{ M}^{-1} \text{ s}^{-1}$.

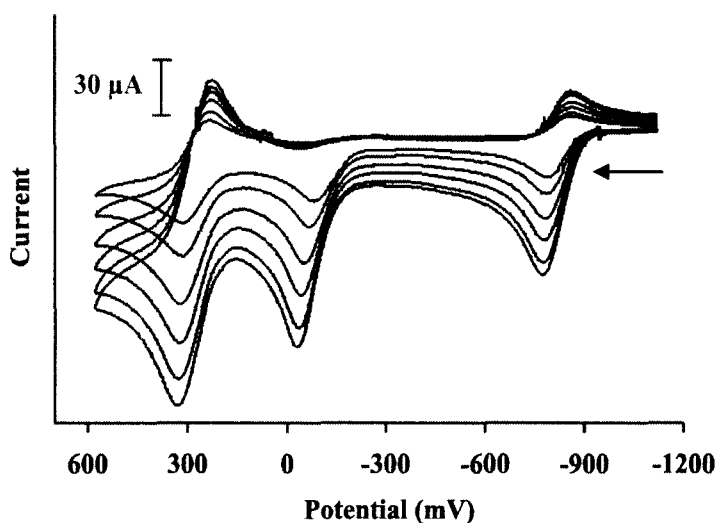


Figure IV-10. Cyclic voltammogram of 2.0 mM complex $[\text{Ru-1}]^-$ in acetonitrile with 0.1 M TBAHFP was obtained in the presence of dipentene (0.20 M) at multiple scan rates, 100 mV/s to 1000 mV/s. Potentials referenced to Fc^+/Fc .

The reactions of $[\text{Ru-1}]^+$ are demonstrated as ligand-centered reactivity toward dienes. From the comparable conformation, 1,3-butadiene addition toward the reactive $[\text{Ru-1}]^+$ reveals the faster rate constant than 2,3-dimethyl-1,3-butadiene, Table IV-3. The dipentene addition rate is in between the two dienes.

Table IV-3: CV data for $[\text{Ru-1}\cdot\text{diene}]^{2+/+}$ with rate constants.

	Potential (vs Fc^+/Fc)	Rate Constant	Shift Potential
	(mV)	($\text{M}^{-1} \text{s}^{-1}$)	(mV)
	E_4	k_f	ΔE
1,3-butadiene	271	2.4×10^5	1101
2,3-dimethyl-1,3-butadiene	267	1.1×10^3	1097
Dipentene	269	2.5×10^4	1099

Overall, the addition of unsaturated substrates to metal-stabilized thiyl radical shows general trend, Table IV-4. The multi-substituted alkenes react slower than the mono-substituted alkenes. The rate constant for alkyne addition are found to be

approximately 100 times lower than the alkenes with an electrophilic metal-coordinated thiyl radical. From alkynes to dienes, the observation revealed the faster addition is dienes but in contrast, the general preference is still alkenes.

Table IV-4: CV data for $[\text{Ru-1}\cdot\text{substrate}]^{2+/+}$ with rate constants.

Substrates	Rate Constant, k_f ($\text{M}^{-1} \text{s}^{-1}$)
styrene	4.6×10^7
<i>m</i> -methyl styrene	7.2×10^7
<i>p</i> -methyl styrene	3.6×10^7
<i>n</i> -propyl vinyl ether	2.0×10^7
<i>tert</i> -butyl vinyl ether	2.6×10^6
1-hexene	7.0×10^5
acrylonitrile	2.7×10^4
norbornene	4.0×10^7
cyclopentene	6.0×10^6
cyclohexene	2.9×10^3
<i>cis</i> -stilbene	8.8×10^2
<i>trans</i> -stilbene	$\leq 1.1 \times 10^1$
2-methyl-2-butene	1.4×10^2
2,3-dimethyl-2-butene	$\leq 3.2 \times 10^1$
phenyl acetylene	1.2×10^4
1-octyne	8.7×10^3
1-phenyl-1-propyne	2.3×10^2
1,3-butadiene	2.4×10^5
dipentene	2.5×10^4
2,3-dimethyl-1,3-butadiene	1.1×10^3

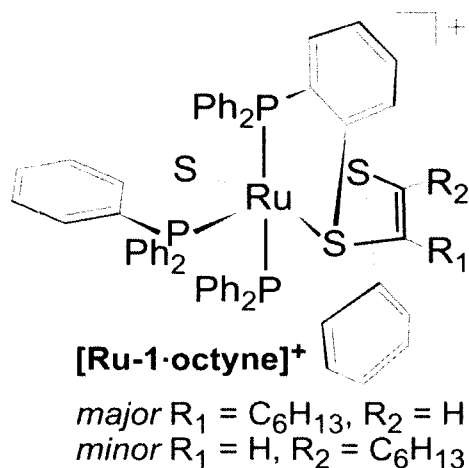
Chemical Syntheses

All the above mentioned data from the electrochemical technique clearly indicate that $[\text{Ru-1}]^+$ intermediate reacts with various substrates to yield the respective Ru-dithioether compounds in case of multi-substituted alkenes and dienes or Ru-dithiolene in case of alkynes. The CV simulation data provide the addition rate constants. For further characterization, the chemical method is applied. Spectroscopic analyses of the chemically synthesized complexes (such as CV, IR, UV-vis, ESI-MS, and EA) confirm a

dialkylated product. The ^{31}P NMR data is utilized to show the number of isomer products as demonstrated previously in Chapter III. Further, X-ray crystallographic studies provide the most definitive assignment of structure.

The chemical synthesis follow the same experimental methodology as described in Chapter III, with the slight change that reactions are allowed to stir overnight. In case of 1-octyne, single crystals of **[Ru-1-octyne]PF₆** are obtained. The yellow solid of **[Ru-1-octyne]PF₆** is crystallized from THF/hexane. The ESI-MS spectrum displays a parent peak at $m/z = 1091.18$, for the desired product, Figure C-6 in Appendix C. Moreover, the cyclic voltammogram of **[Ru-1-octyne]⁺** reveals a single, reversible redox event at +300 mV (vs. ferrocenium/ferrocene), Figure E-25 in Appendix E, assigned to the Ru^{III/II} couple. No other redox couples are observed.

Single crystals of **[Ru-1-octyne]PF₆** for X-ray diffraction studies were obtained by evaporation of chlorobenzene/hexane mixtures. The asymmetric unit consists of co-crystallized mixtures of two geometric isomers, Scheme IV-5. Unlike the related alkene addition product **[Ru-1-*p*-methylstyrene]PF₆**, the isomers of **[Ru-1-octyne]PF₆** could not be separated by crystallization or other methods.⁷⁵ Analyses of multiple crystals consistently reveal co-crystallized products. The isomers differ based on the relative position of the hexyl side chain, which can be located either at the R₁ (nearest S trans to S, major) or R₂ (nearest S trans to P, minor) position.



Scheme IV-5. Representation of [Ru-1-octyne]⁺.

An ORTEP representation of the major [Ru-1-octyne]⁺ isomer is provided in Figure IV-11.⁸⁶ The [Ru-1-octyne]⁺ complex contains a pseudo-octahedral Ru ion in a meridional P₃S₃ donor environment. Ru-S and Ru-P bond lengths range from 2.3106(15) to 2.3890(14) Å and 2.3294(14) to 2.3823(14) Å, respectively, in accord with related structures, Table IV-5.^{32,42,75}

The alkynyl carbon atoms of 1-octyne provide a bridge, C55 and C56, between the *cis*-sulfur donors, S2 and S3. The S2-C55 and S3-C56 bond lengths of 1.798(8) and 1.796(7) Å, respectively, confirm covalent attachment of 1-octyne to the metal-stabilized thiyl radical core with values similar to those observed in alkene addition products such as [Ru-1-C₂H₄]⁺. The S2-C55-C56-S3 torsion angle, 8.3(8)°, approaches zero as expected for an S-alkylated dithiolene chelate; in contrast to the torsion angle of -47.3(3)° for the dithioether fragment in [Ru-1-C₂H₄]⁺. The C55-C56 bond length, 1.322(10) Å, matches the values of 1.312(9) and 1.394(10) Å reported by Yan in their alkyne addition products and is consistent with a C-C double bond.^{84,85}

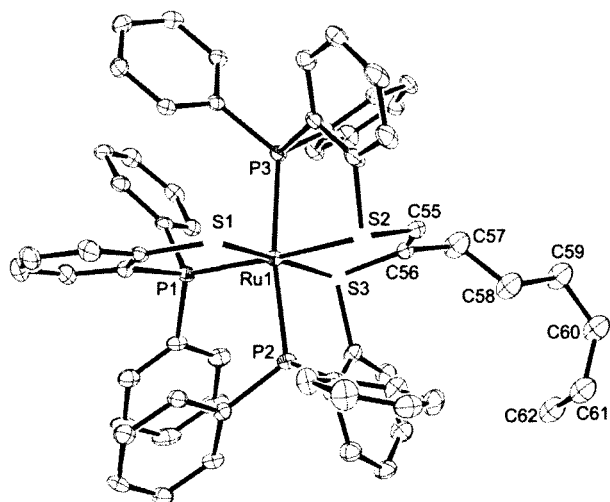


Figure IV-11. ORTEP representations of the complex cations $[\text{Ru-1}\cdot\text{octyne}]^+$.

Table IV-5. Selected bond distances (Å) and bond angles (deg) for $[\text{Ru-1}\cdot\text{octyne}]^+$, $[\text{Ru-1}\cdot\text{C}_2\text{H}_4]^+$, and $[\text{Ru-1}]^+$

	$[\text{Ru-1}\cdot\text{octyne}]^+$	$[\text{Ru-1}\cdot\text{C}_2\text{H}_4]^+$	$[\text{Ru-1}]^+$
Ru-S1	2.3890(14)	2.3856(9)	2.402(1)
Ru-S2	2.3663(15)	2.3749(9)	2.445(1)
Ru-S3	2.3106(15)	2.3365(9)	2.394(1)
Ru-P1	2.3294(14)	2.3290(9)	2.295(1)
Ru-P2	2.3422(14)	2.3965(10)	2.353(1)
Ru-P3	2.3823(14)	2.3648(9)	2.340(1)
S2-C55	1.798(8)	1.836(4)	
S3-C56	1.796(7)	1.843(4)	
C55-C56	1.322(10)	1.510(5)	
S2-Ru-S3	86.22(6)	87.71(3)	89.77(2)
Ru-S2-C55	103.1(3)	104.52(12)	
Ru-S3-C56	105.2(3)	103.59(12)	
S2-C55-C56-S3	8.3(8)	-47.3(3)	

The ^{31}P NMR of crystalline $[\text{Ru-1}\cdot\text{octyne}]^+$ displays a pair of second-order spectra, Figure IV-12. The relative intensities, chemical shifts, and coupling constants are also recorded in Figure IV-12. The two isomers have similar values to previously reported for the two isomers of $[\text{Ru-1}\cdot p\text{-methylstyrene}]^+$.⁷⁵ In that study, the isomer with the substituted carbon positioned nearest the S trans to S was identified as the major

product. This is consistent with the higher spin density than the S trans to P. Given similar product ratios, we assign the major isomer of $[\text{Ru-1-octyne}]^+$ likewise.

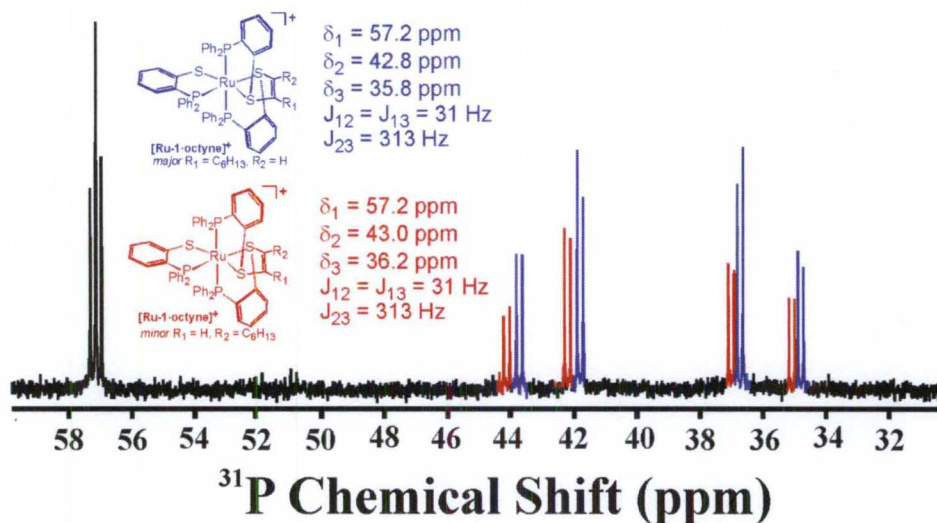


Figure IV-12. ^{31}P NMR of $[\text{Ru-1-octyne}]^+$ as isolated in CD_3CN shows a pair of second order spectra assigned to a pair of structural isomers that differ by the relative position of the alkene substituent.

A summary of results with various substrates from the chemical method is reported in Table IV-6. Products were confirmed by all applicable techniques including electrochemistry, mass spectrometry, and ^{31}P NMR for all substrates. As compared with mono-substituted alkenes, the selected alkenes include *m*-methylstyrene, *p*-methylstyrene, and cyclohexene corresponding to (1), (2), and (3), respectively. The multi-substituted alkenes, alkynes, and dienes put as entries from (4) to (11) referring to *cis*-stilbene, *trans*-stilbene, phenyl acetylene, 1-octyne, 1-phenyl-1-propyne, 1,3-butadiene, 2,3-dimethyl-1,3-butadiene, and dipentene.

Table IV-6: Properties of Ru(II)-substrate complexes.

Substrates	Yield (%)	+ESI-MS (<i>m/z</i>)	Voltammetry $E_{1/2}$ (Ru ^{III/II}) mV
<i>m</i> -methylstyrene(1)	82	1099.20	224
<i>p</i> -methylstyrene(2)	80	1099.20	284
cyclohexene(3)	76	1063.17	269
<i>cis</i> -stilbene(4)	57	1161.20	361
<i>trans</i> -stilbene (5)	70	1161.17	337
phenyl acetylene(6)	42	1083.12	361
1-octyne(7)	43	1091.18	356
1-phenyl-1-propyne(8)	76	1097.13	368
1,3-butadiene(9)	78	1035.12	321
2,3-dimethyl-1,3-butadiene(10)	62	1063.15	332
dipentene(11)	56	1117.20	320

The highest reported yields correspond with the fastest addition rates. As such alkenes addition reactions, achieve yields between 57% to 82%. The alkyne addition yields are slightly lower between 42% to 76%. The diene product yields are between 56% to 78%.

The mass spectra for (4) – (11) show parent peaks with *m/z* values and isotopic distribution similar to theoretical values, Appendix C-4 to Appendix C-11. In each case, the mass spectrum of all products is a single complex. The $E_{1/2}$ value shows a single redox event which indicates one complex for each substrate.

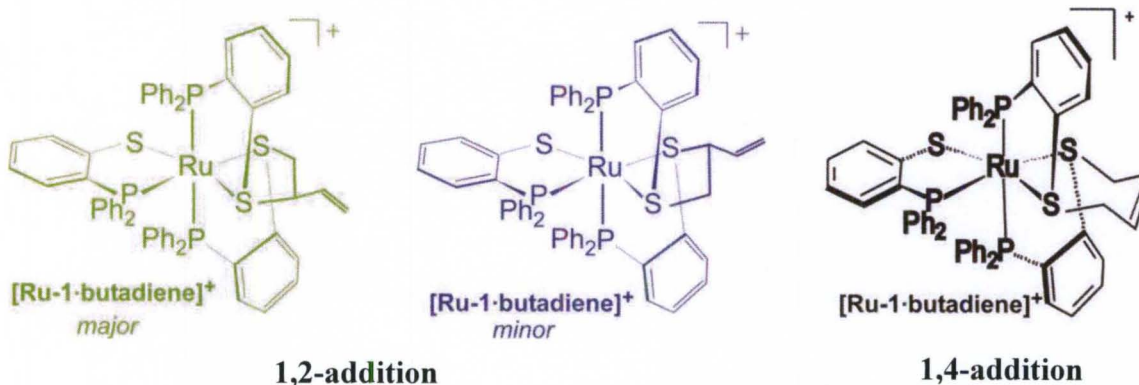
Furthermore, the ³¹P NMR of (4) – (8) show second-order spectra for each substrate from which chemical shifts and coupling constants are extracted, Table IV-7. The ³¹P NMR of alkenes and alkynes observed as two sets of peaks consistent with two similar, but non-magnetically equivalent meridional P₃ donor sets. This is attributed to the presence of two isomers as described above. In contrast, chemical shifts and coupling constants of dienes substrates are not displayed in the table due to complications in product isolation. The electrophilic metal-stabilized thiyl radical may add the conjugated

dienes in two distinct manners, Scheme IV-6. The first product results from 1,2-addition and can be lead to two isomers. In the second product, 1,4-addition, leads to cyclic addition. The transition state leading to 1,2-addition has a lower energy than that leading to 1,4-addition product as well-known. So the 1,2-addition is formed faster (kinetic product). The 1,2-addition product is not as stable as the 1,4-product. If equilibrium is reached, the 1,4-addition product predominates (thermodynamic product). Our hypothesis is 1,2-addition in this case. Based on our ^{31}P NMR, 1,3-butadiene addition is obtained in three compounds which are hardly to isolate, Figure F-8 in Appendix F. Further investigations underway.

Table IV-7: ^{31}P NMR of (4)-(11).

Substrates	Yield (%)		Chemical Shift (ppm)		Coupling Constant (Hz)	
	Major	Minor	Major	Minor	Major	Minor
(1)	65	35	59.3	54.8	30	32
			39.1	44.3	30	32
			35.2	35.9	300	318
(2)	65	35	59.2	54.7	30	30
			39.2	39.2	30	30
			35.1	35.1	300	316
(3)	100		54.8		29	
			39.5		29	
			36.5		313	
(4)	70	30	52.5	54.0	29	30
			42.9	43.7	29	30
			35.6	35.2	315	317
(5)	69	31	57.9	54.1	30	30
			38.5	43.7	30	30
			35.6	35.2	303	318
(6)	57	43	56.7	57.2	30	30
			42.7	43.0	30	30
			36.5	36.0	312	312
(7)	60	40	57.2	57.2	31	31
			42.8	43.0	31	31
			35.8	36.2	313	313
(8)	55	45	55.8	55.5	25	25
			43.3	45.0	25	25

			37.1	35.7	315	316
(11)	62	38	55.0	58.9	30	30
			39.7	43.7	30	30
			34.8	35.8	299	316



Scheme IV-6. Representation of $[\text{Ru-1-butadiene}]^+$.

All substrates react with an electrophilic metal-coordinated thiyl radical yielding C-S bond formation. Even though, the preference is still alkenes. The products are isolated by the chemical synthesis. From the electrochemical and UV-vis data, single product is revealed. But from ^{31}P -NMR, the isomers are observed and also hard to separate these isomers.

CHAPTER V

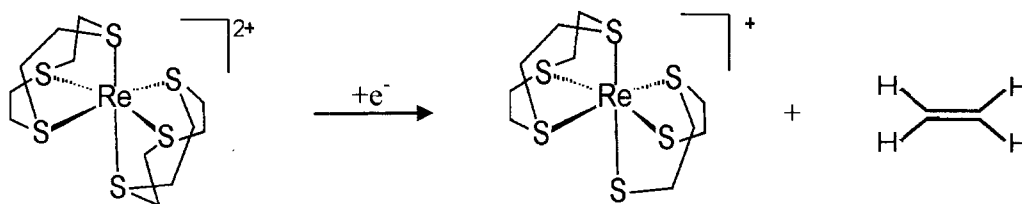
CONCLUSION

In 2001 Wang and Stiefel reported the metal-assisted separation of ethylene from feedstock chemicals utilizing electrochemically regulated C-S bond formation/cleavage as an alternative to current energy intensive purification.¹⁵ However, further studies by Fekl and coworkers indicate that the mechanism was more complicated and not feasible. First, the major products of alkene addition are the deleterious intraligand product leading to decomposition while the desired interligand addition is only a minor product. Second, the reduction potential required for ethylene release complex degradation.^{17,18} In 2009, we published a system that overcomes these obstacles with rapid and reversible C-S bond formation/cleavage in a redox-regulated process.⁵⁵

As highlighted in Chapter III, the oxidation of **[Ru-1]⁻** proceeds in two one-electron steps. The first oxidation, previously assigned as metal-centered, can be readily accomplished by applying potential. Then the product **[Ru-1]** can be further oxidized to **[Ru-1]⁺**. The fully oxidized, **[Ru-1]⁺** complex has been described as a reactive metal-coordinated thiyl radicals.⁴⁰ The generation of a ruthenium-coordinated thiyl radical was demonstrated, and the observed rate of decay to a disulfide was calculated at $10^{-2} \text{ M}^{-1} \text{ s}^{-1}$.

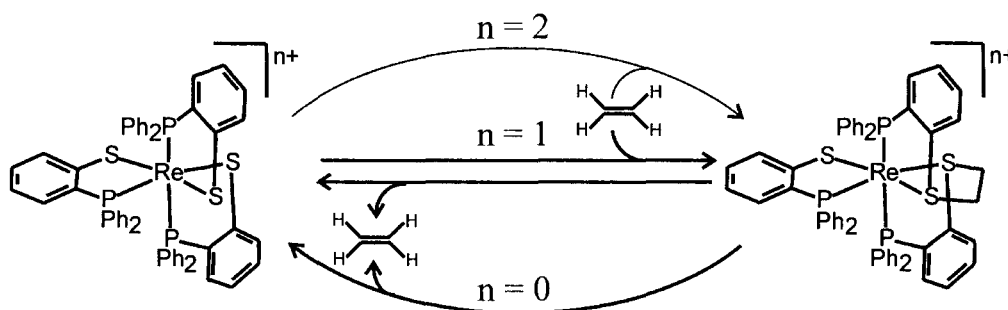
Since the rate of decay is slow enough for detection but fast enough for reactivity, new bond formation utilizing alkenes leading to ruthenium-thioether complexes.

Density functional theory (DFT) investigations by Holly Frye in the Grapperhaus group have sought to determine the ground state of the reactive intermediate, $[\mathbf{Ru-1}]^+$. From those studies, the ground of $[\mathbf{Ru-1}]^+$ is best explained as singlet diradical, as fully mentioned on Chapter III.³⁵ The diradical generated can react with various alkenes at a rate sufficient to prevent observation of the intermediate. The reactivity is proven by reactions with alkenes ranging from simple alkenes, like ethylene, to bulkier, bridged alkenes, like norbornene. In all cases, the resulting product is a Ru(II)-dithioether.⁴² However, the addition of alkenes to $[\mathbf{Ru-1}]^+$ is an irreversible process. To overcome this obstacle, prior work from Went suggests a better choice for reversibility is rhenium (Re).⁴³ Reports of C-S bond cleavage with release of ethylene upon reduction of the Re(II) complex, $[\mathbf{Re}(\mathbf{TTCN})_2]^{2+}$ (TTCN = 1,4,7-trithiacyclononane) provided a lead, Scheme V-1.⁴³ The $\mathbf{Re-1}$ is utilized to see the reactivity with alkenes. Although, $\mathbf{Re-1}$ and $[\mathbf{Ru-1}]^+$ are isoelectronic addition of ethylene proceeds for the ruthenium but not the rhenium complex. This may be due to a charge matter.



Scheme V-1. Reversible C-S bond cleavage $[\mathbf{Re}(\mathbf{TTCN})_2]^{2+}$.

Reversible C-S bond formation/cleavage between a rhenium-thiolate complex and ethylene was described in Chapter III. By regulation of oxidation state and therefore the charge of the complex, the affinity of complex for ethylene can be tuned. The ethylene can be “locked on” in the higher oxidation state or “locked off” in the lower oxidation state. Ethylene binding to the intermediate oxidation state is concentration dependent, Scheme IV-2.



Scheme V-2. Reversible C-S bond formation/cleavage between $[\mathbf{Re-1}]^{n+}$, $[\mathbf{Re-1}\cdot\mathbf{C}_2\mathbf{H}_4]^{n+}$, and oxidized derivatives.

Overall, our sulfur radicals react with alkenes to generate C-S bond formation. This product, which must result from interligand addition, is proven to be stable under nitrogen purge, vacuum and reflux condition. C-S bond cleavage to release alkenes depends on metal and oxidation state. Further studies of $[\mathbf{Re-1}]^+$ investigated the kinetic and the reactivity with other alkenes which is revealed from the oxidized ruthenium thiolate formed C-S bond with alkene addition including 1-hexene, styrene, cyclohexene, and norbornene.

Attempts to measure rate constants for the addition of various alkenes to $[\mathbf{Re-1}]^+$ were unsuccessful. From UV-visible, a rate constant of styrene addition is on the order of $10^{-5} \text{ M}^{-1}\cdot\text{s}^{-1}$, which is below our CV detection limit of $10^{-3} \text{ M}^{-1}\cdot\text{s}^{-1}$. Since the fast

irreversible addition of alkenes $[\mathbf{Ru-1}]^+$ and the assumed rate constants are $\geq 10^{-2} \text{ M}^{-1} \text{ s}^{-1}$, the kinetic study are achieved with this reactive ruthenium thiolate complex. There are three selected group of alkenes. The *para* and *meta*-substituted styrenes are including methoxyl, methyl, chloro and fluoro-substituents. The observed rate constants are using in Hammett Plot to obtain a substituent rate, ρ . Even though, the high error bars are occurred but the data is shown as general Trans. So, the negative ρ (-0.7) suggests an electrophilic metal-coordinated thiyl radical consistent with similar reactions of haloalkyl and *t*-butoxy radicals with substituted styrenes.^{62,63}

The rate constants for the addition of the open chain alkenes are determined. The data are obtained as remarkable results with the small errors. It is consistent with an electrophilic metal-stabilized thiyl radical. The “electron-rich” alkenes styrene, *n*-propyl vinyl ether, and *t*-butyl vinyl ether add more rapidly, while the “electron-poor” acrylonitrile reduces the addition rate. For the cyclic alkenes, the rate constant is related to the amount of ring strain in the alkene precursors. The more ring strain alkene norbornene shows the faster binding as compared to moderate ring strain cyclopentene and less ring strain cyclohexene. The cyclic alkenes are consistent with the linear alkenes as compared in order of the rate constants.⁷⁵

A qualitative overview of the frontier molecular orbitals of $[\mathbf{Ru-1}]^+$ determined by density functional theory calculations is provided in, Figure V-1a. Orbital analysis of the highest singly occupied molecular orbital (SOMO) of $[\mathbf{Ru-1}]^+$ reveals significant contributions from the d_{xz} orbital on Ru and the co-planar, in phase S2- p_z and S3- p_x orbitals in the higher right corner. The highest fully occupied molecular orbital (HOMO) lies in the same plane. The orientation of the sulfur p-type lone pairs perpendicular to the

respective PS chelate plane are shown out phase along with the assigned coordinate system in the lower left corner.³⁵ This half-occupied, frontier molecular orbital has the proper symmetry to interact with the HOMO of the approaching alkene as illustrated in Figure V-1b. The in phase orbital interacts with π -bonding of alkene and out phase orbital interacts with π -antibonding of alkene.

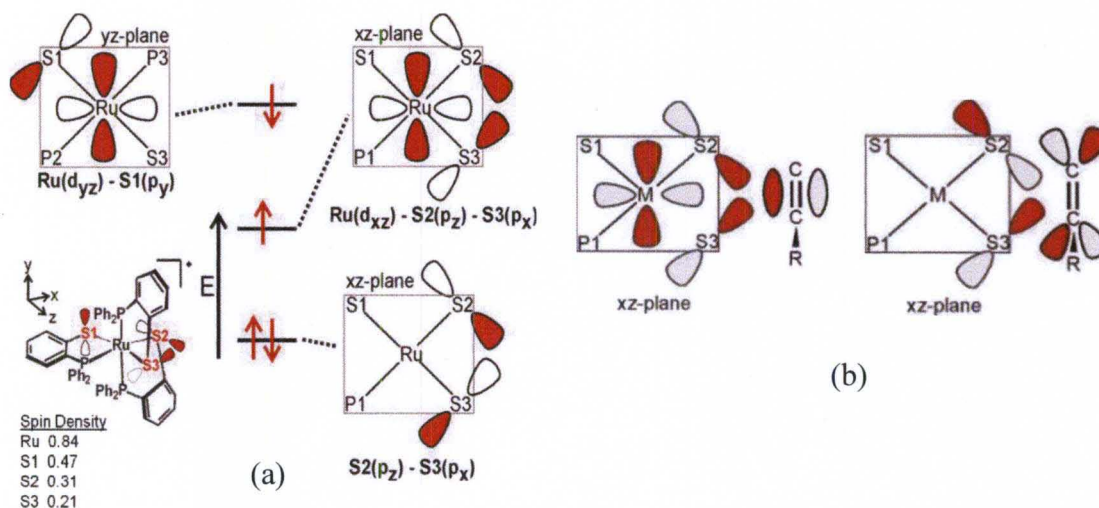
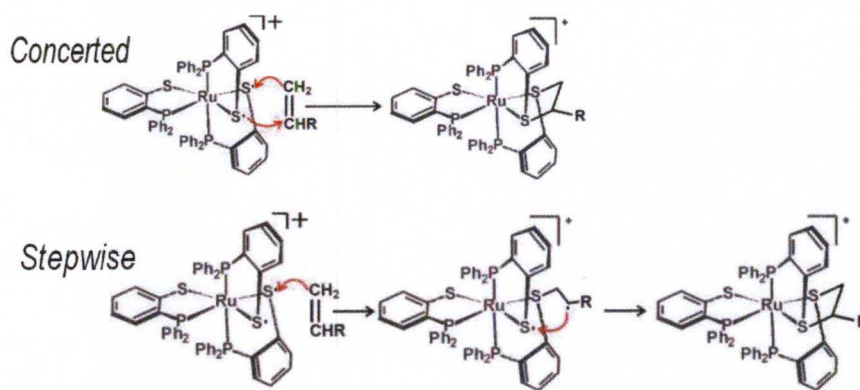


Figure V-1. (a) Qualitative overview of the frontier molecular orbitals of $[\text{Ru-1}]^+$ and (b) site of alkene addition.

The binding mechanism can be concerted or stepwise with the mono-substituted alkenes, Scheme V-3. Tedder's rules suggest that radical addition to alkene occur at least substituted site. Since spin density of S2 (0.31) has greater than S3 (0.21), the preferred addition reveals with unsubstituted carbon. Moreover, S1 (0.47) has greatest spin density, but the directionality of orbitals is incorrect for the alkene addition. From point of view, the mechanism is tending to stepwise with the alkene addition.

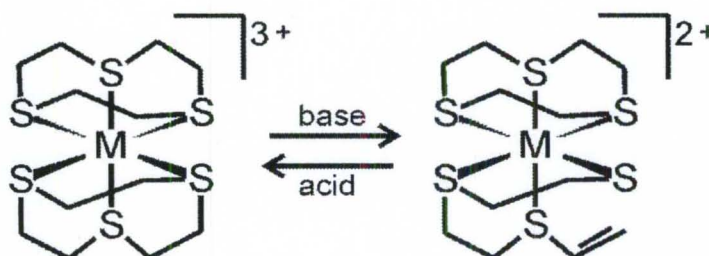


Scheme V-3. Proposed mechanism.

The earlier summary addition reaction of alkenes to the metal-stabilized thiyl radical $[Ru-1]^+$ are extended to multi-substituted alkenes, alkynes, and dienes. The exploration of these additions is allowed us to establish the scope and limits of this reactivity. As shown in Table IV-4, the multi-substituted alkenes rate constants are lower values than the mono-substituted alkenes. This is consistent with the steric effect for the multi-substituted alkenes. The alkynes are efficiently added to $[Ru-1]^+$ forming an S-alkylated dithiolene ligand that remains coordinated to the metal center. The rate constants for alkynes are found to be approximately 100 times lower than those of corresponding alkenes. For dienes, the rate additions are higher values to be 10 orders of magnitude than the alkyne addition to the electrophilic a metal-stabilized thiyl radical. The site of dienes addition is still not solved during this investigation. So the mechanism of reaction will be explored. However, alkenes are still preferred for the reactivity.

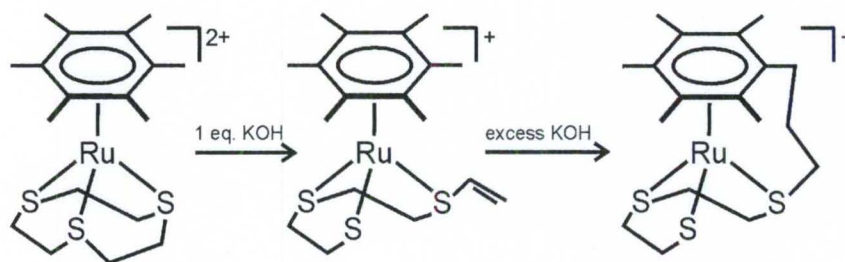
The ligand center reactivity of dithioether metal complexes is under current investigation by Rajat Chauhan. A full description of results will appear in his dissertation. A number of cationic dithioether metal complexes have been reported to undergo base induced eliminations yielding a metal complex with one thiolate and one

vinyl sulfide donor.⁸⁷ Wieghardt reported such reactions for $[M(\text{TTCN})_2]^{3+}$ complexes (M = Co, Rh, Ir) more than 20 years ago, Scheme V-4.



Scheme V-4. Base induced elimination.

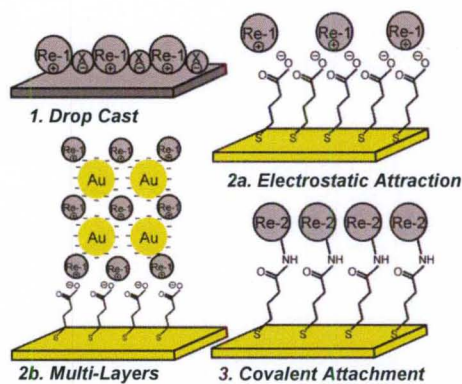
Goh and Webster have reported the $[(\eta^6\text{-C}_6\text{Me}_6)\text{Ru}(\text{TTCN})]^{2+}$ complexes that undergo intramolecular C-C coupling between the C_6Me_6 ring and the vinyl sulfide, Scheme V-5. The reaction occurs in the presence of excess base, which is proposed to generate a $(\eta^6\text{-C}_6\text{Me}_5\text{CH}_2)^-$ carbanion that attacks the metal-coordinated vinyl sulfide.^{88,89} This is a potentially advantageous alternate methods to further investigate with our dithioether complex $[\text{Ru-1}\cdot\text{C}_2\text{H}_4]^+$ and $[\text{Re-1}\cdot\text{C}_2\text{H}_4]^{2+}$. The deprotonation of these dithioether complexes with KOH in acetonitrile yields metalloculfonium derivatives $[\text{Ru-1}\cdot\text{vinyl}]$ and $[\text{Re-1}\cdot\text{vinyl}]$ in an elimination reaction. Moreover, the next step introduces the nucleophilic group to attack forming catalyst cycle and an organic product.



Scheme V-5. Nucleophilic attack on vinyl metalloculfonium.

Instead of the DPPBTH ligand, the TTCN ligand based models are less sterically encumbering and may allow more facile to study the kinetic and reactivity following our methods as the extension system. This catalytic functionalized ligand centered provides the freedom of choosing metal center and consequently making use probe the earth abundant metals dithioether complexes as vinyl metallosulfonium precursors. The synthesis and characterization of $[M-2 \cdot C_2H_4]^{2+}$ ($M = Fe, Co, Ni$) have been previously reported which allows to further explore the similar reactivity.⁸⁷

After the promise of Stiefel, our system is overcome the problem by using **Re-1** complex to regulate ethylene binding and releasing in the very small potential window. This experiment was performed in the solution. The next goal is to immobilize Re-coordinated thiy radical as ethylene sensors, Scheme V-6. This work will be the focus of Rajat's dissertation.



Scheme V-6. Immobilization Strategies.

REFERENCES

- (1) In *Chem. Eng. News* 1999; Vol. 77, p 34.
- (2) In *Chem. Eng. News* 2011; Vol. 89, p 20.
- (3) In *Kirk-Othmer concise encyclopedia of chemical technology*; Howe-Grant, M., Ed.; Wiley: New York, **1999**.
- (4) Mark, F. H.; Othmer, F. D.; Overberger, C. G.; Seabord, T. G. In *Encyclopedia of chemical technology*; John Wiley & Sons, Inc.: New York, 1978; Vol. 9.
- (5) Smith, A. L.; Hardcastle, K. I.; Soper, J. D. *J. Am. Chem. Soc.* **2010**, *132*, 14358.
- (6) Blackmore, K. J.; Lal, N.; Ziller, J. W.; Heyduk, A. F. *J. Am. Chem. Soc.* **2008**, *130*, 2728.
- (7) Chirik, P. J. *Inorg. Chem.* **2011**, *50*, 9737.
- (8) Chirik, P. J.; Wieghardt, K. *Science* **2010**, *327*, 794.
- (9) Bart, S. C.; Lobkovsky, E.; Chirik, P. J. *J. Am. Chem. Soc.* **2004**, *126*, 13794.
- (10) Sylvester, K. T.; Chirik, P. J. *J. Am. Chem. Soc.* **2009**, *131*, 8772.
- (11) Stiefel, E. I.; Matsumoto, K. In *Transition Metal Sulfur Chemistry - Biological and Industrial Significance* 1996; Vol. 653, p 2.
- (12) Thomson, A. J. In *Metalloproteins* Verlag Chemie: Deerfield Beach, FL, **1985**
- (13) Reedijk, J. *Bioinorganic Catalysis* Marcel Dekker, Inc.: New Year, **1993**.
- (14) Constable, E. C. *Metals and Ligand Reactivity: An Introduction to the Organic Chemistry of Metal Complexes 2nd ed.*; VCH, Weinheim, Germany, **1996**.
- (15) Wang, K.; Stiefel, E. I. *Science* **2001**, *291*, 106.
- (16) Ray, K.; Weyhermüller, T.; Neese, F.; Wieghardt, K. *Inorg. Chem.* **2005**, *44*, 5345.

- (17) Harrison, D. J.; Nguyen, N.; Lough, A. J.; Fekl, U. *J. Am. Chem. Soc.* **2006**, *128*, 11026.
- (18) Geiger, W. E. *Inorg. Chem.* **2002**, *41*, 136.
- (19) Alfassi, Z. B. *"S-centered radicals"*; John Wiley & Sons: Chichester, **1999**.
- (20) Walling, C.; Helmreich, W. *J. Am. Chem. Soc.* **1959**, *81*, 1144.
- (21) Ichinose, Y.; Oshima, K.; Utimoto, K. *Chem. Lett.* **1988**, 669.
- (22) Huheey, E. J. *"Inorganic Chemistry"*; 3rd ed.; Harper & Row: New York, **1983**.
- (23) Thompson, M. C.; Busch, D. H. *J. Am. Chem. Soc.* **1964**, *86*, 3651.
- (24) Ashby, M. T.; Enemark, J. H.; Lichtenberger, D. L. *Inorg. Chem.* **1988**, *27*, 191.
- (25) McGuire, D. G.; Khan, M. A.; Ashby, M. T. *Inorg. Chem.* **2002**, *41*, 2202.
- (26) Fox, D. C.; Fiedler, A. T.; Halfen, H. L.; Brunold, T. C.; Halfen, J. A. *J. Am. Chem. Soc.* **2004**, *126*, 7627.
- (27) Darensbourg, M. Y.; Longridge, E. M.; Payne, V.; Reibenspies, J.; Riordan, C. G.; Springs, J. J.; Calabrese, J. C. *Inorg. Chem.* **1990**, *29*, 2721.
- (28) Fiedler, A. T.; Halfen, H. L.; Halfen, J. A.; Brunold, T. C. *J. Am. Chem. Soc.* **2005**, *127*, 1675.
- (29) Bellefeuille, J. A.; Grapperhaus, C. A.; Derecskei-Kovacs, A.; Reibenspies, J. H.; Darensbourg, M. Y. *Inorg. Chim. Acta* **2000**, *300*, 73.
- (30) Grapperhaus, C. A.; Mullins, C. S.; Kozlowski, P. M.; Mashuta, M. S. *Inorg. Chem.* **2004**, *43*, 2859.
- (31) Dilworth, J.; Zheng, Y.; Lu, S.; Wu, Q. *Transition Met. Chem.* **1992**, *17*, 364.
- (32) Grapperhaus, C. A.; Poturovic, S.; Mashuta, M. S. *Inorg. Chem.* **2002**, *41*, 4309.
- (33) Poturovic, S.; Mashuta, M. S.; Grapperhaus, C. A. *Angewandte Chemie-International Edition* **2005**, *44*, 1883.
- (34) Farmer, P. J.; Reibenspies, J. H.; Lindahl, P. A.; Darensbourg, M. Y. *J. Am. Chem. Soc.* **1993**, *115*, 4665.
- (35) Grapperhaus, C. A.; Kozlowski, P. M.; Kumar, D.; Frye, H. N.; Venna, K. B.; Poturovic, S. *Angewandte Chemie-International Edition* **2007**, *46*, 4085.

- (36) Kimura, S.; Bill, E.; Bothe, E.; Weyhermüller, T.; Wieghardt, K. *J. Am. Chem. Soc.* **2001**, *123*, 6025.
- (37) Ghosh, P.; Bill, E.; Weyhermüller, T.; Neese, F.; Wieghardt, K. *J. Am. Chem. Soc.* **2003**, *125*, 1293.
- (38) Herebian, D.; Bothe, E.; Bill, E.; Weyhermüller, T.; Wieghardt, K. *J. Am. Chem. Soc.* **2001**, *123*, 10012.
- (39) Hsieh, C.-H.; Hsu, I. J.; Lee, C.-M.; Ke, S.-C.; Wang, T.-Y.; Lee, G.-H.; Wang, Y.; Chen, J.-M.; Lee, J.-F.; Liaw, W.-F. *Inorg. Chem.* **2003**, *42*, 3925.
- (40) Grapperhaus, C. A.; Poturovic, S. *Inorg. Chem.* **2004**, *43*, 3292.
- (41) Musie, G.; Farmer, P. J.; Tuntulani, T.; Reibenspies, J. H.; Darensbourg, M. Y. *Inorg. Chem.* **1996**, *35*, 2176.
- (42) Grapperhaus, C. A.; Venna, K. B.; Mashuta, M. S. *Inorg. Chem.* **2007**, *46*, 8044.
- (43) Mullen, G. E. D.; Blower, P. J.; Price, D. J.; Powell, A. K.; Howard, M. J.; Went, M. J. *Inorg. Chem.* **2000**, *39*, 4093.
- (44) Maurer, P.; Magistrato, A.; Rothlisberger, U. *The Journal of Physical Chemistry A* **2004**, *108*, 11494.
- (45) Magistrato, A.; Maurer, P.; Fässler, T.; Rothlisberger, U. *The Journal of Physical Chemistry A* **2004**, *108*, 2008.
- (46) Gordon, A. J. *"The Chemistry Companion"*; John Wiley & Sons Inc.: Canada, **1972**.
- (47) Connelly, N. G.; Geiger, W. E. *Chem. Rev.* **1996**, *96*, 877.
- (48) Block, E.; Ofori-Okai, G.; Zubieta, J. *J. Am. Chem. Soc.* **1989**, *111*, 2327.
- (49) Dilworth, J. R.; Hutson, A. J.; Morton, S.; Harman, M.; Hursthouse, M. B.; Zubieta, J.; Archer, C. M.; Kelly, J. D. *Polyhedron* **1992**, *11*, 2151.
- (50) Bard, J. A., Faulkner, R. L. *"Electrochemical Methods: Fundamentals and Applications"*; 2nd ed.; John Wiley & Sons, Inc., **2001**.
- (51) Sawyer, D. T., Heineman, L. R., and Beebe, J. M., *"Chemistry Experiments for Instrumental Methods"*; J. Wiley & Sons, **1984**, Chapter 4.
- (52) Rudolph, M.; Feldberg, S. W.; *DigiSim* (3.03b) ed.; Bioanalytical Systems, Inc.: West Lafayette, IN, 2004.
- (53) www.epsison-web.net/Ec/digisim/tutorials/tut_2.html.

- (54) Kissinger, P. T., Heineman, W. R. In *In Laboratory Techniques in Electroanalytical Chemistry*; 2nd ed.; Marcel Dekker, Inc.: New York, **1996**, p 695.
- (55) Grapperhaus, C. A.; Ouch, K.; Mashuta, M. S. *J. Am. Chem. Soc.* **2009**, *131*, 64.
- (56) In *Chem. Eng. News* 2011; Vol. 89, p 22.
- (57) In *Chem. Eng. News* 1999; Vol. 77, p 34.
- (58) In *Chem. Eng. News* 2008; Vol. 77, p 61.
- (59) Grantom, L. R., Royer, J. D. In *Ullmann's Encyclopedia of Industrial Chemistry*; 5th ed.; VCH: New York, **1987**, p 45.
- (60) Bond, A. M.; Oldham, K. B.; Snook, G. A. *Anal. Chem.* **2000**, *72*, 3492.
- (61) Grapperhaus, C. A.; Mullins, C. S.; Mashuta, M. S. *Inorg. Chim. Acta* **2005**, *358*, 623.
- (62) Sakurai, H.; Hayashi, S.; Hosomi, A. *Bull. Chem. Soc. Jpn.* **1971**, *44*, 1945.
- (63) Jones, M. J.; Moad, G.; Rizzardo, E.; Solomon, D. H. *The Journal of Organic Chemistry* **1989**, *54*, 1607.
- (64) Brown, H. C.; Okamoto, Y. *J. Am. Chem. Soc.* **1958**, *80*, 4979.
- (65) Kadish, K. M.; Morrison, M. M. *J. Am. Chem. Soc.* **1976**, *98*, 3326.
- (66) P.Zuman "*Substituent Effects in Organic Polarography*"; Plenum Press: New York, N. Y., 1967.
- (67) Dilworth, J. R.; Wheatley, N. *Coord. Chem. Rev.* **2000**, *199*, 89.
- (68) Tedder, J. M.; Walton, J. C. *Tetrahedron* **1980**, *36*, 701.
- (69) Tedder, J. M. *Angew. Chem., Int. Ed. Engl.* **1982**, *21*, 401.
- (70) *Introduction to Spectroscopy: A Guide for Students of Organic Chemistry*; Donald L. Pavia, G. M. L., George S. Kriz, Jr., Ed.; W.B. Saunders Company, **1979**.
- (71) Dilworth, J. R.; Lu, C.; Miller, J. R.; Zheng, Y. *J. Chem. Soc., Dalton Trans.* **1995**, 1957.
- (72) Sheldrick, G. M. *Acta Crystallographica Section A* **1990**, *46*, 467.
- (73) Sheldrick, G. M.; University Gottingen: Gottingen, Germany, 1997.

- (74) SHELXTL (v6.14) ed.; Brucker Advanced X-ray Solutions, Inc. : Madison, WI, 2000.
- (75) Ouch, K.; Mashuta, M. S.; Grapperhaus, C. A. *Inorg. Chem.* **2011**, 9904
- (76) Geiger, W. E.; Barrière, F.; LeSuer, R. J.; Trupia, S. *Inorg. Chem.* **2001**, 40, 2472.
- (77) Kerr, M. J.; Harrison, D. J.; Lough, A. J.; Fekl, U. *Inorg. Chem.* **2009**, 48, 9043.
- (78) King, R. B. *Inorg. Chem.* **1963**, 2, 641.
- (79) Stiefel, E. I.; Eisenberg, R.; Rosenberg, R. C.; Gray, H. B. *J. Am. Chem. Soc.* **1966**, 88, 2956.
- (80) Cervilla, A.; Llopis, E.; Marco, D.; Pérez, F. *Inorg. Chem.* **2001**, 40, 6525.
- (81) Harrison, D. J.; Lough, A. J.; Nguyen, N.; Fekl, U. *Angew. Chem. Int. Ed.* **2007**, 46, 7644.
- (82) Nguyen, N.; Harrison, D. J.; Lough, A. J.; De Crisci, A. G.; Fekl, U. *Eur. J. Inorg. Chem.* **2010**, 2010, 3577.
- (83) Ye, H.; Xu, B.; Xie, M.; Li, Y.; Yan, H. *Dalton Transactions* **2011**, 40, 6541.
- (84) Wu, D.; Li, Y.; Han, L.; Li, Y.; Yan, H. *Inorg. Chem.* **2008**, 47, 6524.
- (85) Wu, D.-H.; Ji, C.; Li, Y.-Z.; Yan, H. *Organometallics* **2007**, 26, 1560.
- (86) Farrugia, L. J. *J. Appl. Crystallogr.* **1997**, 30, 565.
- (87) Weighardt, K.; Kueppers, H. J.; Weiss, J. *Inorg. Chem.* **1985**, 24, 3067.
- (88) Bennett, M. A.; Goh, L. Y.; Willis, A. C. *J. Am. Chem. Soc.* **1996**, 118, 4984.
- (89) Shin, R. Y. C.; Tan, G. K.; Koh, L. L.; Goh, L. Y. *Organometallics* **2004**, 23, 6293.

APPENDIX A

Tables for Cyclic Voltammetry Simulation Parameters

Appendix	Page
A-1 Table for <i>n</i> -propyl vinyl ether.....	120
A-2 Table for <i>t</i> -butyl vinyl ether.....	120
A-3 Table for <i>n</i> -hexene.....	120
A-4 Table for acrylonitrile.....	120
A-5 Table for cyclohexene.....	121
A-6 Table for cyclopentene.....	121
A-7 Table for norbornene.....	121
A-8 Table for styrene.....	121
A-9 Table for <i>p</i> -methoxystyrene.....	122
A-10 Table for <i>p</i> -methylstyrene.....	122
A-11 Table for <i>p</i> -chlorostyrene.....	123
A-12 Table for <i>p</i> -fluorostyrene.....	123
A-13 Table for <i>m</i> -methoxystyrene.....	123
A-14 Table for <i>m</i> -methylstyrene.....	124
A-15 Table for <i>m</i> -chlorostyrene.....	124
A-16 Table for <i>m</i> -fluorostyrene.....	125

A-17	Table for <i>o</i> -methoxystyrene.....	125
A-18	Table for <i>o</i> -methylstyrene.....	125
A-19	Table for <i>o</i> -fluorostyrene.....	126
A-20	Table for <i>cis</i> -stilbene.....	126
A-21	Table for <i>trans</i> -stilbene.....	126
A-22	Table for 2-methyl-2-butene.....	127
A-23	Table for 2,3-dimethyl-2-butene.....	127
A-24	Table for 1-octyne.....	127
A-25	Table for phenyl acetylene.....	127
A-26	Table for 1-phenyl -1-propyne.....	127
A-27	Table for 1,3-butadiene.....	128
A-28	Table for 2,3-dimethyl-1,3-butadiene.....	128
A-29	Table for dipentene.....	128

Table A-1: Cyclic voltammetry simulation parameters*n*-propyl vinyl ether, EECE Mechanism

	Potential (vs Fc ⁺ /Fc) (mV)			Rate constant *10 ⁷ M ⁻¹ s ⁻¹	Diffusion coefficient *10 ⁻⁶ cm ² /s	Uncompensated resistance (Ω)
	E ₂	E ₁ ²	E ₄	k _f	D ₀	R _u
Trial 1	-30.0	-830	262	1.924	9.236	182
Trial 2	-30.0	-830	263	1.972	8.205	181
Trial 3	-29.9	-830	263	2.186	8.552	186

Table A-2: Cyclic voltammetry simulation parameters*t*-butyl vinyl ether, EECE Mechanism

	Potential (vs Fc ⁺ /Fc) (mV)			Rate constant *10 ⁶ M ⁻¹ s ⁻¹	Diffusion coefficient *10 ⁻⁶ cm ² /s	Uncompensated resistance (Ω)
	E ₂	E ₁	E ₄	k _f	D ₀	R _u
Trial 1	-30.0	-830	262	1.990	7.960	196
Trial 2	-30.0	-830	262	3.527	8.649	188
Trial 3	-30.0	-830	259	2.306	8.847	172

Table A-3: Cyclic voltammetry simulation parameters*n*-hexene, EECE Mechanism

	Potential (vs Fc ⁺ /Fc) (mV)			Rate constant *10 ⁵ M ⁻¹ s ⁻¹	Diffusion coefficient *10 ⁻⁶ cm ² /s	Uncompensated resistance (Ω)
	E ₂	E ₁	E ₄	k _f	D ₀	R _u
Trial 1	-30.0	-830	253	4.620	9.533	179
Trial 2	-30.0	-830	251	7.612	8.645	175
Trial 3	-33.8	-830	249	8.340	8.750	175

Table A-4: Cyclic voltammetry simulation parameters

acrylonitrile, EECE Mechanism

	Potential (vs Fc ⁺ /Fc) (mV)			Rate constant *10 ⁴ M ⁻¹ s ⁻¹	Diffusion coefficient *10 ⁻⁶ cm ² /s	Uncompensated resistance (Ω)
	E ₂	E ₁	E ₄	k _f	D ₀	R _u
Trial 1	-30.0	-830	342	2.666	9.683	210
Trial 2	-30.0	-830	344	2.446	8.508	201
Trial 3	-30.0	-830	343	2.911	9.310	178

² This was set as internal reference.

Table A-5: Cyclic voltammetry simulation parameters
cyclohexene, EECE Mechanism

	Potential (vs Fc ⁺ /Fc) (mV)			Rate constant *10 ³ M ⁻¹ s ⁻¹	Diffusion coefficient *10 ⁻⁶ cm ² /s	Uncompensated resistance (Ω)
	E ₂	E ₁	E ₄	k _f	D ₀	R _u
Trial 1	-29.9	-830	233	2.745	8.145	185
Trial 2	-30.0	-830	240	3.211	7.062	222
Trial 3	-30.0	-830	235	2.743	9.060	202

Table A-6: Cyclic voltammetry simulation parameters
cyclopentene, EECE Mechanism

	Potential (vs Fc ⁺ /Fc) (mV)			Rate constant *10 ⁶ M ⁻¹ s ⁻¹	Diffusion coefficient *10 ⁻⁶ cm ² /s	Uncompensated resistance (Ω)
	E ₂	E ₁	E ₄	k _f	D ₀	R _u
Trial 1	-30.0	-830	253	4.364	8.916	171
Trial 2	-30.0	-830	255	6.535	9.063	201
Trial 3	-30.0	-830	255	6.140	9.140	170

Table A-7: Cyclic voltammetry simulation parameters
norbornene, EECE Mechanism

	Potential (vs Fc ⁺ /Fc) (mV)			Rate constant *10 ⁷ M ⁻¹ s ⁻¹	Diffusion coefficient *10 ⁻⁶ cm ² /s	Uncompensated resistance (Ω)
	E ₂	E ₁	E ₄	k _f	D ₀	R _u
Trial 1	-30.0	-830	272	3.050	9.664	179
Trial 2	-30.0	-830	274	5.826	9.202	183
Trial 3	-30.0	-830	276	3.231	7.874	184

Table A-8: Cyclic voltammetry simulation parameters
styrene, EECE Mechanism

	Potential (vs Fc ⁺ /Fc) (mV)			Rate constant *10 ⁷ M ⁻¹ s ⁻¹	Diffusion coefficient *10 ⁻⁶ cm ² /s	Uncompensated resistance (Ω)
	E ₂	E ₁	E ₄	k _f	D ₀	R _u
Trial 1	-30.0	-830	271	3.025	7.094	200
Trial 2	-30.0	-830	271	3.570	7.582	172
Trial 3	-30.0	-830	273	9.389	8.807	200 ³

³ Outlier

Trial 4	-30.0	-830	272	3.517	8.499	214
Trial 5	-30.0	-830	269	4.874	8.430	192
Trial 6	-30.0	-830	269	4.798	7.426	205
Trial 7	-30.0	-830	269	4.012	8.759	177
Trial 8	-30.0	-830	272	4.860	8.401	210
Trial 9	-30.0	-830	272	4.605	8.948	203
Trial 10	-30.0	-830	271	5.496	8.589	231

Table A-9: Cyclic voltammetry simulation parameters

p-methoxystyrene, EECE Mechanism

	Potential (vs Fc ⁺ /Fc) (mV)			Rate constant *10 ⁷ M ⁻¹ s ⁻¹	Diffusion coefficient *10 ⁻⁶ cm ² /s	Uncompensated resistance (Ω)
	E ₂	E ₁	E ₄	k _f	D ₀	R _u
Trial 1	-30.0	-830	261	2.537	8.690	255
Trial 2	-30.0	-830	265	2.260	8.172	214
Trial 3	-30.0	-830	261	2.332	11.00	210
Trial 4	-30.0	-830	259	6.290	9.658	229
Trial 5	-30.0	-830	258	6.382	8.633	206
Trial 6	-30.0	-830	266	3.413	9.333	213
Trial 7	-30.0	-830	268	6.170	8.904	258
Trial 8	-30.0	-830	266	2.395	9.355	313
Trial 9	-30.0	-830	266	5.290	8.941	222
Trial 10	-30.0	-830	263	4.468	9.005	209

Table A-10: Cyclic voltammetry simulation parameters

p-methylstyrene, EECE Mechanism

	Potential (vs Fc ⁺ /Fc) (mV)			Rate constant *10 ⁷ M ⁻¹ s ⁻¹	Diffusion coefficient *10 ⁻⁶ cm ² /s	Uncompensated resistance (Ω)
	E ₂	E ₁	E ₄	k _f	D ₀	R _u
Trial 1	-30.0	-830	265	1.856	8.430	267
Trial 2	-30.0	-830	264	2.953	8.301	201
Trial 3	-30.0	-830	270	4.257	8.537	215
Trial 4	-30.0	-830	265	3.194	8.607	228
Trial 5	-30.0	-830	270	3.071	8.265	396
Trial 6	-30.0	-830	270	3.588	8.454	270
Trial 7	-30.0	-830	270	3.552	8.601	243
Trial 8	-30.0	-830	270	4.468	8.378	268
Trial 9	-30.0	-830	268	5.477	8.126	229
Trial 10	-30.0	-830	266	3.509	8.738	182

Table A-11: Cyclic voltammetry simulation parameters*p*-chlorostyrene, EECE Mechanism

	Potential (vs Fc ⁺ /Fc) (mV)			Rate constant *10 ⁷ M ⁻¹ s ⁻¹	Diffusion coefficient *10 ⁻⁶ cm ² /s	Uncompensated resistance (Ω)
	E ₂	E ₁	E ₄	k _f	D ₀	R _u
Trial 1	-30.0	-830	284	1.412	6.525	188
Trial 2	-30.0	-830	280	0.828	7.918	183
Trial 3	-30.0	-830	280	1.417	9.038	128
Trial 4	-30.0	-830	280	1.514	8.948	196
Trial 5	-30.0	-830	282	1.910	8.908	197
Trial 6	-30.0	-830	280	2.669	9.637	187
Trial 7	-30.0	-830	273	1.100	9.809	201
Trial 8	-30.0	-830	282	2.586	8.602	203
Trial 9	-30.0	-830	283	3.603	9.088	193
Trial 10	-30.0	-830	283	3.087	8.347	204

Table A-12: Cyclic voltammetry simulation parameters*p*-fluorostyrene, EECE Mechanism

	Potential (vs Fc ⁺ /Fc) (mV)			Rate constant *10 ⁷ M ⁻¹ s ⁻¹	Diffusion coefficient *10 ⁻⁶ cm ² /s	Uncompensated resistance (Ω)
	E ₂	E ₁	E ₄	k _f	D ₀	R _u
Trial 1	-30.0	-830	273	0.657	5.834	210
Trial 2	-30.0	-830	275	1.804	8.523	218
Trial 3	-30.0	-830	272	1.779	8.934	284
Trial 4	-30.0	-830	276	2.134	8.585	237
Trial 5	-30.0	-830	278	2.682	8.176	236
Trial 6	-30.0	-830	278	1.882	8.863	274
Trial 7	-30.0	-830	279	1.392	8.974	464
Trial 8	-30.0	-830	276	0.882	8.426	293
Trial 9	-30.0	-830	276	1.214	9.057	410
Trial 10	-30.0	-830	270	3.071	8.265	396

Table A-13: Cyclic voltammetry simulation parameters*m*-methoxystyrene, EECE Mechanism

	Potential (vs Fc ⁺ /Fc) (mV)			Rate constant *10 ⁷ M ⁻¹ s ⁻¹	Diffusion coefficient *10 ⁻⁶ cm ² /s	Uncompensated resistance (Ω)
	E ₂	E ₁	E ₄	k _f	D ₀	R _u
Trial 1	-30.0	-830	265	2.290	8.883	210
Trial 2	-30.0	-830	265	6.548	8.851	229
Trial 3	-30.0	-830	265	7.321	8.443	201

Trial 4	-30.0	-830	265	7.795	8.891	217
Trial 5	-30.0	-830	266	7.456	8.789	219
Trial 6	-30.0	-830	266	2.526	9.392	208
Trial 7	-30.0	-830	268	4.193	9.040	213
Trial 8	-30.0	-830	268	7.081	9.277	220
Trial 9	-30.0	-830	227	3.775	8.818	198
Trial 10	-30.0	-830	267	4.443	8.056	216

Table A-14: Cyclic voltammetry simulation parameters

m-methylstyrene, EECE Mechanism

	Potential (vs Fc ⁺ /Fc) (mV)			Rate constant *10 ⁷ M ⁻¹ s ⁻¹	Diffusion coefficient *10 ⁻⁶ cm ² /s	Uncompensated resistance (Ω)
	E ₂	E ₁	E ₄	k _f	D ₀	R _u
Trial 1	-30.0	-830	265	4.051	9.510	222
Trial 2	-30.0	-830	267	6.104	8.896	227
Trial 3	-30.0	-830	266	8.923	9.148	202
Trial 4	-30.0	-830	265	11.56	9.466	210
Trial 5	-30.0	-830	268	9.281	8.889	219
Trial 6	-30.0	-830	272	2.313	8.699	221
Trial 7	-30.0	-830	270	6.472	7.894	223
Trial 8	-30.0	-830	266	11.47	9.107	212
Trial 9	-30.0	-830	266	6.732	8.839	207
Trial 10	-30.0	-830	267	5.255	9.206	214

Table A-15: Cyclic voltammetry simulation parameters

m-chlorostyrene, EECE Mechanism

	Potential (vs Fc ⁺ /Fc) (mV)			Rate constant *10 ⁷ M ⁻¹ s ⁻¹	Diffusion coefficient *10 ⁻⁶ cm ² /s	Uncompensated resistance (Ω)
	E ₂	E ₁	E ₄	k _f	D ₀	R _u
Trial 1	-30.0	-830	278	2.569	9.435	225
Trial 2	-30.0	-830	277	1.555	9.258	200
Trial 3	-30.0	-830	279	2.858	8.937	205
Trial 4	-30.0	-830	277	1.830	7.599	210
Trial 5	-30.0	-830	274	0.996	8.271	205
Trial 6	-30.0	-830	276	2.183	8.252	215
Trial 7	-30.0	-830	277	2.595	8.551	212
Trial 8	-30.0	-830	276	2.969	7.925	210
Trial 9	-30.0	-830	277	2.390	8.123	227
Trial 10	-30.0	-830	281	2.702	8.440	216

Table A-16: Cyclic voltammetry simulation parameters*m*-fluorostyrene, EECE Mechanism

	Potential (vs Fc ⁺ /Fc) (mV)			Rate constant *10 ⁷ M ⁻¹ s ⁻¹	Diffusion coefficient *10 ⁻⁶ cm ² /s	Uncompensated resistance (Ω)
	E ₂	E ₁	E ₄	k _f	D ₀	R _u
Trial 1	-30.0	-830	275	0.911	8.304	222
Trial 2	-30.0	-830	275	1.192	8.168	207
Trial 3	-30.0	-830	277	2.196	8.387	202
Trial 4	-30.0	-830	279	1.347	8.639	221
Trial 5	-30.0	-830	277	2.008	8.683	218
Trial 6	-30.0	-830	276	1.232	8.813	210
Trial 7	-30.0	-830	279	1.731	9.132	216
Trial 8	-30.0	-830	275	0.962	9.030	192
Trial 9	-30.0	-830	278	1.762	8.651	220
Trial 10	-30.0	-830	279	1.803	8.587	214

Table A-17: Cyclic voltammetry simulation parameters*o*-methoxystyrene, EECE Mechanism

	Potential (vs Fc ⁺ /Fc) (mV)			Rate constant *10 ⁷ M ⁻¹ s ⁻¹	Diffusion coefficient *10 ⁻⁶ cm ² /s	Uncompensated resistance (Ω)
	E ₂	E ₁	E ₄	k _f	D ₀	R _u
Trial 1	-30.0	-830	256	9.191	7.853	234
Trial 2	-30.0	-830	261	2.185	8.747	212
Trial 3	-30.0	-830	261	5.935	7.480	250
Trial 4	-30.0	-830	256	5.200	8.775	231
Trial 5	-30.0	-830	260	6.227	8.536	226
Trial 6	-30.0	-830	258	11.28	8.781	213
Trial 7	-30.0	-830	259	19.06	8.587	209
Trial 8	-30.0	-830	259	33.59	8.680	201
Trial 9	-30.0	-830	259	17.73	8.748	204
Trial 10	-30.0	-830	252	12.80	9.902	185

Table A-18: Cyclic voltammetry simulation parameters*o*-methylstyrene, EECE Mechanism

	Potential (vs Fc ⁺ /Fc) (mV)			Rate constant *10 ⁷ M ⁻¹ s ⁻¹	Diffusion coefficient *10 ⁻⁶ cm ² /s	Uncompensated resistance (Ω)
	E ₂	E ₁	E ₄	k _f	D ₀	R _u
Trial 1	-30.0	-830	249	8.252	7.405	202 ⁴

⁴ Outlier

Trial 2	-30.0	-830	246	0.434	9.573	202
Trial 3	-30.0	-830	251	1.734	8.257	211
Trial 4	-30.0	-830	246	2.384	9.099	201
Trial 5	-30.0	-830	253	1.386	7.187	226
Trial 6	-30.0	-830	247	3.563	7.855	203
Trial 7	-30.0	-830	251	1.855	9.284	204
Trial 8	-30.0	-830	251	3.556	9.846	182
Trial 9	-30.0	-830	251	2.625	8.113	216
Trial 10	-30.0	-830	249	2.833	9.125	210

Table A-19: Cyclic voltammetry simulation parameters
o-fluorostyrene, EECE Mechanism

	Potential (vs Fc ⁺ /Fc) (mV)			Rate constant *10 ⁷ M ⁻¹ s ⁻¹	Diffusion coefficient *10 ⁻⁶ cm ² /s	Uncompensated resistance (Ω)
	E ₂	E ₁	E ₄	k _f	D ₀	R _u
Trial 1	-30.0	-830	274	0.656	8.878	200
Trial 2	-30.0	-830	277	2.029	7.874	204
Trial 3	-30.0	-830	275	1.475	9.211	200
Trial 4	-30.0	-830	275	1.859	1.013	208
Trial 5	-30.0	-830	276	0.901	9.651	194
Trial 6	-30.0	-830	273	1.824	9.049	208
Trial 7	-30.0	-830	273	2.976	9.651	209
Trial 8	-30.0	-830	278	0.620	8.723	210
Trial 9	-30.0	-830	279	0.159	8.983	217
Trial 10	-30.0	-830	273	0.256	9.427	192

Table A-20: Cyclic voltammetry simulation parameters
cis-stilbene, EECE Mechanism

	Potential (vs Fc ⁺ /Fc) (mV)			Rate constant *10 ² M ⁻¹ s ⁻¹	Diffusion coefficient *10 ⁻⁶ cm ² /s	Uncompensated resistance (Ω)
	E ₂	E ₁	E ₄	k _f	D ₀	R _u
Trial 1	-30.0	-830	300	8.8	9.749	187

Table A-21: Cyclic voltammetry simulation parameters
trans-stilbene, EECE Mechanism

	Potential (vs Fc ⁺ /Fc) (mV)			Rate constant *10 ¹ M ⁻¹ s ⁻¹	Diffusion coefficient *10 ⁻⁶ cm ² /s	Uncompensated resistance (Ω)
	E ₂	E ₁	E ₄	k _f	D ₀	R _u
Trial 1	-30.0	-830	280	1.1	9.03	187

Table A-22: Cyclic voltammetry simulation parameters						
2-methyl-2-butene, EECE Mechanism						
	Potential (vs Fc ⁺ /Fc) (mV)			Rate constant *10 ² M ⁻¹ s ⁻¹	Diffusion coefficient *10 ⁻⁶ cm ² /s	Uncompensated resistance (Ω)
	E ₂	E ₁	E ₄	k _f	D ₀	R _u
Trial 1	-30.0	-830	252	1.4	10.04	187

Table A-23: Cyclic voltammetry simulation parameters						
2,3-dimethyl-2-butene, EECE Mechanism						
	Potential (vs Fc ⁺ /Fc) (mV)			Rate constant *10 ¹ M ⁻¹ s ⁻¹	Diffusion coefficient *10 ⁻⁶ cm ² /s	Uncompensated resistance (Ω)
	E ₂	E ₁	E ₄	k _f	D ₀	R _u
Trial 1	-30.0	-830	240	3.2	8.74	187

Table A-24: Cyclic voltammetry simulation parameters						
1-octyne, EECE Mechanism						
	Potential (vs Fc ⁺ /Fc) (mV)			Rate constant *10 ⁴ M ⁻¹ s ⁻¹	Diffusion coefficient *10 ⁻⁶ cm ² /s	Uncompensated resistance (Ω)
	E ₂	E ₁	E ₄	k _f	D ₀	R _u
Trial 1	-29.7	-830	292	1.5	13.5	187

Table A-25: Cyclic voltammetry simulation parameters						
phenyl acetylene, EECE Mechanism						
	Potential (vs Fc ⁺ /Fc) (mV)			Rate constant *10 ⁴ M ⁻¹ s ⁻¹	Diffusion coefficient *10 ⁻⁶ cm ² /s	Uncompensated resistance (Ω)
	E ₂	E ₁	E ₄	k _f	D ₀	R _u
Trial 1	-30.0	-830	293	1.5	3.94	187

Table A-26: Cyclic voltammetry simulation parameters						
1-phenyl-1-propyne, EECE Mechanism						
	Potential (vs Fc ⁺ /Fc) (mV)			Rate constant *10 ² M ⁻¹ s ⁻¹	Diffusion coefficient *10 ⁻⁶ cm ² /s	Uncompensated resistance (Ω)
	E ₂	E ₁	E ₄	k _f	D ₀	R _u
Trial 1	-30.0	-830	291	2.3	8.69	187

Table A-27: Cyclic voltammetry simulation parameters						
1,3-butadiene, EECE Mechanism						
	Potential (vs Fc^+/Fc) (mV)			Rate constant $*10^5 \text{ M}^{-1} \text{ s}^{-1}$	Diffusion coefficient $*10^{-6} \text{ cm}^2/\text{s}$	Uncompensated resistance (Ω)
	E_2	E_1	E_4	k_f	D_0	R_u
Trial 1	-30.0	-830	253	1.7	4.57	187

Table A-28: Cyclic voltammetry simulation parameters						
2,3-dimethyl-1,3-butadiene, EECE Mechanism						
	Potential (vs Fc^+/Fc) (mV)			Rate constant $*10^3 \text{ M}^{-1} \text{ s}^{-1}$	Diffusion coefficient $*10^{-6} \text{ cm}^2/\text{s}$	Uncompensated resistance (Ω)
	E_2	E_1	E_4	k_f	D_0	R_u
Trial 1	-30.0	-830	260	1.1	5.65	187

Table A-29: Cyclic voltammetry simulation parameters						
dipentene, EECE Mechanism						
	Potential (vs Fc^+/Fc) (mV)			Rate constant $*10^4 \text{ M}^{-1} \text{ s}^{-1}$	Diffusion coefficient $*10^{-6} \text{ cm}^2/\text{s}$	Uncompensated resistance (Ω)
	E_2	E_1	E_4	k_f	D_0	R_u
Trial 1	-30.0	-830	259	2.5	6.35	187

APPENDIX B

Experimental and Simulated Cyclic Voltammograms

Appendix	Page
B-1 Figure for <i>n</i> -propyl vinyl ether	131
B-2 Figure for <i>t</i> -butyl vinyl ether.....	131
B-3 Figure for <i>n</i> -hexene.....	132
B-4 Figure for acrylonitrile.....	132
B-5 Figure for cyclohexene	133
B-6 Figure for cyclopentene	133
B-7 Figure for norbornene	134
B-8 Figure for <i>p</i> -methoxystyrene	134
B-9 Figure for <i>p</i> -methylstyrene	135
B-10 Figure for <i>p</i> -chlorostyrene	135
B-11 Figure for <i>p</i> -fluorostyrene.....	136
B-12 Figure for <i>m</i> -methoxystyrene.....	136
B-13 Figure for <i>m</i> -methylstyrene.....	137
B-14 Figure for <i>m</i> -chlorostyrene	137
B-15 Figure for <i>m</i> -fluorostyrene.....	138
B-16 Figure for <i>o</i> -methoxystyrene	138

B-17	Figure for <i>o</i> -methylstyrene	139
B-18	Figure for <i>o</i> -fluorostyrene.....	139
B-19	Figure for <i>cis</i> -stilbene	140
B-20	Figure for <i>trans</i> -stilbene	140
B-21	Figure for 2-methyl-2-butene.....	141
B-22	Figure for 2,3-dimethyl-2-butene.....	141
B-23	Figure for 1-octyne	142
B-24	Figure for phenyl acetylene	142
B-25	Figure for 1-phenyl-1-propyne	143
B-26	Figure for 1,3-butadiene.....	143
B-27	Figure for 2,3-dimethyl-1,3-butadiene.....	144
B-28	Figure for dipentene.....	144

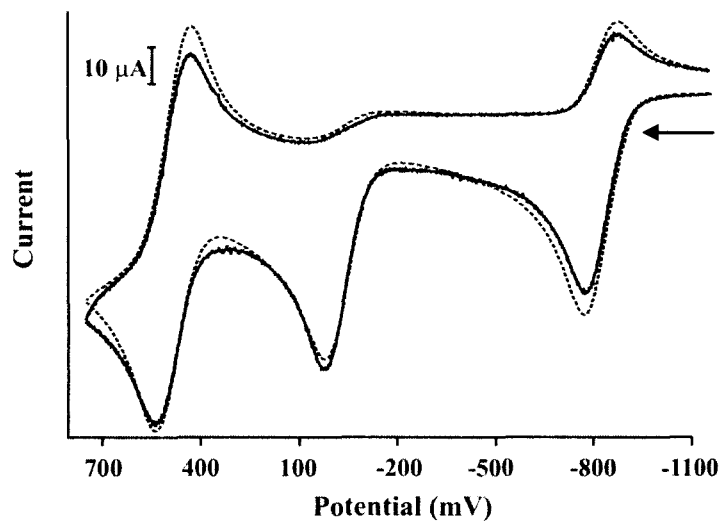


Figure B-1. Experimental (—) and simulated (---) cyclic voltammograms of [Ru-1]⁺ in presence of *n*-propyl vinyl ether at a scan rate 400 mV/s.

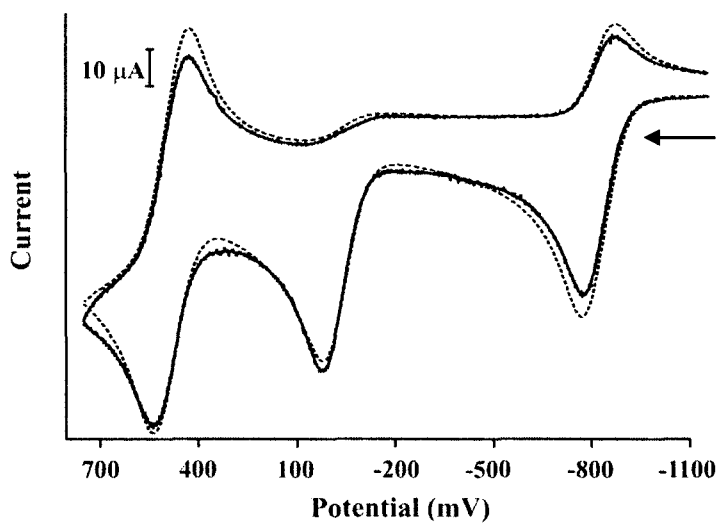


Figure B-2. Experimental (—) and simulated (---) cyclic voltammograms of [Ru-1]⁺ in presence of *t*-butyl vinyl ether at a scan rate 400 mV/s.

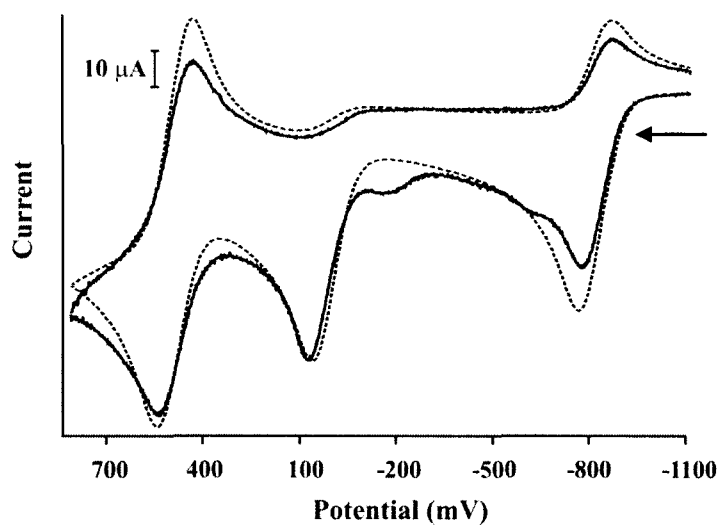


Figure B-3. Experimental (—) and simulated (---) cyclic voltammograms of [Ru-1] in presence of *n*-hexene at a scan rate 400 mV/s.

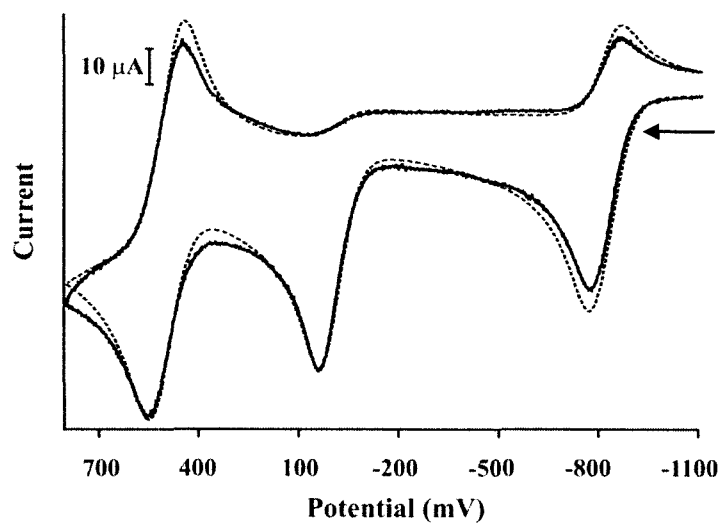


Figure B-4. Experimental (—) and simulated (---) cyclic voltammograms of [Ru-1] in presence of acrylonitrile at a scan rate 400 mV/s.

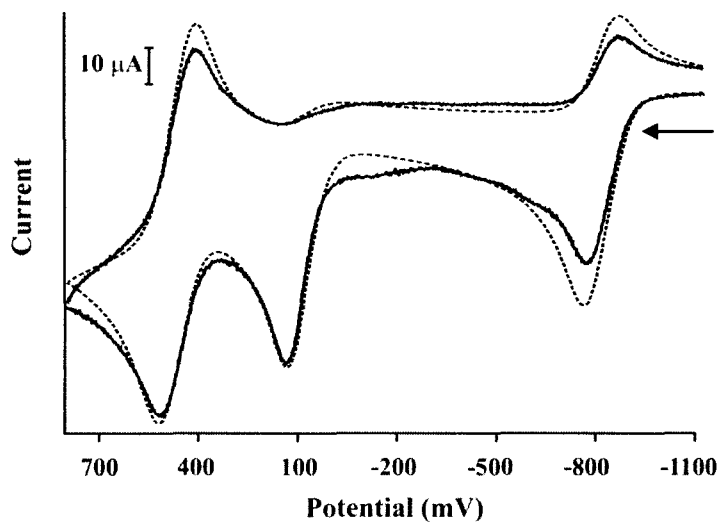


Figure B-5. Experimental (—) and simulated (---) cyclic voltammograms of [Ru-1]⁺ in presence of cyclohexene at a scan rate 400 mV/s.

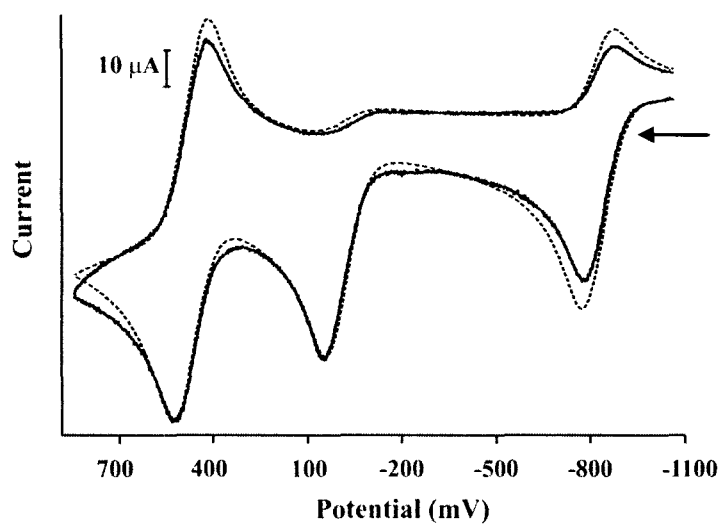


Figure B-6. Experimental (—) and simulated (---) cyclic voltammograms of [Ru-1]⁺ in presence of cyclopentene at a scan rate 400 mV/s.

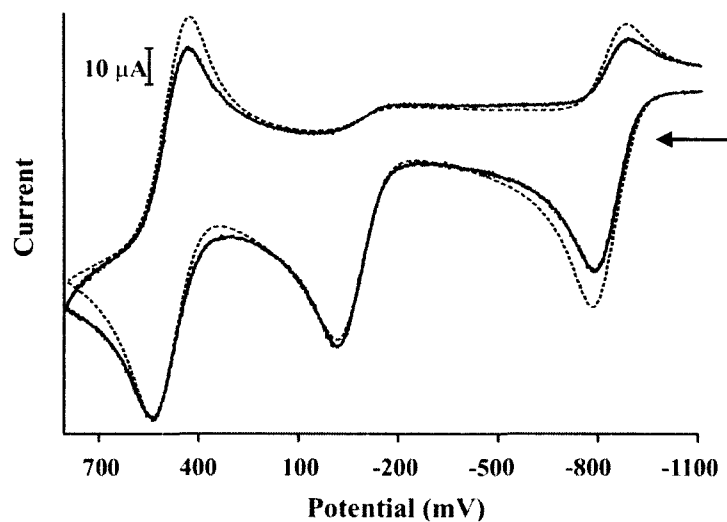


Figure B-7. Experimental (—) and simulated (---) cyclic voltammograms of [Ru-1]⁺ in presence of norbornene at a scan rate 400 mV/s.

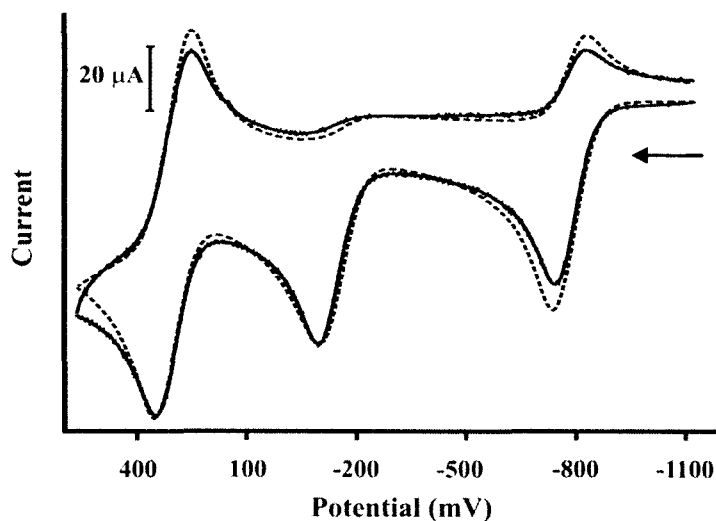


Figure B-8. Experimental (—) and simulated (---) cyclic voltammograms of [Ru-1]⁺ in presence of *p*-methoxystyrene at a scan rate 400 mV/s.

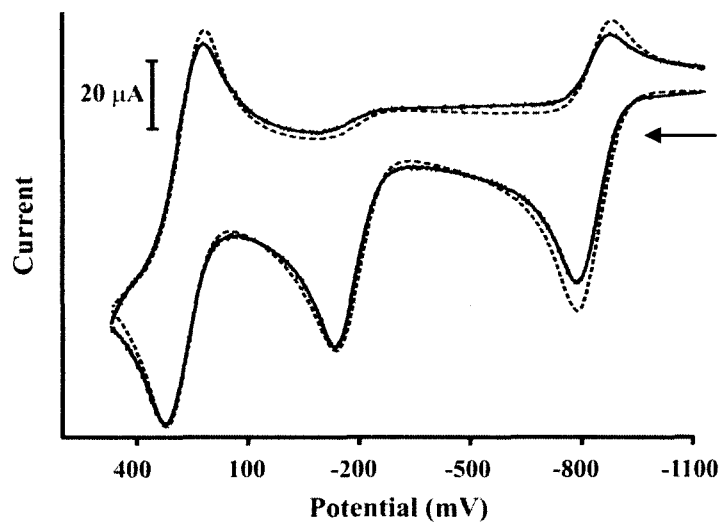


Figure B-9. Experimental (—) and simulated (---) cyclic voltammograms of [Ru-1]⁺ in presence of *p*-methylstyrene at a scan rate 400 mV/s.

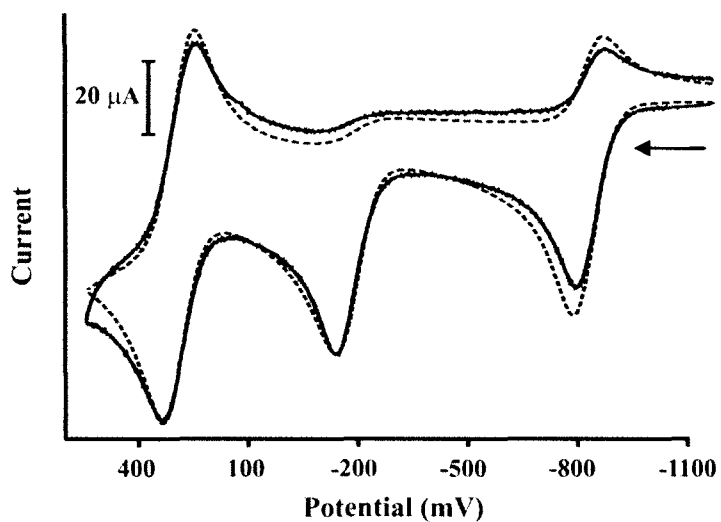


Figure B-10. Experimental (—) and simulated (---) cyclic voltammograms of [Ru-1]⁺ in presence of *p*-chlorostyrene at a scan rate 400 mV/s.

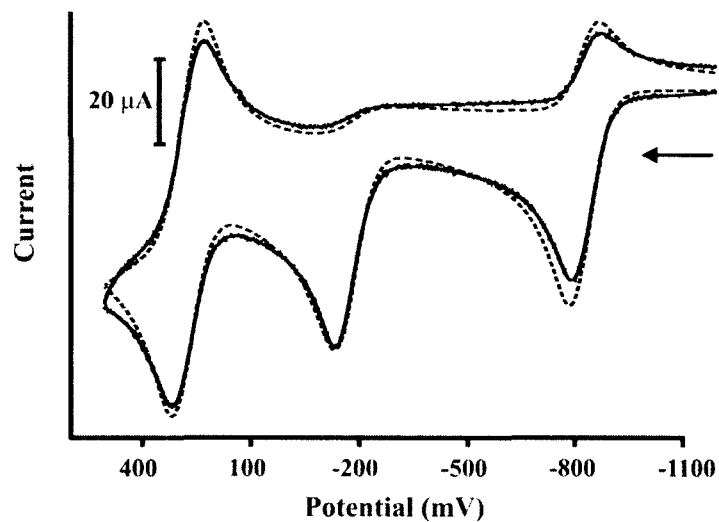


Figure B-11. Experimental (—) and simulated (---) cyclic voltammograms of [Ru-1]⁺ in presence of *p*-fluorostyrene at a scan rate 400 mV/s.

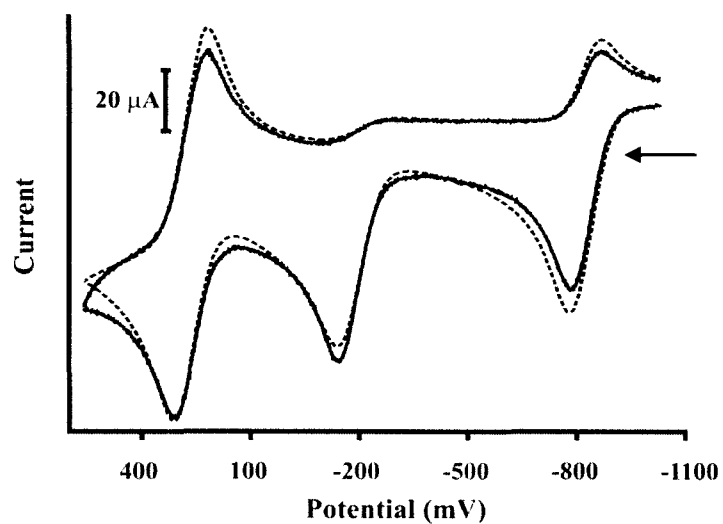


Figure B-12. Experimental (—) and simulated (---) cyclic voltammograms of [Ru-1]⁺ in presence of *m*-methoxystyrene at a scan rate 400 mV/s.

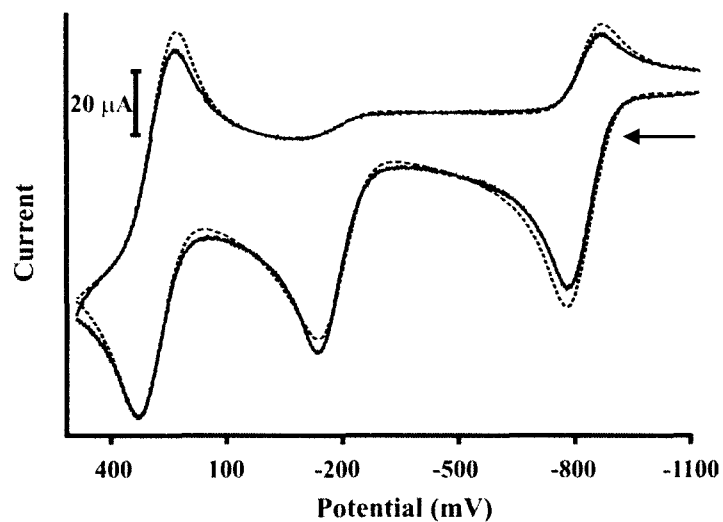


Figure B-13. Experimental (—) and simulated (---) cyclic voltammograms of [Ru-1]⁺ in presence of *m*-methylstyrene at a scan rate 400 mV/s.

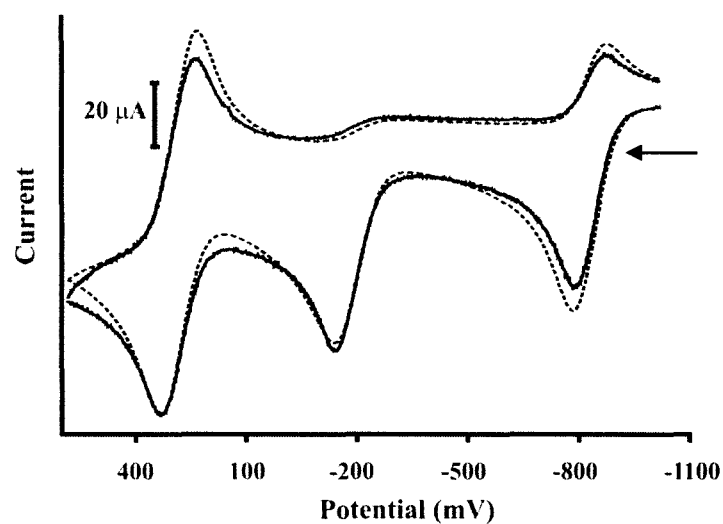


Figure B-14. Experimental (—) and simulated (---) cyclic voltammograms of [Ru-1]⁺ in presence of *m*-chlorostyrene at a scan rate 400 mV/s.

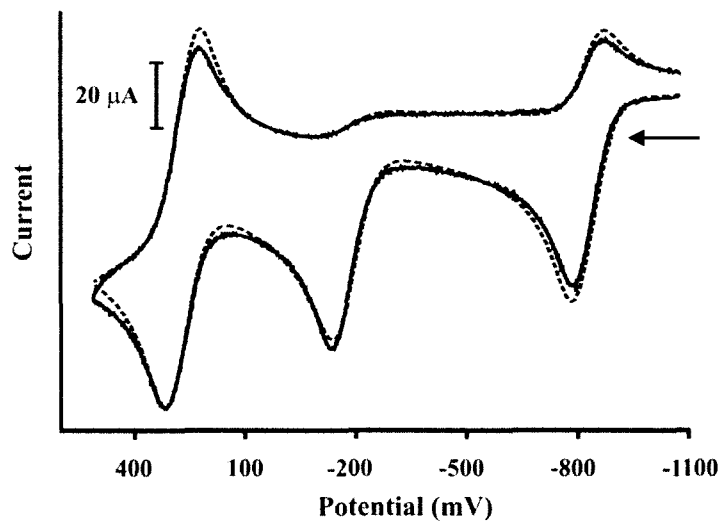


Figure B-15. Experimental (—) and simulated (---) cyclic voltammograms of [Ru-1]⁺ in presence of *m*-fluorostyrene at a scan rate 400 mV/s.

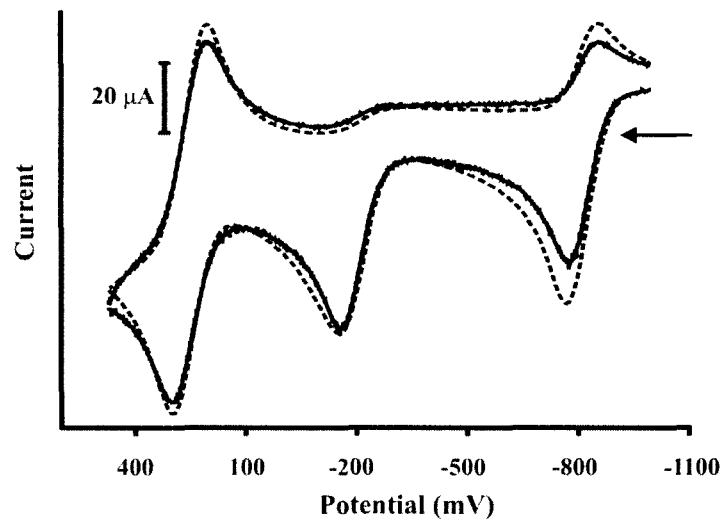


Figure B-16. Experimental (—) and simulated (---) cyclic voltammograms of [Ru-1]⁺ in presence of *o*-methoxystyrene at a scan rate 400 mV/s.

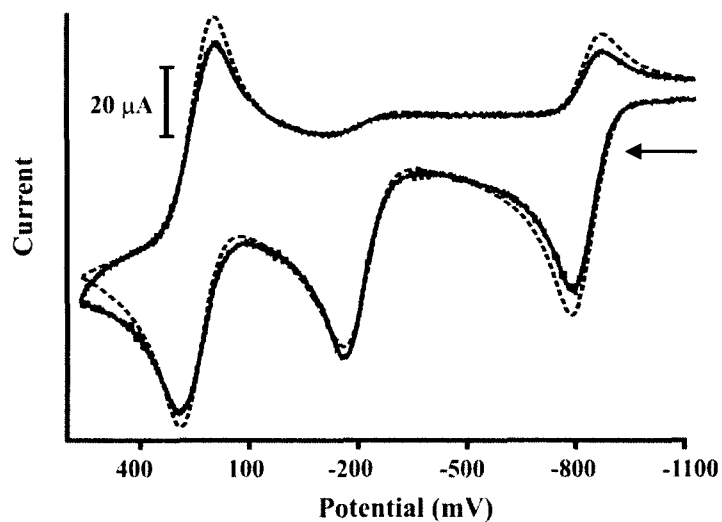


Figure B-17. Experimental (—) and simulated (---) cyclic voltammograms of [Ru-1] in presence of *o*-methylstyrene at a scan rate 400 mV/s.

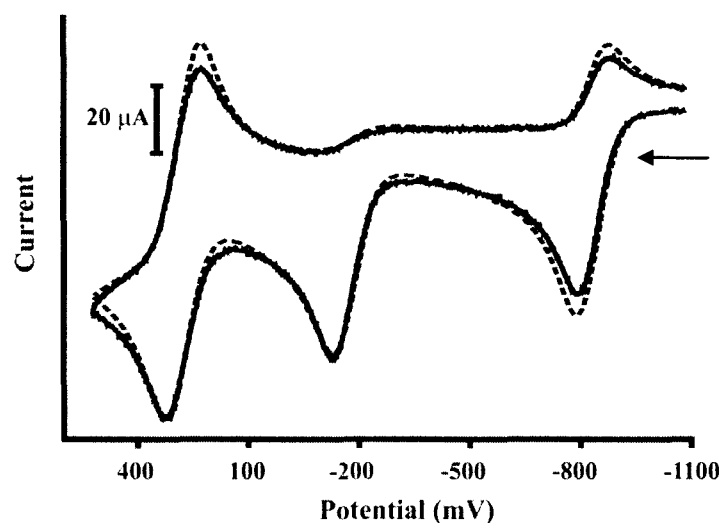


Figure B-18. Experimental (—) and simulated (---) cyclic voltammograms of [Ru-1] in presence of *o*-fluorostyrene at a scan rate 400 mV/s.

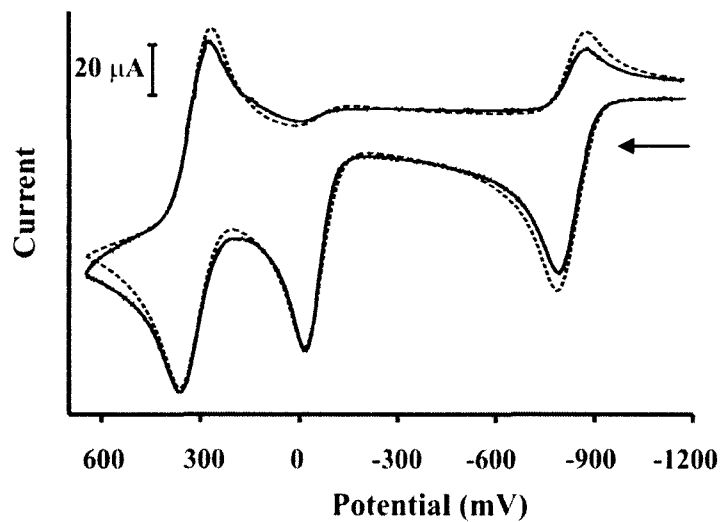


Figure B-19. Experimental (—) and simulated (---) cyclic voltammograms of [Ru-1] in presence of *cis*-stilbene at a scan rate 400 mV/s.

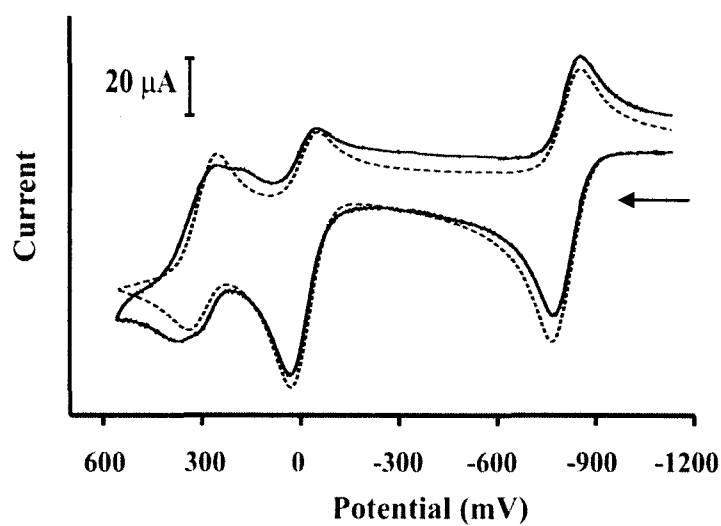


Figure B-20. Experimental (—) and simulated (---) cyclic voltammograms of [Ru-1] in presence of *trans*-stilbene at a scan rate 400 mV/s.

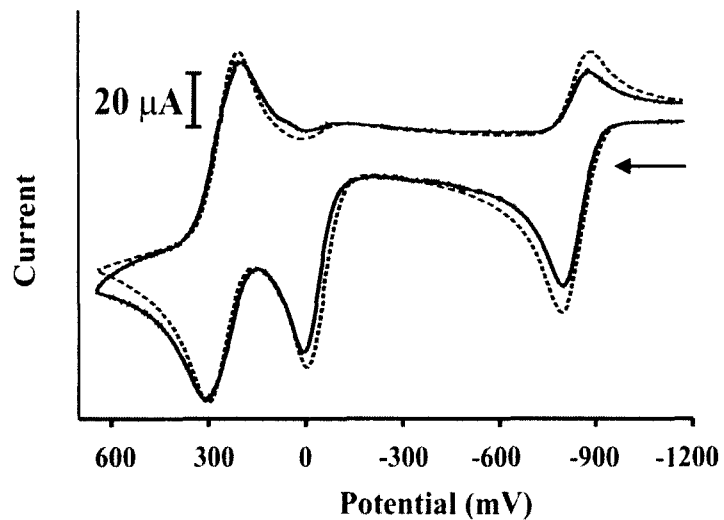


Figure B-21. Experimental (—) and simulated (---) cyclic voltammograms of [Ru-1] in presence of 2-methyl-2-butene at a scan rate 400 mV/s.

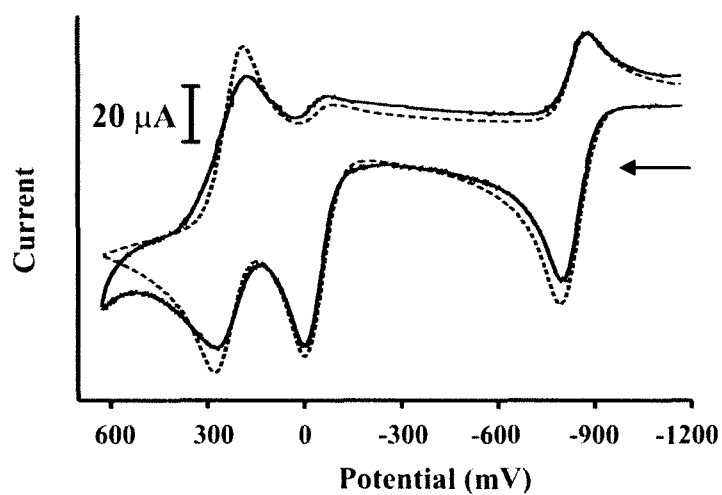


Figure B-22. Experimental (—) and simulated (---) cyclic voltammograms of [Ru-1] in presence of 2,3-dimethyl-2-butene at a scan rate 400 mV/s.

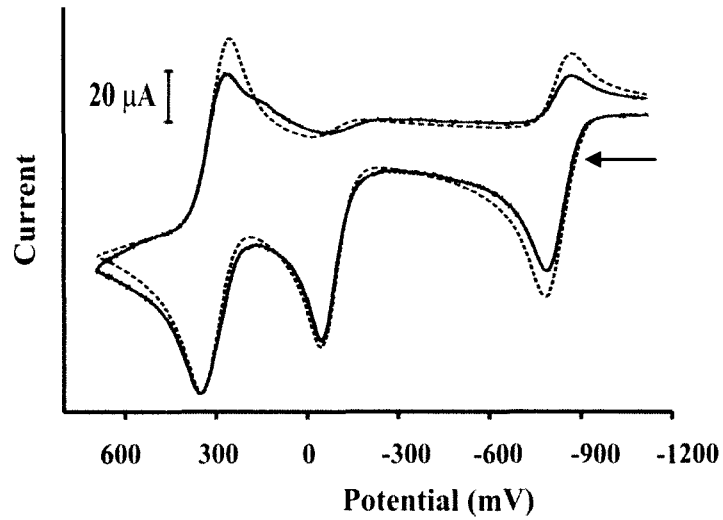


Figure B-23. Experimental (—) and simulated (---) cyclic voltammograms of [Ru-1] in presence of 1-octyne at a scan rate 400 mV/s.

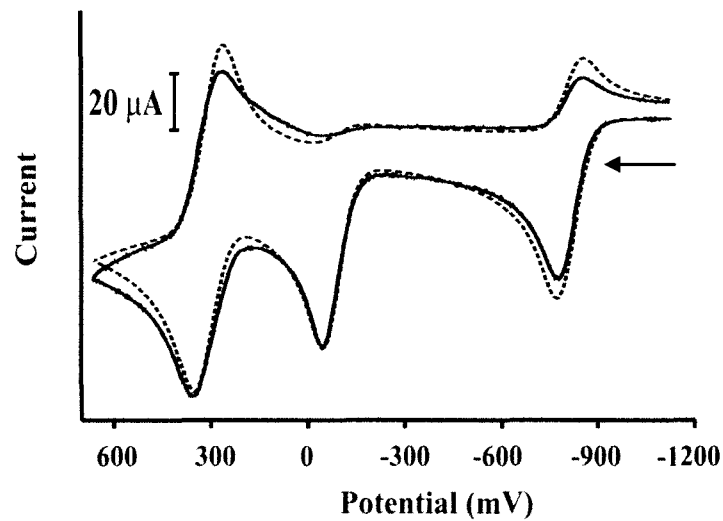


Figure B-24. Experimental (—) and simulated (---) cyclic voltammograms of [Ru-1] in presence of phenyl acetylene at a scan rate 400 mV/s.

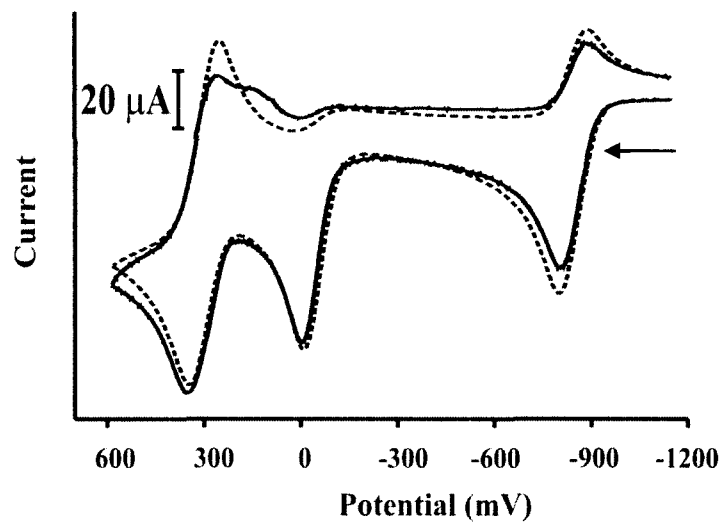


Figure B-25. Experimental (—) and simulated (---) cyclic voltammograms of [Ru-1]⁺ in presence of 1-phenyl-1-propyne at a scan rate 400 mV/s.

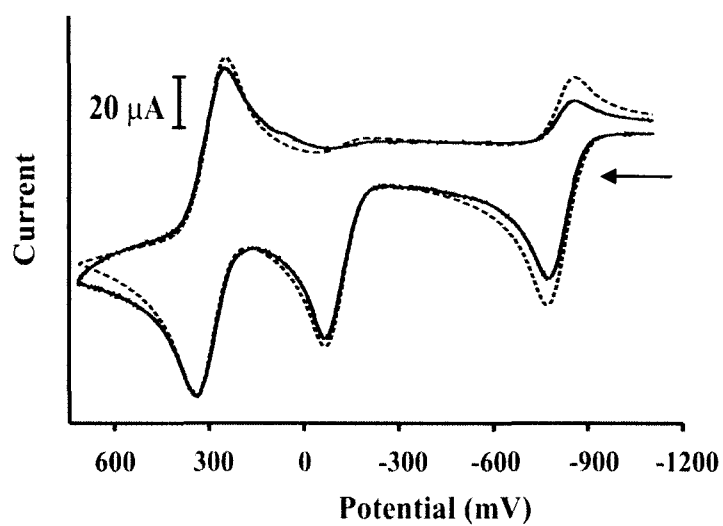


Figure B-26. Experimental (—) and simulated (---) cyclic voltammograms of [Ru-1]⁺ in presence of 1,3-butadiene at a scan rate 400 mV/s.

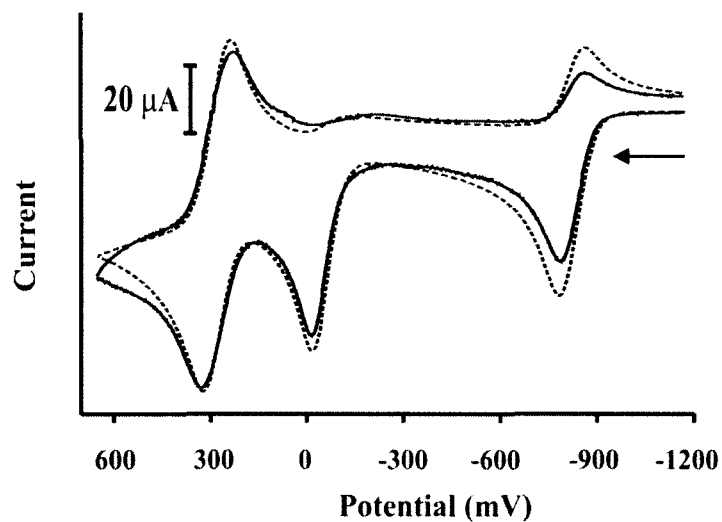


Figure B-27. Experimental (—) and simulated (---) cyclic voltammograms of **[Ru-1]** in presence of 2,3-dimethyl-1,3-butadiene at a scan rate 400 mV/s.

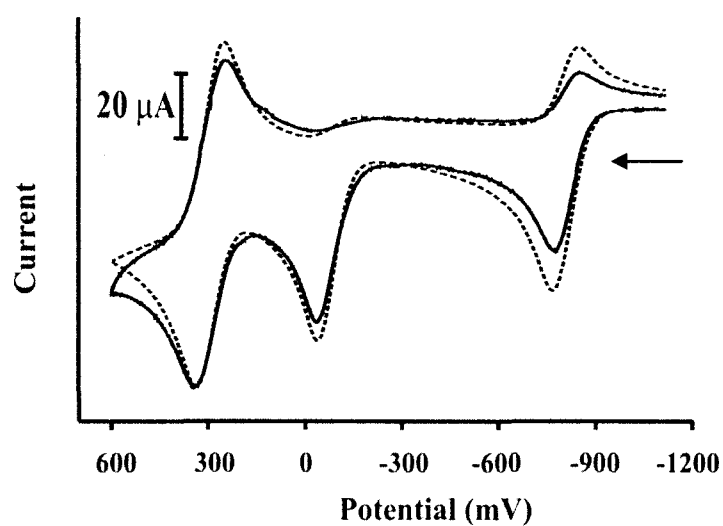


Figure B-28. Experimental (—) and simulated (---) cyclic voltammograms of **[Ru-1]** in presence of dipentene at a scan rate 400 mV/s.

APPENDIX C
Mass Spectroscopy

Appendix	Page
C-1 +ESI-MS of [Ru-1·<i>p</i>-methylstyrene]⁺ in acetonitrile	146
C-2 +ESI-MS of [Ru-1·<i>m</i>-methylstyrene]⁺ in acetonitrile	146
C-3 +ESI-MS of [Ru-1·cyclohexene]⁺ in acetonitrile	147
C-4 +ESI-MS of [Ru-1·<i>cis</i>-stilbene]⁺ in acetonitrile	147
C-5 +ESI-MS of [Ru-1·<i>trans</i>-stilbene]⁺ in acetonitrile	148
C-6 +ESI-MS of [Ru-1·octyne]⁺ in acetonitrile	148
C-7 +ESI-MS of [Ru-1·phenylacetylene]⁺ in acetonitrile	149
C-8 +ESI-MS of [Ru-1·MePhkyne]⁺ in acetonitrile	149
C-9 +ESI-MS of [Ru-1·butadiene]⁺ in acetonitrile	150
C-10 +ESI-MS of [Ru-1·2Mediene]⁺ in acetonitrile	150
C-11 +ESI-MS of [Ru-1·dipentene]⁺ in acetonitrile	151

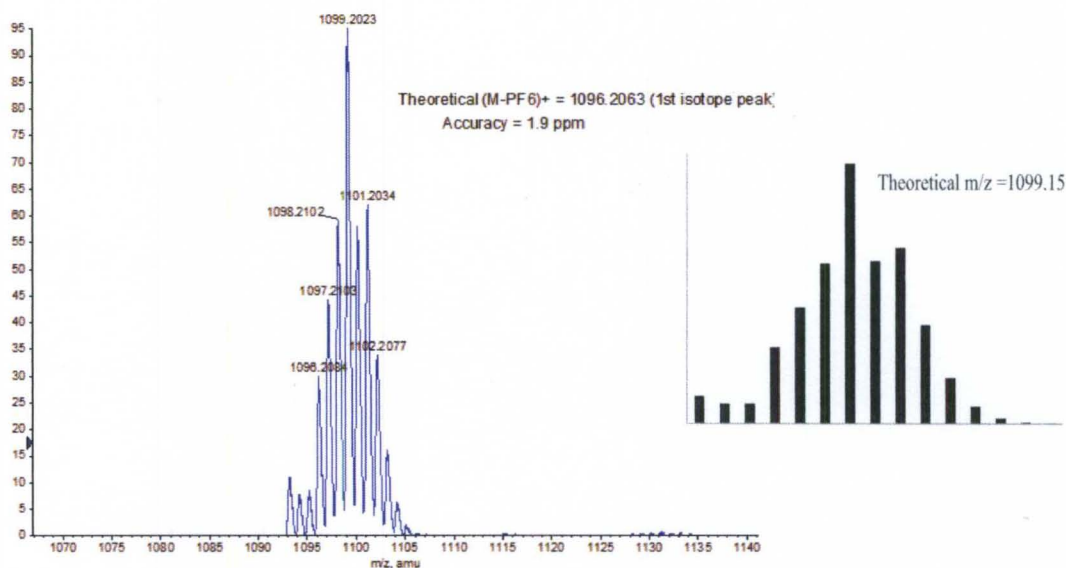


Figure C-1. +ESI-MS of [Ru-1-*p*-methylstyrene]⁺ in acetonitrile.

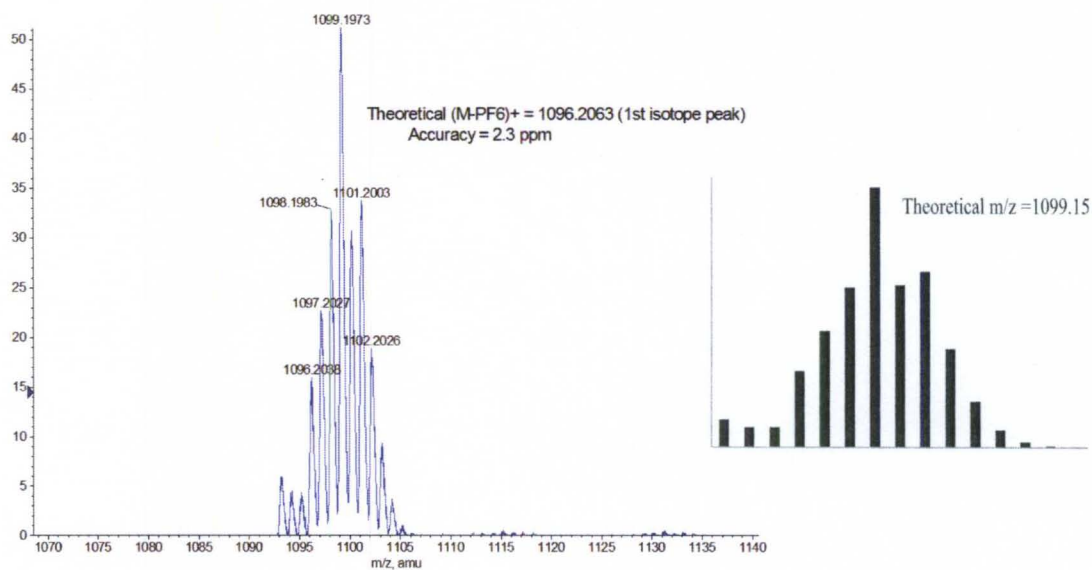


Figure C-2. +ESI-MS of [Ru-1-*m*-methylstyrene]⁺ in acetonitrile

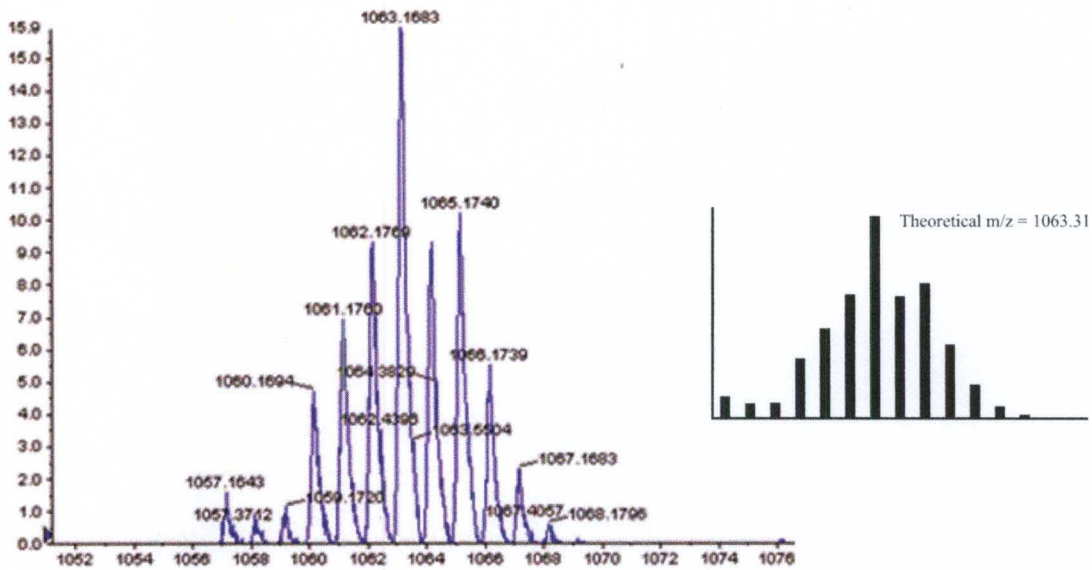


Figure C-3. +ESI-MS of $[\text{Ru-1}\cdot\text{cyclohexene}]^+$ in acetonitrile.

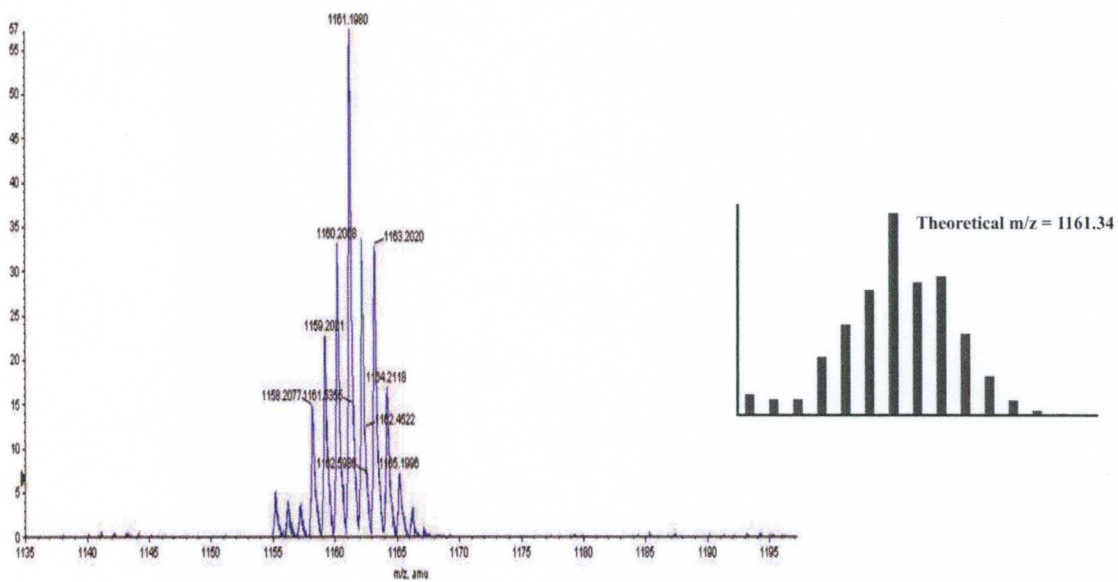


Figure C-4. +ESI-MS of $[\text{Ru-1}\cdot\text{cis-stilbene}]^+$ in acetonitrile.

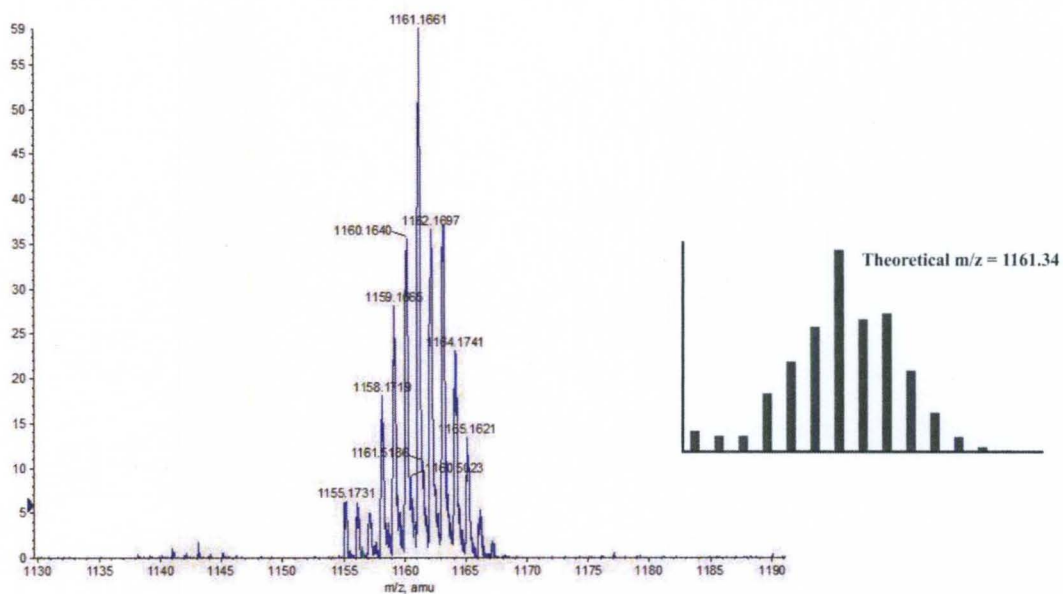


Figure C-5. +ESI-MS of $[\text{Ru-1-}i>\text{trans-stilbene}]^+$ in acetonitrile.

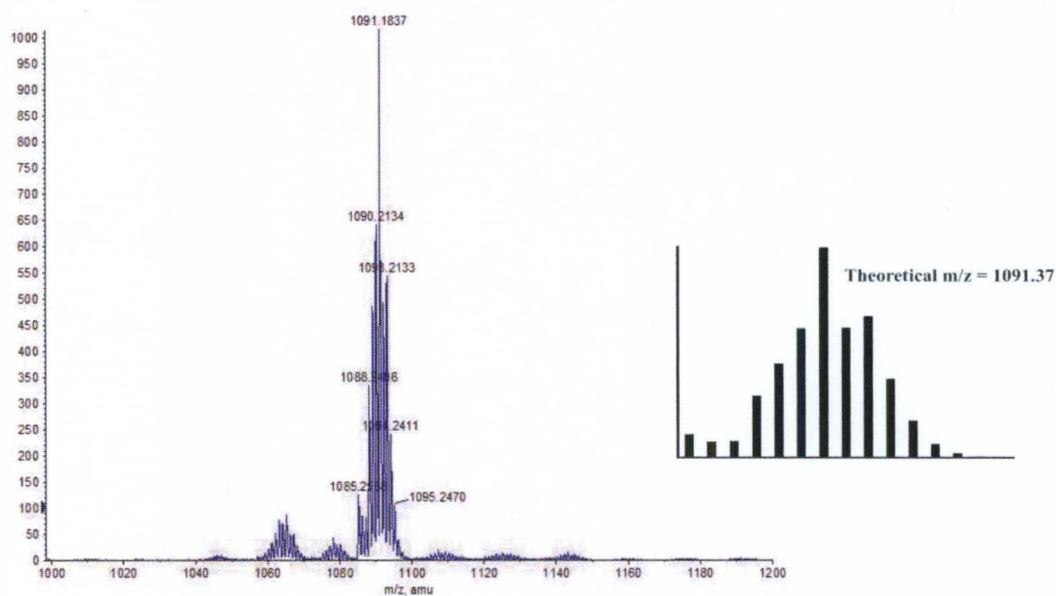


Figure C-6. +ESI-MS of $[\text{Ru-1-octyne}]^+$ in acetonitrile.

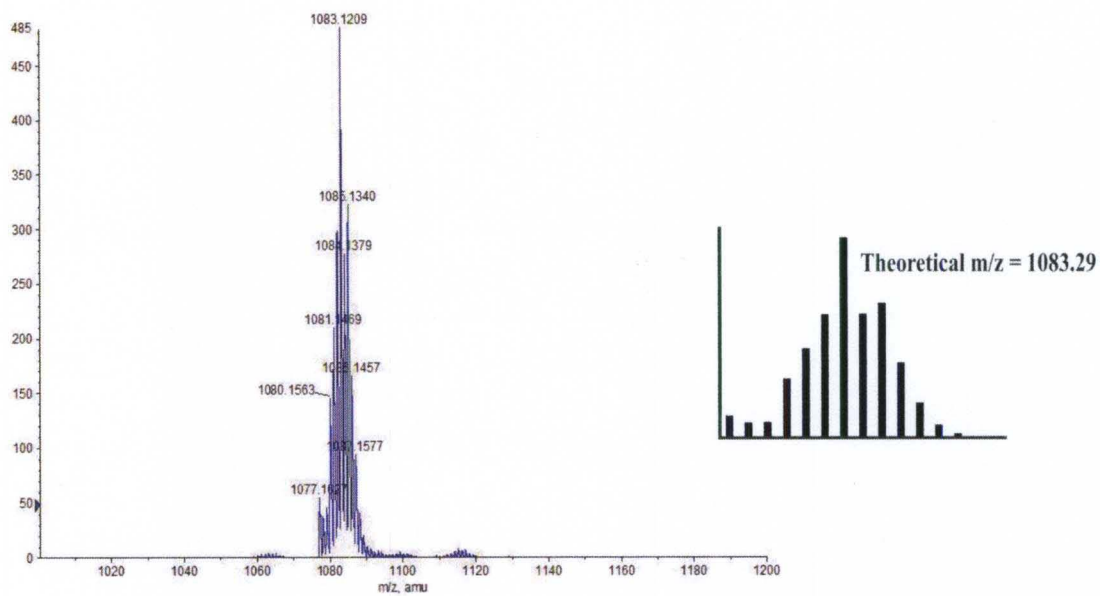


Figure C-7. +ESI-MS of $[\text{Ru-1-phenyl acetylene}]^+$ in acetonitrile.

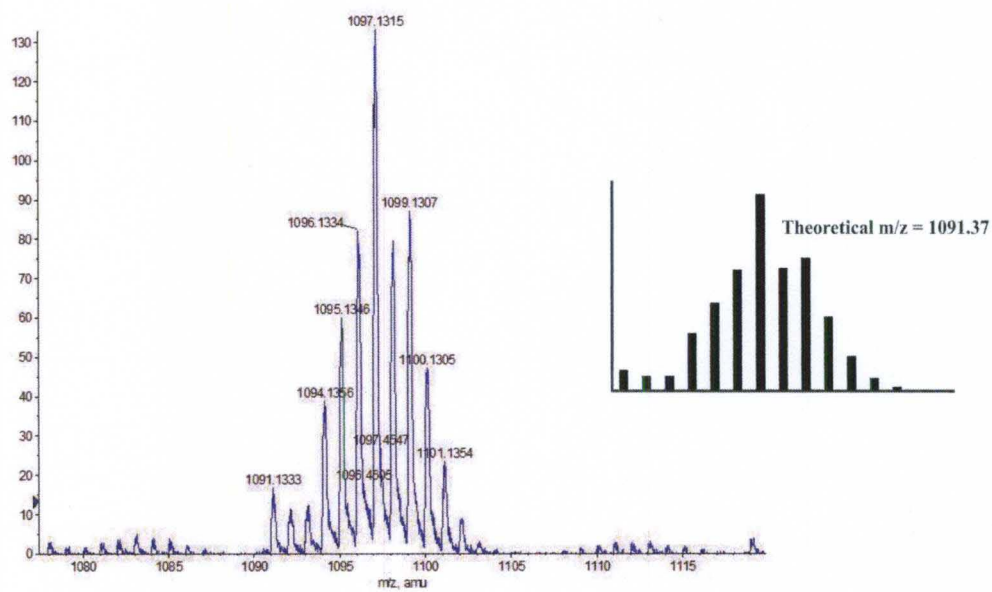


Figure C-8. +ESI-MS of $[\text{Ru-1-MePhkyne}]^+$ in acetonitrile.

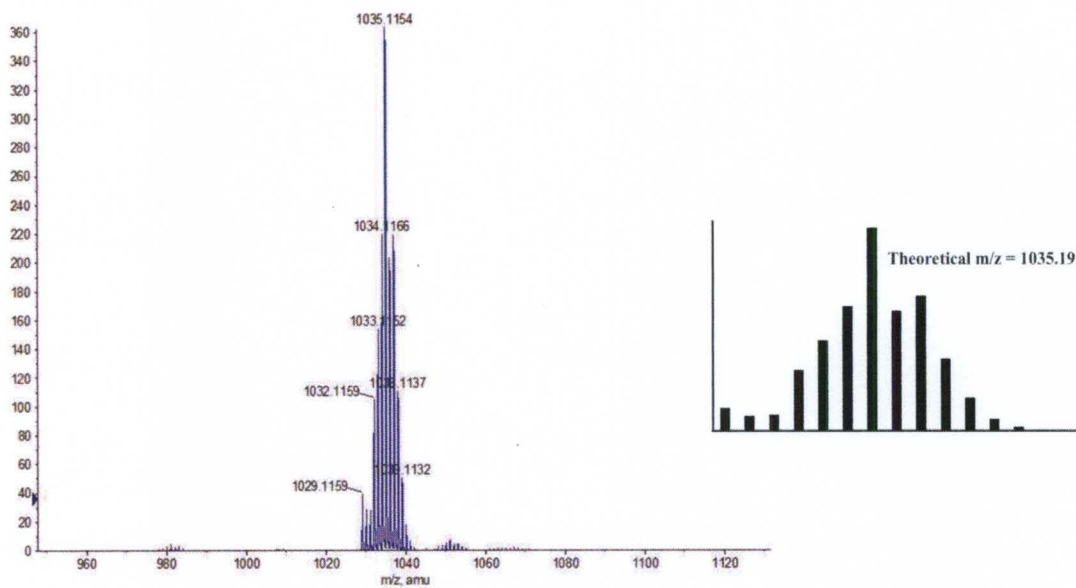


Figure C-9. +ESI-MS of $[\text{Ru-1-butadiene}]^+$ in acetonitrile.

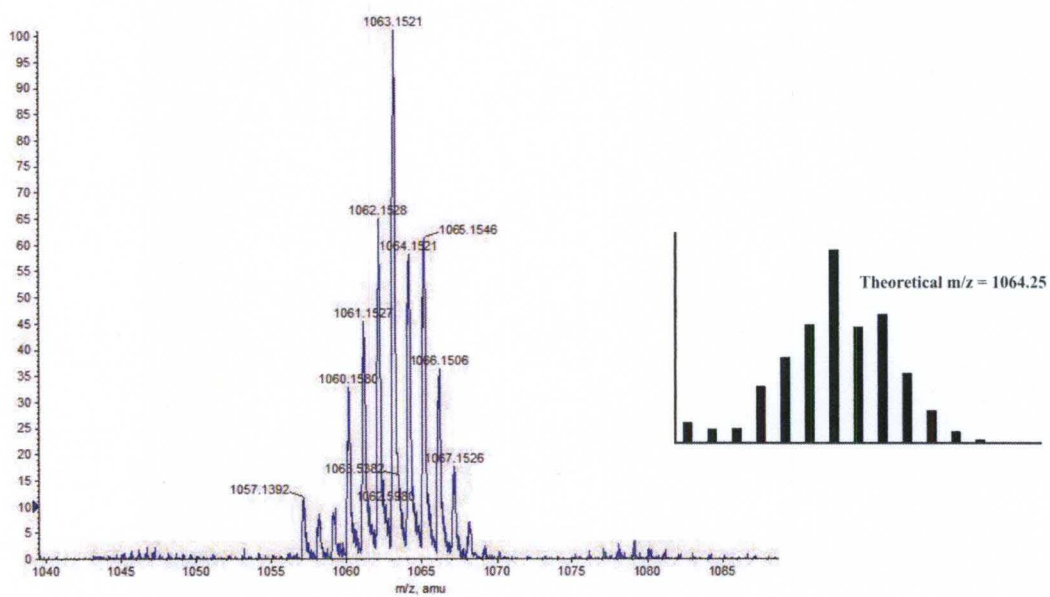


Figure C-10. +ESI-MS of $[\text{Ru-1-2Mediene}]^+$ in acetonitrile.

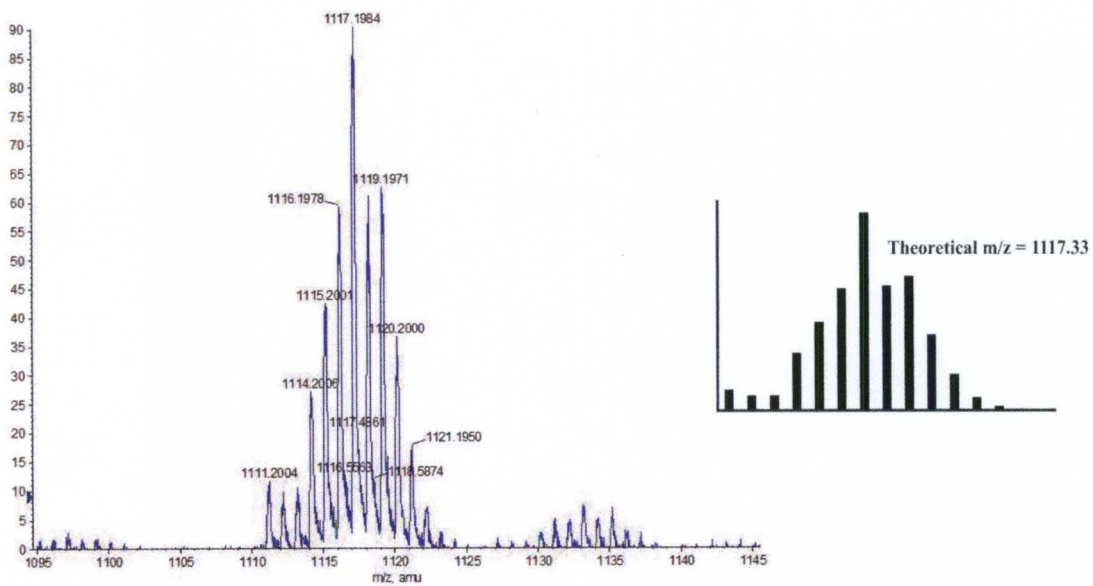


Figure C-11. +ESI-MS of [Ru-1-dipentene]⁺ in acetonitrile.

APPENDIX D

UV-visible Spectroscopy

Appendix	Page
D-1 Electronic spectra of [Ru-1·<i>p</i>-methylstyrene] ⁺ in acetonitrile.....	153
D-2 Electronic spectra of [Ru-1·<i>m</i>-methylstyrene] ⁺ in acetonitrile.....	153
D-3 Electronic spectra of [Ru-1·cyclohexene] ⁺ in acetonitrile.....	154
D-4 Electronic spectra of [Ru-1·<i>cis</i>-stilbene] ⁺ in acetonitrile	154
D-5 Electronic spectra of [Ru-1·<i>trans</i>-stilbene] ⁺ in acetonitrile	155
D-6 Electronic spectra of [Ru-1·octyne] ⁺ in acetonitrile	155
D-7 Electronic spectra of [Ru-1·phenylacetylene] ⁺ in acetonitrile	156
D-8 Electronic spectra of [Ru-1·MePhkyne] ⁺ in acetonitrile.....	156
D-9 Electronic spectra of [Ru-1·butadiene] ⁺ in acetonitrile	157
D-10 Electronic spectra of [Ru-1·dipentene] ⁺ in acetonitrile.....	157
D-11 Electronic spectra of [Ru-1·2Mediene] ⁺ in acetonitrile.....	158

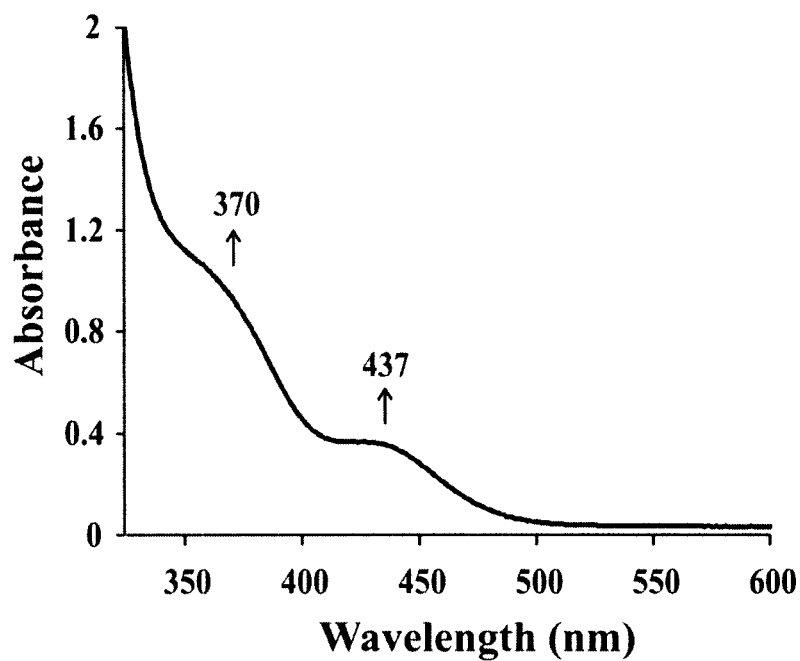


Figure D-1. Electronic spectra of [Ru-1-*p*-methylstyrene]⁺ in acetonitrile.

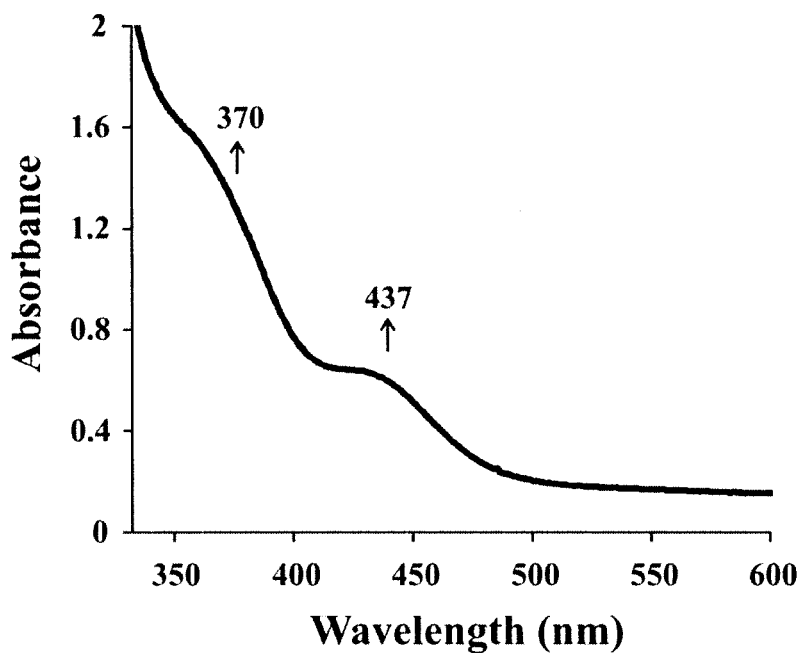


Figure D-2. Electronic spectra of [Ru-1-*m*-methylstyrene]⁺ in acetonitrile

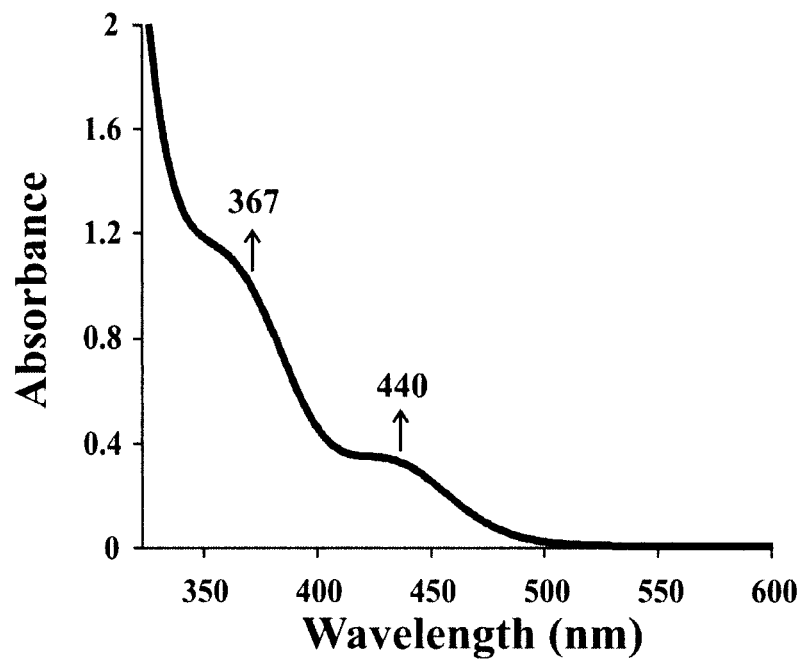


Figure D-3. Electronic spectra of [Ru-1·cyclohexene]⁺ in acetonitrile.

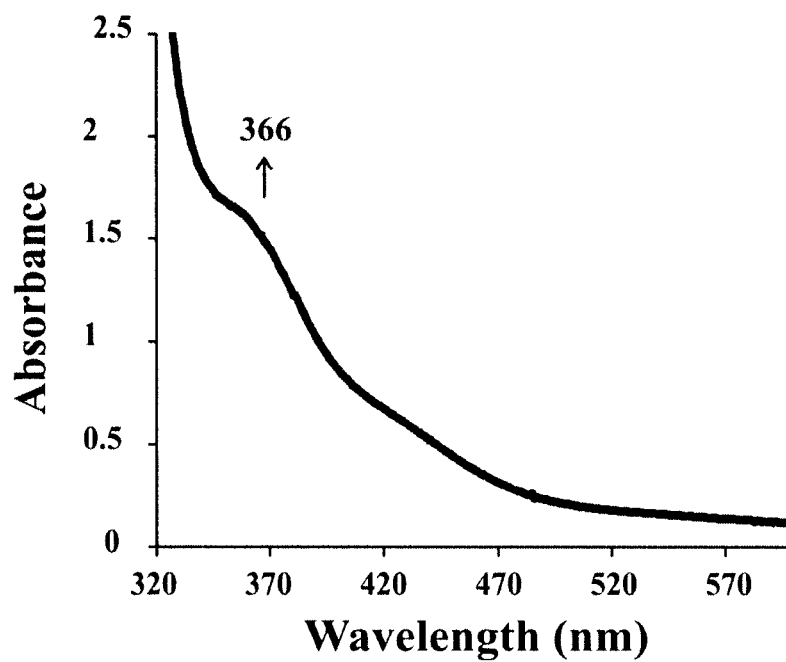


Figure D-4. Electronic spectra of [Ru-1·cis-stilbene]⁺ in acetonitrile.

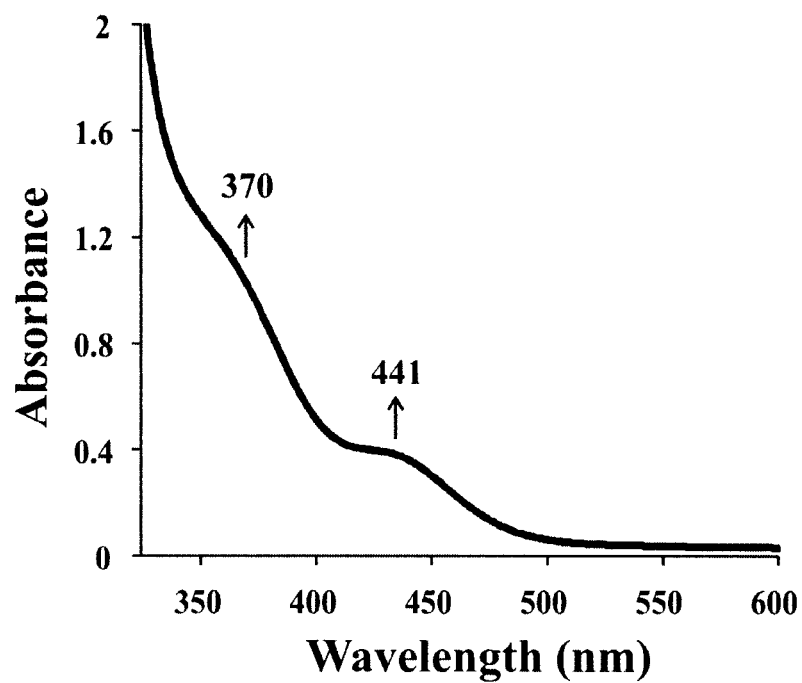


Figure D-5. Electronic spectra of [Ru-1·*trans*-stilbene]⁺ in acetonitrile.

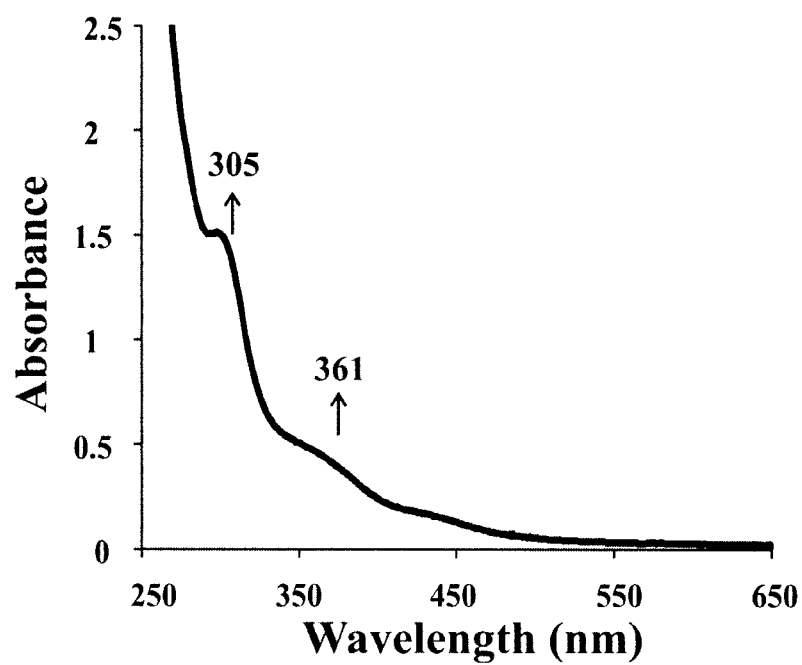


Figure D-6. Electronic spectra of [Ru-1·octyne]⁺ in acetonitrile.

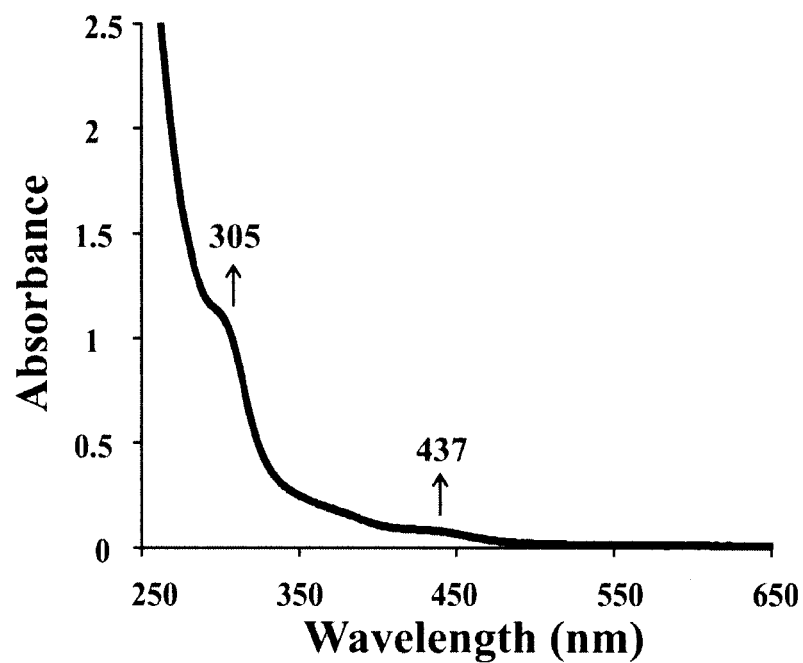


Figure D-7. Electronic spectra of [Ru-1·phenylacetylene]⁺ in acetonitrile.

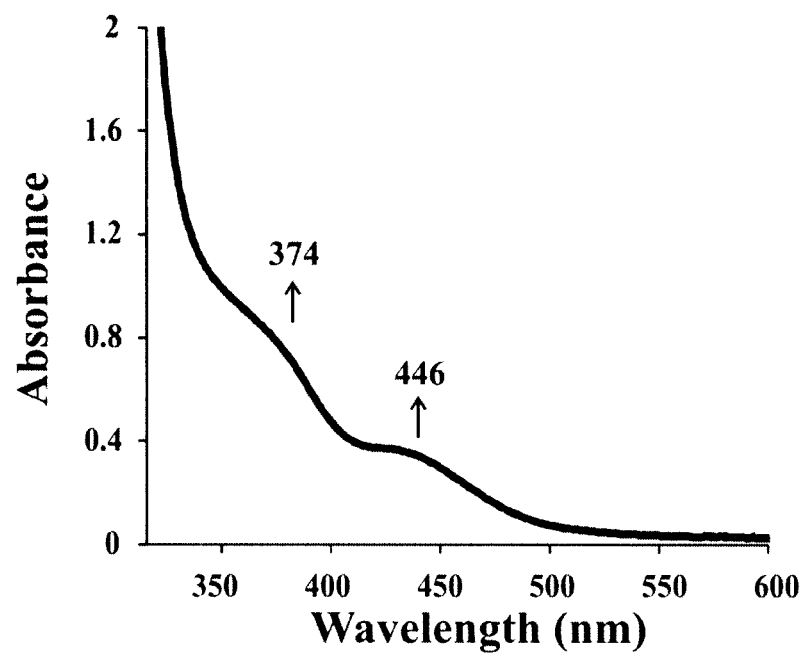


Figure D-8. Electronic spectra of [Ru-1·MePhkyne]⁺ in acetonitrile.

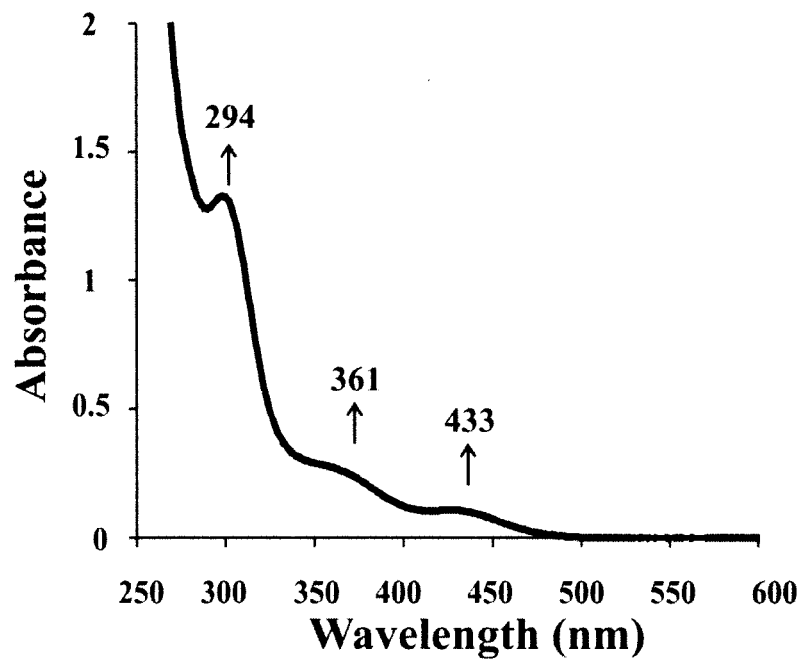


Figure D-9. Electronic spectra of [Ru-1-butadiene]⁺ in acetonitrile.

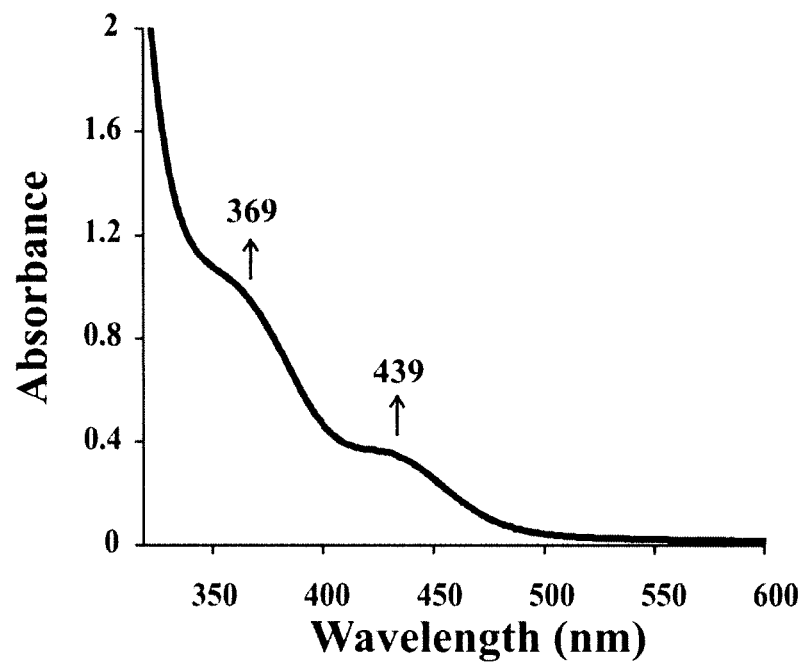


Figure D-10. Electronic spectra of [Ru-1-dipentene]⁺ in acetonitrile.

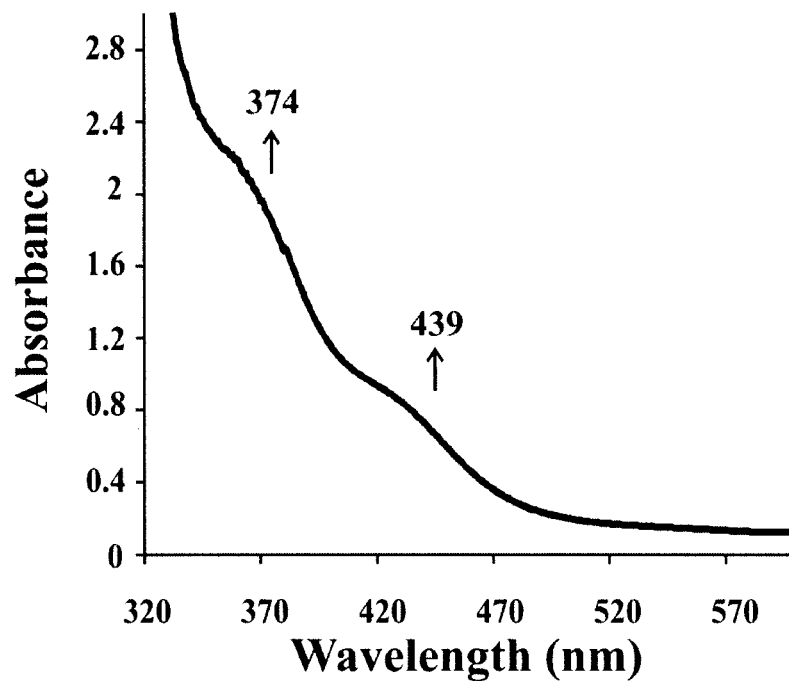


Figure D-11. Electronic spectra of [Ru-1·2Mediene]⁺ in acetonitrile.

APPENDIX E

Electrochemistry

Appendix	Page
E-1 CV of [Re-1 ·styrene] ²⁺ in dichloromethane	161
E-2 CV of [Ru-1] ⁻ in presence of styrene.....	161
E-3 CV of [Ru-1] ⁻ in presence of <i>n</i> -propyl vinyl ether	162
E-4 CV of [Ru-1] ⁻ in presence of <i>t</i> -butyl vinyl ether	162
E-5 CV of [Ru-1] ⁻ in presence of <i>n</i> -hexene.....	163
E-6 CV of [Ru-1] ⁻ in presence of acrylonitrile.....	163
E-7 CV of [Ru-1] ⁻ in presence of cyclohexene	164
E-8 CV of [Ru-1] ⁻ in presence of cyclopentene	164
E-9 CV of [Ru-1] ⁻ in presence of norbornene	165
E-10 CV of [Ru-1 · <i>p</i> -methylstyrene] ⁺ in acetonitrile	165
E-11 CV of [Ru-1 · <i>m</i> -methylstyrene] ⁺ in acetonitrile	166
E-12 CV of [Ru-1 ·cyclohexene] ⁺ in acetonitrile.....	166
E-13 SW of [Ru-1] ⁻ in presence of <i>cis</i> -stilbene.....	167
E-14 SW of [Ru-1] ⁻ in presence of <i>trans</i> -stilbene.....	167
E-15 SW of [Ru-1] ⁻ in presence of 2-methyl-2-butene	168
E-16 SW of [Ru-1] ⁻ in presence of 2,3-dimethyl-2-butene	168

E-17	SW of [Ru-1] ⁻ in presence of 1-octyne.....	169
E-18	SW of [Ru-1] ⁻ in presence of phenyl acetylene.....	169
E-19	SW of [Ru-1] ⁻ in presence of 1-phenyl-1-propyne.....	170
E-20	SW of [Ru-1] ⁻ in presence of 1,3-butadiene.....	170
E-21	SW of [Ru-1] ⁻ in presence of 2,3-dimethyl-1,3-butadiene.....	171
E-22	SW of [Ru-1] ⁻ in presence of dipentene.....	171
E-23	CV of [Ru-1·cis-stilbene] ⁺ in acetonitrile.....	172
E-24	CV of [Ru-1·trans-stilbene] ⁺ in acetonitrile.....	172
E-25	CV of [Ru-1·octyne] ⁺ in acetonitrile.....	173
E-26	CV of [Ru-1·phenyl acetylene] ⁺ in acetonitrile.....	173
E-27	CV of [Ru-1·MePhkyne] ⁺ in acetonitrile.....	174
E-28	CV of [Ru-1·butadiene] ⁺ in acetonitrile.....	174
E-29	CV of [Ru-1·2Mebutadiene] ⁺ in acetonitrile.....	175
E-30	CV of [Ru-1·dipentene] ⁺ in acetonitrile.....	175

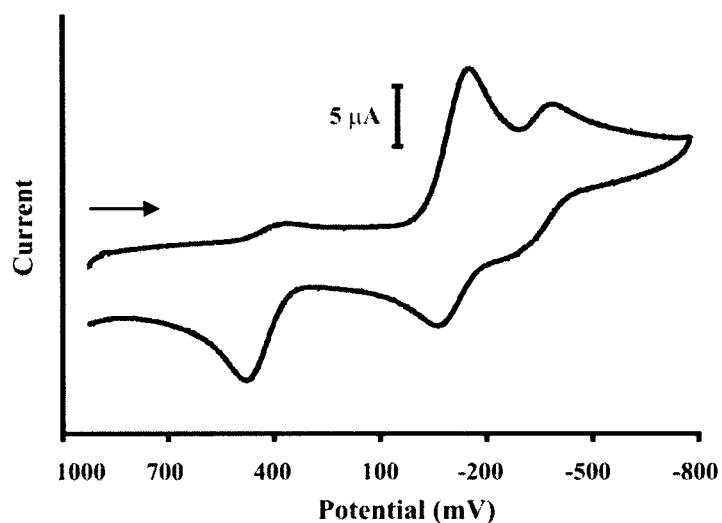


Figure E-1. Cyclic voltammogram of 1.0 mM complex $[\text{Re-1}\cdot\text{styrene}]^{2+}$ in acetonitrile with 0.1 M TBAHFP was obtained at 200 mV/s. Potentials referenced to

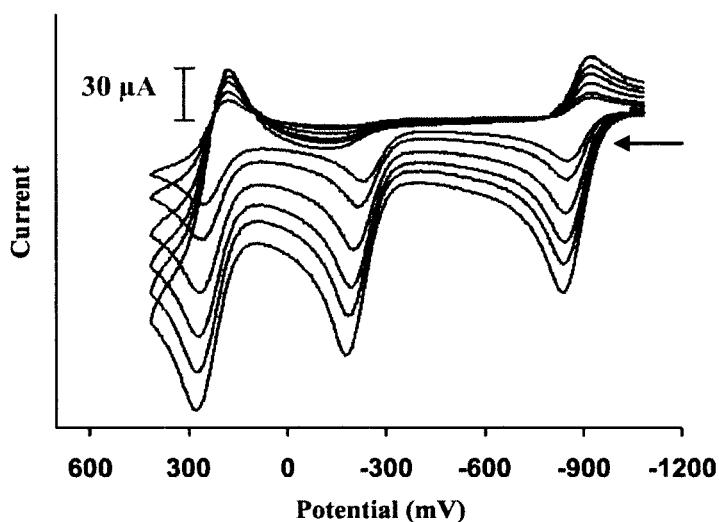


Figure E-2. Cyclic voltammogram of 2.0 mM complex $[\text{Ru-1}]$ in acetonitrile with 0.1 M TBAHFP was obtained in the presence of styrene (0.20 M) at multiple scan rates, 100 mV/s to 1000 mV/s. Potentials referenced to Fc^+/Fc .

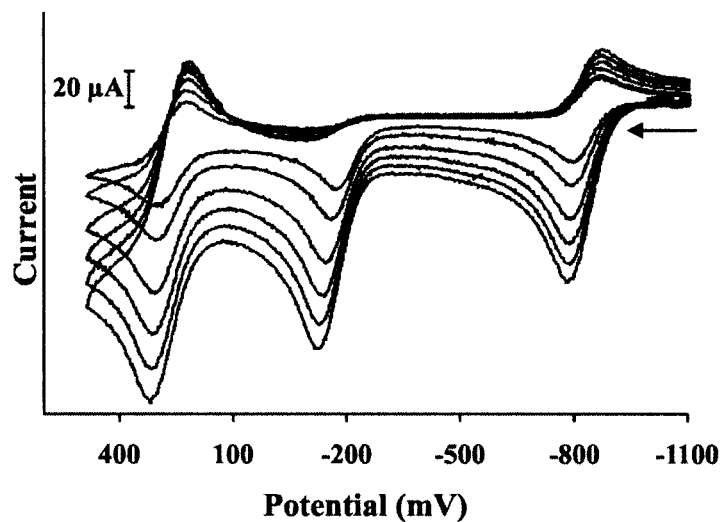


Figure E-3. Cyclic voltammogram of 2.0 mM complex [Ru-1]⁻ in acetonitrile with 0.1 M TBAHFP was obtained in the presence of *n*-propyl vinyl ether (0.20 M) at multiple scan rates, 100 mV/s to 1000 mV/s. Potentials referenced to Fc⁺/Fc.

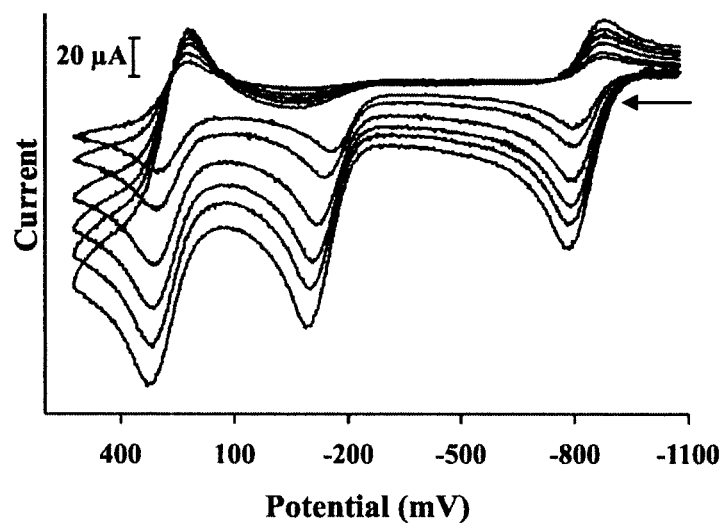


Figure E-4. Cyclic voltammogram of 2.0 mM complex [Ru-1]⁻ in acetonitrile with 0.1 M TBAHFP was obtained in the presence of *t*-butyl vinyl ether (0.20 M) at multiple scan rates, 100 mV/s to 1000 mV/s. Potentials referenced to Fc⁺/Fc.

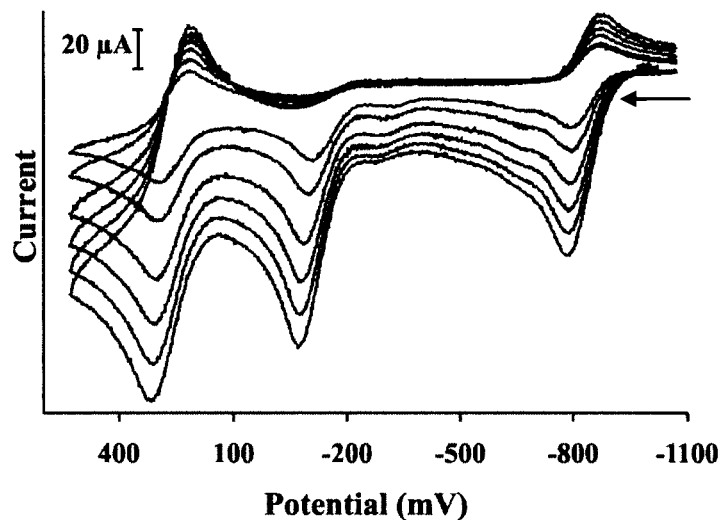


Figure E-5. Cyclic voltammogram of 2.0 mM complex [Ru-1]⁻ in acetonitrile with 0.1 M TBAHFP was obtained in the presence of *n*-hexene (0.20 M) at multiple scan rates, 100 mV/s to 1000 mV/s. Potentials referenced to Fc⁺/Fc.

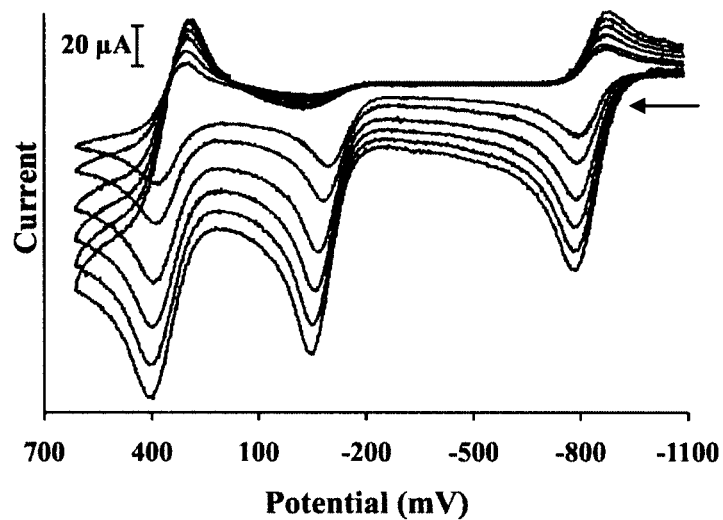


Figure E-6. Cyclic voltammogram of 2.0 mM complex [Ru-1]⁻ in acetonitrile with 0.1 M TBAHFP was obtained in the presence of acrylonitrile (0.20 M) at multiple scan rates, 100 mV/s to 1000 mV/s. Potentials referenced to Fc⁺/Fc.

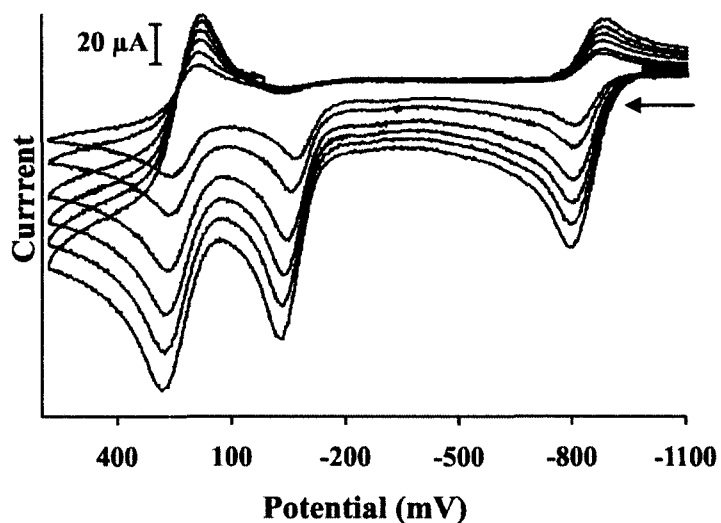


Figure E-7. Cyclic voltammogram of 2.0 mM complex [Ru-1] in acetonitrile with 0.1 M TBAHFP was obtained in the presence of cyclohexene (0.20 M) at multiple scan rates, 100 mV/s to 1000 mV/s. Potentials referenced to Fc^+/Fc .

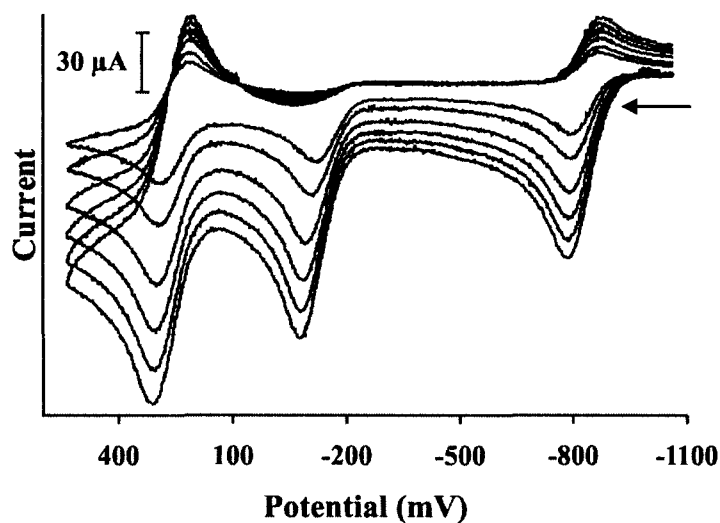


Figure E-8. Cyclic voltammogram of 2.0 mM complex [Ru-1] in acetonitrile with 0.1 M TBAHFP was obtained in the presence of cyclopentene (0.20 M) at multiple scan rates, 100 mV/s to 1000 mV/s. Potentials referenced to Fc^+/Fc .

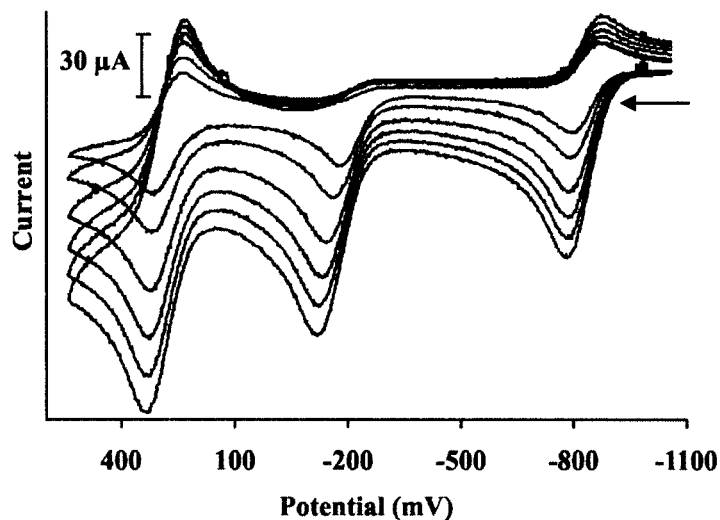


Figure E-9. Cyclic voltammogram of 2.0 mM complex $[\text{Ru-1}]^-$ in acetonitrile with 0.1 M TBAHFP was obtained in the presence of norbornene (0.20 M) at multiple scan rates, 100 mV/s to 1000 mV/s. Potentials referenced to Fc^+/Fc .

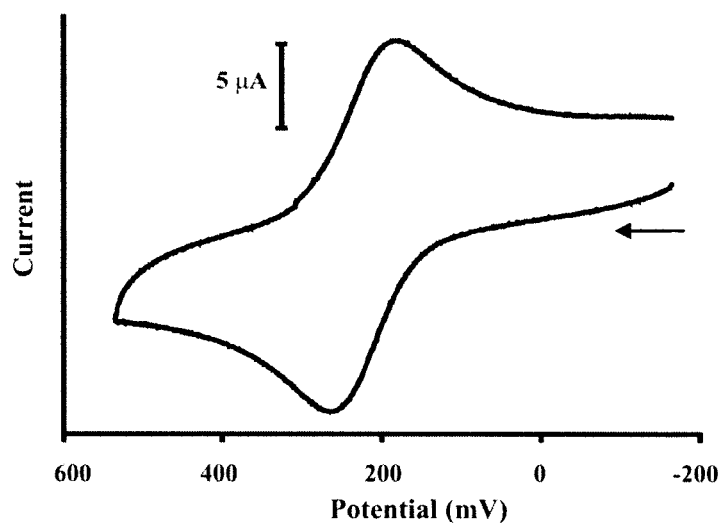


Figure E-10. Cyclic voltammogram of 1.0 mM complex $[\text{Ru-1}\cdot p\text{-methylstyrene}]^+$ in acetonitrile with 0.1 M TBAHFP was obtained at 200 mV/s. Potentials referenced to

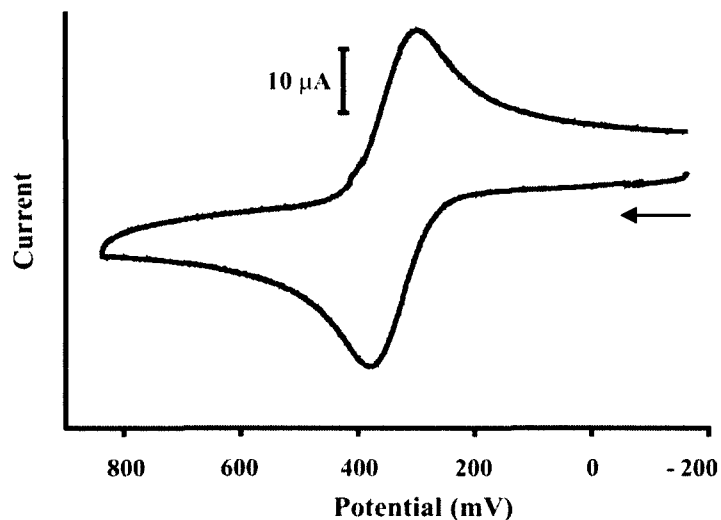


Figure E-11. Cyclic voltammogram of 1.0 mM complex $[\text{Ru-1}\cdot m\text{-methylstyrene}]^+$ in acetonitrile with 0.1 M TBAHFP was obtained at 200 mV/s. Potentials referenced to

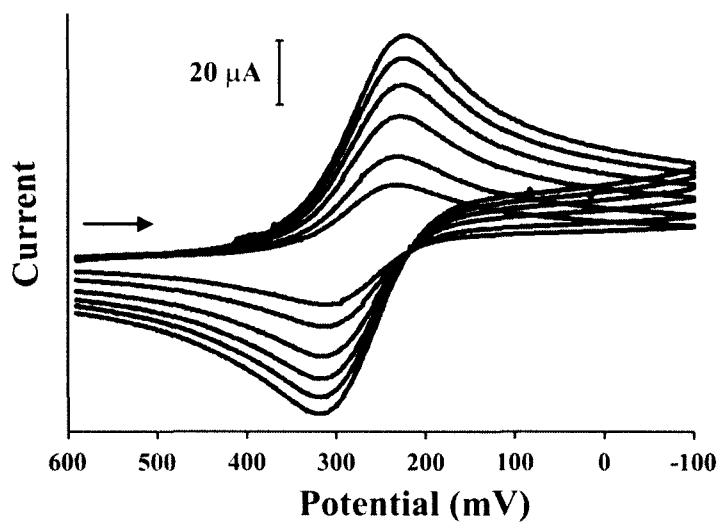


Figure E-12. Cyclic voltammogram of 1.0 mM complex $[\text{Ru-1}\cdot\text{cyclohexene}]^+$ in acetonitrile with 0.1 M TBAHFP was obtained at multiple scan rates, 100 mV/s to 1000 mV/s. Potentials referenced to Fc^+/Fc .

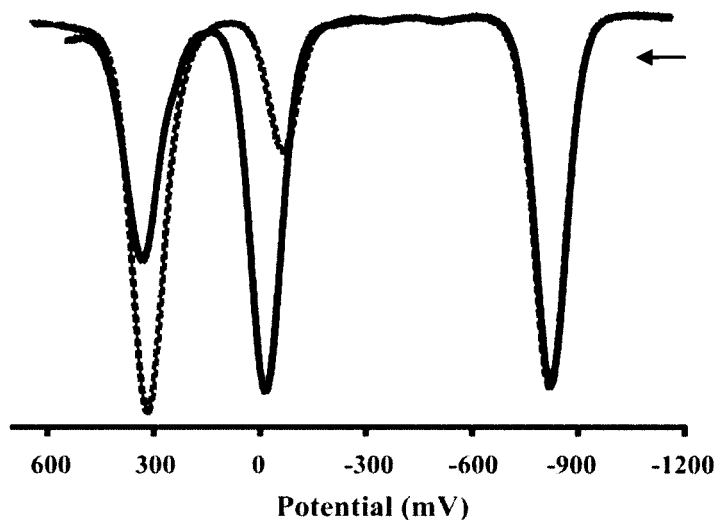


Figure E-13. Anodic square wave voltammograms of 2.0 mM complex PPN[Ru-1] (dark line) and in the presence of 0.2 M *cis*-stilbene (dotted line) measured at room temperature versus Ag/AgCl reference electrode. Reported potentials are scaled to a ferrocenium/ferrocene reference.

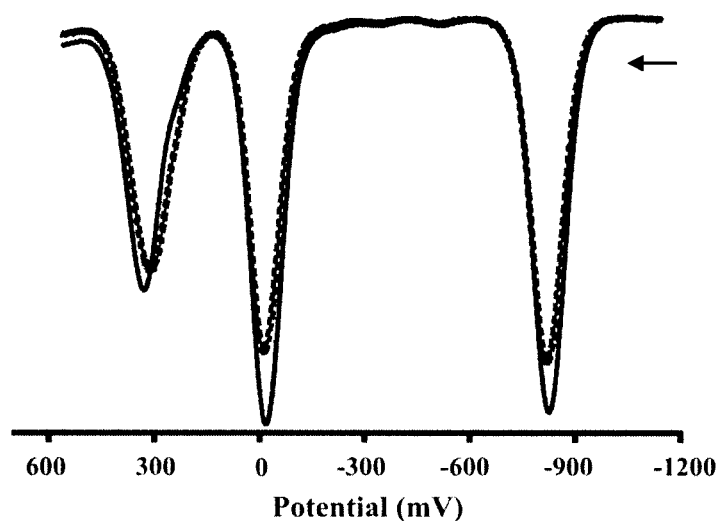


Figure E-14. Anodic square wave voltammograms of 2.0 mM complex PPN[Ru-1] (dark line) and in the presence of 0.2 M *trans*-stilbene (dotted line) measured at room temperature versus Ag/AgCl reference electrode. Reported potentials are scaled to a ferrocenium/ferrocene reference.

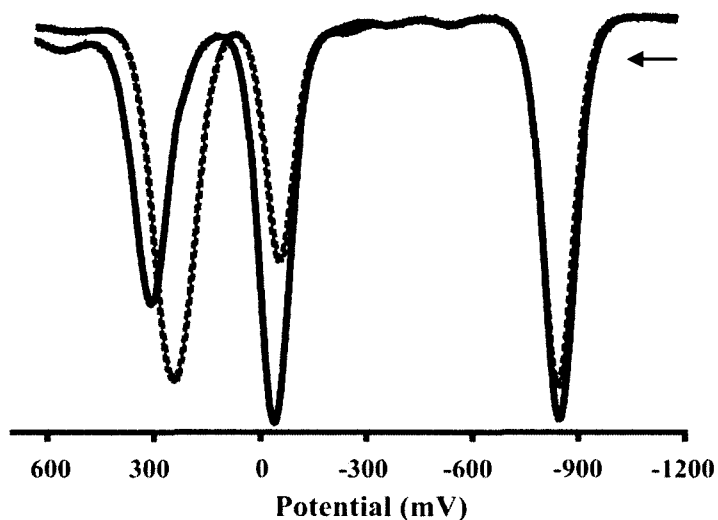


Figure E-15. Anodic square wave voltammograms of 2.0 mM complex PPN[Ru-1] (dark line) and in the presence of 0.2 M 2-methyl-2-butene (dotted line) measured at room temperature versus Ag/AgCl reference electrode. Reported potentials are scaled to a ferrocenium/ferrocene reference.

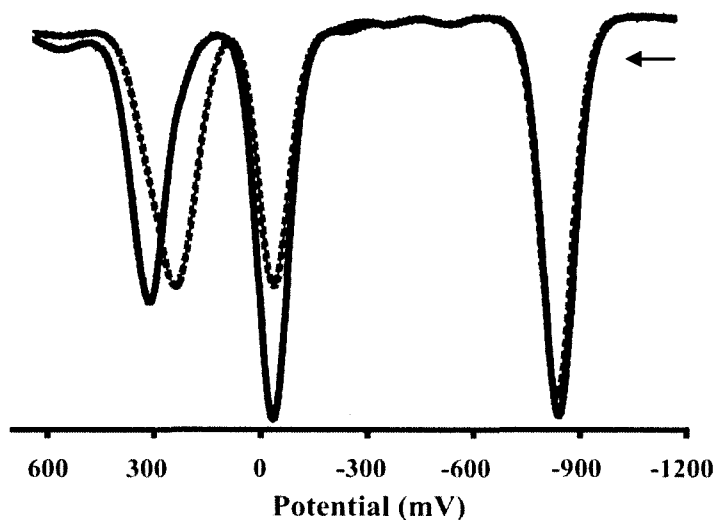


Figure E-16. Anodic square wave voltammograms of 2.0 mM complex PPN[Ru-1] (dark line) and in the presence of 0.2 M 2,3-dimethyl-2-butene (dotted line) measured at room temperature versus Ag/AgCl reference electrode. Reported potentials are scaled to a ferrocenium/ferrocene reference.

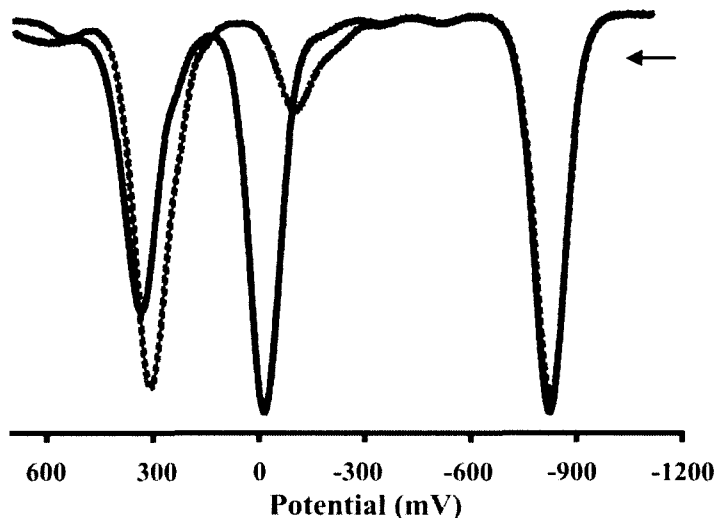


Figure E-17. Anodic square wave voltammograms of 2.0 mM complex **PPN[Ru-1]** (dark line) and in the presence of 0.2 M 1-octyne (dotted line) measured at room temperature versus Ag/AgCl reference electrode. Reported potentials are scaled to a ferrocenium/ferrocene reference.

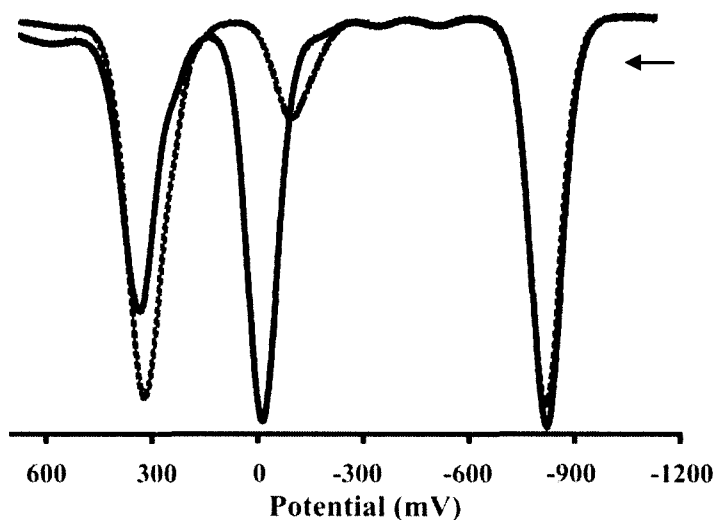


Figure E-18. Anodic square wave voltammograms of 2.0 mM complex **PPN[Ru-1]** (dark line) and in the presence of 0.2 M phenyl acetylene (dotted line) measured at room temperature versus Ag/AgCl reference electrode. Reported potentials are scaled to a ferrocenium/ferrocene reference.

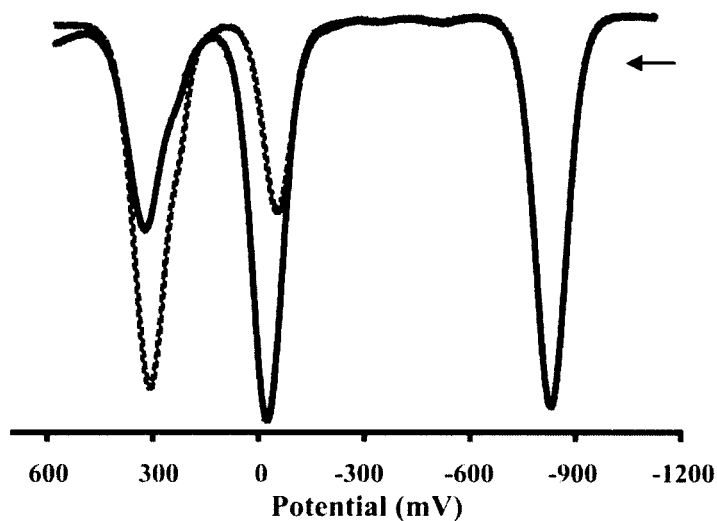


Figure E-19. Anodic square wave voltammograms of 2.0 mM complex **PPN[Ru-1]** (dark line) and in the presence of 0.2 M 1-phenyl-1-propyne (dotted line) measured at room temperature versus Ag/AgCl reference electrode. Reported potentials are scaled to a ferrocenium/ferrocene reference.

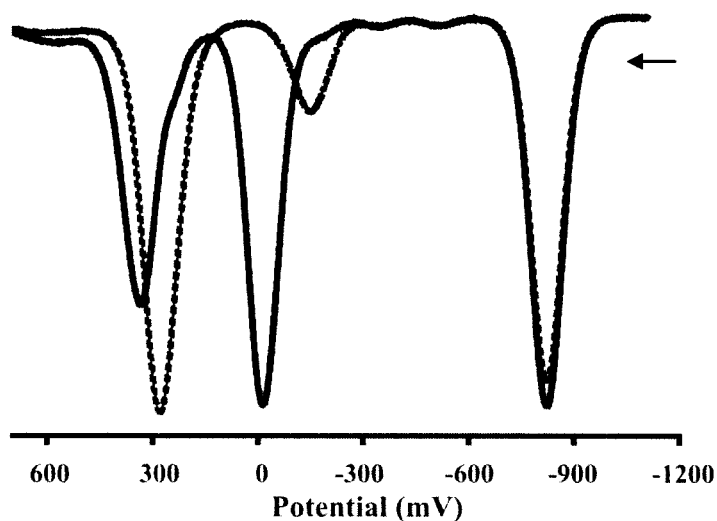


Figure E-20. Anodic square wave voltammograms of 2.0 mM complex **PPN[Ru-1]** (dark line) and in the presence of 0.2 M 1,3-butadiene (dotted line) measured at room temperature versus Ag/AgCl reference electrode. Reported potentials are scaled to a ferrocenium/ferrocene reference.

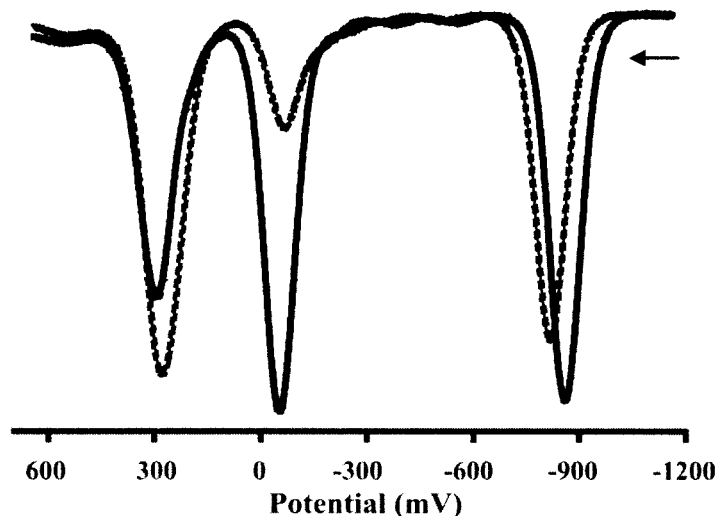


Figure E-21. Anodic square wave voltammograms of 2.0 mM complex **PPN[Ru-1]** (dark line) and in the presence of 0.2 M 2,3-dimethyl-1,3-butadiene (dotted line) measured at room temperature versus Ag/AgCl reference electrode. Reported potentials are scaled to a ferrocenium/ferrocene reference.

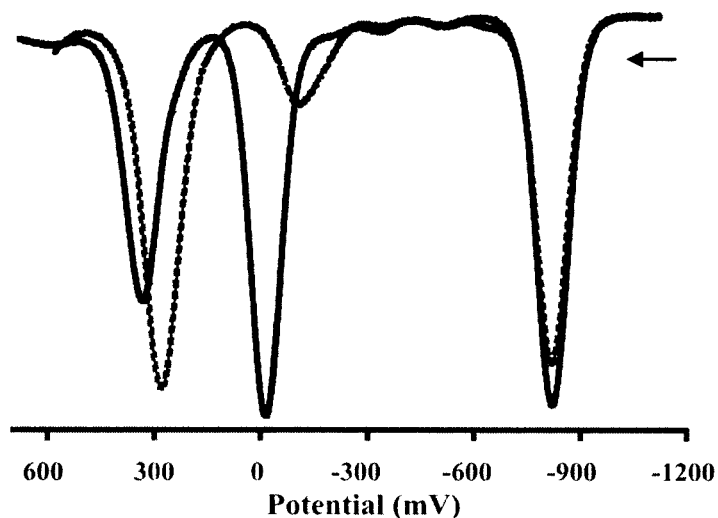


Figure E-22. Anodic square wave voltammograms of 2.0 mM complex **PPN[Ru-1]** (dark line) and in the presence of 0.2 M dipentene (dotted line) measured at room temperature versus Ag/AgCl reference electrode. Reported potentials are scaled to a ferrocenium/ferrocene reference.

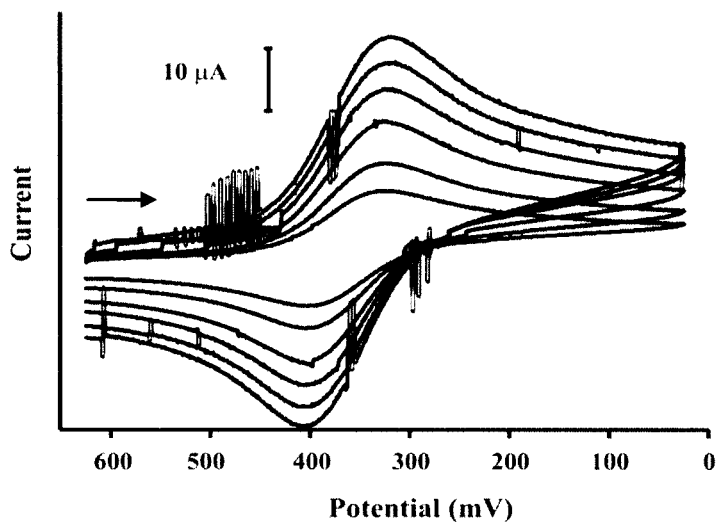


Figure E-23. Cyclic voltammogram of 1.0 mM complex [Ru-1-*cis*-stilbene]⁺ in acetonitrile with 0.1 M TBAHFP was obtained at multiple scan rates, 100 mV/s to 1000 mV/s. Potentials referenced to Fc⁺/Fc.

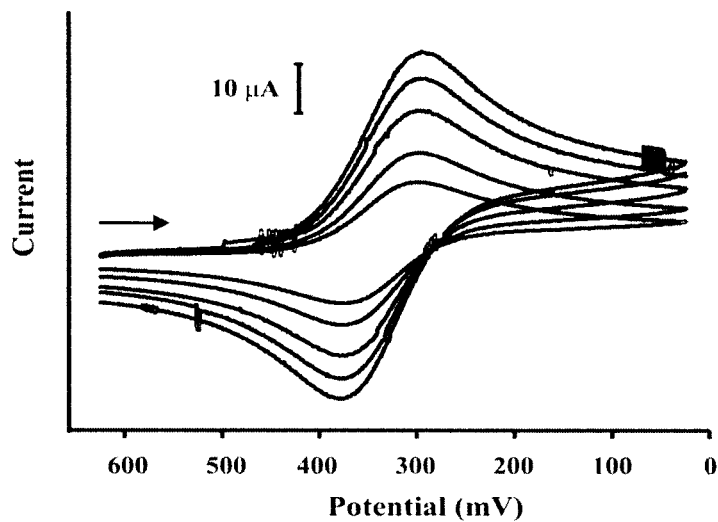


Figure E-24. Cyclic voltammogram of 1.0 mM complex [Ru-1-*trans*-stilbene]⁺ in acetonitrile with 0.1 M TBAHFP was obtained at multiple scan rates, 100 mV/s to 1000 mV/s. Potentials referenced to Fc⁺/Fc.

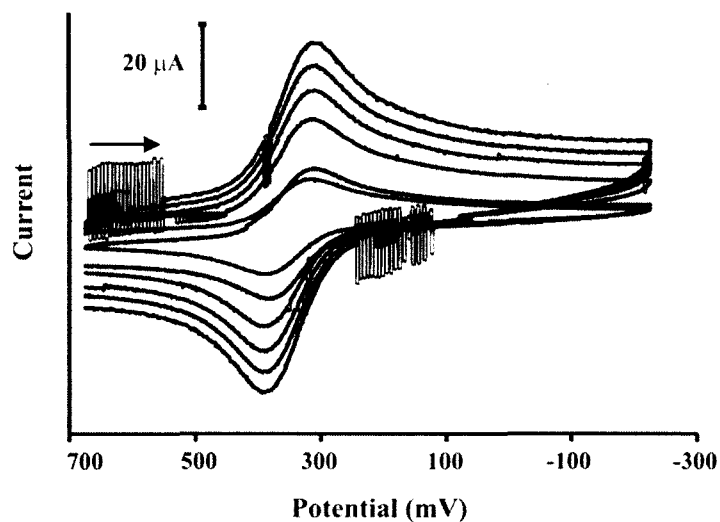


Figure E-25. Cyclic voltammogram of 1.0 mM complex $[\text{Ru-1-octyne}]^+$ in acetonitrile with 0.1 M TBAHFP was obtained at multiple scan rates, 100 mV/s to 1000 mV/s. Potentials referenced to Fc^+/Fc .

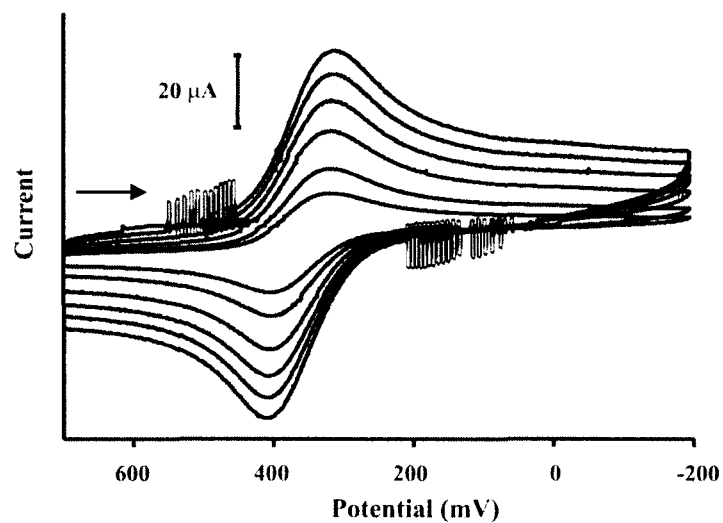


Figure E-26. Cyclic voltammogram of 1.0 mM complex $[\text{Ru-1-phenyl acetylene}]^+$ in acetonitrile with 0.1 M TBAHFP was obtained at multiple scan rates, 100 mV/s to 1000 mV/s. Potentials referenced to Fc^+/Fc .

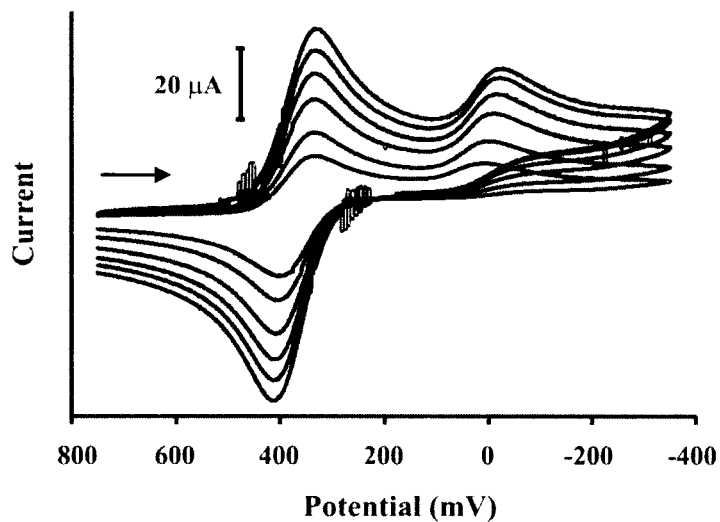


Figure E-27. Cyclic voltammogram of 1.0 mM complex [Ru-1·MePhkyne]⁺ in acetonitrile with 0.1 M TBAHFP was obtained at multiple scan rates, 100 mV/s to 1000 mV/s. Potentials referenced to Fc⁺/Fc.

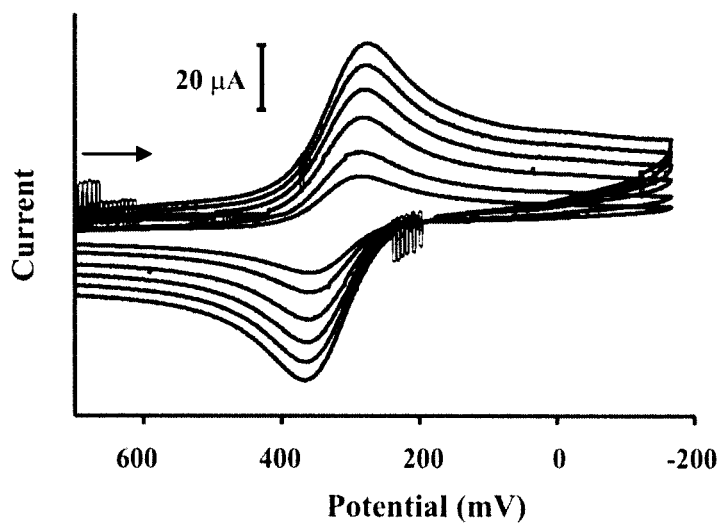


Figure E-28. Cyclic voltammogram of 1.0 mM complex [Ru-1·butadiene]⁺ in acetonitrile with 0.1 M TBAHFP was obtained at multiple scan rates, 100 mV/s to 1000 mV/s. Potentials referenced to Fc⁺/Fc.

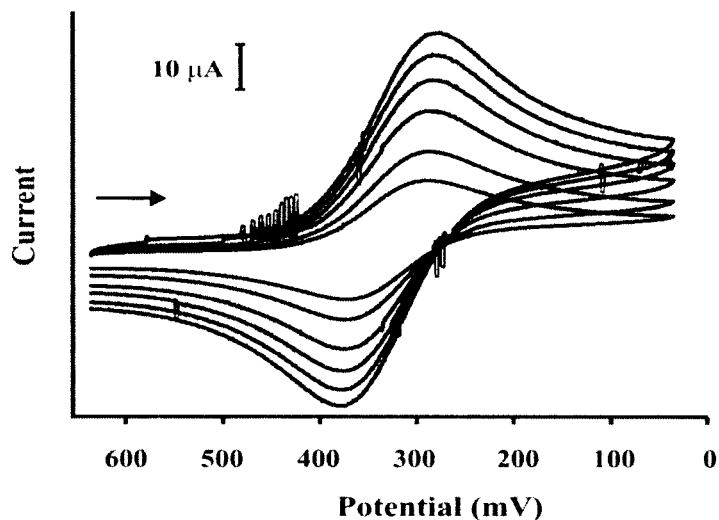


Figure E-29. Cyclic voltammogram of 1.0 mM complex [Ru-1-2Mebutadiene]⁺ in acetonitrile with 0.1 M TBAHFP was obtained at multiple scan rates, 100 mV/s to 1000 mV/s. Potentials referenced to Fc⁺/Fc.

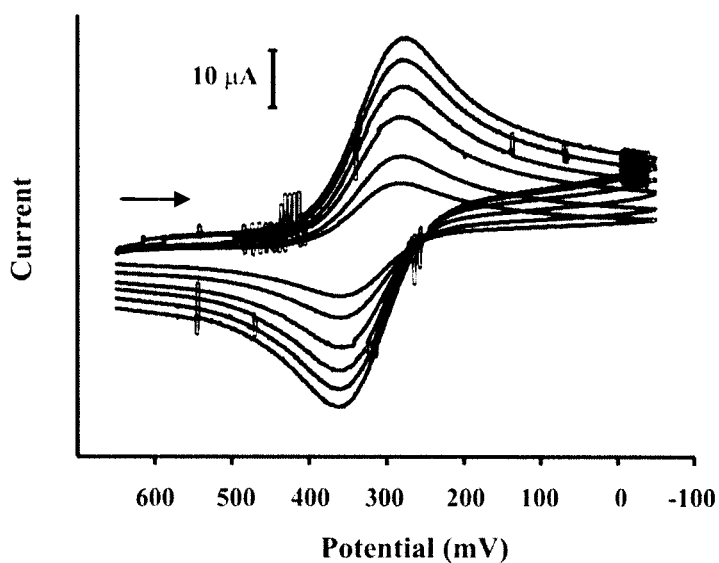


Figure E-30. Cyclic voltammogram of 1.0 mM complex [Ru-1-dipentene]⁺ in acetonitrile with 0.1 M TBAHFP was obtained at multiple scan rates, 100 mV/s to 1000 mV/s. Potentials referenced to Fc⁺/Fc.

APPENDIX F
NMR Spectroscopy

Appendix	Page
F-1 ^{31}P NMR spectrum of [Ru-1·<i>m</i>-methylstyrene]⁺ in deuterated acetonitrile.....	177
F-2 ^{31}P NMR spectrum of [Ru-1·<i>cis</i>-stilbene]⁺ in deuterated acetonitrile.....	177
F-3 ^{31}P NMR spectrum of [Ru-1·<i>trans</i>-stilbene]⁺ in deuterated acetonitrile.....	178
F-4 ^{31}P NMR spectrum of [Ru-1·phenyl acetylene]⁺ in deuterated acetonitrile.....	178
F-5 ^{31}P NMR spectrum of [Ru-1·MePhkyne]⁺ in deuterated acetonitrile.....	179
F-6 ^{31}P NMR spectrum of [Ru-1·butadiene]⁺ in deuterated acetonitrile.....	179
F-7 ^{31}P NMR spectrum of [Ru-1·2Mebutadiene]⁺ in deuterated acetonitrile.....	180
F-8 ^{31}P NMR spectrum of [Ru-1·dipentene]⁺ in deuterated acetonitrile.....	180

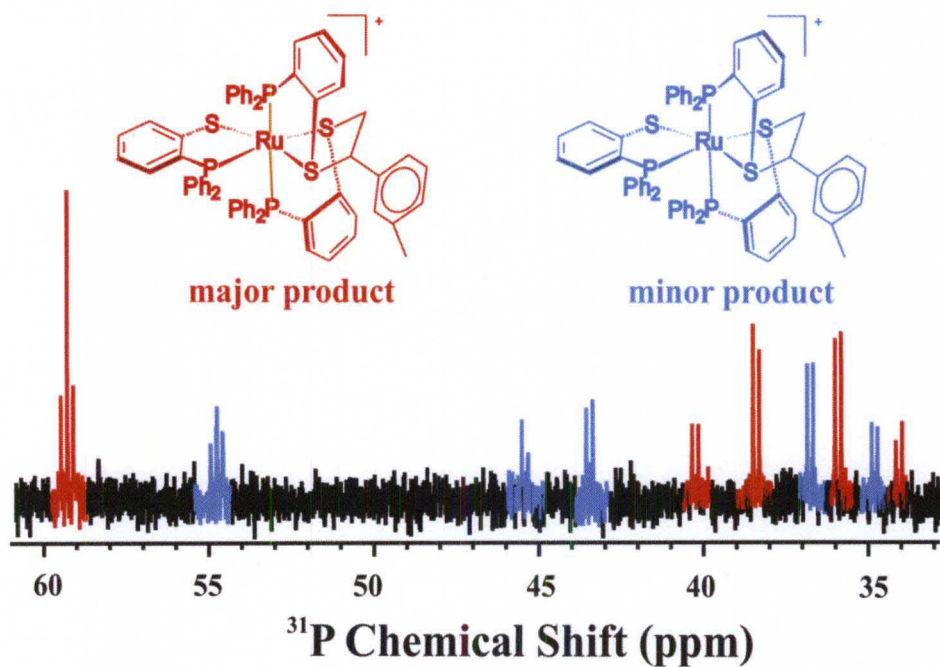


Figure F-1. ^{31}P NMR spectrum of $[\text{Ru-1-}m\text{-methylstyrene}]^+$ in deuterated acetonitrile

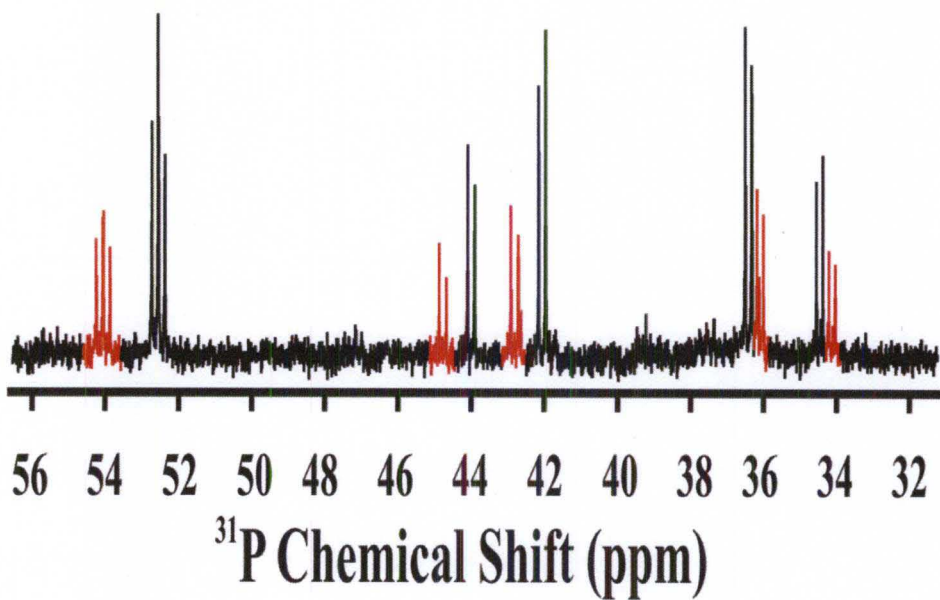


Figure F-2. ^{31}P NMR spectrum of $[\text{Ru-1-}cis\text{-stilbene}]^+$ in deuterated acetonitrile

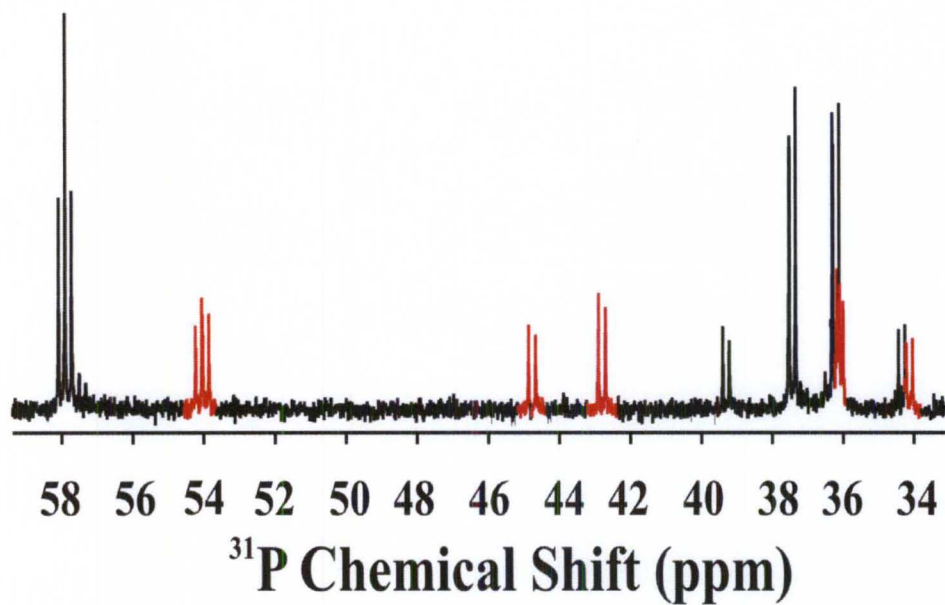


Figure F-3. ^{31}P NMR spectrum of $[\text{Ru-1}\cdot\text{trans-stilbene}]^+$ in deuterated acetonitrile

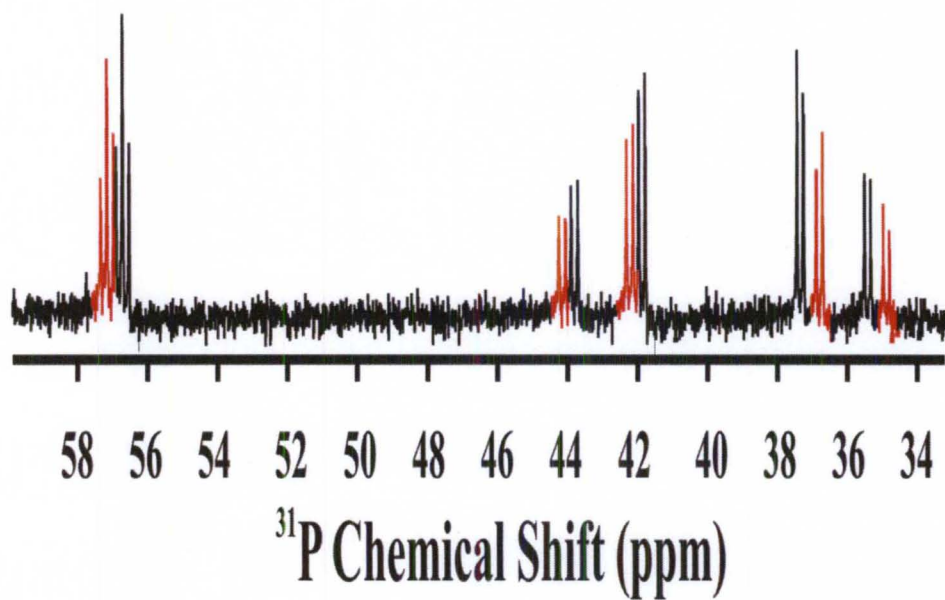


Figure F-4. ^{31}P NMR spectrum of $[\text{Ru-1}\cdot\text{phenyl acetylene}]^+$ in deuterated acetonitrile

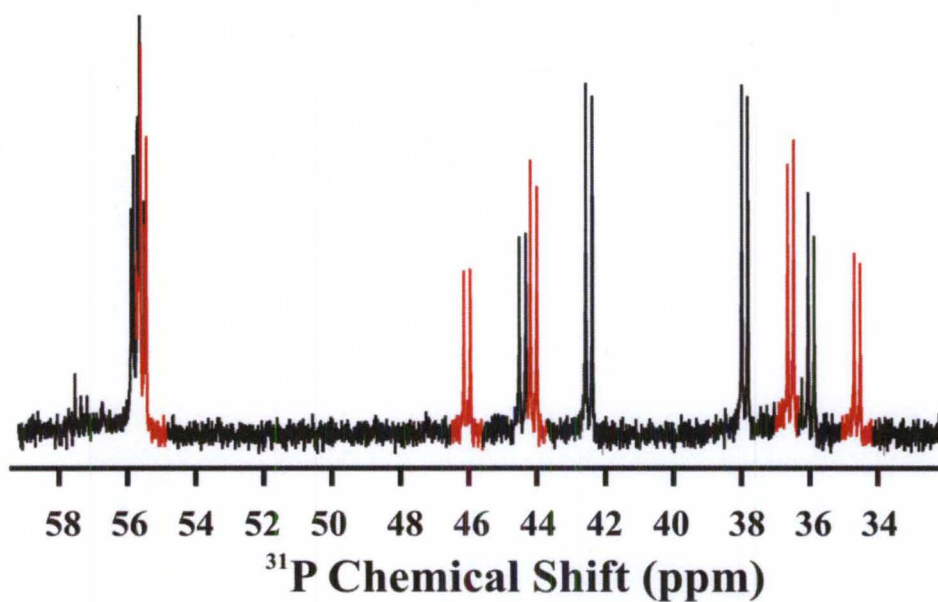


Figure F-5. ^{31}P NMR spectrum of $[\text{Ru-1}\cdot\text{MePhkyne}]^+$ in deuterated acetonitrile

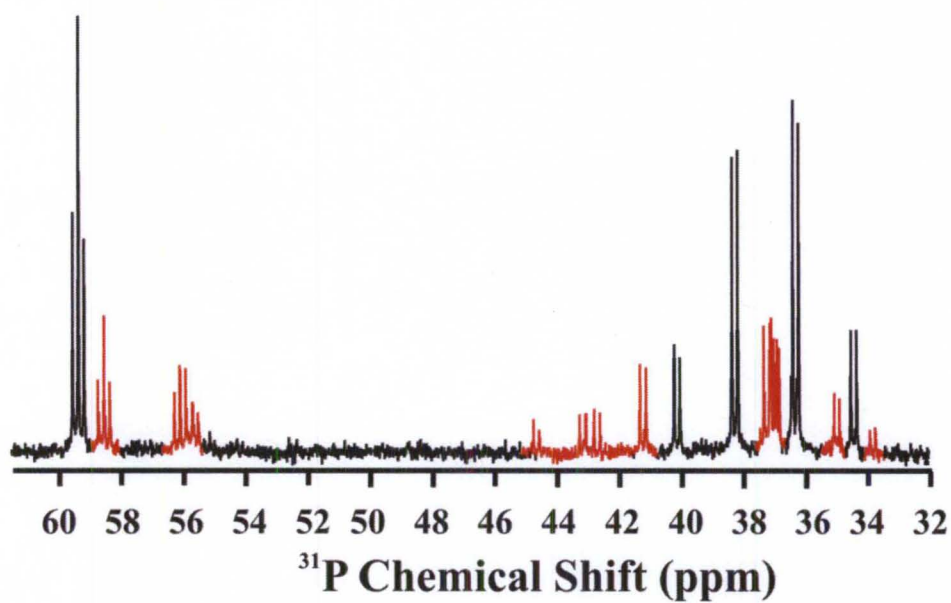


Figure F-6. ^{31}P NMR spectrum of $[\text{Ru-1}\cdot\text{butadiene}]^+$ in deuterated acetonitrile

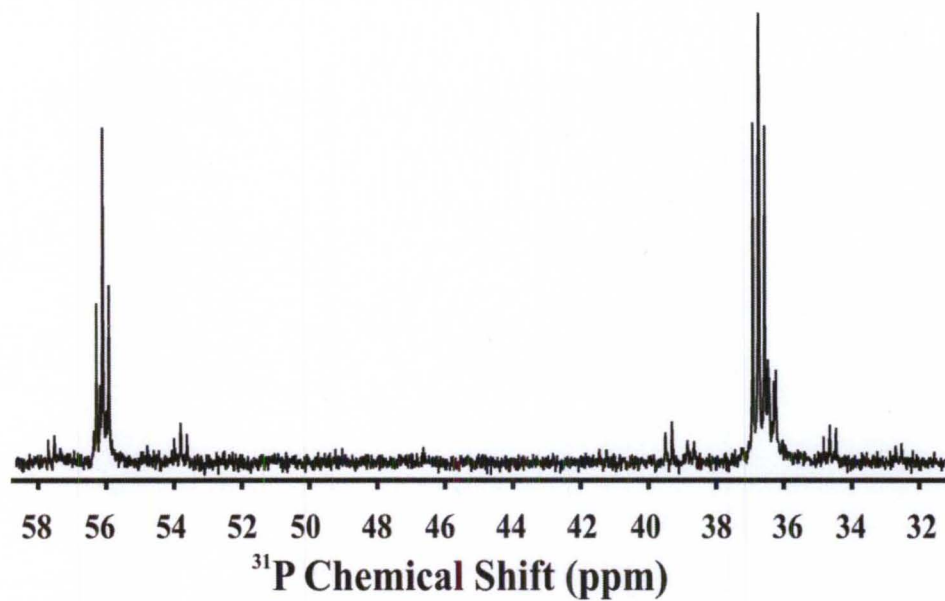


Figure F-7. ^{31}P NMR spectrum of $[\text{Ru-1}\cdot 2\text{Mebutadiene}]^+$ in deuterated acetonitrile

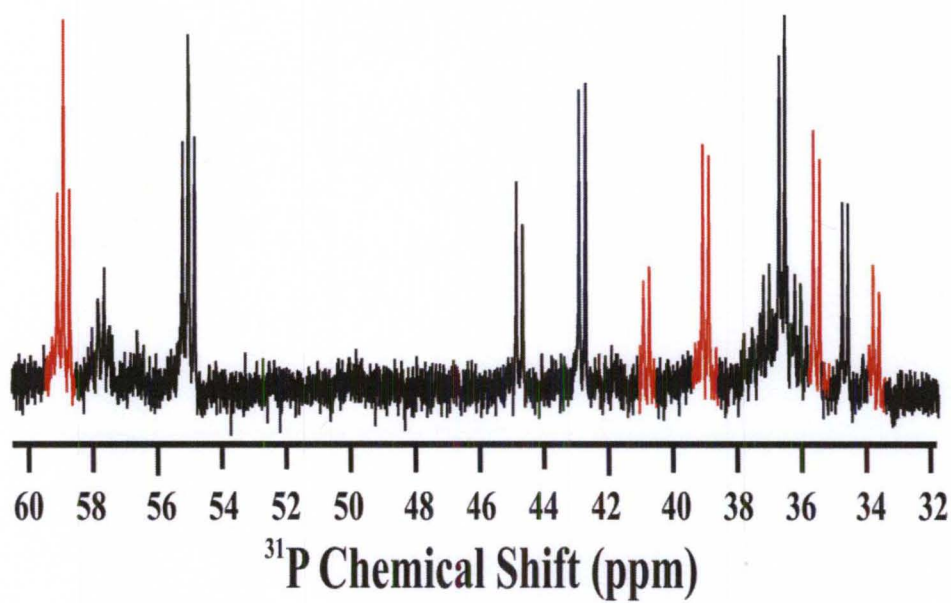


Figure F-8. ^{31}P NMR spectrum of $[\text{Ru-1}\cdot \text{dipentene}]^+$ in deuterated acetonitrile

APPENDIX G

Tables for Crystallographic Data

Appendix	Page
G-1	Experimental data for the X-ray crystal structure of [Ru-1·<i>m</i>-methylstyrene]⁺182
G-2	Atomic coordinates ($\times 10^4$) and equivalent isotropic displacement parameters ($\text{\AA}^2 \times 10^3$) for [Ru-1·<i>m</i>-methylstyrene]⁺183
G-3	Experimental data for the X-ray crystal structure of [Ru-1·<i>p</i>-methylstyrene]⁺186
G-4	Atomic coordinates ($\times 10^4$) and equivalent isotropic displacement parameters ($\text{\AA}^2 \times 10^3$) for [Ru-1·<i>p</i>-methylstyrene]⁺187
G-5	Experimental data for the X-ray crystal structure of [Ru-1·cyclohexene]⁺190
G-6	Atomic coordinates ($\times 10^4$) and equivalent isotropic displacement parameters ($\text{\AA}^2 \times 10^3$) for [Ru-1·cyclohexene]⁺191
G-7	Bond Lengths (\AA) and bond angles for [Ru-1·cyclohexene]⁺193
G-8	Experimental data for the X-ray crystal structure of [Ru-1·octyne]⁺202
G-9	Atomic coordinates ($\times 10^4$) and equivalent isotropic displacement parameters ($\text{\AA}^2 \times 10^3$) for [Ru-1·octyne]⁺203

Table G-1. Crystal data and structure refinement for [Ru-1-*m*-methylstyrene]⁺

Empirical formula	C _{64.5} H ₆₁ Cl ₃ F ₆ P ₄ Ru S ₃
Formula weight	1368.54
Temperature	100(2) K
Wavelength	0.71073 Å
Crystal system	Monoclinic
Space group	P2 ₁
Unit cell dimensions	a = 105855(4) Å α = 90° b = 16.8551(5) Å β = 104.576(3)° c = 17.7704(4) Å γ = 90°
Volume	3068.53(18) Å ³
Z	2
Density (calculated)	1.481 Mg/m ³
Absorption coefficient	0.651 mm ⁻¹
F(000)	1392
Crystal color, habit	yellow cut-block
Crystal size	0.31 x 0.14 x 0.10 mm ³
Theta range for data collection	3.38 to 29.65°
Index ranges	-14 ≤ h ≤ 13, -23 ≤ k ≤ 23, -24 ≤ l ≤ 22
Reflections collected	50963
Independent reflections	15701 [R(int) = 0.0498]
Completeness to theta = 29.62°	94.5 %
Completeness to theta = 27.04°	99.8 %
Absorption correction	SCALE3 ABSPACK
Max. and min. transmission	0.952 and 0.926
Refinement method	Full-matrix least-squares on F ²
Data / restraints / parameters	15701 / 27 / 778
Goodness-of-fit on F ²	1.014
Final R indices [I > 2σ(I)]	R1 = 0.0483, wR2 = 0.1042
R indices (all data)	R1 = 0.0563, wR2 = 0.1136
Largest diff. peak and hole	1.372 and -0.564 e.Å ⁻³

Note: crystallographic data in CIF format (CCDC 814546 and 814547). This material is available free of charge via the internet at <http://pubs.acs.org>.

Table G-2. Atomic coordinates ($\times 10^4$) and equivalent isotropic displacement parameters ($\text{\AA}^2 \times 10^3$) for **[Ru-1-*m*-methylstyrene]⁺**. U(eq) is defined as one third of the trace of the orthogonalized U^{ij} tensor.

	x	y	z	U(eq)
Ru(1)	1605(1)	9493(1)	1969(1)	14(1)
S(1)	651(1)	10090(1)	749(1)	19(1)
S(2)	3638(1)	9796(1)	1705(1)	18(1)
S(3)	2767(1)	8852(1)	3100(1)	17(1)
P(1)	-542(1)	9284(1)	2054(1)	16(1)
P(2)	1718(1)	8268(1)	1344(1)	18(1)
P(3)	1842(1)	10758(1)	2574(1)	16(1)
C(1)	-1036(4)	10013(2)	619(2)	20(1)
C(2)	-1838(4)	10324(3)	-74(2)	28(1)
C(3)	-3184(4)	10290(3)	-216(3)	32(1)
C(4)	-3759(4)	9960(3)	334(3)	29(1)
C(5)	-2982(3)	9655(2)	1009(2)	24(1)
C(6)	-1614(3)	9666(2)	1160(2)	19(1)
C(7)	3987(3)	10825(2)	1937(2)	19(1)
C(8)	5039(4)	11176(2)	1729(2)	24(1)
C(9)	5249(4)	11979(2)	1849(3)	27(1)
C(10)	4399(4)	12438(2)	2147(2)	25(1)
C(11)	3337(4)	12086(2)	2343(2)	21(1)
C(12)	3132(4)	11266(2)	2242(2)	18(1)
C(13)	2907(3)	7827(2)	2857(2)	21(1)
C(14)	3399(4)	7302(2)	3465(2)	26(1)
C(15)	3466(4)	6493(3)	3303(3)	34(1)
C(16)	3069(4)	6221(3)	2550(3)	35(1)
C(17)	2578(4)	6742(2)	1952(3)	28(1)
C(18)	2463(4)	7554(2)	2100(2)	22(1)
C(19)	-1215(3)	9758(2)	2809(2)	18(1)
C(20)	-1149(3)	9390(2)	3522(2)	22(1)
C(21)	-1629(4)	9748(2)	4093(2)	28(1)
C(22)	-2195(4)	10498(3)	3960(3)	30(1)
C(23)	-2280(4)	10875(2)	3260(2)	26(1)
C(24)	-1798(4)	10508(2)	2686(2)	21(1)
C(25)	-1022(3)	8258(2)	2197(2)	20(1)
C(26)	-195(4)	7837(2)	2795(2)	24(1)
C(27)	-513(4)	7071(2)	2994(3)	32(1)
C(28)	-1672(5)	6736(3)	2600(3)	37(1)
C(29)	-2503(4)	7147(3)	1991(3)	32(1)
C(30)	-2189(4)	7906(2)	1794(3)	27(1)

C(31)	247(3)	7787(2)	750(2)	19(1)
C(32)	-444(4)	8183(2)	75(2)	24(1)
C(33)	-1572(4)	7852(3)	-391(3)	30(1)
C(34)	-2013(4)	7125(3)	-210(2)	29(1)
C(35)	-1344(4)	6729(2)	451(3)	27(1)
C(36)	-234(4)	7064(2)	941(2)	25(1)
C(37)	2827(4)	8238(2)	693(2)	22(1)
C(38)	2587(4)	8751(3)	49(2)	27(1)
C(39)	3411(4)	8755(3)	-438(3)	37(1)
C(40)	4480(4)	8253(3)	-310(3)	38(1)
C(41)	4727(4)	7747(3)	315(3)	41(1)
C(42)	3911(4)	7740(3)	825(3)	34(1)
C(43)	611(4)	11546(2)	2422(2)	20(1)
C(44)	-6(4)	11758(2)	1657(2)	22(1)
C(45)	-933(4)	12358(2)	1515(3)	30(1)
C(46)	-1235(4)	12753(3)	2125(3)	34(1)
C(47)	-604(5)	12556(3)	2883(3)	36(1)
C(48)	315(4)	11955(2)	3037(3)	28(1)
C(49)	2520(4)	10763(2)	3634(2)	20(1)
C(50)	1801(4)	10399(2)	4097(2)	25(1)
C(51)	2271(5)	10391(2)	4901(2)	30(1)
C(52)	3469(5)	10734(3)	5247(2)	35(1)
C(53)	4177(5)	11078(3)	4786(3)	39(1)
C(54)	3721(4)	11110(3)	3993(2)	30(1)
C(55)	4839(3)	9273(2)	2451(2)	22(1)
C(56)	4490(4)	9210(2)	3217(2)	24(1)
C(57)	5447(4)	8737(3)	3836(3)	32(1)
C(58)	5574(5)	8922(3)	4605(3)	42(1)
C(59)	6478(6)	8490(4)	5197(3)	56(2)
C(60)	7209(5)	7906(4)	4952(4)	58(2)
C(61)	7102(5)	7715(3)	4205(4)	49(1)
C(62)	6214(4)	8130(3)	3641(3)	39(1)
C(63)	6600(8)	8660(6)	6017(4)	81(2)
P(4)	3854(1)	9739(1)	7457(1)	30(1)
F(1A)	2625(10)	9954(7)	6758(6)	47(1)
F(2A)	5041(6)	9519(4)	8160(3)	47(1)
F(3A)	4724(8)	9613(5)	6859(5)	47(1)
F(4A)	2952(7)	9934(4)	8036(4)	47(1)
F(5A)	4235(6)	10661(3)	7457(5)	47(1)
F(6A)	3382(7)	8837(4)	7410(5)	47(1)
F(1B)	2917(15)	10095(10)	6752(10)	39(5)
F(2B)	4755(12)	9255(8)	8228(7)	32(3)
F(3B)	5005(12)	9620(9)	7062(7)	30(4)
F(4B)	2694(10)	9700(6)	7941(6)	16(3)
F(5B)	4333(10)	10571(6)	7844(7)	16(2)

F(6B)	3409(12)	8816(7)	7178(6)	17(3)
F(1C)	2519(16)	9823(10)	6754(10)	21(3)
F(2C)	5338(11)	9727(8)	8024(7)	28(3)
F(3C)	4499(11)	9410(7)	6757(7)	16(3)
F(4C)	3362(12)	10151(7)	8130(7)	29(3)
F(5C)	4237(14)	10621(8)	7163(8)	39(4)
F(6C)	3671(12)	8883(7)	7681(7)	24(3)
C(70)	2623(5)	8365(3)	5439(4)	52(1)
Cl(1A)	948(7)	8207(7)	5053(5)	62(2)
Cl(2A)	3512(5)	7481(3)	5714(5)	39(1)
Cl(1B)	3525(10)	7502(6)	5663(7)	89(3)
Cl(2B)	1015(11)	8096(10)	5016(7)	98(4)
C(80)	118(12)	4826(8)	2580(6)	69(3)
Cl(3A)	1146(5)	4383(3)	2079(3)	35(1)
Cl(3B)	700(8)	4587(5)	1792(5)	75(2)
Cl(4A)	660(8)	4905(5)	3420(5)	57(2)
Cl(4B)	872(7)	5066(4)	3587(4)	48(2)

Table G-3. Crystal data and structure refinement for [Ru-1-*p*-methylstyrene]⁺

Empirical formula	C ₇₅ H ₆₁ Cl ₂ F ₆ P ₃ Ru S ₃
Formula weight	1234.38
Temperature	100.1 K
Wavelength	0.7107 Å
Crystal system	Triclinic
Space group	P -1
Unit cell dimensions	a = 11.2718(5) Å α = 101.715(3)° b = 12.0524(3) Å β = 98.154(4)° c = 23.6075(10) Å γ = 105.209(3)°
Volume	2965.04(21) Å ³
Z	2
Density (calculated)	1.383 Mg/m ³
Absorption coefficient	0.496 mm ⁻¹
F(000)	1278
Crystal color, habit	yellow cut-block
Crystal size	0.25 x 0.13 x 0.10 mm ³
Theta range for data collection	3.37 to 29.62°
Index ranges	-15 ≤ h ≤ 14, -16 ≤ k ≤ 15, -31 ≤ l ≤ 31
Reflections collected	67874
Independent reflections	15439 [R(int) = 0.041]
Completeness to theta = 29.62°	92.4 %
Completeness to theta = 27.04°	99.8 %
Absorption correction	Semi-empirical from equivalents
Max. and min. transmission	0.952 and 0.926
Refinement method	Full-matrix least-squares on F ²
Data / restraints / parameters	15439 / 7 / 735
Goodness-of-fit on F ²	1.043
Final R indices [I > 2σ(I)]	R1 = 0.0383, wR2 = 0.0763
R indices (all data)	R1 = 0.0562, wR2 = 0.0849
Largest diff. peak and hole	0.763 and -0.736 e.Å ⁻³

Note: crystallographic data in CIF format (CCDC 814546 and 814547). This material is available free of charge via the internet at <http://pubs.acs.org>.

Table G-4. Atomic coordinates ($\times 10^4$) and equivalent isotropic displacement parameters ($\text{\AA}^2 \times 10^3$) for **[Ru-1-*p*-methylstyrene]⁺**. U(eq) is defined as one third of the trace of the orthogonalized U^{ij} tensor.

	x	y	z	U(eq)
Ru(1)	4719(1)	7900(1)	10309(1)	16(1)
S(1)	3954(2)	8249(2)	12087(2)	22(1)
S(2)	6861(2)	7792(2)	10817(2)	19(1)
S(3)	5638(2)	7626(2)	8617(2)	19(1)
P(1)	2517(2)	8087(2)	10022(2)	19(1)
P(2)	4547(3)	9808(2)	9998(2)	21(1)
P(3)	5307(3)	5929(2)	10656(2)	19(1)
C(1)	2240(10)	8481(8)	12127(7)	25(1)
C(2)	1499(10)	8768(9)	13058(8)	25(1)
C(3)	140(9)	8980(8)	13164(7)	25(1)
C(4)	-503(10)	8895(8)	12282(7)	25(1)
C(5)	192(9)	8556(8)	11354(7)	25(1)
C(6)	1610(10)	8441(8)	11250(7)	25(1)
C(7)	7485(10)	6456(8)	11392(7)	22(1)
C(8)	8635(9)	6210(8)	11903(7)	22(1)
C(9)	9073(9)	5235(8)	12426(7)	22(1)
C(10)	8339(9)	4476(8)	12480(7)	22(1)
C(11)	7171(9)	4686(8)	11988(6)	22(1)
C(12)	6734(9)	5663(8)	11433(7)	22(1)
C(13)	5569(10)	8979(9)	8063(7)	31(1)
C(14)	5994(10)	9026(9)	7017(7)	31(1)
C(15)	5982(10)	10045(8)	6565(8)	31(1)
C(16)	5522(10)	11023(9)	7159(7)	31(1)
C(17)	5079(10)	10967(9)	8159(7)	31(1)
C(18)	5079(10)	9961(9)	8650(8)	31(1)
C(19)	1967(8)	6899(7)	9559(7)	18(2)
C(20)	1906(9)	6729(8)	8518(7)	22(2)
C(21)	1524(10)	5837(8)	8181(8)	34(1)
C(22)	1139(10)	5114(9)	8886(8)	34(1)
C(23)	1171(10)	5257(9)	9923(8)	34(1)
C(24)	1596(9)	6146(8)	10277(7)	24(2)
C(25)	1730(10)	9149(8)	9066(7)	22(2)
C(26)	2361(9)	9172(8)	8097(7)	25(2)
C(27)	1811(10)	9824(8)	7300(8)	29(2)
C(28)	517(10)	10496(8)	7463(8)	30(2)
C(29)	-136(10)	10485(8)	8424(8)	29(2)
C(30)	444(9)	9837(8)	9206(7)	26(2)

C(31)	2956(10)	10868(8)	10218(8)	32(1)
C(32)	2345(10)	10948(8)	11226(9)	32(1)
C(33)	1111(10)	11730(8)	11429(9)	32(1)
C(34)	520(10)	12379(8)	10651(8)	32(1)
C(35)	1068(10)	12312(8)	9694(8)	32(1)
C(36)	2300(10)	11539(8)	9457(9)	32(1)
C(37)	5655(9)	10438(7)	10665(7)	23(2)
C(38)	5508(10)	10548(9)	11739(8)	35(1)
C(39)	6270(10)	11044(9)	12262(8)	35(1)
C(40)	7200(10)	11468(9)	11742(8)	35(1)
C(41)	7396(10)	11337(9)	10695(8)	35(1)
C(42)	6642(10)	10834(9)	10174(8)	35(1)
C(43)	4306(9)	5129(7)	11394(7)	22(2)
C(44)	3824(9)	5443(8)	12398(7)	28(2)
C(45)	3150(10)	4808(9)	12986(8)	35(2)
C(46)	2941(10)	3863(9)	12588(8)	35(2)
C(47)	3414(10)	3540(9)	11626(8)	35(2)
C(48)	4116(10)	4142(8)	11026(8)	33(3)
C(49)	5963(10)	5009(8)	9537(7)	24(2)
C(50)	5184(10)	5067(8)	8713(7)	31(2)
C(51)	5616(10)	4358(8)	7865(8)	32(2)
C(52)	6854(10)	3613(8)	7823(7)	32(3)
C(53)	7647(10)	3545(8)	8618(7)	28(2)
C(54)	7234(10)	4258(8)	9480(7)	24(2)
C(55)	7881(10)	7674(8)	9587(7)	25(1)
C(56)	7444(10)	7073(9)	8768(7)	25(1)
C(57)	8195(10)	6978(10)	7732(8)	29(2)
C(58)	8183(9)	6119(10)	7098(7)	35(3)
C(59)	8817(9)	5993(8)	6100(7)	29(2)
C(60)	9533(10)	6730(9)	5748(7)	30(2)
C(61)	9550(9)	7608(9)	6385(7)	29(2)
C(62)	8895(9)	7743(9)	7358(7)	29(2)
C(63)	10223(11)	6571(10)	4664(8)	47(3)
P(4)	7495(3)	2445(3)	4744(2)	31(1)
F(1)	8709(6)	1989(5)	3898(4)	38(1)
F(2)	6288(6)	2922(5)	5590(4)	38(1)
F(3)	7992(6)	3546(5)	4882(4)	40(1)
F(4)	7020(6)	1331(5)	4614(4)	40(1)
F(5)	8393(6)	1853(5)	5658(4)	40(1)
F(6)	6600(6)	3062(5)	3858(4)	40(1)
Cl(1)	1948(6)	3783(4)	6260(4)	118(2)
C(70)	5527(7)	7457(6)	4614(6)	48(1)
C(71)	5883(7)	6314(6)	4520(6)	48(1)
C(72)	5069(8)	5705(6)	4951(6)	48(1)
C(73)	3898(7)	6240(6)	5477(6)	48(1)

C(74)	3542(7)	7383(6)	5572(5)	48(1)
C(75)	4356(7)	7992(6)	5141(6)	48(1)
Cl(2)	6555(3)	8225(3)	4070(3)	61(1)
C(80)	2289(8)	2664(6)	5450(6)	53(1)
C(81)	3606(8)	2204(7)	5126(6)	53(1)
C(82)	3963(8)	1292(7)	4463(6)	53(1)
C(83)	3003(8)	840(6)	4123(6)	53(1)
C(84)	1686(8)	1300(7)	4447(6)	53(1)
C(85)	1329(8)	2212(7)	5110(6)	53(1)

Table G-5. Crystal data and structure refinement for **[Ru-1·cyclohexene]⁺**

Empirical formula	C ₆₁ H ₅₄ Cl ₂ F ₆ P ₄ Ru S ₃
Formula weight	1293.07
Temperature	100.0 K
Wavelength	0.71073 Å
Crystal system	Triclinic
Space group	P-1
Unit cell dimensions	a = 12.4717(6) Å α = 89.638(4)° b = 12.7535(6) Å β = 74.032(4)° c = 18.2603(9) Å γ = 89.193(4)°
Volume	2792.1(2) Å ³
Z	2
Density (calculated)	1.538 Mg/m ³
Absorption coefficient	0.664 mm ⁻¹
F(000)	1320
Crystal size	0.21 x 0.17 x 0.04 mm ³
Theta range for data collection	3.23 to 30.04°
Index ranges	-16 ≤ h ≤ 17, -16 ≤ k ≤ 17, -24 ≤ l ≤ 25
Reflections collected	47997
Independent reflections	14961 [R(int) = 0.0407]
Completeness to theta = 27.62°	99.8 %
Absorption correction	Semi-empirical from equivalents
Max. and min. transmission	1.000 and 0.903
Refinement method	Full-matrix least-squares on F ²
Data / restraints / parameters	14961 / 0 / 682
Goodness-of-fit on F ²	1.093
Final R indices [I > 2σ(I)]	R1 = 0.0549, wR2 = 0.1090
R indices (all data)	R1 = 0.0992, wR2 = 0.1265
Largest diff. peak and hole	1.799 and -1.603 e.Å ⁻³

Table G-6. Atomic coordinates ($\times 10^4$) and equivalent isotropic displacement parameters ($\text{\AA}^2 \times 10^3$) for **[Ru-1·cyclohexene]⁺**. U(eq) is defined as one third of the trace of the orthogonalized U^{ij} tensor.

	x	y	z	U(eq)
Ru(1)	7062(1)	7859(1)	7248(1)	14(1)
S(1)	8451(1)	9095(1)	6649(1)	17(1)
S(2)	8257(1)	7004(1)	7880(1)	19(1)
S(3)	5712(1)	6695(1)	7922(1)	18(1)
P(1)	5976(1)	8665(1)	6543(1)	15(1)
P(2)	8031(1)	6673(1)	6249(1)	16(1)
P(3)	6438(1)	8956(1)	8297(1)	15(1)
C(1)	7894(3)	9810(3)	6012(2)	18(1)
C(2)	8587(3)	10518(3)	5512(2)	21(1)
C(3)	8233(3)	11046(3)	4968(2)	27(1)
C(4)	7158(3)	10909(3)	4900(2)	27(1)
C(5)	6459(3)	10218(3)	5388(2)	23(1)
C(6)	6817(3)	9651(3)	5938(2)	17(1)
C(7)	9497(3)	6732(3)	7138(2)	21(1)
C(8)	10519(3)	6710(3)	7302(2)	26(1)
C(9)	11493(3)	6601(3)	6715(2)	26(1)
C(10)	11434(3)	6482(3)	5973(2)	23(1)
C(11)	10413(3)	6489(3)	5811(2)	19(1)
C(12)	9435(3)	6632(3)	6391(2)	18(1)
C(13)	4813(3)	7445(3)	8680(2)	20(1)
C(14)	3803(3)	7001(3)	9069(2)	25(1)
C(15)	3104(3)	7529(3)	9673(2)	28(1)
C(16)	3393(3)	8495(3)	9885(2)	24(1)
C(17)	4392(3)	8942(3)	9487(2)	19(1)
C(18)	5118(3)	8425(3)	8870(2)	18(1)
C(19)	5510(3)	7789(3)	5893(2)	14(1)
C(20)	4821(3)	6957(3)	6215(2)	19(1)
C(21)	4452(3)	6262(3)	5758(2)	23(1)
C(22)	4755(3)	6389(3)	4982(2)	26(1)
C(23)	5441(3)	7203(3)	4655(2)	26(1)
C(24)	5835(3)	7898(3)	5106(2)	22(1)
C(25)	4643(3)	9343(3)	6998(2)	20(1)
C(26)	3764(3)	8787(3)	7466(2)	26(1)
C(27)	2744(3)	9273(4)	7805(2)	36(1)
C(28)	2588(4)	10323(4)	7678(2)	38(1)
C(29)	3450(4)	10895(4)	7224(2)	36(1)
C(30)	4468(3)	10409(3)	6890(2)	26(1)

C(31)	6201(3)	10373(3)	8234(2)	18(1)
C(32)	5144(3)	10824(3)	8388(2)	23(1)
C(33)	5010(4)	11908(3)	8394(2)	28(1)
C(34)	5922(4)	12542(3)	8244(2)	31(1)
C(35)	6987(4)	12105(3)	8057(2)	31(1)
C(36)	7124(3)	11027(3)	8047(2)	24(1)
C(37)	7346(3)	8972(3)	8946(2)	17(1)
C(38)	8474(3)	9215(3)	8640(2)	23(1)
C(39)	9178(3)	9282(3)	9107(2)	28(1)
C(40)	8774(3)	9098(3)	9882(2)	29(1)
C(41)	7673(3)	8825(3)	10187(2)	24(1)
C(42)	6961(3)	8759(3)	9719(2)	20(1)
C(43)	8291(3)	6899(3)	5224(2)	17(1)
C(44)	8786(3)	7817(3)	4886(2)	20(1)
C(45)	8941(3)	8007(3)	4117(2)	24(1)
C(46)	8630(3)	7267(3)	3667(2)	26(1)
C(47)	8168(3)	6342(3)	3987(2)	28(1)
C(48)	7988(3)	6159(3)	4762(2)	23(1)
C(49)	7696(3)	5262(3)	6308(2)	17(1)
C(50)	6589(3)	4956(3)	6512(2)	20(1)
C(51)	6319(3)	3900(3)	6555(2)	22(1)
C(52)	7152(3)	3148(3)	6379(2)	24(1)
C(53)	8257(3)	3447(3)	6185(2)	24(1)
C(54)	8531(3)	4491(3)	6151(2)	21(1)
C(55)	7637(3)	5675(3)	8085(2)	25(1)
C(56)	8257(4)	5015(3)	8538(2)	31(1)
C(57)	8008(4)	5346(3)	9369(2)	34(1)
C(58)	6753(3)	5358(4)	9729(2)	34(1)
C(59)	6174(3)	6100(3)	9319(2)	29(1)
C(60)	6402(3)	5790(3)	8481(2)	22(1)
P(4)	2929(1)	4426(1)	7949(1)	24(1)
F(1)	2704(2)	3257(2)	8262(2)	52(1)
F(2)	3158(2)	5598(2)	7637(2)	52(1)
F(3)	1756(2)	4441(2)	7751(1)	36(1)
F(4)	4104(2)	4420(2)	8153(1)	32(1)
F(5)	2333(2)	4867(2)	8772(1)	35(1)
F(6)	3531(2)	3986(2)	7121(2)	52(1)
CI(1)	-424(1)	3408(1)	10350(1)	51(1)
CI(2)	-249(1)	2403(1)	8885(1)	54(1)
C(61)	362(4)	3281(4)	9402(3)	52(1)

Table G-7. Bond lengths [\AA] and angles [$^\circ$] for **[Ru-1-cyclohexene]⁺**

Ru(1)-P(3)	2.3273(9)
Ru(1)-P(1)	2.3351(9)
Ru(1)-S(3)	2.3363(9)
Ru(1)-S(2)	2.3722(9)
Ru(1)-S(1)	2.3866(9)
Ru(1)-P(2)	2.4172(9)
S(1)-C(1)	1.756(4)
S(2)-C(7)	1.785(4)
S(2)-C(55)	1.865(4)
S(3)-C(13)	1.795(4)
S(3)-C(60)	1.886(4)
P(1)-C(6)	1.811(3)
P(1)-C(19)	1.846(3)
P(1)-C(25)	1.847(4)
P(2)-C(43)	1.831(3)
P(2)-C(12)	1.839(3)
P(2)-C(49)	1.849(4)
P(3)-C(18)	1.827(4)
P(3)-C(31)	1.835(4)
P(3)-C(37)	1.850(3)
C(1)-C(6)	1.404(5)
C(1)-C(2)	1.405(5)
C(2)-C(3)	1.364(5)
C(2)-H(2)	0.9300
C(3)-C(4)	1.394(5)
C(3)-H(3)	0.9300
C(4)-C(5)	1.384(5)
C(4)-H(4)	0.9300
C(5)-C(6)	1.399(5)
C(5)-H(5)	0.9300
C(7)-C(8)	1.387(5)
C(7)-C(12)	1.395(5)
C(8)-C(9)	1.388(5)
C(8)-H(8)	0.9300
C(9)-C(10)	1.386(5)
C(9)-H(9)	0.9300
C(10)-C(11)	1.384(5)
C(10)-H(10)	0.9300
C(11)-C(12)	1.389(5)
C(11)-H(11)	0.9300
C(13)-C(18)	1.385(5)
C(13)-C(14)	1.391(5)
C(14)-C(15)	1.376(5)
C(14)-H(14)	0.9300

C(15)-C(16)	1.375(5)
C(15)-H(15)	0.9300
C(16)-C(17)	1.387(5)
C(16)-H(16)	0.9300
C(17)-C(18)	1.399(5)
C(17)-H(17)	0.9300
C(19)-C(24)	1.388(5)
C(19)-C(20)	1.396(5)
C(20)-C(21)	1.387(5)
C(20)-H(20)	0.9300
C(21)-C(22)	1.371(5)
C(21)-H(21)	0.9300
C(22)-C(23)	1.380(5)
C(22)-H(22)	0.9300
C(23)-C(24)	1.397(5)
C(23)-H(23)	0.9300
C(24)-H(24)	0.9300
C(25)-C(26)	1.391(5)
C(25)-C(30)	1.396(5)
C(26)-C(27)	1.391(5)
C(26)-H(26)	0.9300
C(27)-C(28)	1.377(6)
C(27)-H(27)	0.9300
C(28)-C(29)	1.377(6)
C(28)-H(28)	0.9300
C(29)-C(30)	1.388(5)
C(29)-H(29)	0.9300
C(30)-H(30)	0.9300
C(31)-C(32)	1.388(5)
C(31)-C(36)	1.394(5)
C(32)-C(33)	1.389(5)
C(32)-H(32)	0.9300
C(33)-C(34)	1.369(6)
C(33)-H(33)	0.9300
C(34)-C(35)	1.387(6)
C(34)-H(34)	0.9300
C(35)-C(36)	1.383(5)
C(35)-H(35)	0.9300
C(36)-H(36)	0.9300
C(37)-C(42)	1.388(5)
C(37)-C(38)	1.401(5)
C(38)-C(39)	1.385(5)
C(38)-H(38)	0.9300
C(39)-C(40)	1.386(5)
C(39)-H(39)	0.9300

C(40)-C(41)	1.381(5)
C(40)-H(40)	0.9300
C(41)-C(42)	1.396(5)
C(41)-H(41)	0.9300
C(42)-H(42)	0.9300
C(43)-C(44)	1.391(5)
C(43)-C(48)	1.392(5)
C(44)-C(45)	1.383(5)
C(44)-H(44)	0.9300
C(45)-C(46)	1.382(5)
C(45)-H(45)	0.9300
C(46)-C(47)	1.375(5)
C(46)-H(46)	0.9300
C(47)-C(48)	1.389(5)
C(47)-H(47)	0.9300
C(48)-H(48)	0.9300
C(49)-C(50)	1.388(5)
C(49)-C(54)	1.394(5)
C(50)-C(51)	1.390(5)
C(50)-H(50)	0.9300
C(51)-C(52)	1.377(5)
C(51)-H(51)	0.9300
C(52)-C(53)	1.384(5)
C(52)-H(52)	0.9300
C(53)-C(54)	1.377(5)
C(53)-H(53)	0.9300
C(54)-H(54)	0.9300
C(55)-C(60)	1.515(5)
C(55)-C(56)	1.522(5)
C(55)-H(55)	0.9800
C(56)-C(57)	1.524(6)
C(56)-H(56A)	0.9700
C(56)-H(56B)	0.9700
C(57)-C(58)	1.522(6)
C(57)-H(57A)	0.9700
C(57)-H(57B)	0.9700
C(58)-C(59)	1.499(6)
C(58)-H(58A)	0.9700
C(58)-H(58B)	0.9700
C(59)-C(60)	1.530(5)
C(59)-H(59A)	0.9700
C(59)-H(59B)	0.9700
C(60)-H(60)	0.9800
P(4)-F(5)	1.585(2)
P(4)-F(6)	1.593(3)

P(4)-F(1)	1.594(3)
P(4)-F(2)	1.598(3)
P(4)-F(3)	1.600(2)
P(4)-F(4)	1.609(2)
Cl(1)-C(61)	1.747(6)
Cl(2)-C(61)	1.778(5)
C(61)-H(99A)	0.9700
C(61)-H(99B)	0.9700
P(3)-Ru(1)-P(1)	94.72(3)
P(3)-Ru(1)-S(3)	85.60(3)
P(1)-Ru(1)-S(3)	97.04(3)
P(3)-Ru(1)-S(2)	88.92(3)
P(1)-Ru(1)-S(2)	175.91(3)
S(3)-Ru(1)-S(2)	85.07(3)
P(3)-Ru(1)-S(1)	90.65(3)
P(1)-Ru(1)-S(1)	85.35(3)
S(3)-Ru(1)-S(1)	175.70(3)
S(2)-Ru(1)-S(1)	92.77(3)
P(3)-Ru(1)-P(2)	168.71(3)
P(1)-Ru(1)-P(2)	95.54(3)
S(3)-Ru(1)-P(2)	97.79(3)
S(2)-Ru(1)-P(2)	80.69(3)
S(1)-Ru(1)-P(2)	85.50(3)
C(1)-S(1)-Ru(1)	105.91(12)
C(7)-S(2)-C(55)	101.93(17)
C(7)-S(2)-Ru(1)	104.04(12)
C(55)-S(2)-Ru(1)	103.00(12)
C(13)-S(3)-C(60)	100.48(16)
C(13)-S(3)-Ru(1)	105.90(12)
C(60)-S(3)-Ru(1)	107.57(12)
C(6)-P(1)-C(19)	105.59(15)
C(6)-P(1)-C(25)	104.62(16)
C(19)-P(1)-C(25)	99.61(15)
C(6)-P(1)-Ru(1)	108.04(11)
C(19)-P(1)-Ru(1)	115.08(11)
C(25)-P(1)-Ru(1)	122.36(12)
C(43)-P(2)-C(12)	103.81(16)
C(43)-P(2)-C(49)	100.57(15)
C(12)-P(2)-C(49)	100.72(16)
C(43)-P(2)-Ru(1)	125.93(12)
C(12)-P(2)-Ru(1)	101.52(11)
C(49)-P(2)-Ru(1)	120.41(11)
C(18)-P(3)-C(31)	105.90(16)
C(18)-P(3)-C(37)	104.82(15)

C(31)-P(3)-C(37)	98.86(15)
C(18)-P(3)-Ru(1)	106.69(11)
C(31)-P(3)-Ru(1)	124.23(11)
C(37)-P(3)-Ru(1)	114.61(11)
C(6)-C(1)-C(2)	118.4(3)
C(6)-C(1)-S(1)	123.1(3)
C(2)-C(1)-S(1)	118.3(3)
C(3)-C(2)-C(1)	121.4(3)
C(3)-C(2)-H(2)	119.3
C(1)-C(2)-H(2)	119.3
C(2)-C(3)-C(4)	120.6(3)
C(2)-C(3)-H(3)	119.7
C(4)-C(3)-H(3)	119.7
C(5)-C(4)-C(3)	118.9(3)
C(5)-C(4)-H(4)	120.6
C(3)-C(4)-H(4)	120.6
C(4)-C(5)-C(6)	121.3(3)
C(4)-C(5)-H(5)	119.4
C(6)-C(5)-H(5)	119.4
C(5)-C(6)-C(1)	119.4(3)
C(5)-C(6)-P(1)	123.1(3)
C(1)-C(6)-P(1)	117.4(2)
C(8)-C(7)-C(12)	120.8(3)
C(8)-C(7)-S(2)	119.5(3)
C(12)-C(7)-S(2)	119.4(3)
C(9)-C(8)-C(7)	119.6(3)
C(9)-C(8)-H(8)	120.2
C(7)-C(8)-H(8)	120.2
C(10)-C(9)-C(8)	119.8(3)
C(10)-C(9)-H(9)	120.1
C(8)-C(9)-H(9)	120.1
C(11)-C(10)-C(9)	120.6(3)
C(11)-C(10)-H(10)	119.7
C(9)-C(10)-H(10)	119.7
C(10)-C(11)-C(12)	120.2(3)
C(10)-C(11)-H(11)	119.9
C(12)-C(11)-H(11)	119.9
C(11)-C(12)-C(7)	119.0(3)
C(11)-C(12)-P(2)	124.4(3)
C(7)-C(12)-P(2)	116.6(3)
C(18)-C(13)-C(14)	121.5(3)
C(18)-C(13)-S(3)	121.1(3)
C(14)-C(13)-S(3)	117.4(3)
C(15)-C(14)-C(13)	119.5(4)
C(15)-C(14)-H(14)	120.3

C(13)-C(14)-H(14)	120.3
C(16)-C(15)-C(14)	120.4(4)
C(16)-C(15)-H(15)	119.8
C(14)-C(15)-H(15)	119.8
C(15)-C(16)-C(17)	119.9(3)
C(15)-C(16)-H(16)	120.0
C(17)-C(16)-H(16)	120.0
C(16)-C(17)-C(18)	121.0(3)
C(16)-C(17)-H(17)	119.5
C(18)-C(17)-H(17)	119.5
C(13)-C(18)-C(17)	117.7(3)
C(13)-C(18)-P(3)	117.9(3)
C(17)-C(18)-P(3)	124.4(3)
C(24)-C(19)-C(20)	118.7(3)
C(24)-C(19)-P(1)	123.5(3)
C(20)-C(19)-P(1)	117.8(2)
C(21)-C(20)-C(19)	120.7(3)
C(21)-C(20)-H(20)	119.6
C(19)-C(20)-H(20)	119.6
C(22)-C(21)-C(20)	120.3(3)
C(22)-C(21)-H(21)	119.9
C(20)-C(21)-H(21)	119.9
C(21)-C(22)-C(23)	119.8(3)
C(21)-C(22)-H(22)	120.1
C(23)-C(22)-H(22)	120.1
C(22)-C(23)-C(24)	120.6(3)
C(22)-C(23)-H(23)	119.7
C(24)-C(23)-H(23)	119.7
C(19)-C(24)-C(23)	119.9(3)
C(19)-C(24)-H(24)	120.0
C(23)-C(24)-H(24)	120.0
C(26)-C(25)-C(30)	117.5(3)
C(26)-C(25)-P(1)	120.0(3)
C(30)-C(25)-P(1)	122.6(3)
C(25)-C(26)-C(27)	121.2(4)
C(25)-C(26)-H(26)	119.4
C(27)-C(26)-H(26)	119.4
C(28)-C(27)-C(26)	120.1(4)
C(28)-C(27)-H(27)	119.9
C(26)-C(27)-H(27)	119.9
C(29)-C(28)-C(27)	119.9(4)
C(29)-C(28)-H(28)	120.1
C(27)-C(28)-H(28)	120.1
C(28)-C(29)-C(30)	119.9(4)
C(28)-C(29)-H(29)	120.1

C(30)-C(29)-H(29)	120.1
C(29)-C(30)-C(25)	121.4(4)
C(29)-C(30)-H(30)	119.3
C(25)-C(30)-H(30)	119.3
C(32)-C(31)-C(36)	118.6(3)
C(32)-C(31)-P(3)	122.9(3)
C(36)-C(31)-P(3)	118.4(3)
C(31)-C(32)-C(33)	120.4(4)
C(31)-C(32)-H(32)	119.8
C(33)-C(32)-H(32)	119.8
C(34)-C(33)-C(32)	120.3(4)
C(34)-C(33)-H(33)	119.8
C(32)-C(33)-H(33)	119.8
C(33)-C(34)-C(35)	120.0(4)
C(33)-C(34)-H(34)	120.0
C(35)-C(34)-H(34)	120.0
C(36)-C(35)-C(34)	119.8(4)
C(36)-C(35)-H(35)	120.1
C(34)-C(35)-H(35)	120.1
C(35)-C(36)-C(31)	120.6(4)
C(35)-C(36)-H(36)	119.7
C(31)-C(36)-H(36)	119.7
C(42)-C(37)-C(38)	118.6(3)
C(42)-C(37)-P(3)	123.1(3)
C(38)-C(37)-P(3)	118.3(3)
C(39)-C(38)-C(37)	120.7(3)
C(39)-C(38)-H(38)	119.7
C(37)-C(38)-H(38)	119.7
C(38)-C(39)-C(40)	120.1(4)
C(38)-C(39)-H(39)	120.0
C(40)-C(39)-H(39)	120.0
C(41)-C(40)-C(39)	119.9(3)
C(41)-C(40)-H(40)	120.0
C(39)-C(40)-H(40)	120.0
C(40)-C(41)-C(42)	120.1(3)
C(40)-C(41)-H(41)	119.9
C(42)-C(41)-H(41)	119.9
C(37)-C(42)-C(41)	120.6(3)
C(37)-C(42)-H(42)	119.7
C(41)-C(42)-H(42)	119.7
C(44)-C(43)-C(48)	118.1(3)
C(44)-C(43)-P(2)	121.0(3)
C(48)-C(43)-P(2)	120.8(3)
C(45)-C(44)-C(43)	121.1(3)
C(45)-C(44)-H(44)	119.5

C(43)-C(44)-H(44)	119.5
C(44)-C(45)-C(46)	120.1(4)
C(44)-C(45)-H(45)	120.0
C(46)-C(45)-H(45)	120.0
C(47)-C(46)-C(45)	119.7(3)
C(47)-C(46)-H(46)	120.2
C(45)-C(46)-H(46)	120.2
C(46)-C(47)-C(48)	120.3(4)
C(46)-C(47)-H(47)	119.8
C(48)-C(47)-H(47)	119.8
C(43)-C(48)-C(47)	120.6(4)
C(43)-C(48)-H(48)	119.7
C(47)-C(48)-H(48)	119.7
C(50)-C(49)-C(54)	118.8(3)
C(50)-C(49)-P(2)	119.6(3)
C(54)-C(49)-P(2)	121.6(3)
C(49)-C(50)-C(51)	120.6(3)
C(49)-C(50)-H(50)	119.7
C(51)-C(50)-H(50)	119.7
C(52)-C(51)-C(50)	120.0(3)
C(52)-C(51)-H(51)	120.0
C(50)-C(51)-H(51)	120.0
C(51)-C(52)-C(53)	119.7(4)
C(51)-C(52)-H(52)	120.1
C(53)-C(52)-H(52)	120.1
C(54)-C(53)-C(52)	120.5(4)
C(54)-C(53)-H(53)	119.7
C(52)-C(53)-H(53)	119.7
C(53)-C(54)-C(49)	120.3(3)
C(53)-C(54)-H(54)	119.8
C(49)-C(54)-H(54)	119.8
C(60)-C(55)-C(56)	112.9(3)
C(60)-C(55)-S(2)	109.2(3)
C(56)-C(55)-S(2)	111.1(3)
C(60)-C(55)-H(55)	107.8
C(56)-C(55)-H(55)	107.8
S(2)-C(55)-H(55)	107.8
C(57)-C(56)-C(55)	113.2(3)
C(57)-C(56)-H(56A)	108.9
C(55)-C(56)-H(56A)	108.9
C(57)-C(56)-H(56B)	108.9
C(55)-C(56)-H(56B)	108.9
H(56A)-C(56)-H(56B)	107.8
C(58)-C(57)-C(56)	109.5(3)
C(58)-C(57)-H(57A)	109.8

C(56)-C(57)-H(57A)	109.8
C(58)-C(57)-H(57B)	109.8
C(56)-C(57)-H(57B)	109.8
H(57A)-C(57)-H(57B)	108.2
C(59)-C(58)-C(57)	111.2(3)
C(59)-C(58)-H(58A)	109.4
C(57)-C(58)-H(58A)	109.4
C(59)-C(58)-H(58B)	109.4
C(57)-C(58)-H(58B)	109.4
H(58A)-C(58)-H(58B)	108.0
C(58)-C(59)-C(60)	110.7(3)
C(58)-C(59)-H(59A)	109.5
C(60)-C(59)-H(59A)	109.5
C(58)-C(59)-H(59B)	109.5
C(60)-C(59)-H(59B)	109.5
H(59A)-C(59)-H(59B)	108.1
C(55)-C(60)-C(59)	112.6(3)
C(55)-C(60)-S(3)	110.4(2)
C(59)-C(60)-S(3)	113.3(3)
C(55)-C(60)-H(60)	106.7
C(59)-C(60)-H(60)	106.7
S(3)-C(60)-H(60)	106.7
F(5)-P(4)-F(6)	179.76(17)
F(5)-P(4)-F(1)	90.08(14)
F(6)-P(4)-F(1)	90.14(16)
F(5)-P(4)-F(2)	89.82(15)
F(6)-P(4)-F(2)	89.96(16)
F(1)-P(4)-F(2)	179.73(16)
F(5)-P(4)-F(3)	89.74(13)
F(6)-P(4)-F(3)	90.38(13)
F(1)-P(4)-F(3)	89.86(14)
F(2)-P(4)-F(3)	90.39(14)
F(5)-P(4)-F(4)	89.78(12)
F(6)-P(4)-F(4)	90.11(13)
F(1)-P(4)-F(4)	90.42(14)
F(2)-P(4)-F(4)	89.34(13)
F(3)-P(4)-F(4)	179.44(15)
Cl(1)-C(61)-Cl(2)	112.3(3)
Cl(1)-C(61)-H(99A)	109.1
Cl(2)-C(61)-H(99A)	109.1
Cl(1)-C(61)-H(99B)	109.1
Cl(2)-C(61)-H(99B)	109.1
H(99A)-C(61)-H(99B)	107.9

Table G-8. Crystal data and structure refinement for [Ru-1·octyne]⁺

Empirical formula	C ₆₂ H ₅₅ P ₃ Ru S ₃ • P F ₆
Formula weight	1235.22
Temperature	100.0 K
Wavelength	0.7107 Å
Crystal system	Monoclinic
Space group	P 2 ₁ /n
Unit cell dimensions	a = 12.0367(4) Å □ = 90.0°. b = 24.2458(10) Å □ = 98.291(3)°. c = 20.1572(9) Å □ = 90.0°.
Volume	5821.2(7) Å ³
Z	4
Density (calculated)	1.409 Mg/m ³
Absorption coefficient	0.545 mm ⁻¹
F(000)	2532
Crystal color. habit	yellow prism
Crystal size	0.20 x 0.18 x 0.16 mm ³
Theta range for data collection	3.29 to 28.89°
Index ranges	-10 ≤ h ≤ 15, -31 ≤ k ≤ 30, -24 ≤ l ≤ 23
Reflections collected	16557
Independent reflections	13711 [R(int) = 0.0747]
Completeness to theta = 29.01°	88.5 %
Absorption correction	Semi-empirical from equivalents
Max. and min. transmission	1.000 and 0.981
Refinement method	Full-matrix least-squares on F ²
Data / restraints / parameters	13711 / 23 / 679
Goodness-of-fit on F ²	1.056
Final R indices [I > 2σ(I)]	R1 = 0.0778, wR2 = 0.1332
R indices (all data)	R1 = 0.1337, wR2 = 0.1495
Largest diff. peak and hole	1.418 and -1.112 e.Å ⁻³

Note: crystallographic data in CIF format (CCDC 844993). This material is available free of charge via the internet at www.ccdc.cam.ac.uk/data_request/cif.

Table G-9. Atomic coordinates ($\times 10^4$) and equivalent isotropic displacement parameters ($\text{\AA}^2 \times 10^3$) for **[Ru-1·octyne]⁺**. U(eq) is defined as one third of the trace of the orthogonalized U^{ij} tensor.

	x	y	z	U(eq)
Ru(1)	2297(1)	8065(1)	1435(1)	21(1)
S(1)	1499(1)	7458(1)	562(1)	26(1)
S(2)	522(1)	8136(1)	1803(1)	38(1)
S(3)	2957(1)	8617(1)	2341(1)	35(1)
P(1)	3956(1)	7971(1)	977(1)	21(1)
P(2)	2690(1)	7322(1)	2176(1)	24(1)
P(3)	1579(1)	8833(1)	771(1)	22(1)
C(1)	2602(4)	7276(2)	127(3)	26(1)
C(2)	2403(5)	6900(2)	-405(3)	35(1)
C(3)	3214(5)	6759(3)	-779(3)	43(2)
C(4)	4286(5)	6987(3)	-638(3)	41(2)
C(5)	4508(5)	7350(2)	-117(3)	32(1)
C(6)	3697(4)	7490(2)	283(3)	25(1)
C(7)	-407(5)	8429(2)	1105(3)	33(1)
C(8)	-1554(5)	8325(3)	1050(3)	40(2)
C(9)	-2236(5)	8510(3)	493(3)	40(2)
C(10)	-1801(4)	8814(2)	12(3)	32(1)
C(11)	-667(4)	8921(2)	78(3)	30(1)
C(12)	49(4)	8726(2)	629(3)	25(1)
C(13)	3443(4)	8175(2)	3045(3)	29(1)
C(14)	3928(5)	8412(3)	3646(3)	38(2)
C(15)	4246(5)	8080(3)	4198(3)	38(2)
C(16)	4113(5)	7524(3)	4154(3)	38(2)
C(17)	3664(5)	7279(3)	3556(3)	34(1)
C(18)	3327(4)	7606(2)	2981(3)	28(1)
C(19)	4571(4)	8566(2)	604(3)	23(1)
C(20)	5134(4)	8971(2)	1024(3)	27(1)
C(21)	5642(4)	9413(2)	748(3)	33(1)
C(22)	5638(4)	9451(2)	66(3)	33(1)
C(23)	5071(4)	9064(2)	-351(3)	30(1)
C(24)	4528(4)	8630(2)	-84(3)	26(1)
C(25)	5226(4)	7728(2)	1526(3)	26(1)
C(26)	5536(4)	8009(3)	2125(3)	34(1)
C(27)	6504(5)	7879(3)	2546(3)	43(2)
C(28)	7197(5)	7466(3)	2369(3)	45(2)
C(29)	6903(5)	7177(3)	1783(3)	42(2)
C(30)	5914(4)	7305(2)	1361(3)	32(1)

C(31)	3588(4)	6757(2)	1982(3)	26(1)
C(32)	3283(4)	6468(2)	1391(3)	29(1)
C(33)	3940(5)	6041(2)	1195(3)	35(1)
C(34)	4934(5)	5907(2)	1600(3)	39(2)
C(35)	5261(5)	6191(2)	2179(3)	34(1)
C(36)	4611(4)	6618(2)	2377(3)	28(1)
C(37)	1456(4)	6964(2)	2419(3)	27(1)
C(38)	913(5)	6557(3)	2016(3)	39(2)
C(39)	-29(5)	6296(3)	2196(4)	47(2)
C(40)	-440(5)	6443(3)	2764(3)	43(2)
C(41)	63(5)	6860(3)	3154(3)	46(2)
C(42)	1008(5)	7121(3)	2985(3)	37(1)
C(43)	1835(4)	9000(2)	-78(3)	21(1)
C(44)	1824(4)	8577(2)	-544(3)	26(1)
C(45)	1992(4)	8698(2)	-1195(3)	30(1)
C(46)	2155(4)	9236(2)	-1387(3)	30(1)
C(47)	2116(4)	9654(2)	-930(3)	28(1)
C(48)	1969(4)	9540(2)	-283(3)	23(1)
C(49)	1720(4)	9506(2)	1187(3)	23(1)
C(50)	2796(5)	9710(2)	1405(3)	32(1)
C(51)	2952(5)	10211(2)	1737(3)	37(2)
C(52)	2038(5)	10506(2)	1864(3)	36(1)
C(53)	969(5)	10310(2)	1647(3)	35(1)
C(54)	805(4)	9822(2)	1311(3)	28(1)
C(55)	711(7)	8699(3)	2388(3)	53(2)
C(56)	1723(7)	8872(3)	2645(3)	53(2)
C(57)	1626(13)	9280(6)	3163(6)	51(2)
C(58)	1238(13)	9087(5)	3829(6)	51(2)
C(59)	1242(14)	9595(5)	4373(6)	51(2)
C(60)	1297(18)	9363(6)	5063(8)	51(2)
C(61)	1843(11)	8849(6)	5354(8)	51(2)
C(62)	3078(11)	8957(6)	5504(7)	51(2)
C(63)	-143(14)	8998(8)	2661(8)	81(3)
C(64)	45(15)	9474(8)	3162(7)	81(3)
C(65)	314(13)	9313(9)	3880(7)	81(3)
C(66)	1400(14)	9308(10)	4280(8)	81(3)
C(67)	1170(20)	9218(10)	4987(9)	81(3)
C(68)	2307(15)	8902(9)	5228(9)	81(3)
P(4A)	6576(3)	9730(2)	2794(2)	49(1)
F(1AB)	7175(5)	9451(2)	2209(3)	105(1)
F(2A)	5832(9)	10013(5)	3296(5)	105(1)
F(3A)	5714(10)	9251(5)	2711(5)	105(1)
F(4A)	7324(12)	10221(6)	3037(6)	105(1)
F(5A)	7230(11)	9443(5)	3435(5)	105(1)
F(6A)	5936(9)	10031(5)	2185(5)	105(1)

P(4B)	7665(3)	9578(1)	2822(2)	43(1)
F(2B)	8293(11)	9639(5)	3550(5)	116(2)
F(3B)	6698(12)	9256(5)	3106(6)	116(2)
F(4B)	8647(10)	9874(4)	2552(5)	116(2)
F(5B)	8224(11)	9007(4)	2857(6)	116(2)
F(6B)	7302(14)	10187(5)	2772(6)	116(2)

Appendix H

Tables for Cyclic Voltammetry Experimental Parameters

Appendix	Page
H-1 Table for <i>para</i> -substituted styrene.....	207
H-2 Table for <i>meta</i> -substituted styrene.....	208
H-3 Table for <i>ortho</i> -substituted styrene.....	209
H-4 Table for alkenes.....	210

Table H-1. CV data for 2.0 mM PPN[Ru-1] + 0.2 M *para*-substituted styrenes in dry degassed CH₃CN with 0.1 M TBAHFP.

Alkene	Potential (vs Fc ⁺ /Fc) (mV)			Uncompensated resistance (Ω)	Measured potential (mV)
	E ₁	E ₂	E ₄	R _u	
Styrene	-830	-171	286	200	-1288
Styrene	-830	-111	283	172	-1146
Styrene	-830	-130	277	195	-1148
Styrene	-830	-118	274	214	-1160
Styrene	-830	-123	268	192	-1160
Styrene	-830	-117	276	205	-1217
Styrene	-830	-122	277	177	-1005
Styrene	-830	-120	282	210	-956
Styrene	-830	-120	278	203	-943
Styrene	-830	-122	278	231	-955
<i>p</i> -chlorostyrene	-830	-112	286	188	-1165
<i>p</i> -chlorostyrene	-830	-107	282	183	-1138
<i>p</i> -chlorostyrene	-830	-112	287	128	-1027
<i>p</i> -chlorostyrene	-830	-66	283	196	-1061
<i>p</i> -chlorostyrene	-830	-112	290	197	-1059
<i>p</i> -chlorostyrene	-830	-114	286	187	-1072
<i>p</i> -chlorostyrene	-830	-105	280	201	-1069
<i>p</i> -chlorostyrene	-830	-116	286	203	-1033
<i>p</i> -chlorostyrene	-830	-119	288	193	-1008
<i>p</i> -chlorostyrene	-830	-167	289	204	-1022
<i>p</i> -fluorostyrene	-830	-101	281	210	-1028
<i>p</i> -fluorostyrene	-830	-108	282	218	-993
<i>p</i> -fluorostyrene	-830	-103	285	284	-963
<i>p</i> -fluorostyrene	-830	-109	281	237	982
<i>p</i> -fluorostyrene	-830	-105	283	236	-1006
<i>p</i> -fluorostyrene	-830	-102	286	274	-974
<i>p</i> -fluorostyrene	-830	-59	294	464	-1061
<i>p</i> -fluorostyrene	-830	-93	278	293	1059
<i>p</i> -fluorostyrene	-830	-75	289	410	-981
<i>p</i> -fluorostyrene	-830	-100	281	396	-1259
<i>p</i> -methylstyrene	-830	-109	275	267	-950
<i>p</i> -methylstyrene	-830	-121	271	201	-1055
<i>p</i> -methylstyrene	-830	-123	275	215	-1046
<i>p</i> -methylstyrene	-830	-119	273	228	-1063
<i>p</i> -methylstyrene	-830	-100	281	396	-1259
<i>p</i> -methylstyrene	-830	-117	276	270	-1055
<i>p</i> -methylstyrene	-830	-50	278	243	-993
<i>p</i> -methylstyrene	-830	-116	278	268	-1008
<i>p</i> -methylstyrene	-830	-124	273	229	-955

<i>p</i> -methylstyrene	-830	-122	273	182	-955
<i>p</i> -methoxystyrene	-830	-174	213	255	-1046
<i>p</i> -methoxystyrene	-830	-123	337	214	-1044
<i>p</i> -methoxystyrene	-830	-136	265	210	-1035
<i>p</i> -methoxystyrene	-830	-68	272	229	-1012
<i>p</i> -methoxystyrene	-830	-130	264	206	-961
<i>p</i> -methoxystyrene	-830	-167	265	213	-953
<i>p</i> -methoxystyrene	-830	-116	280	258	-1005
<i>p</i> -methoxystyrene	-830	-105	274	313	-986
<i>p</i> -methoxystyrene	-830	-130	268	222	-991
<i>p</i> -methoxystyrene	-830	-129	266	209	-990

Table H-2. CV data for 2.0 mM PPN[Ru-1] + 0.2 M *meta*-substituted styrenes in dry degassed CH₃CN with 0.1 M TBAHFP.

Alkene	Potential (vs Fc ⁺ /Fc) (mV)			Uncompensated resistance (Ω)	Measured potential (mV)
	E ₁	E ₂	E ₄		
<i>m</i> -chlorostyrene	-830	-82	286	225	-1022
<i>m</i> -chlorostyrene	-830	-109	287	200	-955
<i>m</i> -chlorostyrene	-830	-116	289	205	-952
<i>m</i> -chlorostyrene	-830	-114	286	210	-957
<i>m</i> -chlorostyrene	-830	-113	284	205	-956
<i>m</i> -chlorostyrene	-830	-114	288	215	-955
<i>m</i> -chlorostyrene	-830	-114	286	212	-952
<i>m</i> -chlorostyrene	-830	-119	285	210	-956
<i>m</i> -chlorostyrene	-830	-113	286	227	-961
<i>m</i> -chlorostyrene	-830	-116	292	216	-952
<i>m</i> -fluorostyrene	-830	-103	283	222	-958
<i>m</i> -fluorostyrene	-830	-110	284	207	-956
<i>m</i> -fluorostyrene	-830	-116	283	202	-959
<i>m</i> -fluorostyrene	-830	-108	284	221	-961
<i>m</i> -fluorostyrene	-830	-113	282	218	-956
<i>m</i> -fluorostyrene	-830	-105	284	210	-958
<i>m</i> -fluorostyrene	-830	-106	286	216	-957
<i>m</i> -fluorostyrene	-830	-104	278	192	-964
<i>m</i> -fluorostyrene	-830	-111	285	220	-957
<i>m</i> -fluorostyrene	-830	-113	285	214	-957
<i>m</i> -methylstyrene	-830	-115	274	222	-958
<i>m</i> -methylstyrene	-830	-126	268	227	-959
<i>m</i> -methylstyrene	-830	-128	272	202	-959
<i>m</i> -methylstyrene	-830	-126	271	210	-1179
<i>m</i> -methylstyrene	-830	-125	272	219	-1006
<i>m</i> -methylstyrene	-830	-113	276	221	-1016

<i>m</i> -methylstyrene	-830	-124	279	223	-957
<i>m</i> -methylstyrene	-830	-125	274	212	-923
<i>m</i> -methylstyrene	-830	-123	273	207	-928
<i>m</i> -methylstyrene	-830	-120	274	214	926
<i>m</i> -methoxystyrene	-830	-111	271	210	-1012
<i>m</i> -methoxystyrene	-830	-122	263	229	-965
<i>m</i> -methoxystyrene	-830	-126	271	201	-951
<i>m</i> -methoxystyrene	-830	-125	275	217	-956
<i>m</i> -methoxystyrene	-830	-122	275	219	-965
<i>m</i> -methoxystyrene	-830	-112	275	208	-963
<i>m</i> -methoxystyrene	-830	-119	274	213	-957
<i>m</i> -methoxystyrene	-830	-123	274	220	-979
<i>m</i> -methoxystyrene	-830	-121	273	198	-974
<i>m</i> -methoxystyrene	-830	-121	270	216	-967

Table H-3. CV data for 2.0 mM PPN[Ru-1] + 0.2 M *ortho*-substituted styrene in dry degassed CH₃CN with 0.1 M TBAHFP.

Alkene	Potential (vs Fc ⁺ /Fc) (mV)			Uncompensated resistance (Ω)	Measured potential (mV)
	E ₁	E ₂	E ₄		
<i>o</i> -fluorostyrene	-830	-126	278	200	-1168
<i>o</i> -fluorostyrene	-830	-136	282	204	-1057
<i>o</i> -fluorostyrene	-830	-110	280	200	-1058
<i>o</i> -fluorostyrene	-830	-112	278	208	-1047
<i>o</i> -fluorostyrene	-830	-106	281	194	-954
<i>o</i> -fluorostyrene	-830	-113	282	208	-959
<i>o</i> -fluorostyrene	-830	-91	281	209	-957
<i>o</i> -fluorostyrene	-830	-100	285	210	-961
<i>o</i> -fluorostyrene	-830	-84	285	217	-960
<i>o</i> -fluorostyrene	-830	-90	279	192	-957
<i>o</i> -methylstyrene	-830	-128	255	202	-1056
<i>o</i> -methylstyrene	-830	-86	253	202	-956
<i>o</i> -methylstyrene	-830	-108	252	211	-956
<i>o</i> -methylstyrene	-830	-65	251	201	-960
<i>o</i> -methylstyrene	-830	-105	256	226	-1001
<i>o</i> -methylstyrene	-830	-118	250	203	-1170
<i>o</i> -methylstyrene	-830	-134	255	204	-1065
<i>o</i> -methylstyrene	-830	-144	250	182	-1057
<i>o</i> -methylstyrene	-830	-138	254	216	-964
<i>o</i> -methylstyrene	-830	-136	252	210	-976
<i>o</i> -methoxystyrene	-830	-124	269	234	-1244
<i>o</i> -methoxystyrene	-830	-120	264	212	-1151
<i>o</i> -methoxystyrene	-830	-124	267	250	-1047

<i>o</i> -methoxystyrene	-830	-122	265	231	-1007
<i>o</i> -methoxystyrene	-830	-129	264	226	-939
<i>o</i> -methoxystyrene	-830	-137	261	213	-1102
<i>o</i> -methoxystyrene	-830	-139	265	209	-1054
<i>o</i> -methoxystyrene	-830	-147	262	201	-952
<i>o</i> -methoxystyrene	-830	-137	265	204	-977
<i>o</i> -methoxystyrene	-830	-133	257	185	-961

Table H-4. CV data for 2.0 mM PPN[Ru-1] + 0.2 M alkenes in dry degassed CH₃CN with 0.1 M TBAHFP.

Alkene	Potential (vs Fc ⁺ /Fc) (mV)			Uncompensated resistance (Ω)	Measured potential (mV)
	E ₁	E ₂	E ₄		
Styrene	-830	-117	276	205	-1217
Styrene	-830	-122	277	177	-1005
Styrene	-830	-120	282	210	-956
<i>n</i> -propyl vinyl ether	-830	-113	270	182	-1039
<i>n</i> -propyl vinyl ether	-830	-115	273	181	-996
<i>n</i> -propyl vinyl ether	-830	-117	272	186	-965
<i>t</i> -butyl vinyl ether	-830	-87	273	196	-988
<i>t</i> -butyl vinyl ether	-830	-95	269	188	-954
<i>t</i> -butyl vinyl ether	-830	-89	269	172	-968
1-hexene	-830	-65	263	179	-987
1-hexene	-830	-69	263	175	-963
1-hexene	-830	-69	267	175	-963
acrylonitrile	-830	-71	347	210	-984
acrylonitrile	-830	-42	348	201	-982
acrylonitrile	-830	-90	300	178	-1007
cyclohexene	-830	-22	228	185	-1065
cyclohexene	-830	-7	251	222	-978
cyclohexene	-830	-7	245	202	-976
cyclopentene	-830	-73	250	171	-1092
cyclopentene	-830	-9	263	201	-1038
cyclopentene	-830	-79	262	170	-988
norbornene	-830	-113	285	179	-995
norbornene	-830	-116	287	183	-912
norbornene	-830	-119	286	184	-917

CURRICULUM VITAE

NAME: Kagna Ouch Sampson

ADDRESS: Department of Chemistry
University of Louisville
2320 South Brook Street
Louisville, KY 40292

E. Mail ADDRESS: ouch.kagna@gmail.com

DOB: Phnom Penh, Cambodia, June 05, 1983

EDUCATION
& TRAINING: B.S., Chemistry
Royal University of Phnom Penh
2000-2004

M.S., Chemistry
University of Louisville
2006-2008

AWARDS: Golden Key Awards Association, University of Louisville, KY
2009

M.S. outstanding student from University of Louisville, KY
2008

PUBLICATIONS: Ouch, K.; Mashuta, M.S.; Grapperhaus, C.A. (2012) Alkyne Addition to a Metal-Stabilized Thiyl Radical: Carbon-Sulfur Bond formation between 1-Octyne and $[\text{Ru}(\text{SP})_3]^+$. *Eur. J. Inorg. Chem.*, 2012, 475-478

Ouch, K.; Mashuta, M.S.; Grapperhaus, C.A. (2011) Metal-Stabilized Thiyl Radicals as Scaffolds for Reversible Alkene Addition via C-S Bond Formation/Cleavage. *Inorg. Chem.*, 50, 9904-9914

Grapperhaus, C.A.; Ouch, K.; Mashuta, M.S. (2009) Redox-Regulated Ethylene Binding to a Rhenium-Thiolate Complex. *J. Am. Chem. Soc.*, 131, 64-65